ADHESION FAILURE AND DELAMINATION DAMAGE ANALYSES OF BONDED JOINTS IN LAMINATED FRP COMPOSITES

Thesis Submitted for the Partial Fulfillment
of the Requirements for the Degree of

Doctor of Philosophy in Engineering

by

Sashi Kanta Panigrahi

Under the supervision of

Prof. B. Pradhan

Department of Mechanical Engineering
Indian Institute of Technology
Kharagpur – 721 302, India

August, 2007

Dedicated to my beloved

Teacher and Father

Department of Mechanical Engineering
Indian Institute of Technology
Kharagpur – 721 302, India

CERTIFICATE

This is to certify that the Thesis entitled **"Adhesion Failure and Delamination Damage Analyses of Bonded Joints in Laminated FRP Composites"** submitted by Mr. Sashi Kanta Panigrahi to the Indian Institute of Technology, Kharagpur, is a record of bonafide Research work carried out by him under my guidance and supervision in the Department of Mechanical Engineering, Indian Institute of Technology, Kharagpur. This Thesis is, in my opinion, worthy for the award of the Degree of *Doctor of Philosophy in Engineering* in accordance with the regulations of this Institute. The results presented in this Thesis have not been submitted to any other University or Institution for the award of any other Degree or Diploma.

(Prof. B. Pradhan)
Professor
Mechanical Engineering Department
Indian Institute of Technology
Kharagpur

August 30, 2007
IIT, Kharagpur

ACKNOWLEDGEMENT

The meticulous style of reviewing and guidance by Professor B. Pradhan, Department of Mechanical Engineering, Indian Institute of Technology, Kharagpur, throughout my research work has left an indelible impression on me. I am highly indebted and grateful to him for his constant inspiration, discussion of intricacies of investigation, help and support during the entire period of work of this dissertation. I received many useful and excellent academic training from him, which has stood in good stead while writing this Thesis. Nevertheless, it helped me acquire, develop and sharpen some of the skills and scientific methodologies of good independent research. In fact, I availed the excellent moral support, advice, philosophy and many other helps during my research period, for which I am very much grateful to my professor for ever.

I am thankful to the Head of the Mechanical Engineering Department, IIT Kharagpur, for providing me the necessary facilities to carry out my research work. I take this opportunity to express my warm regards to all the faculty members of the Mechanical Engineering Department and Doctoral Scrutiny Members in particular for their encouragement and advice extended to me. I am highly grateful to the Director of my parent Institution NERIST (Deemed University), Arunachal Pradesh for sponsoring me under Quality Improvement Programme to pursue my research programme leading to Ph.D. Degree in Engineering.

Sincere thanks are due to my research scholar friends, Mr. P. Ramesh Babu, Mr. Sambit Kumar Parida, Mr. J. Sivakumar, Mr. Arun Kumar Pradhan and many others for their cooperation and help rendered to me. Thanks are due to Mr. M. K. Mukherjee and Mr. N. Tulsaya of the Material Testing Laboratory for their assistance.

It gives me immense pleasure and satisfaction to express my gratitude to my wife Lisa, daughter Goodul and son Om for their constant patience, inspiration and unconditional moral support. I would like to share my appreciation with my mother and all family members of my brother, whose all endeavours have been always available to provide all encouragements during my research work. How much I do wish my father to be here at this moment, let his soul may live in peace in heaven and bless me all along. At the last, but not the least, I am greatly grateful to my father-in-law for his inspiration and help for the completion of my Thesis.

I take the opportunity to be highly grateful to the family members of my Professor for their incessant encouragements and support during the entire period of this Dissertation.

August 30, 2007 **Sashi Kanta Panigrahi**

ABSTRACT

This Thesis deals with three-dimensional non-linear Finite Element Analyses (FEA) of adhesion failure and delamination damages in four different types of adhesively bonded joints of laminated FRP composites. They are: Single Lap Joint (SLJ), Lap Shear Joint (LSJ), Double Lap Joint (DLJ) and Spar Wingskin Joint (SWJ). Different concepts of SWJ along with varying aspect ratios (ratio of spar base to height) with improved performance for integral structural construction of aircraft wings under out-of-plane loads have been studied. Comprehensive and relevant geometric and material parameters appropriate for damage analyses of different types of bonded joints have been considered in the present research. Layered solid and brick finite elements have been used for 3D modelling of the laminated FRP composite adherends and the epoxy adhesive layer, respectively, with appropriate orthotropic material characteristics. Sublaminate modelling techniques have been adopted for modelling of delaminations which have been presumed either to pre-exist or get evolved due to the coupled stress failure criteria in the laminated FRP composite adherends. Multi-point constraints have been used along the adhesion failure and the delamination damage fronts for maintaining the interface continuity. By sequential release of these constraints, self similar delamination progression has been realized. 3D Contact elements have been used inside the damaged region for preventing the interpenetration of damaged surfaces. The three individual components of Strain Energy Release Rate (SERR), G_I, G_{II} and G_{III} have been used as the defining parameters for assessing the adhesion failure and the delamination damage propagation behaviours. Modified Crack Closure Techniques (MCCI) based on the concepts of Linear Elastic Fracture Mechanics (LEFM) have been employed for computation of the SERR components.

Pertinent three-dimensional issues relating to stress states and damage onset and propagations have been dealt with in details. The distributions of out-of-plane stresses in the adhesive layer and the interfacial surfaces, the interlaminar stress distributions along the adhesion failure and the delamination damage fronts, and the SERR corresponding to the three individual modes have been evaluated for the SLJ, LSJ, DLJ and SWJ with laminated FRP composite adherends. Coupled stress failure criteria have been used to determine the locations of onset of the adhesion failure and the delamination induced damages. The critical locations for onset of the adhesion failure are found to be from the edges of stress singularity points in case of SLJ and DLJ. Delamination induced damages are found to occur near the overlap ends beneath the ply adjacent to the overlap region, and at the transition points where the spar changes its orientation from horizontal to inclined for LSJ and SWJ, respectively. The variations of the interlaminar stresses and the SERRs along the delamination fronts are found to be significantly different at the two ends of any such delamination indicating dissimilar rate of propagation of the delamination fronts. For a DLJ, it is seen that there is a significant difference in SERR values along the adhesion failure front and the delamination front. The trend of damage front propagation indicates, in general, that the straight delamination front may tend to propagate in non-self similar manner towards a curved delamination front. Suitable modified elliptical load coupler profiles have been developed from the stress and damage analyses of SWJ for improved performance. Associated recommendations have been made for arresting the delamination damages emanating from the toe ends of the spar of the SWJ.

Keywords: Adhesively bonded joints, Adhesion failure, Delamination damage, FRP composites, Interlaminar stresses, Sublaminate modelling, SERR, SWJ.

PREFACE

Damages in adhesively bonded laminated FRP composites may manifest itself in the forms of cohesive failure, adhesion failure, interlaminar/intralaminar delamination, debonding of fiber matrix interface, matrix cracking and fiber breakage, etc. While all or some of the above damage modes may simultaneously be present in any structural bonded joint applications, damages due to the cohesive failure, the adhesion failure and the delamination are of prime concern, because they may reduce significantly the strength and stiffness of the structure leading to the problems of loss in structural integrity and stability and to the final catastrophic failure. Delamination mode of failure in the laminated FRP composite adherends is especially of insidious nature. In this study, these damage behaviours in adhesively bonded joints of laminated FRP composites have been studied in details using the Finite Element Analysis (FEA). The joint specimens have been modelled using the solid elements, and Multi-Point Constraints along with the contact elements have been used for the delaminated damaged surfaces. Individual modes of Strain Energy Release Rates (SERR) near the free edges of the composite structure or along the delamination fronts computed using 2D models showed erroneous results when compared with the values obtained from three dimensional models. This happens as the stress state there is three-dimensional. Therefore, three-dimensional analyses are essential for modelling various types of such damages. In the present work 3D finite element analyses have been performed for various adhesively bonded joints in FRP laminated composites with adhesion failure and delamination damages. The three components of SERR viz. G_I, G_{II} and G_{III} have been used as characterizing parameters for assessing the damage growth behaviour. The Modified Crack Closure Integral (MCCI) techniques based on the concepts of Linear Elastic Fracture Mechanics (LEFM) have been employed to evaluate the individual modes of strain energy release rates during the adhesion failure and delamination damage propagation.

There are a large variety of bonded joint configurations used in the current structural applications. Among some typical classifications, adhesively bonded Single Lap Joint (SLJ), Lap Shear Joint (LSJ) and Double Lap Joint (DLJ) are used in practice and the damage analyses pertaining to these joints have been considered in the present Thesis. Also, one of the most important applications of adhesively bonded joints is found in the aircraft structure known as Spar Wingskin Joints (SWJ), which is intended for transferring and sharing the wing load and the fluid pressure. This type of joint is subjected to out-of-plane loads. The space between base flanges of the spar called core is filled up with some suitable adhesive or bonding materials called load couplers. The damage analyses of the SWJ having various load coupler profiles have been also dealt with in this Thesis.

The impetus of this research work is to formulate and facilitate such guidelines, which will enable to establish a better and effective design philosophy of adhesively bonded

joints in laminated FRP structures. The objectives of the present work have been set as follows:

An introduction to FRP composite materials, configurations of adhesively bonded joints of laminated FRP composites and damages commonly observed in the laminated FRP composite adherends and in the joints are presented in Chapter 1.

Chapter 2 is devoted to the review of literatures on the subjects of damage analyses of various types of adhesively bonded joints, interlaminar fracture behaviour and damage characteristics of laminated FRP composite adherends. The Strain Energy Release Rate (SERR) analyses based on Linear Elastic Fracture Mechanics (LEFM) for use of damage analyses in bonded joints in FRP composite have also been presented.

Compact descriptions of constitutive formulations in anisotropic and orthotropic media, finite element modeling and simulation of adhesion failure and delamination propagation and procedure for evaluation of SERR for characterizing the damage initiation and progression have been described in Chapter 3.

Chapter 4 deals with the three-dimensional FE analyses of adhesively bonded Single Lap Joint (SLJ). The three-dimensional issues involved, onset of damages and their growth have been discussed in details in this Chapter.

The effect of pre-embedded adhesion failures at the two ends of the adhesive layer of an SLJ on the stress distributions, joint strengths, SERR variations and adhesion failure propagations have been studied in Chapter 5.

Chapter 6 gives the delamination damage analyses in SLJ for varied positions of through-the-width pre-embedded delaminations in the adherends.

Chapter 7 is devoted to analyze the effect of delamination damage propagation pre-embedded beneath the surface ply of the strap adherend of the Lap Shear Joint (LSJ) on out-of-plane stress distributions in the adhesive layer, the interlaminar stresses and SERR variations along the delamination front.

The prediction of onset of adhesion failure and delamination induced damages and their propagations in an adhesively bonded laminated FRP composite Double Lap Joint (DLJ) have been presented in Chapter 8.

Design and development of load coupler profiles of Spar Wingskin Joints (SWJ) with improved performance for integral structural construction of aircraft wings have been described in Chapter 9. This Chapter also includes the study of delamination damage initiation and their propagations for the SWJ with modified elliptical load coupler profile.

Conclusions and Scope for further work are given in Chapter 10. References are put at the end of the Thesis accompanied with a list of publications by the author during the course of this Dissertation.

Contents

NOMENCLATURE

a	Damage length
$\{a^e\}$	Nodal displacement vector
b	Element width
$[B]$	Strain-displacement matrix
c	Overlap length
c_1, c_2	Adhesion failure lengths
C_{ijkl}	Stiffness or elastic moduli matrix for a general anisotropic material
e_a	Adhesion failure index
e_c	Cohesive failure index
e_d	Delamination damage index
E_1, E_2, E_3	Young's moduli referred to principal material directions
E_f, E_m	Elastic moduli of fiber and matrix, respectively
E_x, E_y, E_z	Young's moduli referred to geometric axes (x, y, z)
F_x, F_y, F_z	Nodal forces at the crack tip
G_T	Total Strain Energy Release Rate (SERR)
G_c	Critical SERR
G_{12}, G_{23}, G_{31}	Shear moduli in principal material directions
G_I, G_{II}, G_{III}	Mode I, Mode II and Mode III SERR
$G_{IC}, G_{IIC}, G_{IIIC}$	Critical SERR for mode : I, II and III
G_{xy}, G_{yz}, G_{zx}	Shear moduli referred to orthogonal axes
h	Ply thickness
$[J]$	Jacobian matrix
K	Stress intensity factor
$K_{IC}, K_{IIC}, K_{IIIC}$	Critical fracture toughness parameters for mode: *I*, *II* and *III*
$[K]$	Assembled global elastic stiffness matrix
$[K^e]$	Element elastic stiffness matrix
L	Adherend lengths of adhesively bonded joint
M_{max}	Maximum bending moment in a simply supported beam identical in all respect to that of the wingskin member of the SWJ
$[N]$	Element shape function matrix

$[q^e]$	Element nodal force vector
Q	Expression for Quadratic Stress Criterion
$[Q]$	Elasticity matrix for special orthotropic lamina
$[\bar{Q}]$	Elasticity matrix for generally orthotropic lamina
$\{r\}$	Nodal displacement vector
$\{R\}$	Nodal force vector for assemblage
S_{ijkl}	Compliance matrix of anisotropic material
S_{xy}, S_{yz}, S_{zx}	Shear strengths in orthogonal coordinate system
t_a	Thickness of adhesive layer
t_1, t_{20}	Thickness of bottom and top adherends of a Single Lap Joint (SLJ), respectively
$[T]$	Transformation matrix
u, v, w	Displacement components along x, y, z directions
$\{\bar{u}\}$	Displacement vector at any point within the element
U	Total elastic energy called strain energy
W	Work required to close the incremental damage Also, width of the joint adhesively bonded joint specimen
X, Y, Z	Material strength in orthogonal coordinate system
Y_C, Y_T	Young's modulus in tension and compression, respectively
Δ	Uniform extension applied through the end of the joint
Δa	Virtual crack extension
ΔA	Incremental delaminated area
$\Delta u, \Delta v, \Delta w$	Damage opening displacements along x, y, z directions
ε	Applied strain
ε_{ij}	Strain tensor
θ	Fiber orientation angle from x-axis in anticlockwise direction
$\nu_{12}, \nu_{23}, \nu_{31}$	Poisson's ratio referred to principal material direction
$\nu_{xy}, \nu_{yz}, \nu_{zx}$	Poisson's ratio referred to orthogonal axes
$\sigma_x, \sigma_y, \sigma_z$	Normal stresses in orthogonal coordinate
$\tau_{xy}, \tau_{yz}, \tau_{zx}$	Shear stresses in orthogonal coordinate

ABBREVIATIONS

ASTM	American Society for Testing and Materials
BS	British Standards
DLJ	Double Lap Joint
EU	European Standard
ESDU	Engineering Science Data Unit
FEA	Finite Element Analysis
FEM	Finite Element Method
FRP	Fiber Reinforced Polymeric/ Fiber Reinforced Plastic
GFRP	Graphite Fiber Reinforced Plastic
Gr/E	Graphite/Epoxy
ISO	International Standards Organization
LEFM	Linear Elastic Fracture Mechanics
LSJ	Lap Shear Joint
MCCI	Modified Crack Closure Integral
MPC	Multi- Point Constraint
SERR	Strain Energy Release Rate
SIF	Stress Intensity factor
SLJ	Single Lap Joint
SWJ	Spar Wingskin Joint
VCCT	Virtual Crack Closure Technique
VCEM	Virtual Crack Extension Method

1

Introduction

1.1 Introduction

Most structures consist of assemblage of individual components connected in the form of joints to form an integral load transmission path. These connections are generally referred to as joints and can be achieved in different ways such as by bolting, riveting, brazing, soldering, welding of metallic (isotropic) components, or by adhesive bonding of both isotropic and orthotropic materials. One of the major advantages of adhesive bonding is that it enables dissimilar materials to be joined, even when one of the components is non-metallic, and also it allows for a uniform diffusion of the load into the structure, thus reducing the localized stresses encountered compared to other joining methods, particularly mechanical fastening. A major application of adhesive bonding is therefore found in joining of Fiber Reinforced Polymeric (FRP) composite materials which are widely used in composite structures. No matter what forms of connections are used in any structure, the joints are potentially be considered as the weakest points. By the use of FRP composite materials, these weakest points increase, which may lead to the loss of structural integrity of the structure. Thus, adhesively bonded structural joints of FRP composite materials must be designed appropriately to meet the specific design requirements.

1.2 FRP composites: Constituents and characteristics

Composite materials are composed of two or more materials on a macro-scale resulting in a macroscopically homogeneous medium. Fiber reinforced composite materials consist of fibers of high strength and modulus embedded in or bonded to a matrix with distinct interface between them. In this form, both fibers and matrix retain their physical and chemical identities. Thus, FRP composites exhibit the best qualities compared to its constituents and often possess the better qualities that neither of their constituents possesses. In general, fibers are the principal load carrying members, while the matrix keeps them at the desired location and orientation, acts as a load transfer medium between them, and protects from environmental damages. Eventhough the fibers provide reinforcement to the matrix,

the latter also serves as a member of metal functions [1-4] in FRP composite materials.

The FRP composite materials are used in large scale due to the improved properties such as specific strength, specific weight, stiffness, corrosion resistance, wear resistance, fatigue life, temperature dependant behaviour, thermal insulation, thermal conductivity, acoustical insulation, etc. Naturally, not all of these properties are improved at the same time nor is there usually any requirement to do so. Due to the above desired characteristics, FRP composite materials find wide scale applications in the industries like aircraft, automotive, marine, sporting goods, biomedical sciences, electronics and defence, etc. Unlike traditional monolithic materials, FRP composites can have their strengths oriented to meet specific design requirements of applications. Real composite structures consist of multi layered laminae having different ply orientations of continuous fiber as shown in Fig. 1.1. A wide variety of fibers and matrix materials are now available for use. The principal fibers in commercial use are various types of Glass, Carbon, Graphite, Aramid as well as Kevlar. Other fibers, such as Boron, Silicon Carbide and Aluminium Oxide are used in limited applications. All these fibers are incorporated into the appropriate matrix phase in continuous or discontinuous (chopped) lengths. The matrix material may be a polymer, a metal or a ceramic. Specific fillers, additives and core materials are also sometimes added to enhance and modify the final product.

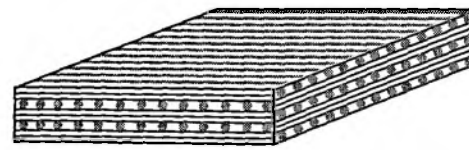

Figure 1.1 An example of a continuous fiber laminated FRP composite.

The fibrous composite material is one of the most important ones from the application point of view. The filamentary type of composite material is that material system consisting of selected fiber-macro constituents. Such material systems have desirable properties which are discussed above. The classification of such type of fibrous composite system is shown in Fig. 1.2.

Schematics of various types of composite laminates used for structural applications are shown in Fig. 1.3. The basic constituents of composite material system are the reinforcements, the matrix (usually epoxy or polyester) and the

coupling agents (coatings/fillers). Depending on the reinforcement type they are classified as:

- Fibrous : Composed of continuous or chopped fibers,
- Particulate : Composed of particles,
- Laminated : Composed of layers or laminae with desired fiber orientation,
- Flake : Composed of flat flakes reinforcements.

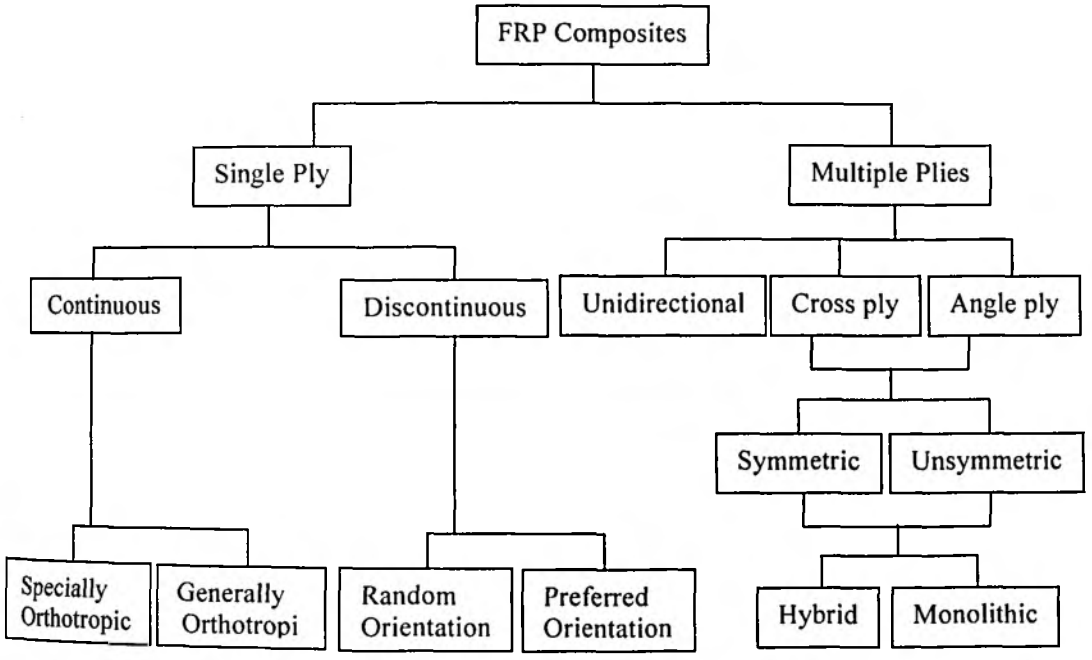

Figure 1.2 Classification of FRP composites.

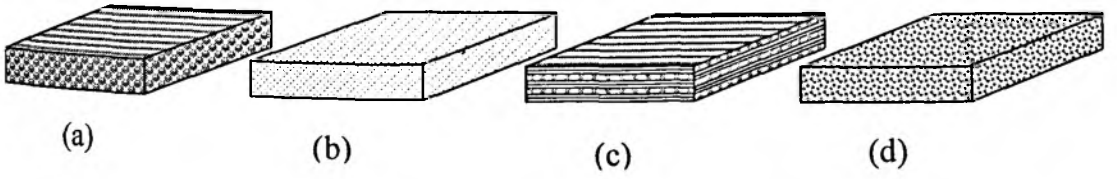

Figure 1.3 Various types of polymeric composites; (a) fibrous, (b) particulate, (c) laminated and (d) flake.

The selection of a specific composite material system must be carefully chosen in order to enhance the structural integrity and the structural efficiency of any composite structure. The composite must be resistant to debonding or delamination damages at the fiber/matrix interface and it must be resistant to fiber breakage and

matrix cracking. However, in applications where it is desired to dissipate energy during the failure process (such as crashworthy or impact resistant structures), progressive fiber failure and fiber matrix debonding are positive features because they dissipate energy. Thus, a major challenge for the mechanism and material community is to understand the factors influencing damage development and its propagation in the structural applications. The different types of damages, propagation of damages and the mechanics of initiation of damages are discussed vividly in the subsequent sections.

Damages in adhesively bonded laminated FRP composites may manifest itself in the forms of cohesive failure, adhesion failure, interlaminar/intralaminar delamination, debonding of fiber matrix interface, and fiber breakage. While all or some of the above damage modes may simultaneously be present in any structural bonded joint applications, damages due to the cohesive failure, the adhesion failure and the delamination are of prime concern, because they may reduce significantly the strength and stiffness of the structure. So this has been a subject of major concern in engineering applications of the adhesively bonded joints because of the problems of structural integrity and stability, reduction in load carrying capacity, stiffness reduction, and exposure of the interior to adverse environment, and final catastrophic failure of the structure. Delamination mode of failure in the laminated FRP composite adherends is especially of insidious nature. In this Thesis, these damage mechanisms in bonded joints of laminated FRP composites have been studied in details using the Finite Element Analysis (FEA). FRP composites exhibit relatively poor resistance to delamination damages. These damages may arise from micro cracks and cavities or voids formed during manufacturing stages, service or maintenance induced damages, or from low velocity impact damage [5-7]. Their susceptibility to out-of-plane loading, such as transverse loading is due to the fact that matrix constituents mainly control properties in a transverse direction. Liu [8] has performed a three-dimensional Finite Element Analysis (FEA) for studying the delamination damage propagation characteristics due to the impact of indentor. Strain Energy Release Rate (SERR) calculations along the straight or curved delamination fronts have been evaluated by many researchers [9-14] for a wide range of problems on FRP composites to assess the delamination or debonding growth.

On the whole, most of the analyses performed to date have been restricted to simple models for studying the delamination damages. However, the general problem of modelling the delamination of any shape when existing in laminated FRP

composites of adhesively bonded joints in composite structures can be tackled effectively by using a rigorous three-dimensional analysis. The reason, why a full three-dimensional FEA is used, in spite of its large computational cost in terms of space and memory requirements, is to keep the study as general and versatile as possible. This would require very few embedded assumptions in comparison to 2D FEA and closed form analytical formulations, thereby the modelling and simulations would be very close to the real life situation.

1.3 Joining of FRP composite laminates

Adhesive bonding represents one of the most important enabling technologies for developing innovative design concepts and structural configurations as well as exploiting the new materials. The evolution of the adhesive bonding method and its current knowledge were made possible by the explosive growth in the adhesive applications in a great variety of industries over the past few decades. While it is easy for everyone to identify examples of adhesive bonding in the world around us, analysis and design of structural bonded joints represent one of the challenging jobs in terms of analysis, design and structural integrity assessment. Compared to other mechanically fastened joints, adhesively bonded joints can offer substantially improved performance and economic advantages which are listed below:

- Joining of dissimilar materials
- Continuous bond
- Stronger and stiffer joints
- More uniform stress distribution (shown in Fig. 1.4) in the joint cross section
- Low local stress concentrations
- Bonding of porous adherends possible

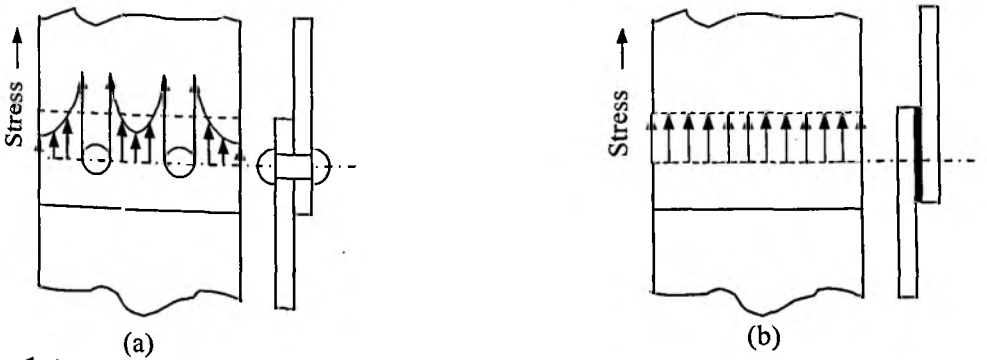

Figure 1.4 Comparison of stress distribution in (a) mechanically fastened joint and (b) adhesively bonded joint.

- No finishing costs
- Improved fatigue resistance
- Vibration damping and no noise
- Reduced weight and part count
- Large areas (both planar as well as non-planar) can be bonded
- Small areas can be accommodated for bonding
- Fast and slow curing systems available
- Easy to combine with other fastening methods such as pin/rivet/bolted joints
- Easily automated/mechanized.

Analysis and design of adhesively bonded joints is a multi disciplinary task, and it can involve concepts from the surface and polymer chemistry, stress analysis, manufacturing technology and fracture mechanics. The following important aspects need to be considered for designing the adhesively bonded joints when used in structural applications.

- Selection of suitable adhesive and its characteristics.
- Appropriate surface preparation of adherends.
- Development of design based on stress and failure analyses.

This thesis is intended to focus on various aspects of analysis and design of adhesively bonded joints of laminated FRP composites including stress analysis, strength prediction and failure analysis.

1.4 Adhesively bonded joint classifications

There are a large variety of bonded joint configurations used in current structural applications. Figures 1.5-1.6 show some typical classifications of adhesively bonded joints used in practice. One of the most important applications of adhesively bonded joints is found in the aircraft structure known as Spar Wingskin Joint (SWJ) of various adhesive core profiles and, are illustrated in Fig. 1.6.

Any appropriate design of a structural bonded joint must be based on a reliable stress analysis and strength evaluation. It is a challenging task to adequately determine the stress distribution as it is complex even for the simplest lap joint configurations as shown in Fig. 1.5. This is because the tensile loads in an SLJ are not co-linear, and thus the joint is subjected to a bending moment. The effects of bending moment is quite large initially and decreases progressively as described by Volkersen [15], Goland and Reissner [16]. Hart-Smith [17, 18] Oplinger [19], etc. The stresses in the adhesive layer are developed not only in shearing but also by peeling (called

the normal or tearing stress in through-the-thickness direction). These stresses are developed when the lap joints are subjected to different boundary conditions as shown in Fig. 1.7. For the type 1 boundary condition, the failure of the joint is by shearing of adhesive layer and is known as the cohesive failure. Due to the Type 2 and the Type 3 boundary conditions, failures are expected to occur either at the interfacial surfaces, known as the adhesion failures, or in the laminated FRP composite adherends known as the delamination failure. The details of these failures pertaining to the adhesively bonded joints are discussed in a later section. Since the adhesive is normally strong in shearing compared to peeling, the peel stress components should always be avoided, or minimized if unavoidable. There are various methods discussed in the literatures [20, 21] to reduce these peel stresses.

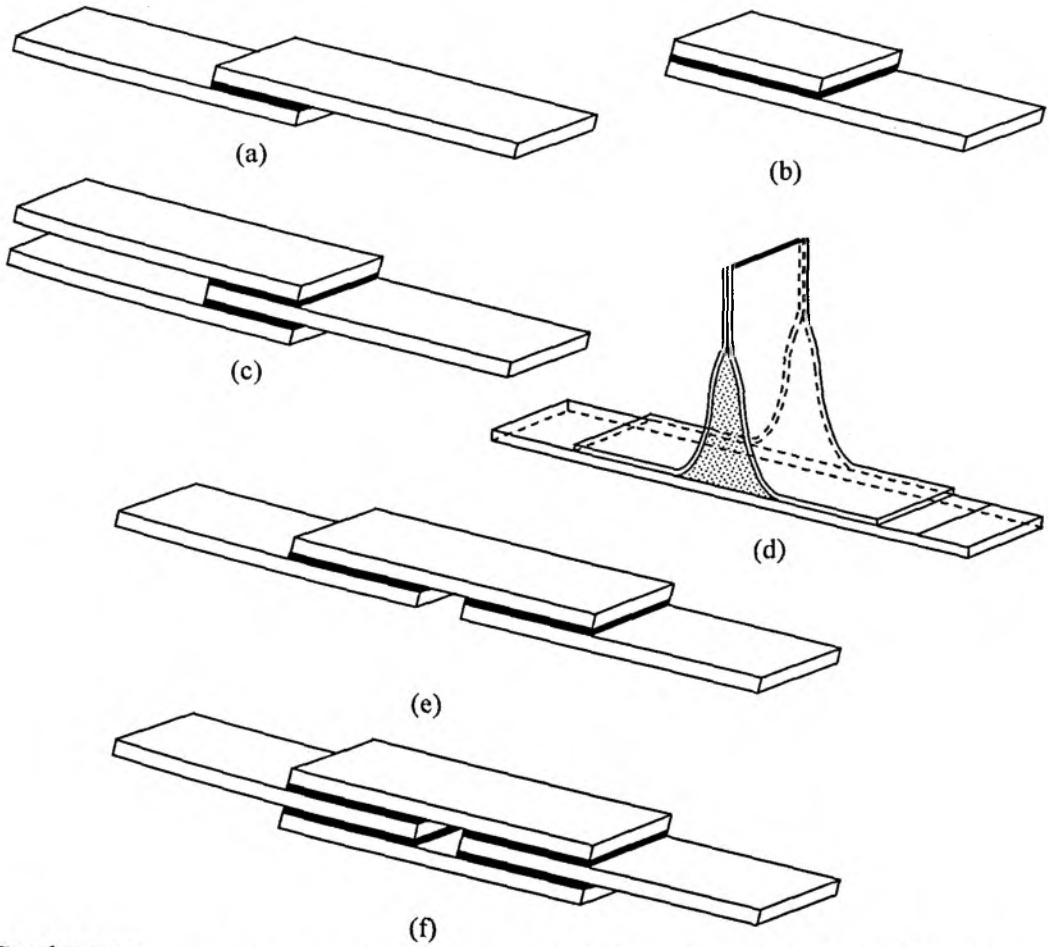

Figure 1.5 Different types of adhesively bonded joints; (a) Single Lap Joint (SLJ), (b) Lap Shear Joint (LSJ), (c) Double Lap Joint (DLJ), (d) Spar Wingskin Joint (SWJ), (e) Double SLJ (DSLJ) and (f) Double DLJ (DDLJ).

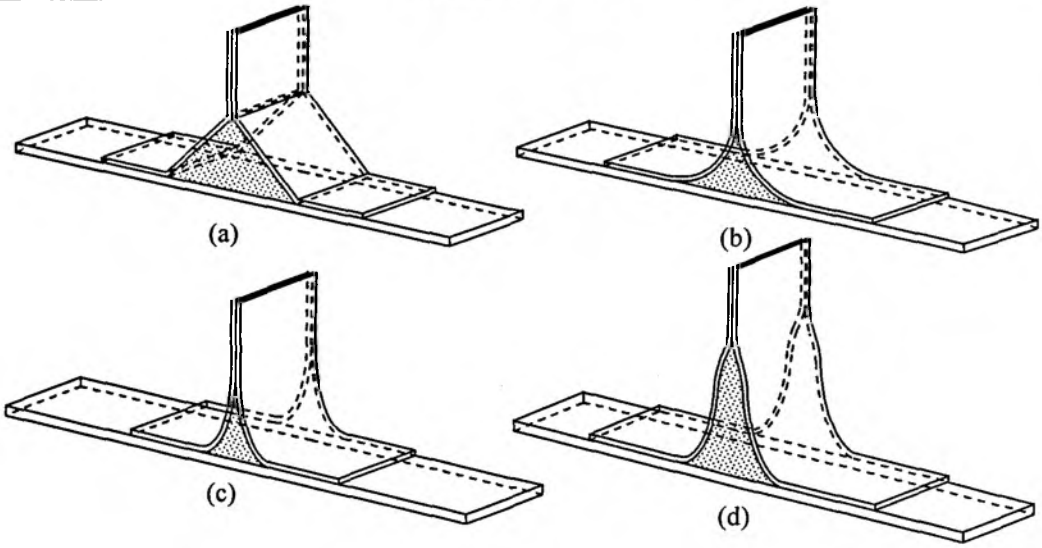

Figure 1.6 Development of FRP composite SWJ with various adhesive core profiles; (a) Triangular, (b) Circular, (c) Elliptical and (d) Modified elliptical.

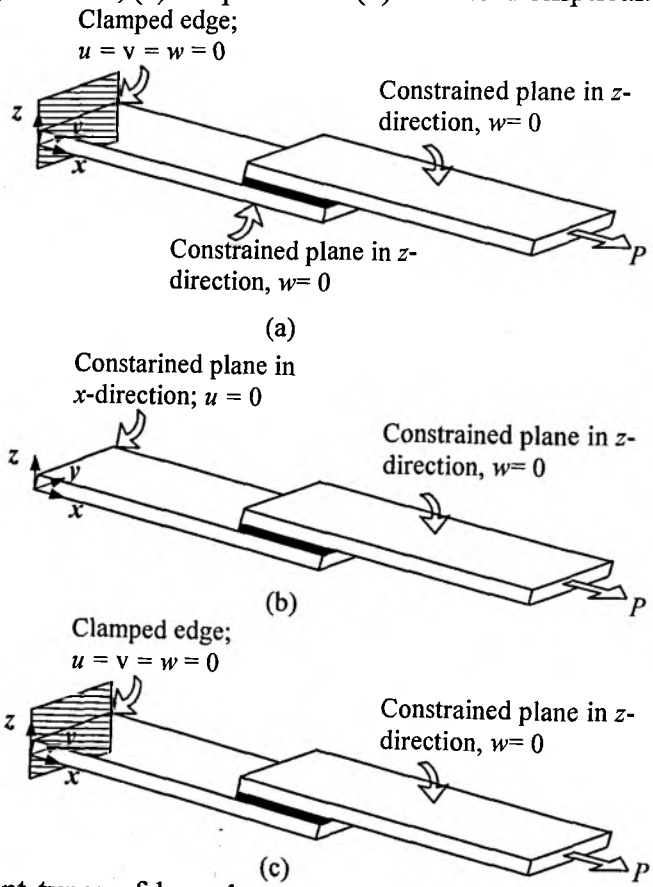

Figure 1.7 Different types of boundary conditions; (a) Type I, (b) Type II and (c) Type III.

1.5 Characterization of bonded joint constituents

Any rational design of structural bonded joints must be based on adequate knowledge of the stresses and strength in the joint. To determine the stresses and further to predict the performance (strength, stiffness and service life, etc.) of the bonded joint, it is inevitable to know the material characterization of the constituents. In general, the bonded joint is composed of two distinct constituents: (i) the adhesive and (ii) the adherend. It is necessary to discuss the material characterization of bonded joint constituents.

1.5.1 Adhesive

According to the need, adhesive materials are considered to be isotropic one. For linear stress analyses, Young's modulus and Poisson's ratio are the two input data, whereas for non-linear analyses, stress-strain curves may be considered and material yielding and hardening rules may also be needed. Fracture toughness and fatigue properties are required to characterize the failure strength and service life of the adhesive, respectively.

A great variety of test methods have been developed by researchers to characterize the adhesive material when sandwiched between the laminated FRP composite adherends. Accurate test methods are published in ASTM (American Society for Testing and Materials) standards, BS (British Standard), ISO (International Standards Organization) standards and the EU (European) standard. These tests evaluate not only the material properties of adhesive such as strength, modulus and fracture toughness but also the bonding techniques, effectiveness of surface preparations and curing cycle, etc. All tests are generally classified into four different groups i.e. shearing, tension, peeling and fracture toughness. The details of these tests are described in literatures [20, 22]

Adhesive materials can be classified into two categories; (i) brittle adhesive and (ii) ductile adhesive. For a brittle adhesive, a proportional linear relationship exists between the stress and the strain, while for a ductile adhesive, a non-linear stress strain relationship is generally observed as shown in Fig. 1.8. For brittle adhesives Young's modulus and Poisson's ratio are the two properties required for linear analyses of bonded joint. Figure 1.8 depicts the non-linear characteristics of the ductile adhesive and the entire non-linear adhesive behaviour must be adequately determined in order to predict the stresses and strains accurately, and to further study the damages in a bonded joint.

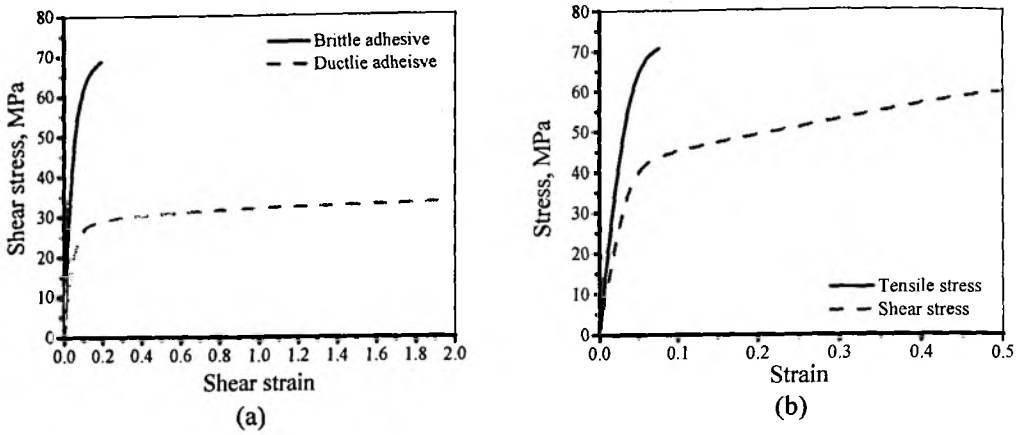

Figure 1.8 Characteristics of adhesives; (a) Comparison of shear stress-strain for brittle and ductile adhesives and (b) True shear and tensile stress-strain curves of adhesive [21].

1.5.2 Adherend

One of the major advantages of the adhesive bonding is that it enables orthotropic materials to be joined, eventhough it can be used for metallic adherends or combination of both. In many applications, laminated FRP composites are used as adherends for joining. The techniques of analyses are essentially same as when isotropic adherends are used, although due attention must be paid to the low longitudinal shear stiffness of unidirectional composites. With unidirectional composites the shear modulus is of the order of 25-30% of Young's modulus. It may be as low as 2%, and so the adherend shears becomes extremely important. The use of lamination techniques in which fibers are placed at different orientation to the plate axis leads to reduced longitudinal and increased shear moduli. However, transverse modulus remains low. In addition, the transverse strength of FRP composite adherend is low, usually being the same order or less than that of the matrix. Thus, if the joint experiences transverse (peel) loading, there is a strong likelihood that the composite will fail in transverse tension before the adhesive fails. Adhesive peel stresses should therefore be minimized when composite adherends are used, lest this leads to adherend failure.

Compared to isotropic materials, the analysis of joints between FRP composites is complicated by the anisotropy and heterogeneity of the adherends. A

rigorous analysis may also be carried out to include the effects of residual thermal strains arising from curing and thermal mismatch when bonding to metals. When laminated FRP composite adherends are used, there are such additional variables of lay-up i.e. combination of ply orientation, and stacking sequence as the order in which the plies are placed through-the-thickness, it being possible to change the latter without altering the former. Both these parameters affect the performance of the bonded joints, the stacking sequence playing the important role with thin adherends particularly because of its remarkable effect on bending stiffness which, in turn, determines the deformation of the joint and subsequent failure.

Matthews et al.[23] concluded that it is necessary to consider the non-linear analysis to predict the joint strengths in their review paper. Various types of failures encountered in FRP composite bonded joints are as follows:

- Tensile failure in the fiber direction.
- Tensile failure perpendicular to the fiber direction.
- Interlaminar shear failure.
- Cohesive failure.
- Adhesion failure.

However, since the laminated FRP composites have comparatively low interlaminar strength, the three prominent modes of failure in FRP composite bonded joints are as shown in Fig. 1.9.

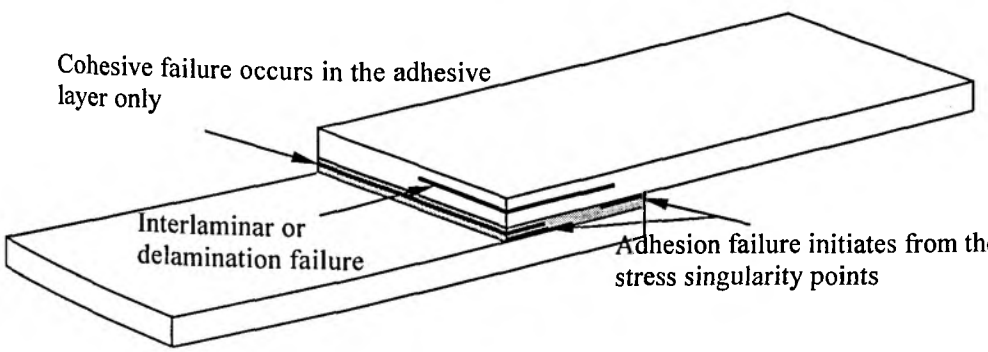

Figure 1.9 Prominent failure modes in an adhesively bonded single lap laminated FRP composite joint.

1.6 Adhesively bonded joints: Applications

There are enormous applications of adhesively bonded composite structures used in various industries. For example, bonding of composite pipe work is one of the largest

industrial composite assembly operations existing. The applications of adhesively bonded joint which are used in the joining of stiffeners where it is required to stiffen the large areas of FRP composite panel by attaching deep sections. Also this type of joining is used in large ship structures including the joining of stiffeners to sandwich the panels. Apart from these, its application is found in chemical industries, transport industries, aircraft structures, wood industries, etc.

1.7 Bonded joint design philosophy

The design of adhesively bonded joint must be based on; (i) the nature of the materials to be joined, (ii) the configuration of the joint i.e. geometry and configuration, (iii) the joining methods, and (iv) the strength and failure analysis. So for a structural bonded joint, a designer should consider the following aspects.

- Service conditions such as stresses and environmental conditions which are likely to be encountered in service.
- Selection of material combinations such as selection of suitable adhesive and FRP composite adherends.
- Selection of specific joint configuration according to the need.
- Manufacturing specifications such as surface pre-treatment and fabrication procedures.

Many theories for adhesively bonded joints have been developed for stress and strength analysis. Many authors have made various assumptions regarding the behaviour of adhesive and adherends in terms of differential equations and have investigated the effects of various factors on the stress and strength. These factors are the adhesive plasticity, large deformations and rotations, satisfaction of the boundary conditions at the overlap ends, spew fillet and geometry, bondline thickness, overlap length, etc. It has been shown that in addition to the large deformation, adhesive plasticity is another important factor and can not be ignored for appropriate prediction of joint strength. While implementing the non-linearity of the adhesive, the analytical solutions of the joint become cumbersome. Analytical and closed form solution analysis would be very difficult or may be impossible when material (both adhesive and adherend) non-linearity, delamination and debonding damages are considered. The mechanics of materials and fracture mechanics based approach are considered as the most suitable analysis tool for prediction of strength of adhesively bonded joints.

It has been observed that adhesively bonded joints often fail due to the damages initiated from the stress singularity locations and their propagation either in

the adhesive layer or along the interfacial surfaces or in a combination of both. Thus, fracture mechanics has been widely used to correlate damage propagation behaviour in adhesively bonded joints. For characterizing the strength, service life and designing rationally adhesively bonded joints, the main governing parameters are Strain Energy Release Rate (SERR). Figure 1.10 shows the three separate individual modes of damage propagation in the laminated FRP composite joints. These modes are: (i) opening mode called Mode *I*, (ii) shearing mode known as Mode *II*, and (iii) tearing mode designated as Mode *III*. A mixed mode of delamination damage in laminated FRP composite bonded joint is shown in Fig. 1.11. A crack line damage in the bondline of adhesively bonded joint is constrained and will propagate under mixed mode conditions in a direction such that the crack tips are in pure Mode *I* [24].

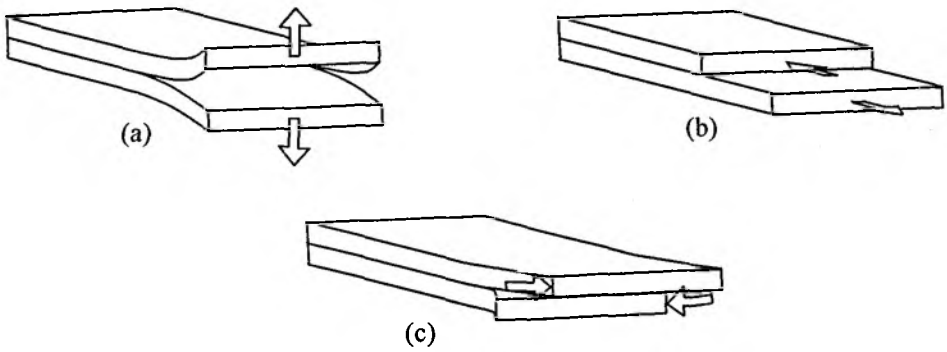

Figure 1.10 Three different individual modes; (a) Mode *I*, (b) Mode *II*, and (c) Mode *III* of delamination damage in laminated FRP composite joint.

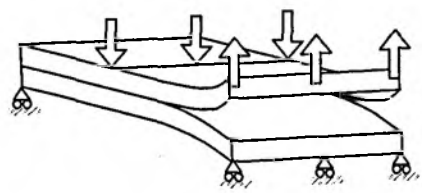

Figure 1.11 Mixed mode delamination damage in laminated FRP composite joint.

During the last few decades, numerous joint theories have been developed by a large number of authors using a lot of simplifying assumptions concerning the behaviour of the adherend and the adhesive. These assumptions may enable to remove the stress singularities which occur at the stress singularity locations. These stress singularities are due to many factors like dissimilar material properties at the interface, discontinuities of geometry, loading and material heterogeneity, etc. and are

the main concerns for the joint designers. The details of assumptions made for stress analysis of bonded joints have been discussed in the pioneering work by Carpenter [25] for obtaining a closed form solution. He concluded that the effect of a given assumption on predicted adhesive stress is difficult to determine from the differential equations.

1.7.1 Stress analyses

Stress analysis is one of the important steps for any structural design. It provides many vital information about the stresses and the strains in the real structures made of adhesively bonded joints subjected to specified loading and service conditions. This information will enable the designer to predict the strength and the life of a bonded joint. The stress analysis of bonded joint is a real challenge for two important aspects of joint design: (i) because bi-material interfaces and geometric discontinuities create stress concentrations and material behaviour uncertainties and (ii) the stress gives the idea of failure initiation in terms of failure index. Failure index refers to a parameter which characterizes the location of failure or damage initiation. Particularly the out-of-plane stresses are most important factors responsible for the propagation of initiated damages. In case of laminated FRP composite adherends, delamination induced damages are the major threat to the bonded joint applications. The details of methodology to predict the location of damage initiation in adhesively bonded joint of laminated FRP composites have been discussed in Chapter 3, using the stress analysis.

Stress analysis techniques can generally be classified into two major categories i.e. analytical solution which is based on a number of mathematically simplified assumptions and numerical solutions using the FEA. Because of the complexities, analytical solutions of the bonded joint exist for simple geometry, loading and boundary conditions. Therefore, more emphasis is put on the use of numerical methods when laminated FRP composites are used as adherend material and the joints involving complicated geometry, loading and boundary conditions. Among various numerical techniques available, it is seen that the FEA is not only simple and robust but also straight forward and versatile enough to cover all types of bonded joint problems relevant to practical situations. The FEA, as described by Zienkiewicz [26], is a well established numerical means for stress analysis of bonded joints. The FEA avoids the approximation of the closed form theories. Many authors like Adams [27] and his co-authors [28-32] along with many other researchers [33-35] have used finite element techniques exclusively for the bonded joint problems.

1.7.2 Adhesion failure and delamination damage studies: An overview

For practical application of adhesively bonded composite joints, many researchers have investigated the influence of various parameters on the failure behaviour in their studies on composite bonded joints [36-41] experimentally and numerically. In those studies, the typical bonding parameters are surface conditions (e.g., contamination, abrasion, and plasma treatment), fillet, bondline thickness, surface ply angle, stacking sequence, environmental conditions, etc. Many researchers have also predicted the onset of failures for the composite bonded joints[35, 38-40, 42]. But the failure prediction of the composite bonded joints is still difficult because the failure strength and failure mode differ according to the various bonding methods and parameters.

There have been usually two kinds of failure prediction methods discussed: one is a stress or strain based method and the other is based on fracture mechanics approach. The stress or strain based method utilizes failure criterion equations which include maximum stresses or strains in the bonded joint. This method is simple but may not be suitable because there are locations of stress or strain singularities in the bonded joints. In the fracture mechanics method, an initial crack is assumed and crack growth is assessed by comparing the computed strain energy release rate with fracture toughness determined by experiments. The fracture toughness differs according to the mode mix ratios as well as failure modes (for example, interfacial, cohesive, and delamination failure). So, the fracture toughness test is a time (and cost) consuming process. In addition, the fracture mechanics method is not suitable for the bonded joint which fails without an initial crack. These two methods have merits and demerits as mentioned above; and various failure modes may appear due to the mechanical properties of adhesives or bonding methods in the composite bonded joints.

In recent decades, researchers are investigating new material system developments and their applications to existing engineering systems and their failure analysis in an effort to improve these systems. Figures 1.12 (a) and (b) describe the crack tip and crack front configurations for studying the initiation and progression of straight-edged and curved interlaminar fracture. Delamination in a composite material is fundamentally an interlaminar fracture phenomenon involving debonding or separation of two highly anisotropic, fiber-reinforced laminae. In many types of composite structures (e.g. aircraft, marine) delamination is the most common form of defect/damage. Also sometimes manufacturing deficiencies cause inadequate bonding between the layers. This may lead to delamination over a long period in service.

There are several mechanisms which contribute to property degradation, and they have received considerable attention in recent times as they differ remarkably from the failure process observed in conventional metallic components. Fracture mechanics has been extensively used for the damage analysis and prediction for isotropic materials. As such, the application of Linear Elastic Fracture Mechanics (LEFM) has gained the attention of the researchers for investigating the delamination mode of failure pertaining to the adhesively bonded joints of laminated FRP composites.

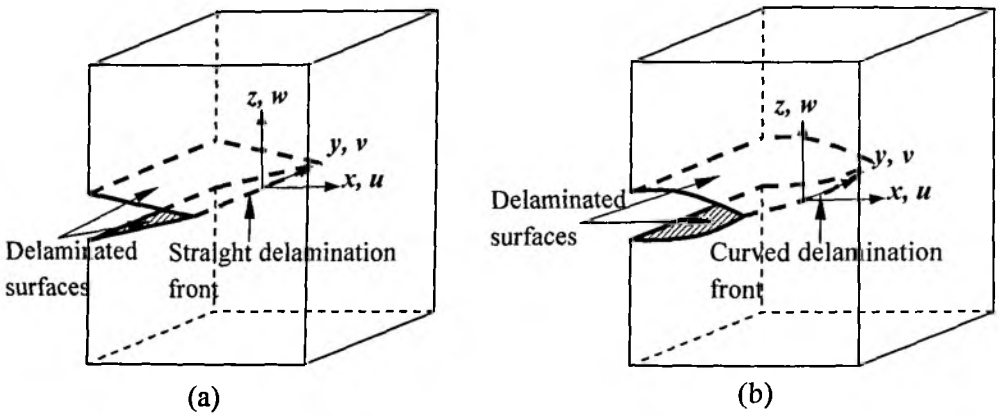

Figure 1.12 Schematic of delamination fronts; (a) straight and (b) curved.

1.7.3 Adhesion failure and delamination damage analyses

Since fibrous composite laminates are most commonly used as adherends, they are susceptible to internal defects such as delamination during manufacture or in service. The stress analysis of laminated composites with defects for predicting the mechanical behaviour of bonded structures is also important and has received considerable attention. However, due to the anisotropic properties of laminated FRP composite adherends, the stress distribution around the defects is complex and a global theory for precise prediction of delamination due to such defects in composite materials is not available. Finite Element Method, because of its ability to model real life structures has been extensively used for stress analysis of such laminates with defects. However, for complete understanding of behaviour of such FRP composite laminates and delamination initiation from such defects, a 3D finite element analysis is necessary. In fact, with the popularity of damage tolerance, fracture mechanics concepts have been in use for analysis of such structures. However, effective

analytical and numerical methods are necessary for analysis of adhesively bonded joints of laminated FRP composite adherends with defects.

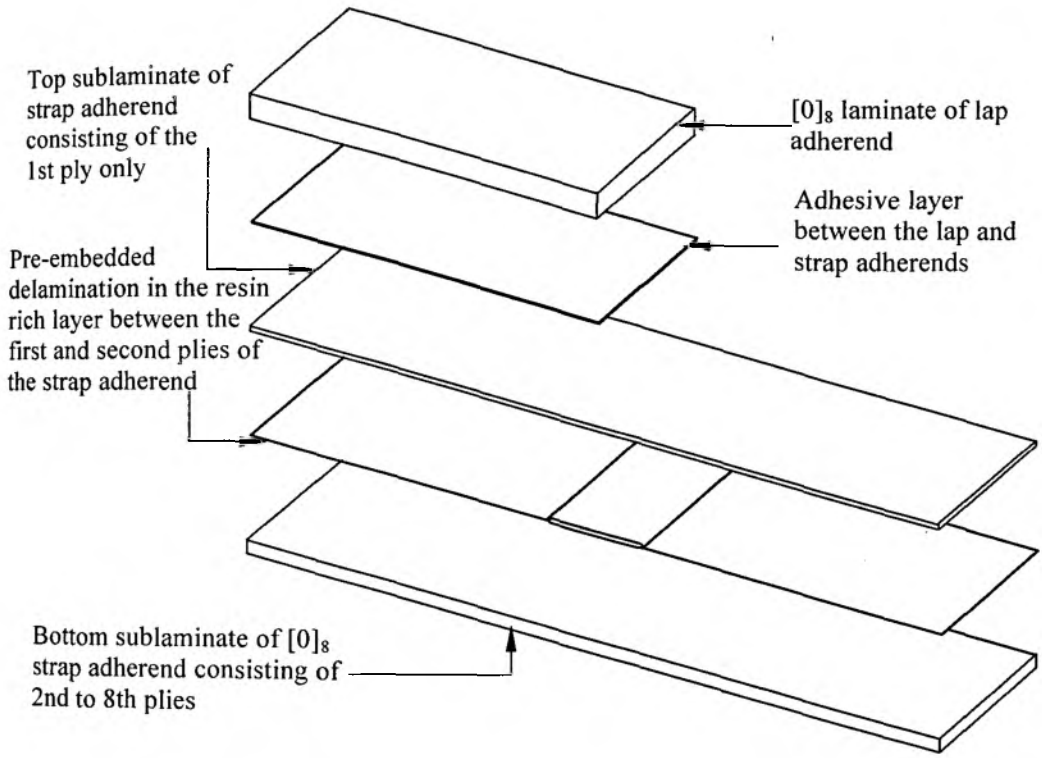

Figure 1.13 Sublaminate configuration with pre-embedded delamination existing in the resin layer of strap adherend of FRP composite LSJ specimen.

Figure 1.13 demonstrates the sublaminate techniques, which are generally used for evaluating the severity of damage growth mechanism in laminated FRP composite bonded joints. The interfacial resin rich layer is presumed to contain the delamination. The problem of delamination in laminated FRP composite adherends is very complex in nature and difficult to solve, because it not only involves geometric and material discontinuities, but also internally coupled mode *I*, mode *II* and mode *III* fractures in layered composites. The mixed mode interlaminar fracture characteristics are investigated by retrieving the stress and displacement field results from the numerical FE analyses using transformed coordinate system. Finite Element Method (FEM) is an approximate numerical method for solving field problems. In principle the analysis domain is divided into finite number of non-overlapping sub-domains of polygonal shapes called the finite elements. First an approximate solution is sought

for each element and the behaviour of the element is characterized by a finite number of unknown parameters. Then by a suitable assembly procedure the relations between the individual elements are combined into a system of equations, which are used to solve these unknown parameters. With the use of finer elements the discretization errors of the field variables can be reduced considerably and near exact solution can be obtained. The unknown parameters are usually the values of the field variables at a finite number of nodal points. Interpolation of these field variables within each element yields the approximate solution.

A stationary condition of a functional based on variational principle, characterizes the equilibrium for the element and subsequently establishes the system of equations for the unknown parameters. The most important feature of the FEM is that it can be realized by using flexible and parametric design concepts and can be applied to a wide range of practical problems.

1.7.4 Adhesion failure and delamination damage onset

According to the study [36], there are two major kinds of failure modes in case of a composite single lap bonded joints. One is failure of the adhesive layer which includes interfacial failure called adhesion failure and cohesion failure of the adhesive. This type of failure may be called bondline failure in an overall concept. The other is the delamination failure of the composite adherends. The characteristic behaviour of the first is progressive failure and the failure propagation occurs in the adhesive layer. The characteristic behaviour of the second is catastrophic failure which occurs abruptly due to the delamination failure without an initial crack.

The present failure prediction method utilizes two kinds of failure criteria which consider separately the bondline and the delamination failures. Therefore, the critical failure mode and failure load can be simultaneously determined by the present method. The details of the present method would be described in the Chapter 3.

1.8 Scope of adhesion failure and delamination damage analyses of bonded joints in laminated FRP composites

All the stiffness and strength advantages of FRP composite materials can not be transformed into the structural advantages. One of the main reasons is that while making parts for members made of composite materials turn out to be more bulky than those of the corresponding metal parts. Hence, well defined bonded joint must have to obtain the required joint efficiency as well as the joint strength in order to

assess the structural integrity fully. The mechanical strength of an adhesively bonded joint depends essentially on four parameters (i) the adhesion between the adhesive layer and the adherends, (ii) the cohesion properties of the adhesive layer, (iii) the delaminated adherends and (iv) the geometry and configuration of the joint. Understanding the fundamental nature of the damage parameters is of utmost importance in the reliability and safe design of the adhesively bonded joints. For practical applications of adhesively bonded composite joints, many researchers investigated the influences of various parameters on the failure behaviours of the composite bonded joints experimentally and numerically. But the failure prediction of the composite bonded joints is still difficult because the failure strength and modes are different according to the various bonding methods and parameters. According to the studies, there are broadly two kinds of failure modes in the composite bonded joints. One is the failure of the adhesive layer, which includes interfacial failure called adhesion failure, and the other cohesion failure of the adhesive. The other is the delamination induced failure which occurs in the laminated FRP composite adherends between the laminae. The characteristic behaviour of the first is progressive failure and the failure propagation occurs in the adhesive layer. The characteristic behaviour of the second is catastrophic failure which occurs abruptly. The present failure prediction method utilizes two kinds of failure criteria which consider separately the bondline failure and the delamination failures.

The joint performance due to the presence of damages has not yet been properly highlighted. The detail methodologies for the prediction of onset of damages in an adhesively bonded joint are not available in the literatures. Adhesively bonded joints having delamination mode of damages in laminated FRP composite adherends has become a subject of intensive research among the researchers. The defects which may lead to premature delamination in composites may arise from micro-cracks and cavities or voids formed during manufacturing stages, service or maintenance induced damages, or from low-velocity impact damage. The structural degradation and stability reduction of composite structures having bonded joints are more critical due to the presence of above mentioned damages.

To study the onset of damages and their growth behaviour, Strain Energy Release Rate (SERR) procedures based on the concepts of Linear Elastic Fracture Mechanics (LEFM) are found to be most suitable. Not only it is based on a sound energy balance principle related to work done in new surface generation, but also the mixed mode damage progression can be separated into individual fracture modes,

which can be suitably compared with experimental observations of critical strain energy release rates. Thus the physics of stable and unstable damage growth characteristics are being modelled as a function of fracture energy release rates both by numerical and analytical approaches for understanding the interface phenomenon.

Among the different types of adhesively bonded joint configurations, Single Lap Joint (SLJ), Lap Shear Joints (LSJ), Double Lap Joints (DLJ) and Spar Wingskin Joints (SWJ) are the most commonly and widely means of connection in the structural fabrication for their simplicity and ease of joining. But, the determination of joint strength for a given configuration and material property is yet to be fully understood. Several researchers have limited their bonded joint analyses pertaining to the study of stress and deformations using two-dimensional plane stress or plane assumptions. The three-dimensional stress analyses of adhesively bonded joint of laminated FRP composites are very rare even today.

It would be interesting to evaluate the optimum values of the various geometrical parameters of different concepts of the Spar Wingskin Joints (SWJ) with different adhesive load coupler profiles. Analysis and determination of design data for SWJ adopted in the integrated modular wing concept fabrication technique in modern aircraft technology is relatively much newer and useful step to add to the literature of this class of joints subjected to out-of-plane loads are desirable to be undertaken. These types of joints with complicated configurations and non-planar loadings are remaining so far intractable and insolvable by the classical continuum mechanics approach. Attempt should be made to study the effects of geometry of the adhesive core profiles on the onset of damages and on their growth. Suitable remedy has to be recommended to arrest the further growth of such damages in such joints.

2

Review of Literature

2.1 Introduction

There is significant written and archaeological evidence to suggest that humans have been using adhesive products for thousands of years in their drive to make objects more decorous, stronger, useful or cheaper. The introduction of adhesives is likely to have been a gradual process, beginning with the application of naturally 'sticky' products before moving on to the preparation of simple adhesives, possibly by-products from cooking [43]. Probably the most important landmark in the history of structural adhesives is the emergence of epoxy resins in the late 1930s. These epoxy adhesive achieved great success in aerospace, automotive, construction, electronic, medical, ship and woodworking applications, largely because of their effectiveness, versatility and mechanical properties. Typically they possessed high shear strength but relatively low toughness and peel strength.

Adhesive bonding is an effective method of joining many materials. As such, adhesives are used widely in many adhesively bonded joint applications to make them functional and capable enough to transmit the load. These joints are known as structural adhesively bonded joint. Clearly, it is important to design structural joints in order to enable them to transmit their loads safely. There are a number of general features of design of adhesive bonding which do not explicitly involve mechanical fastening or other methods of joining. Adhesively bonded joints require a thin layer of adhesive to connect two or more parts together in a structure and are used to transfer of load. One of the most challenging aspects of adhesively bonded joints with laminated Fiber Reinforced Polymeric (FRP) composite adherends is that the well established design procedures, based on years of experience with isotropic and homogeneous materials like metals or their alloys, have to be altered in order to accommodate the anisotropic and non-homogenous properties of FRP composite materials.

The purpose of a review of literature is to assess the state-of-art, analytical, experimental and numerical methodologies for the damage analysis of various types of adhesively bonded structural joints of laminated FRP composites and to achieve a

basic understanding of the subject in order to carry out an investigation of analysis of stress and displacement field for various geometry, loading and constraints. The concerned literature in this area is focused on the development of FRP composites, various types of damages in FRP composite adherends, and state-of-art of damage developments in the joints and their analyses, prediction of strength using different failure theories; and propagation of damages. This Chapter emphasizes the review of literature on stress analyses, prediction of location for onset of the damages in the adherends and in the joint overlap region and damage propagation studies of four important and widely used adhesively bonded joints of laminated FRP composites, viz.

- Single Lap Joint (SLJ)
- Lap Shear Joint (LSJ)
- Double Lap Joint (DLJ)
- Spar Wingskin Joint (SWJ).

2.2 Damage classification of bonded joints

Damage/defect in a bonded structure is defined as any unintentional local variation in the physical state or mechanical properties, which may affect the structural behaviour of the component. This is often termed as a discontinuity or flaw in an intact structure. Damage calumniates the proper functioning of the structure, eventually causing its failure. Failure of a component or structure is defined as a state "When a component or structure is unable to perform its primary functions adequately." Delamination refers to a situation in which failure (or inadequate adhesion) occurs on a plane between adjacent layers within a laminate. This type of failure is dominated by the properties of the matrix and since matrix strength and toughness tend to be relatively low, laminated composites are prone to develop delamination. Heslehurst [44] studied the failure modes and defects types generally found in composite aircraft structures. FRP composites have high strength and stiffness in the direction of fibers, but their strength and stiffness in the direction perpendicular to the fibers are mainly attributed by the matrix properties. When the laminated FRP composites have been used as adherends in structural adhesively bonded joints, the greatest difficulty for the bonded structure is that it performs poorly under out-of-plane loading. The matrix which usually carries the out-of-plane load has very low modulus compared to the longitudinal modulus of fibers. When the FRP composites are used as adherends, the structural integrity of bonded joints is reduced due to the loading eccentricity which

the lap joints generally experience. The existing failure modes of adhesively bonded joints are classified into the following four general groups:

- Adherend failure due to bending, tension or compression,
- Adhesion failure due to interfacial peel and shear stresses,
- Cohesive failure mainly due to shear stress, and
- Out-of-plane adherend failure due to delamination in laminated FRP composite adherend.

Adams and Wake [20] described some possible cohesive and adhesion failure modes in an SLJ and showed the possible locus of onset and propagation of these failures. It has been seen that cohesive failures occur only in the adhesive layer and adhesion failure propagates along the bondline interfaces of the joint. Chai [45] reported a wavy crack path in an adhesive layer between aluminium adherends. The crack jumps periodically from one interface to the other across the adhesive layer. Due to laminated nature of FRP composite adherends and their relative weakness in the out-of-plane direction, the failure mechanism of adhesively bonded joints becomes more complex than that of a joint of isotropic materials as in case of metals or their alloys. Hoskin and Baker [46], Kairouz and Matthews [37] and Tong et al. [47] analyzed the net section fracture and delamination for an adhesively bonded SLJ. The delamination failure with two possibilities such as the surface ply fracture and further growth of delamination may be considered in the damage analyses of bonded joints.

2.3 Damage development analyses of bonded joints in laminated FRP composites: A review

2.3.1 Delamination damage in laminated FRP composite adherends

Talreja [48, 49] analyzed the intralaminar damage (matrix cracking) and the interlaminar damage (interior delamination) in composite laminates. Effect of transverse cracking on stiffness reduction was studied. He observed that the intralaminar damage reduces all elastic moduli for a general orientation of the damage entities (cracks) and changes the initial orthotropic symmetry of a laminate, whereas the interlaminar damage reduces the moduli though it does not change the symmetry. Stout et al. [50] have studied the damage development in laminated composites made of unidirectional layers under quasi-static loading using four-point bend test. Though they found many matrix cracks within individual plies and only a few delamination

cracks between the plies, the delamination cracks had a greater length than that of the matrix cracks. Also the specimen failure occurred as a result of delamination crack propagation. Hart-Smith [51] analyzed mechanical fastened joints for FRP composite laminated structures. Strengths of various composite joints were discussed in detail with reference to section properties and laminae sequence.

Fracture behaviour of embedded delaminations was investigated by Pradhan and Chakraborty [11] by employing strain energy release rate as a characterizing parameter. They studied the influence of ply orientation, stacking sequence, material anisotropic properties and interface resin layer properties on delamination progression behaviour. Higher-order theories based on the discrete layer approach were used by Reddy [52] to account for slope discontinuity at the interfaces in multiply composites. This theory has been used by Nosier et al. [53] for studying the impact characteristics of laminated plates for comparing its results with that of the equivalent single layer theories.

Higher order theories using the C^o finite element concepts and modified Hertzian contact law were employed to analyze the impact response of laminated plates. Swanson and co-workers [54, 55] conducted both the experiments and numerical works to investigate the impact response of composite plates. In their analytical works they estimated the contact features of impact event of the non-linear contact force and displacement relationship with a linearised relationship and a constant contact area. The predicted strain response agreed well with the measured response.

The shortcomings of neglecting the shear deformation of the adherends on bonded lap joints were discussed by Carpenter [25]. This study found a difference of nearly 30% in the estimation of maximum peel stresses. Stress analysis of different types of adhesively bonded joints was conducted by using ANSYS general purpose finite element program. He identified the peek values of stress locations near the edges, from which delamination initiation may take place. Although the delamination studies were not performed, the vast results presented by him cater to the understanding of delamination onset and propagation from the localized stressed zones along the edges. Tong et al. [56, 57] performed both experimental and numerical finite element analyses of the initiation and growth of individual cracks in quasi-isotropic laminates under quasi-static and mechanical fatigue loading.

A detailed review of the developments in damage mechanics studies using various analytical and continuum mechanics approaches were reported by Nairn and

others [58, 59]. Damage modes in polymeric composites such as transverse matrix cracks, micro cracks, ply cracks and delaminations were treated extensively. Variational methods, finite element methods and energy release rate procedures were followed for studying the crack field characteristics and associated laminate response. Lee et al. [60] investigated the mechanical behaviour characteristics of hybrid composites with non-woven carbon tissues. They found that the hybrid specimen is effective for improving the tensile characteristics.

Qing et al. [61] performed both experiment and three-dimensional FEM simulation for studying the effects of reinforcing strips on the notch strength and failure response of laminated composites. Results showed that the notch strength and damage progression of composite laminates could be affected significantly by adding reinforcing strips in front of notches such as crack tips and cut-outs. The change in notch strength strongly depends upon the geometry, properties, and bond strength of the reinforcing strips. The strips could significantly alter the failure progression and failure modes in composite plates. They observed that reinforcing strips with more than six plies delaminated from laminates, leading to premature failure of the reinforced laminates. Such delamination failure was not considered in the model. It is therefore necessary in the future to include delamination analysis in the model for accurate prediction of the failure load of strip reinforced composite structures. Zheng et al. [62] qualitatively evaluated the effect of partial debonding on the reduction of overall elastic moduli and overall elasto-plastic strength of a fiber reinforced composite. Both the homogenization and the finite element calculations disclosed significant effect of the debonding angle on the overall transverse Young's Modulus along the debonding direction, and on the plane strain tensile Bulk Modulus of the composite. In the plastic range the transverse tensile stress-strain curves of the debonded composites were found to be significantly lowered due to the presence of the interface cracks. They used eight nodded isoparametric quadratic elements except at the debonding tip, where triangular quarter-node elements have been employed. The elements surrounding the debonding tip were six-node triangular element with the radial length less than one hundredth of the half of the debonding length. The next layer of elements consisted of quadratic elements with a 20% increase in edge length from those of the inner quarter node elements. Fatigue testing of impact damaged carbon fiber/epoxy laminates [63] revealed that fatigue life was controlled by delamination growth in the direction transverse to the load.

2.3.2 Bondline damages in the bonded joint

Accurate prediction of bonded joint strength and service life is one of the most challenging tasks in structural bonded joints design. First of all, it is not an easy task to determine with certainty an accurate geometry as it can significantly change the stress concentrations. Secondly, it is difficult and expensive to characterize the adhesive properties, such as stress-strain curves and allowable material properties including fracture toughness, especially when environmental effects are present. Last, but not the least, there is a lack of complete understanding and accurate modelling methodologies of failure mechanisms in various bonded joints. Some possible cohesive and adhesion failure modes in an adhesively bonded joint usually assumed to be confined in the adhesive layer and the bondline interfacial surfaces, respectively would be addressed in detail in Chapter 3. The possible loci of adhesion failure initiation are found to be from the locations of stress singularity and such failures usually propagate along the bondline interfaces. The damage formation procedures in the ductile adhesive layer show the void nucleation, growth, and coalescence in the adhesive material. These types of failures are observed by Tong [64] experimentally. More factors have been considered in strength prediction of adhesively bonded joints due to the complexities in the materials properties, geometry, loading and constraints when adhesion failure and delamination damages are present. Due to the presence of delamination damage, the joint may fail because of the surface ply fracture or due to the further growth of embedded delaminations.

The joint failure mechanism includes onset of initial failures such as yielding, fracturing and cracking, followed by stable damage growth, and ultimately fast or catastrophic damage propagation leading to the joint failure. This failure mechanism becomes more complex and involved when the joining members are laminated FRP composites. In such situations, additional affecting factors such as material properties, ply lay up sequence and fiber orientation are involved in joining the components. Usually two approaches are adopted to deal with the damage analyses of adhesively bonded joints. One is the mechanics of materials approach and the other is based on Fracture Mechanics principles [27, 62, 65-67].

2.4 Analytical, experimental and numerical analyses of bonded joints

During past few decades adhesively bonded joints have been of increased importance because of the facts that the stress concentrations in the joint region are relatively low and the weight of the structure does not increase much. Continuous development and

refinement is taking place in the adhesively bonded joint analysis. A good understanding of the process of joining from mechanics view point and of the predictive capability for structural failures in adhesive bonding requires realistic theoretical analysis methods which are able to determine the stress distributions in the joint. The FEA is the most powerful analysis tool that has been used to determine stress and displacement fields in complicated adhesively bonded structures. At present, FEA is one that can take all features of adhesively bonded joints into consideration and has the capability for all desired options. The relevant literature concerning strength and damage analyses of various bonded joints such as SLJ, LSJ, DLJ and SWJ in laminated FRP composites are briefly outlined as follows:

2.4.1 Single Lap Joint (SLJ)

An analysis of adhesive stresses of bonded joints which included the effects of load eccentricity was first performed by Goland and Reissner [16] with the assumptions: (i) adhesive flexibility is negligible, and the joint is homogeneous (i.e. ignore the presence of adhesive); and (ii) no axial stress exists, and other stresses do not vary through-the-thickness of the adhesive layer. With these simplified assumptions, Goland and Reissner developed elasticity solutions for two limiting cases: (i) the case in which the adhesive layer is so thin and stiff that its deformation can be neglected, and (ii) the case in which the adhesive layer is soft and flexible, and the joint flexibility is mainly due to the deformation of the adhesive layer. In the first case, the peel stress is found to be very high at the edge of the joint, while the shear stress is zero. In the second case, the maximum values of the peel and the shear stresses occur at the edges of the joint. The Goland and Reissner analysis is limited to identical adherends in which the joint edge loads are not in equilibrium, and the stresses across the adhesive layer are constant.

Erdogan and Ratwani [68] developed a model for calculating stresses in a stepped lap joint. One adherend was assumed to consist of an isotropic material and the second of an orthotropic material. Linear elastic conditions for the materials were assumed. The variations of the stresses in both the adherends and in the adhesive layer along the thickness were insiginificant. All normal or peel stresses were thus neglected.

Wooley and Carver [69] investigated the stress distributions in an SLJ using FEA. They assumed that the total length of the adherends beyond the lap is long and a plane stress condition exists. They used the constant strain quadrilateral element obtained by combining four constant strain triangular elements. In the way of

boundary conditions, one end of the adherend was assumed to be hinged and the other end was allowed to move freely in the direction parallel to the original bondline. The study dealt with the influence of Young's moduli ratios and geometries on the peel and shear stress distributions. The results could be compared favourably with the results of Goland and Reissner.

Hart-Smith [18] improved upon the approach of Goland and Reissner by considering a third free body diagram for the adherend outside the joint in addition to the two free body diagrams from each of the upper and lower halves of the joint. With these three separate sections collated three relations between displacements and bending moment were obtained. Additional boundary conditions involving displacements and their first derivatives, not considered by Goland and Reissner, were imposed in order to solve for the additional unknowns. In addition to the improvement on the analysis of Goland and Reissner, Hart-Smith also established the quantitative influence of adhesive plasticity in shear. The elasto-plastic theory used by Hart-Smith predicted an increase in joint strength. It was shown to be capable of explaining premature failure predictions found when using linear elastic analysis. The quantitative effects of stiffness imbalance were also accounted for. Hart-Smith's analysis could determine the edge moment and the adhesive stress simultaneously, and take into account the effect of large deflection of the free adherends, but ignored the large deflection effect in the joint overlap.

A further development was conducted by Oplinger [19] who took into account the large deflection effect and presented a more detailed analysis. The edge bending moment factor given by Oplinger was between the Goland and Reissner's solution and the Hart-Smith solution. Tsai and Mortan [70] conducted a 2-dimensional analysis and discussed the limits of the above three solutions for the edge bending moment in the range of short, intermediate long to long overlap.

A FEA for adhesively bonded SLJs using elasticity and elasto-plastic theories was reported by Liu [71]. Stress distributions and concentrations in the adhesive layer for different joining parameters (geometry, material properties and loading) were studied and compared.

The existence of stress gradients through-the-thickness of the adhesive layer, close to the joint edges, was observed by Adams and Peppiatt [72]. They performed a linear elastic FEA on an SLJ, employing more than one element through-the-thickness of the adhesive layer, and also studied the adhesive yielding, using an iterative elasto-plastic FE program.

Humphreys [73] presented a non-linear analysis of an SLJ using FEA. The non-linear stress strain response was represented by a Ramberg-Osgood approximation. Mechanical and thermal loadings were considered but only one element through-the-thickness of the adhesive layer was used. Allman [74] presented an elastic stress analysis based on the strain energy density of a particular joint. The effects of bending, stretching and shearing of the adherends were included, and the shearing and tearing actions accounted for. All conditions of stress equilibrium in the joint and stress free surface conditions were satisfied. It was assumed, however, that the axial stress varies linearly through the adherend thickness and that the shear stress is constant through the adhesive thickness. Allman obtained solutions for an SLJ, although the method also appears to be applicable to other joint configuration. He found that the shear stress concentration is 11% higher than that of Goland and Reissner's first analysis, while the average peel stress at the joint edge is 67% lower. Compared with the second analysis of Goland and Reissner, Allman's method yielded a shear stress concentration of 15% and 31% less for metal and composite adherends, respectively, while the average peel stress at the joint edge was 27% higher and 36 % lower for the same types of adherends, respectively.

Phenomenological considerations were discussed by Hart-Smith [75], which greatly improves the understanding of the sources of non-uniform load transfer viz., adherend extensivity, stiffness imbalance and thermal mismatch. He also explained how the lightly loaded central area of the joint, away from the joint edges, restricts cumulative creep damage, and suggests that this region is vital for long term durability. The amount of lightly loaded central area is a function of the overlap length.

Pickett and Hollaway [76] presented both classical and finite element solutions for elastic-plastic adhesives stress distributions in bonded SLJ. The results showed how the development of adhesive yielding occurred when the joints were loaded to failure condition. The detrimental effect of adherend-stiffness imbalance on the adhesive shear stress distribution was also shown [77].

Jeandrau [78] observed that determination of stress distribution and design data suitable for design engineers could be obtained by the use of available commercial software based on the published analytical methods. His findings are found to be in good agreement with experimental observations in five different epoxy based structural adhesives. With the use of numerical shape optimization technique, Groth and Nordulund [79] found out a substantial decrease in stress level in the

adhesive layer to obtain much lighter joints. They further concluded that it was very difficult to obtain the correct profile of the thin adherend. Capenter [25] tested the lap joint analytical theories of numerous authors and remarked that neglecting assumptions like shear deformation was inconsistent, and error upto 30% was introduced thereby.

A concise method of analysis was used to study the numerous parameters influencing the stress distributions within the adhesive of an SLJ by Renton and Vinson [80]. The formulation included transverse shear and normal strain deformations with both isotropic and anisotropic material systems of similar and dissimilar adherends. The authors concluded that the primary Young's modulus of adherends, overlap length and the adhesive material properties are the most influential parameters in the optimization of an SLJ. However, they neglected the variation of both shear and transverse normal stresses in the thickness direction.

Experimental work by Sage [81] revealed that radiusing (by way of spew filleting) of adherends in an SLJ helps to increase the joint strength substantially. He also discussed several aspects of reducing stress concentration in bonded joints with Carbon Fiber Reinforced Polymeric (CFRP) composite adherends.

Recently Kayupov and Dzenis [38] developed a 2-Dimensional non-linear finite element model for a cracked SLJ with laminated adherends and studied the effects of crack length, load, and the adhesive layer on the joint response. It was shown that stresses, energy release rates and stress intensity factors vary non-linearly with the crack length. Two-dimensional geometrical non-linear plane strain numerical and experimental solutions under rotation boundary conditions were performed by Li and Sullivan [82] who estimated the bending moment factor and the adhesive stresses in an SLJ under tension. They observed significant scatter values of strains at the overlap ends. Andruet et al. [83] described a finite element model to predict the behaviour of an SLJ that minimizes the number of degrees of freedom required to obtain accurate result by including geometric non-linearity, moisture and temperature effects. They concluded that the bonded joint problems are in a real 3D scenario, which cannot be modelled in 2D. Three-dimensional zones in an SLJ were identified form the plane strain behaviour by comparing the 3D results by Pandey and Narasimhan [84] using visco-plastic FEA. Total Langrangian method was formulated to consider geometric non-linearity in the SLJ due to finite rotation of the joint.

Mortensen and Thomsen [85] presented a newly developed unified approach for the analysis of adhesively bonded joints by modelling adherends as beams or wide

plates in cylindrical bending. Comparing the linear and non-linear adhesive solutions, they concluded that the non-linear behaviour shown by many polymeric adhesives exerted a strong influence on the adhesive stress distribution. The severe stress concentrations, predicted by the linear solution procedure, tend to smooth out when a non-linear solution is applied. The non-linear effects become influential even at low load levels, and become very influential at a higher load levels. Thus, in most of the cases non-linear effects are unavoidable, and a certain degree of plasticity in the adhesive layer close to the ends of the overlap end cannot be prevented. Linear elastic solution procedure would therefore underestimate the strength of the bonded joint unless brittle adhesives with approximately linear elastic properties are considered.

2.4.2 Lap Shear Joint (LSJ)

Analytical solutions for other joint configuration have been developed under various assumptions by many researchers in the past few decades. For example, solutions for Lap Shear Joint (LSJ) is representative of many applications in aerospace structures, such as stiffened panel and shell, selective plate reinforcement, bonded edge doublers for flush mechanical attachments , etc. The LSJ has only one end with critical stress concentration, and it has long been known that the doublers must be flexible in bending at the end to diffuse load transfer gradually. This is different from an SLJ, which has two overlap ends with stress concentrations.

To investigate the fracture mechanics behaviour of LSJ, Brussat [86] originally proposed by placing an initial crack in the bondline and, thus forming a cracked LSJ. An ASTM round robin was conducted and reported by Johnson [87] on stress analysis of cracked LSJ. Cracked LSJ specimen was used for studying composite delamination and adhesive joint debonding by many researchers. It is found that the debond tip in the cracked LSJ specimen is predominantly loaded in Mode *II* with approximately 30% Mode *I*. There was no known exact solution for this type of specimen.

Edde and Verreman [88] proposed a stress analysis using an approach similar to that suggested by Goland and Reissner [16]. In their analysis, both adherends are assumed to have same thickness and elastic moduli. These assumptions decouple the normal and shear stress solutions. In a recent study, Lai et al. [89] revisited the cracked LSJ specimen and introduced a new non-dimensional closed form solution for the lateral deflection and bending moment. They considered three types of boundary conditions: clamped-clamped, roller-clamped and roller-roller, as it was found that the testing results are sensitive to boundary conditions [90]. The clamped-

clamped case is representative of typical testing in fixed grips of a Universal Testing Machine (UTM), while the roller-roller case is equivalent to half of the SLJ problem solved by Goland and Reissner [16]. A comparative study for numerous lap joint theories of adhesively bonded joint illustrated by Carpenter [25], shows the effects of the various assumptions.

In addition to the displacement method, stress approach is used by Chen and Cheng [91] and Adams and Mallick [29]. The finite element analysis has been used by many researchers to study the stress distributions in the adherend and adhesive of adhesively bonded joint. The relevant literature reviews can be found in Reddy and Roy [77]. A numerical study of adhesively bonded LSJ used in composite panel flange joints was presented by Tong et al.[92]. Two-dimensional geometric non-linear through-the-thickness plane strain model was used for analyzing a variety of composite panel flange joints. Stress redistributed in the joints when the panel buckled was presented and incorporated with maximum stress failure criterion to predict the failure loads. A parametric study was conducted to investigate the role of the flexibility of the LSJ used in flange panel joint in the design of these types of structures [92].

The failure modes in LSJ were of great practical interest for many years. At first sight, the failure of LSJ specimen might appear to be due to the plastic failure in the adhesive layer so that the shear strength should be given by the adhesive yield stress, and the failure load would increase directly with the overlap dimension. Many experimental results demonstrated that this plastic failure is not the dominant mode of fracture of LSJ specimen. These experimental facts, together with observations of actual failures, lead to the suggestion that LSJ rupture took place predominantly by the propagation of cracks. Thus, Kendall [93] contributed his work in recognizing that failure of LSJ is brought about, not only by the initiation of crack, but also by its continued movement through the adhesive layer. Firstly, a theoretical study was described which employed an energy argument of the Griffith theory [94] and derived a criterion for crack movement under a constant force. Finally, theory and experiment were employed to deduce criteria for designing practical LSJ.

Recently, Wang and Yau [95] studied the elastic behaviour of interfacial cracks in adhesively bonded LSJ using a recently developed method based on conservation laws in elasticity for non-homogenous solids and fundamental relationships in fracture mechanics of dissimilar materials. Fracture parameters such as Stress Intensity Factor (SIF) and associated Energy Release Rate (ERR) were

described for crack tip deformation and stresses under complex failure modes in the LSJ specimen. They obtained solutions for problems with various kinds of adhesives and adherends, joint configurations and interfacial crack lengths. Cheuk and Tong [36] investigated the effects of embedded cracks on failure loads and modes of LSJ specimens, experimentally, numerically and analytically and found that the embedded crack could significantly reduce the failure of the joints.

2.4.3 Double Lap Joint (DLJ)

Another joint configuration that received considerable attention is the Double Lap Joint (DLJ). Hart-Smith [17] studied adhesively bonded DLJ using elastic-plastic analytical techniques. Explicit solutions obtained include sufficiently simple formulas for predicting the shear bond strength and the plastic zone length. It was shown that with a particular geometric configuration and specified material properties; the maximum bond shear strength is achievable between specified adherends in case of a DLJ. Similarly, the Engineering Science Data Unit (ESDU) [96] in its document no. 79016 pointed out that the precise shape of the shear stress and strain curve has no effect on the limiting joint strength, and can affect only the adhesive shear stress distribution along the overlap. Tong [97] proposed a study of adhesive DLJ with arbitrary non-linear adhesive shear stress strain behaviour.

Adams et al. [98] indicated that the internal bending moment are established in the DLJ, which Volkersen [15] accounted for his later work, so that normal stresses arise, acting normal to the adhesive layer. The maximum values of these normal stresses occur in the adhesive layer and the inner adherend at the end of the overlap. These normal stresses called peel stresses influenced significantly on the failure of the joint. This arises for two reasons; firstly, the strain capability of structural adhesives is very limited in tension, as compared with shear and, secondly, the transverse tensile strength of fibrous composite is much lower than the strength parallel to the fibers. Most of the predictions assumed the failure of the adhesive and did not address the problem of interlaminar adherend failure. Adams and Wake [20] presented theoretical studies to draw upon both established analytical and original FEA to describe the shear and tensile stress distributions in the FRP composite to metal DLJ, taking into account the above factors.

Tong et al. [99] showed the effect of the end mismatch on mechanical behaviour of adhesively bonded DLJ. Parametric results showed that the end mismatch had a noticeable effect on the adhesive shear and peel stresses and a significant effect on the normal displacement. Also, they included the effect of end

mismatch in the peel stress formula developed by Tong et al. [100] in their further research. Finally, the surface normal displacement and the peel stress in the adhesive layer were validated by comparing them with the experimental results measured using holographic interferometry technique.

Cheuk et al. [101] presented experimental and numerical investigations of the fatigue crack initiation and growth mechanism in metal to composite bonded DLJ. Fracture surface was examined using scanning electron microscope. They revealed that fatigue cracks were near the interface between the co-cured adhesive and surface ply of the FRP composite adherend. It was concluded that the fatigue failure of metal to composite DLJ was mainly driven by the tensile mode loading due to the peel stress only.

Keer and Chantaramungkorn [102] analyzed a DLJ using integral transform technique. Singular integral equations were derived from integral transform solutions using boundary and continuity conditions appropriate to the DLJ. Stress Intensity Factors (SIF) and contact stresses were calculated and presented for various values of geometrical parameters. Osnes and McGeorge [103] used over laminated technique, where the parts to be joined were connected by laminated adherends directly upon assembly. Analytical solutions of interfacial stress were compared with the finite element solutions.

Altus [33] made a profound study, on three-dimensional aspects of DLJ, including all three modes of fracture simultaneously, to find how far the fracture mechanics approach could be used as a designing tool for further use of DLJ and, to follow the influence of different materials on the three-dimensional behaviour to check the accuracy, using numerical technique. It is highlighted that the singular region for common combinations of adhesives-adherends are so small that regular continuum mechanics tools may be limited in failure predictions and the two-dimensional solutions would show higher critical load for the same problem.

2.4.4 Spar Wingskin Joint (SWJ)

Extensive use of FRP composites was adopted in modern aircraft technology to develop and produce aircraft of better performance and of lower cost by fully exploiting the advantageous characteristics of advanced composite materials. Fabrication of structural components of aircraft were made with the help of joints by replacing the mechanical fastening or other methods of joining which not only reduced the weight, but also minimized the locations of stress concentrations. The

analysis, optimization and design of joints made of fibrous composites in aircraft structures generated interest and special attention.

The use of unidirectional laminae or plies as basic building blocks in the making of multidirectional laminate provided the designer with a unique ability to tailor-make the strength and stiffness of the laminates to withstand the in-plane force resultants only. But, it was not easy to tailor-make the out-of-plane strength and properties of the laminates. The absence of fibers oriented normal to the plane of the laminates resulted in low interlaminar strength properties typical of the resin phase of the material. Consequently, the out-of-plane strength of the laminate was severely limited by the interlaminar strength of these materials.

Application of loads normal to the plane of FRP composite laminates through joints posed a significant problem for the designers, especially in the aircraft industries. The designers resorted to the use of mechanical fasteners in the joints made for carrying out-of-plane loads. Unfortunately, the perforations caused by mechanical fasteners significantly reduce the load carrying capability of the laminate and cause rapid deterioration of the joint strength when subjected to dynamic loads in adverse environment. For these reasons, the need for analysis, optimization and design of out-of-plane load carrying joints in FRP composite laminates utilizing no mechanical fasteners was of paramount importance, especially in aerospace technology.

The joints that were fabricated using the integral modular wing concept techniques for connecting monolithically the lower wingskin to the spars in an aircraft are known as Spar Wingskin Joint (SWJ). The SWJ concept was a novel fabrication method in aircraft technology which permits lay up and co-cure of lower wingskin and the spar-web in one operation. This fabrication technique resulted in significant cost saving by eliminating secondary bonding, use of assembly tools and multiple cycles of curing.

The SWJ used in aircraft structures were intended for transferring and sharing the wing load and fuel pressure. The space between base flanges of the spar called core was filled up with some suitable adhesive or bonding materials. The relevant literature on the analysis of SWJ parameters was not available as the analysis is only at its nascent stage. The complicated shape, loading, boundary conditions and the orthotropic material properties of the joint components were the formidable obstacles in initiating any attempt for closed form solution. Some attempts in experimental as well as finite element analysis had been taken to study the behaviour and predict the

strength of the joint. Lackman et al. [104] developed a method of strengthening bonded structures to cover joints to withstand the combination of structural loads and fuel pressure which generated peeling forces at the end of spar base flanges. The first approach was consisting of using either metallic pins or stitching to reinforce with the conventional I-beams. The metallic pins or stitching concepts were not efficient enough to withstand the external loads acting on the wings.

Gillespie and Pipes [105] conducted experimental and finite element analyses on integral composite joints with titanium and graphite epoxy inserters in the wingskin. The results of the experimental verification were found to be in good agreement with the results of finite element analysis. They found that the load coupler concept increased the load transfer capability of the joints.

Cope and Pipes [106, 107] analyzed SWJ with triangular and circular profile core by finite element technique to predict the ultimate load through the application of maximum stress and Tsai-Wu failure criteria based on span length. However, they did not take any attempt for optimization of spar base or core configuration. Till date no attempt was made with regards to the failure analyses of the SWJ.

2.5 SERR: A fracture mechanics approach for characterization of adhesion failure and delamination damages in bonded joints

Irwin [108] conceptualized that stress field ahead of the crack due to an infinitesimal small crack extension could be made equal to that behind it due to the crack closure, when the crack was assumed to propagate in the same plane. Hellen [109] proposed the Virtual Crack Extension Method (VCEM) to evaluate strain energy release rate to study the crack propagation characteristics. However, using this method total strain energy release rate could only be calculated, but not the individual modes responsible for mixed mode interlaminar fracture. Rybicki and Kanninen [13] discussed the advantage of the method of Modified Crack Closure Integral (MCCI) based on the postulates of Irwin's theory of crack field solution for calculating the individual modes of strain energy release rates for cracks in bi-material interface. This procedure of virtual crack closure along the delamination interface has the advantage that not only it is based on a sound energy balance principle in the light of Linear Elastic Fracture Mechanics, but also it has the advantage of calculating individual modes of interlaminar fracture energy release rates with a single finite element run.

Traditionally strain energy release rate mode ratios of G_I, G_{II} and G_{III} were being used to analyze the interfacial delaminations between two orthotropic solids

using Virtual Crack Closure Technique (VCCT) [14, 110-112]. However, the stress field solutions of the near crack tip field indicated that stresses started to oscillate in the immediate vicinity of the tip, when crack growth occurred at interfaces between materials with dissimilar properties. Interface crack growth studies in orthotropic media were quite complex in nature due to the mismatch of material properties at the interface. Again the finite plate dimensions possessed another problem on the prevalent boundary conditions to evaluate the constant terms in analytical studies, which otherwise simplified the crack growth analysis in an infinite medium and whose analytical expressions were readily available in literature [113, 114]. Sun and Pandey [115] applied beam theory for modelling the interface crack progression and calculating the individual modes of strain energy release rates. Researchers [116-119] found that the energy release rate was not evenly distributed along a straight crack and concluded therefore that the crack tip would become curved. This was studied both analytically and with finite element methods. Carpenter [120] reported the dependence of the wedge corner stress intensity on the integration path for the singular stress field near the interface corner of a bi-material joint. Qian and Sun [121, 122] studied the interlaminar crack growth mechanism by calculating stress intensity factors for different crack propagation lengths. Evaluation of strain energy release rates along the interface delamination suggested the mixed mode crack growth phenomena in orthotropic composite materials [123, 124]. Venkatesha et al. [125-127] employed different generalized modified crack closure formulations to calculate individual modes of strain energy release rates in interfacial cracked laminates. Tian and Swanson [128] studied the effect of internal fiber breakage on the tensile strength of carbon/epoxy laminates. The results showed a significant strength reduction due to internal fiber cut. The prediction of the residual strength was attempted using a principal load carrying ply failure criterion in conjunction with a 3D anisotropic Finite element analysis.

2.6 Objectives of the present Thesis

From the literature survey it is concluded that in most of the cases, out-of-plane loadings result in early damage/failure of laminated FRP adherends. One of the failure modes such as interlaminar or intralaminar delaminations, cohesive failure, adhesion failure or a combination thereof and subsequent propagation/coalescence cause abrupt fracture to the adhesively bonded joints. Most of the analyses so far in this direction are of two-dimensional in nature with simplified assumptions, which

lacks explaining the mixed mode fracture behaviour of adhesively bonded joints of laminated FRP composites under any general state of loading conditions and stacking sequences, which real composite bonded structures experience.

Ascribed to the published works in literature, it is also observed that systematic studies on the subject of three-dimensional stress analyses, prediction methodologies for the onset of damages and propagation behaviour of such damages when per-embedded at the critical locations in the different types of adhesively bonded joints of laminated FRP composites have been very limited because of the complexities of geometry and loading eccentricity, and material anisotropy and heterogeneities involved. The effects of stress raisers on damage evolution should not be ignored for a thorough understanding of fracture and failure phenomena in adhesively bonded joints of laminated FRP laminated composites. This aspect is growing to be interested amongst the researchers recently. The behaviour of adhesively bonded structures is rather complicated by the simultaneous occurrence of three fracture modes even under a simple loading condition due to the presence of damages having linear damage front. This is mainly due to the inherent nature of material heterogeneity and anisotropy as well as by the geometric discontinuity at the interface. From these observations, in this Thesis, the following works are being outlined for investigation of some of the types of damages pre-existing in different types of adhesively bonded joints of laminated FRP composites. The various damage mode studies are carried out using three-dimensional finite element analyses to have a thorough understanding of the damage onset and growth. Strain energy release rate (SERR) procedures based on the concepts of linear elastic fracture mechanics are employed to assess the severity of damage progression due to mechanical loadings.

The objective of the present study is to undertake a detailed investigation of damages in several bonded joint specimens of laminated FRP composite adherends using fracture mechanics approach, where it has been assumed that a straight damage front to pre-exist at the critical location. The damage evolution in the adhesively bonded joint of laminated FRP composites and the fracture behaviour of embedded damages have been discussed with respect to the variation of the individual modes of strain energy release rates as the defining parameters along the damage front. Some of the major aims of the research work are as follows:

- Three-dimensional finite element analyses of adhesively bonded SLJ in laminated FRP composites to predict the onset of failures and study the failure propagation characteristics.

- Delamination damage analyses of adhesively bonded SLJ in laminated FRP composites to study the effect of embedded adhesion failures at both ends of the adhesive layer and their propagations.
- Delamination damage analyses of adhesively bonded SLJ for varied positions of pre-embedded through-the-width delaminations in both the laminated FRP composite adherends.
- The effect of out-of-plane stress distributions in the adhesive layer, the interlaminar stresses and SERR distributions along the delamination front on the delamination damage propagation pre-embedded beneath the surface ply of the strap adherend of the LSJ.
- Prediction of adhesion failure and delamination damage onset and their propagations in adhesively bonded laminated FRP composite DLJ.
- Design and development of load coupler profiles of Spar Wingskin Joints for integral structural construction of aircraft wings and study of delamination damage initiation and propagation in SWJ with modified elliptical load coupler profile.

The aim also has been set to put forth suitable recommendations for improved performance of various adhesively bonded joints under consideration.

3

Adhesion Failure and Delamination Damage Analyses of Bonded Joints in Laminated FRP Composites

3.1 Introduction

Structural adhesively bonded joints fail at different locations and in a variety of damage modes which were discussed in earlier Chapters. Damages in an adhesively bonded joint could occur or initiate in the adhesive layer, or in the adherends, or in the interfacial areas of the adhesive-adherend, depending on the joint configuration, the joint materials, the loading, the type of constraints and the manufacturing procedures. It is quite complex to describe all the possible modes of damages of adhesively bonded joints. There are in general two approaches to deal with the damage analyses of adhesively bonded joints. One is the Mechanics of Materials approach, and the other is based on Fracture Mechanics principles. In the first method, the applied or anticipated design stress or deformation is compared to the strengths of the materials, and then the material is assumed to adequate if the allowable strength values are greater than the evaluated stress or strain under loading. In the second one, there are three important variables, the applied stress, the flaw or damage size and the fracture toughness, and the combinations of these three variables are quantified using fracture mechanics approach to determine the integrity and service life of a structure. Adhesively bonded joints need to be proficiently designed for safe load carrying and/or load transferring device in any structural applications. In this Chapter, the numerical formulations based on Finite Element Analysis (FEA) for different types of adhesively bonded joints viz. Single Lap Joint (SLJ), Lap Shear Joint (LSJ), Double Lap Joint (DLJ), and Spar Wingskin Joint (SWJ) of laminated FRP composite adherends have been discussed. Also, the damage mechanics and the detailed analysis procedures have been discussed to address the various types of damages pertaining to adhesively bonded joints including the delamination induced damage in laminated FRP composite adherends.

3.2 Constitutive relationship of laminated FRP composites

A laminate is an assemblage of laminae stacked together along with supporting adhesive to achieve the desired thickness and stiffness. As shown in Fig. 3.1, multidirectional fiber reinforced laminates can be formed so that the fibers in each lamina are oriented in the same or different directions to achieve the desired load carrying capabilities. The arrangement of various orientations of the fibers in the composite layer in a laminate is called the laminating scheme or stacking sequence.

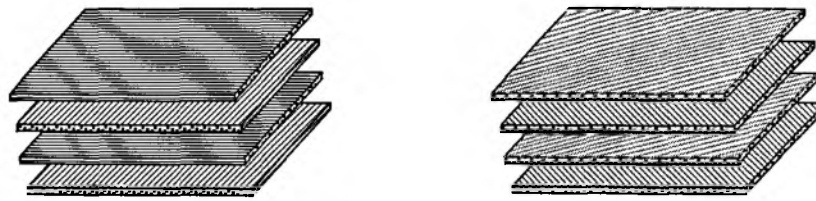

(a) Cross-ply laminate (b) Angle-ply laminate

Figure 3.1 Multidirectional laminate configuration.

The layers are bonded together or cocured with the same matrix materials as that is used for the laminae. Because of the mismatch of material properties between the layers, the shear stresses are induced between the layers which may cause delamination. Also, during the manufacturing of laminates, material defects such as interlaminar voids, delamination, incorrect orientation, damaged fibers, and variation in thickness may be introduced. It is impossible to eliminate the manufacturing defects altogether. Therefore, analysis and design procedures of adhesively bonded joint should account for the defects when laminated FRP composites are used as adherends.

The mechanical behaviour of a single lamina, treating it as a linear, orthotropic, elastic continuum is described below. It is to be emphasized that the postulate of smallness of deformation gives rise to the linear relationship between the strain and stress. This linearity is reflected in the validity of Hooke's law postulated in the linear theory of elasticity. The elastic coefficients of an orthotropic material are expressed in terms of Engineering constants of a lamina. Thus, the generalized Hooke's law [3, 4, 129] is written as

$$\sigma_{ij} = C_{ijkl}\varepsilon_{kl}, \quad i,j,k,l = 1, 2, 3, \ldots\ldots, 6. \tag{3.1}$$

The above are the constitutive equations in tensorial form of the linear theory of elasticity for a most general type of anisotropy material. The coefficients C_{ijkl} are called as the stiffness coefficients and σ_{ij} are the stress components on a three-

dimensional x, y and z coordinates, and ε_{kl} are the corresponding strain components. Invoking symmetry of the stress and the strain tensors, the interchange of indices i and j, as well as of the indices k and l in Eq. (3.1) does not affect the equation. Hence,

$$C_{ijkl} = C_{jikl} = C_{ijlk} \tag{3.2}$$

This results in reducing the number of stiffness constants from 81 for a general anisotropic case to 36. However, less than 36 of the constants can be shown to actually be independent for elastic materials when important characteristics of the strain energy are considered. Elastic materials for which strain energy density function exists have incremental work per unit volume of

$$dW = \sigma_{ij} d\varepsilon_{kl} \tag{3.3}$$

when the stresses σ_{ij} act through $d\varepsilon_{kl}$. However, because of the stress-strain relations, Eq. (3.1), the incremental work becomes

$$dW = C_{ijkl}\varepsilon_{kl} d\varepsilon_{kl} \tag{3.4}$$

Upon integration for all strains, the work per unit of volume is

$$W = \frac{1}{2} C_{ijkl}\varepsilon_{ij}\varepsilon_{kl} \tag{3.5}$$

However, Hooke's law, Eq. (3.1), can be derived from Eq. (3.5):

$$\frac{\partial W}{\partial \varepsilon_{ij}} = C_{ijkl}\varepsilon_{kl} \tag{3.6}$$

whereupon

$$\frac{\partial^2 W}{\partial \varepsilon_{ij}\partial \varepsilon_{kl}} = C_{ijkl} \tag{3.7}$$

Similarly,

$$\frac{\partial^2 W}{\partial \varepsilon_{kl}\partial \varepsilon_{ij}} = C_{ijkl} \tag{3.8}$$

But the order of differentiation is immaterial, So, Eqs. (3.7) and (3.8) yield

$$C_{ijkl} = C_{klij} \tag{3.9}$$

Then the number of distinct stiffness constants reduces to 21 only even for the most general type of anisotropic materials. In the similar manner, the following expression for strain tensor can be written:

$$\varepsilon_{ij} = S_{ijkl}\sigma_{kl} \tag{3.10}$$

where S_{ij} is known as the compliance matrix. By adopting similar procedures and arguments as for stress tensors, it can be easily verified that strain tensor ε_{ij} is also symmetric and the compliance coefficients reduce from 81 to 21.

Now expressing the Eq. (3.1) into the explicit matrix form

$$\begin{bmatrix} \sigma_{11} \\ \sigma_{22} \\ \sigma_{33} \\ \tau_{23} \\ \tau_{31} \\ \tau_{12} \end{bmatrix} = \begin{bmatrix} C_{1111} & C_{1122} & C_{1133} & C_{1123} & C_{1113} & C_{1112} \\ . & C_{2222} & C_{2233} & C_{2223} & C_{2213} & C_{2212} \\ . & . & C_{3333} & C_{3323} & C_{3313} & C_{3312} \\ . & . & . & C_{2323} & c_{2313} & C_{2312} \\ . & Sym & . & . & C_{3113} & C_{3112} \\ . & . & . & . & . & C_{1212} \end{bmatrix} \begin{bmatrix} \varepsilon_{11} \\ \varepsilon_{22} \\ \varepsilon_{33} \\ 2\gamma_{23} \\ 2\gamma_{31} \\ 2\gamma_{12} \end{bmatrix} \tag{3.11}$$

Equation (3.11) signifies the constitutive relations for materials exhibiting the most general elastic anisotropy. It is worth noticing that in the above expression, the doubled components of the shearing strain, appearing in the strain column in Eq. (3.11), comes from the sums of pairs of identical terms, such as $C_{1112}\varepsilon_{12} + C_{1121}\varepsilon_{21}$, obtained from the expansion of Eq. (3.1). The numerical values of the stiffness and compliances are direction dependent. There exist directions, in which the values of the coefficients are the same. Such directions of identical elastic properties are called equivalent.

Whenever a material displays some kind of elastic symmetry, the numbers of distinct coefficients drop below the maximum of 21 elastic constants. If there is only one plane of material symmetry, then the relationship of stress and strain tensor results in the following coefficient matrix.

$$[C_{ijkl}] = \begin{bmatrix} C_{1111} & C_{1122} & C_{1133} & 0 & 0 & C_{1112} \\ . & C_{2222} & C_{2233} & 0 & 0 & C_{2212} \\ . & . & C_{3333} & 0 & 0 & C_{3312} \\ . & . & . & C_{2323} & C_{2313} & 0 \\ . & Sym & . & . & C_{3113} & 0 \\ . & . & . & . & . & C_{1212} \end{bmatrix} \tag{3.12}$$

It is to be noticed that the number of distinct elastic stiffness coefficients reduces to 13. Correspondingly, for an orthotropic material having three mutual planes of material symmetry, the elastic constants can be described by the following matrices as reasoned before.

$$[C_{ijkl}]=\begin{bmatrix} C_{1111} & C_{1122} & C_{1133} & 0 & 0 & 0 \\ . & C_{2222} & C_{2233} & 0 & 0 & 0 \\ . & . & C_{3333} & 0 & 0 & 0 \\ . & . & . & C_{2323} & C_{2313} & 0 \\ . & Sym & . & . & C_{3113} & 0 \\ . & . & . & . & . & C_{1212} \end{bmatrix} \tag{3.13}$$

Hence, the orthotropy of the material reduces the number of distinct material elastic coefficients to nine. The directions perpendicular to the planes of elastic symmetry are customarily called the principal material directions. Typically for a transversely isotropic material the above expressions are more simplified. Transversely isotropic materials possess parallel planes of isotropy, so that all directions in these planes are elastically equivalent. The stiffness coefficients for this are expressed as

$$[C_{ijkl}]=\begin{bmatrix} C_{1111} & C_{1122} & C_{1133} & 0 & 0 & 0 \\ . & C_{2222} & C_{2233} & 0 & 0 & 0 \\ . & . & C_{3333} & 0 & 0 & 0 \\ . & . & . & C_{2323} & C_{2313} & 0 \\ . & Sym & . & . & C_{3113} & 0 \\ . & . & . & . & . & \frac{1}{2}(C_{1111}-C_{1122}) \end{bmatrix} \tag{3.14}$$

Thus, the number of distinct elastic coefficients reduces to 5. To complete the discussion, for isotropic bodies exhibiting no preferred planes of material symmetry directions with regard to their physical properties, the stiffness coefficients are written as below:

$$[C_{ijkl}]=\begin{bmatrix} C_{1111} & C_{1122} & C_{1122} & 0 & 0 & 0 \\ . & C_{1111} & C_{1122} & 0 & 0 & 0 \\ . & . & C_{1111} & 0 & 0 & 0 \\ . & . & . & \frac{1}{2}(C_{1111}-C_{1122}) & 0 & 0 \\ . & Sym & . & . & \frac{1}{2}(C_{1111}-C_{1122}) & 0 \\ . & . & . & . & . & \frac{1}{2}(C_{1111}-C_{1122}) \end{bmatrix} \tag{3.15}$$

Though the four suffix notation of stiffness matrix is imperative for the tensorial formulation of a generalized anisotropic material, a second type of notation in which two indices are appended as suffixes to all quantities involved such as stresses, strains, stiffness and compliances, the double suffix notation is more convenient in handling practical problems, and is often used. For instance, for a thin plate of orthotropic material subjected to a plane state of stress with 1 and 2 respectively representing the major and minor principal material axes of elastic symmetry, it is evident that the strain components ε_{31}, ε_{32} and ε_{33} do not come into analysis consideration and can be safely ignored. For the thin orthotropic plate, then Eq. (3.12) is reduced to

$$\begin{bmatrix}\sigma_1\\ \sigma_2\\ \tau_{12}\end{bmatrix}=\begin{bmatrix}C_{11} & C_{12} & 0\\ C_{12} & C_{22} & 0\\ 0 & 0 & C_{66}\end{bmatrix}\begin{bmatrix}\varepsilon_1\\ \varepsilon_2\\ 2\gamma_{12}\end{bmatrix} \tag{3.16}$$

The strain tensor can be obtained by taking inverse of Eq. (3.16) and is written as below.

$$\begin{bmatrix}\varepsilon_1\\ \varepsilon_2\\ 2\gamma_{12}\end{bmatrix}=\begin{bmatrix}S_{11} & S_{12} & 0\\ S_{12} & S_{22} & 0\\ 0 & 0 & S_{66}\end{bmatrix}\begin{bmatrix}\sigma_1\\ \sigma_2\\ \tau_{12}\end{bmatrix} \tag{3.17}$$

Assuming the lamina is thin, it is natural to consider the state of stress in the lamina as plane, as long as loading is acting parallel to the faces of the lamina. Accordingly, the only meaningful stress components become σ_1, σ_2 and τ_{12}, provided the state is referred to its natural principal material axes. The constitutive equations of a single lamina are then expressed by Eq. (3.17).

Here, in terms of elastic constants,

$$S_{11}=\frac{1}{E_1},\ S_{22}=\frac{1}{E_2},\ S_{12}=-\nu_{21}\frac{1}{E_2}=-\nu_{12}\frac{1}{E_1}\ \text{and}\ S_{66}=\frac{1}{G_{12}}. \tag{3.18}$$

where E_1 and E_2 are the Young's moduli; ν_{12} and ν_{21} are the coupled Poisson's ratios and G_{12} is the shear modulus of the orthotropic lamina referred to the principal material directions 1 and 2. The stiffness matrix coefficients, in turn, are expressed as follows:

$$C_{11} = \frac{E_1}{(1-\nu_{12}\nu_{21})},\ C_{22} = \frac{E_2}{(1-\nu_{12}\nu_{21})},$$

$$C_{12} = \frac{\nu_{12}E_2}{(1-\nu_{12}\nu_{21})} = \frac{\nu_{21}E_1}{(1-\nu_{12}\nu_{21})} \text{ and } C_{66} = G_{12}. \tag{3.19}$$

For an isotropic material the above coefficients become

$$C_{11} = \frac{E}{(1-\nu^2)},\ C_{22} = \frac{E}{(1-\nu^2)},$$

$$C_{12} = \frac{\nu E}{(1-\nu^2)} \text{ and } C_{66} = G \tag{3.19(a))}$$

where E, G and υ represent the Young's modulus, shear modulus and Poisson's ratio, respectively, with implied relationship $E = 2G(1+\upsilon)$.

3.3 Constitutive elastic formulation for laminated FRP composites

Reverting back to the expression in Eq. (3.13) for an orthotropic material, it is worth noticing that instead of using the four subscripts of the original elasticity tensor to describe the nine nonzero elastic constants, it is more convenient to express the generalized Hooke's law in the following form.

$$\sigma_i = Q_{ij}\varepsilon_j, \quad i,j = 1, 2, 3, ...6. \tag{3.20}$$

where σ_i are the stress components as before with a reduced number of indices without loosing the generalization of elasticity formulation. Q_{ij} is the stiffness matrix for the elastic formulation replacing C_{ijkl} matrix of elasticity; through keeping the equivalent identity. To be noted that, hence forward, the ε_j are termed as the Engineering strains instead of tensorial strains. The Engineering strains are different from the tensorial strains used earlier in Eq. (3.11) in as much as that there is a notational change in shearing strain components only. A tensorial shearing strain is half of the corresponding Engineering shearing strain. Now Eq. (3.20) can be written in expanded matrix form as

$$\begin{bmatrix} \sigma_1 \\ \sigma_2 \\ \sigma_3 \\ \tau_{23} \\ \tau_{31} \\ \tau_{12} \end{bmatrix} = \begin{bmatrix} Q_{11} & Q_{12} & Q_{13} & 0 & 0 & 0 \\ Q_{21} & Q_{22} & Q_{23} & 0 & 0 & 0 \\ Q_{31} & Q_{32} & Q_{33} & 0 & 0 & 0 \\ 0 & 0 & 0 & Q_{44} & 0 & 0 \\ 0 & 0 & 0 & 0 & Q_{55} & 0 \\ 0 & 0 & 0 & 0 & 0 & Q_{66} \end{bmatrix} \begin{bmatrix} \varepsilon_{11} \\ \varepsilon_{22} \\ \varepsilon_{33} \\ \gamma_{23} \\ \gamma_{31} \\ \gamma_{12} \end{bmatrix} \tag{3.21}$$

where the elastic symmetry axes of the material are being assumed to coincide with the geometric coordinate axes.

The Engineering strain matrix can be obtained by inverting the constitutive relations given in Eq. (3.20). In abbreviated form this is expressed as

$$\{\varepsilon\} = [Q_{ij}]^{-1}\{\sigma\} \tag{3.22}$$

The individual terms of the elasticity stiffness matrix $[Q_{ij}]$ are written in terms of elastic material constants called as the Engineering Constants as below:

$$Q_{11} = \frac{1-\nu_{23}\nu_{32}}{E_2E_3\Delta}$$

$$Q_{12} = \frac{\nu_{21}+\nu_{31}\nu_{13}}{E_2E_3\Delta} = \frac{\nu_{12}+\nu_{32}\nu_{13}}{E_1E_3\Delta}$$

$$Q_{13} = \frac{\nu_{31}+\nu_{21}\nu_{32}}{E_2E_3\Delta} = \frac{\nu_{13}+\nu_{12}\nu_{23}}{E_1E_2\Delta}$$

$$Q_{22} = \frac{1-\nu_{13}\nu_{31}}{E_2E_3\Delta}$$

$$Q_{23} = \frac{\nu_{32}+\nu_{12}\nu_{31}}{E_1E_3\Delta} = \frac{\nu_{23}+\nu_{21}\nu_{13}}{E_1E_2\Delta}$$

$$Q_{33} = \frac{1-\nu_{12}\nu_{21}}{E_1E_2\Delta}$$

$$Q_{44} = G_{23}$$

$$Q_{55} = G_{31}$$

$$Q_{66} = G_{12}$$

and

$$\Delta = \frac{1-\nu_{12}\nu_{21}-\nu_{23}\nu_{32}-\nu_{31}\nu_{13}-2\nu_{21}\nu_{32}\nu_{13}}{E_1E_2E_3} \tag{3.23}$$

in which, E_1, E_2 and E_3 are the Young's moduli along the principle material axes and ν_{ij} = Poisson's ratios for transverse strain in the j-direction when the applied stress is in i-direction, i.e.,

$$\nu_{ij} = -\frac{\varepsilon_j}{\varepsilon_i} \text{ for } \sigma_i = \sigma \text{ and all other stresses are zero.}$$

G_{12}, G_{23} and G_{31} are the shear moduli in the 1-2, 2-3 and 3-1 planes, respectively. The following reciprocal relations automatically satisfy for the continuum mechanics requirement.

$$\frac{\nu_{12}}{E_1}=\frac{\nu_{21}}{E_2},\ \frac{\nu_{13}}{E_1}=\frac{\nu_{31}}{E_3}\ \text{and}\ \frac{\nu_{23}}{E_2}=\frac{\nu_{32}}{E_3} \tag{3.24}$$

In laminated FRP composites, the principal directions of orthotropy 1-2-3, in general, do not coincide with the geometric natural axes *x-y-z* because of the effective directional utilization of the material system in the composites as shown in Fig. 3.1. The medium, in which the principal material directions are parallel to the natural geometric axes is called a specially orthotropic lamina as shown in Fig. 3.2 (a) and for a generally orthotropic lamina as shown in Fig. 3.2 (b), the principal directions of orthotropy 1-2-3 do not coincide with the geometric natural axes *x-y-z*.

x-y-z: Geometrical natural axes
1-2-3: Principal material directions

Figure 3.2 (a) Specially orthotropic lamina and (b) Generally orthotropic lamina.

For a generally orthotropic medium, the constitutive relationship is written as

$$\begin{bmatrix}\sigma_x\\ \sigma_y\\ \sigma_z\\ \tau_{yz}\\ \tau_{zx}\\ \tau_{xy}\end{bmatrix}=[\bar{Q}]\begin{bmatrix}\varepsilon_x\\ \varepsilon_y\\ \varepsilon_z\\ \gamma_{yz}\\ \gamma_{zx}\\ \gamma_{xy}\end{bmatrix} \tag{3.25}$$

The transformed elasticity matrix is given by

$$[\bar{Q}] = [T]^{-1}[Q][T]^{-T} \tag{3.26}$$

in which, $[Q]$ = Elastic stiffness matrix of specially orthotropic medium given by Eq. (3.21) and (3.23). The transformation matrix $[T]$ can be derived and is given by

$$[T] = \begin{bmatrix} \cos^2\theta & \sin^2\theta & 0 & 0 & 0 & \sin 2\theta \\ \sin^2\theta & \cos^2\theta & 0 & 0 & 0 & -\sin 2\theta \\ 0 & 0 & 0 & 1 & 0 & 0 \\ 0 & 0 & 0 & \cos\theta & -\sin\theta & 0 \\ 0 & 0 & 0 & \sin\theta & \cos\theta & 0 \\ -\frac{1}{2}\sin 2\theta & \frac{1}{2}\sin 2\theta & 0 & 0 & 0 & \cos 2\theta \end{bmatrix} \tag{3.27}$$

Here, θ is the fiber orientation angle with respect to x-axis in a counter-clockwise sense between the x-axis and the principal material direction 1 of the orthotropic medium (Fig. 3.2 (b)).

For a thin lamina, the constitutive relationship given in Eq. (3.25) can be written as

$$\begin{Bmatrix} \sigma_x \\ \sigma_y \\ \tau_{xy} \end{Bmatrix} = [\bar{Q}] \begin{bmatrix} \varepsilon_x \\ \varepsilon_y \\ \gamma_{xy} \end{bmatrix} = \begin{bmatrix} \overline{Q_{11}} & \overline{Q_{12}} & \overline{Q_{16}} \\ \overline{Q_{12}} & \overline{Q_{22}} & \overline{Q_{26}} \\ \overline{Q_{16}} & \overline{Q_{26}} & \overline{Q_{66}} \end{bmatrix} \begin{bmatrix} \varepsilon_x \\ \varepsilon_y \\ \gamma_{xy} \end{bmatrix} \tag{3.28}$$

in which

$$\begin{aligned} \overline{Q_{11}} &= Q_{11}\cos^4\theta + 2\,(Q_{12} + 2Q_{66})\sin^2\theta\cos^2\theta + Q_{22}\sin^4\theta \\ \overline{Q_{12}} &= (Q_{11} + Q_{22} - 4Q_{66})\sin^2\theta\cos^2\theta + Q_{12}(\sin^4\theta + \cos^4\theta) \\ \overline{Q_{22}} &= Q_{11}\sin^4\theta + 2\,(Q_{12} + 2Q_{66})\sin^2\theta\cos^2\theta + Q_{22}\cos^4\theta \\ \overline{Q_{16}} &= (Q_{11} - Q_{12} - 2Q_{66})\sin\theta\cos^3\theta + (Q_{12} - Q_{22} + 2Q_{66})\sin^3\theta\cos\theta \\ \overline{Q_{26}} &= (Q_{11} - Q_{12} - 2Q_{66})\sin^3\theta\cos\theta + (Q_{12} - Q_{22} + 2Q_{66})\sin\theta\cos^3\theta \\ \overline{Q_{66}} &= (Q_{11} + Q_{22} - 2Q_{12} - 2Q_{66})\sin^2\theta\cos^2\theta + Q_{66}(\sin^4\theta + \cos^4\theta) \end{aligned} \tag{3.29}$$

where the bar over the $\overline{Q_{ij}}$ matrix denotes that we are dealing with the transformed reduced stiffnesses instead of the reduced stiffnesses Q_{ij}.

It may be noted that the transformed reduced stiffness matrix $\overline{Q_{ij}}$ has terms in all nine positions in contrast to the presence of zeros in the reduced stiffness matrix Q_{ij}. However, there are still four independent material constants because the lamina is orthotropic. In the generally orthotropic case with geometric coordinate axes x and y, there is coupling between shear strain and normal stresses and between shear stress and normal strains, i.e. shear-extension coupling exists. Thus, in geometric coordinates, even an orthotropic lamina appears to be anisotropic. However, because such a lamina does have orthotropic characteristics in material coordinates, it is called a generally orthotropic lamina because it can be represented by the stress strain relations in Eq. (3.28). That is, a generally orthotropic lamina is an orthotropic lamina whose material coordinate axes are not aligned with the geometric coordinate axes.

3.4 Three-dimensional finite element formulation

The conventional three-dimensional characters of isoparametric solid elements used in the present study have been discussed in this section. The three-dimensional (having eight nodes and three translational degrees of freedom at each node) solid elements as shown in Fig. 3.3 have been used for discretization of the domain. The normal finite element procedures as described below have been adopted for the FEA of adhesively bonded joints [26, 130, 131]:

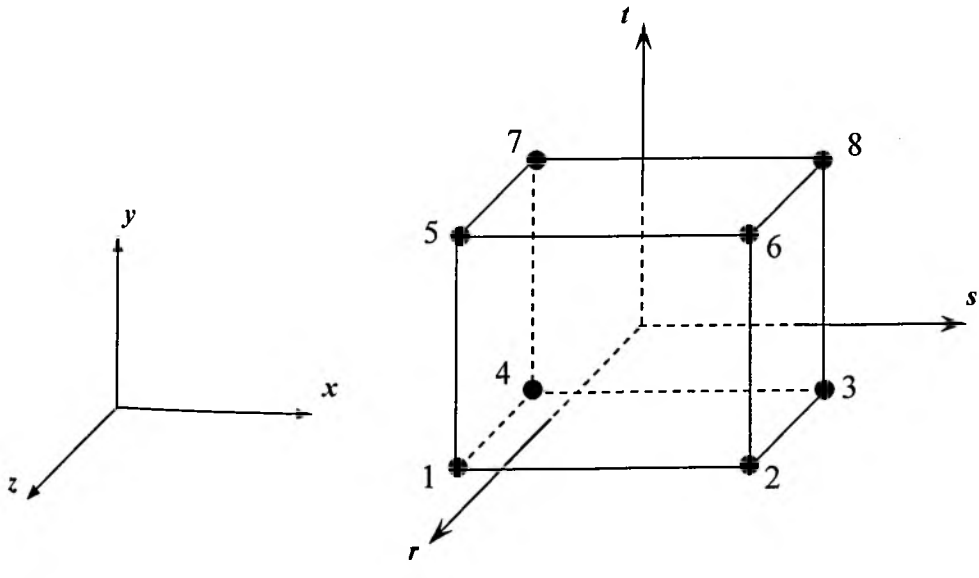

Figure 3.3 3D eight-node isoparametric solid element.

- Discretization of the domain into a set of finite elements (meshing).
- Formulation of differential equation over a typical element.
- Development of the finite element model which consists of a set of algebraic equations among the unknown parameters of the element.
- Assembly of finite elements for the entire problem.
- Imposition of constraints i.e. boundary conditions.
- Solution of equations.
- Post-processing of solution and quantities of interest.

The normal finite element procedure leads to the following expression for the displacement of the element. The primary variables i.e. displacements are expressed in terms of nodal variables in order to enforce their inter-element continuity. Thus, the displacements are being approximated as

$$\{\bar{u}\} = [[N_1][N_2][N_3]].....[N_7][N_8]]\begin{Bmatrix} a_1 \\ a_2 \\ .. \\ .. \\ a_8 \end{Bmatrix} \tag{3.30}$$

In compact form, $\{\bar{u}\} = [N]\{a^e\}$ (3.31)

where, $\{\bar{u}\} = \begin{Bmatrix} u \\ v \\ w \end{Bmatrix}$ and the nodal displacements are given by

$$\{a_i\} = \begin{Bmatrix} u_i \\ v_i \\ w_i \end{Bmatrix} \tag{3.32}$$

The shape function defining the geometry and variation of displacement is given by

$$N_i = \frac{1}{8}(1+rr_i)(1+ss_i)(1+tt_i) \tag{3.33}$$

where r, s, t are the natural coordinates and r_i, s_i and t_i are the values of the natural coordinates for a node i. Thus, the geometry of the element is defined as;

$$\begin{Bmatrix} x \\ y \\ z \end{Bmatrix} = \sum_{i=1}^{8} N_i \begin{Bmatrix} x_i \\ y_i \\ z_i \end{Bmatrix} \tag{3.34}$$

in which x_i, y_i and z_i are the global coordinates of node i. The variation of displacement inside the element can be expressed using the same shape function and given by

$$\begin{Bmatrix} u \\ v \\ w \end{Bmatrix} = \sum_{i=1}^{8} N_i \begin{Bmatrix} u_i \\ v_i \\ w_i \end{Bmatrix} \tag{3.35}$$

where u_i, v_i and w_i are the nodal displacements of node i in the global Cartesian coordinate system. Using the element shape functions, the displacements within the element are given by

$$\begin{aligned} u(x,y,z) = {} & \frac{1}{8}(1-r)(1-s)(1-t)u_1 + \frac{1}{8}(1+r)(1-s)(1-t)u_2 + \frac{1}{8}(1-r)(1+s)(1-t)u_3 + \\ & \frac{1}{8}(1+r)(1+s)(1-t)u_4 + \frac{1}{8}(1-r)(1-s)(1+t)u_5 + \frac{1}{8}(1+r)(1-s)(1+t)u_6 + \\ & \frac{1}{8}(1-r)(1+s)(1+t)u_7 + \frac{1}{8}(1+r)(1+s)(1+t)u_8 \end{aligned}$$

$$\begin{aligned} v(x,y,z) = {} & \frac{1}{8}(1-r)(1-s)(1-t)v_1 + \frac{1}{8}(1+r)(1-s)(1-t)v_2 + \frac{1}{8}(1-r)(1+s)(1-t)v_3 + \\ & \frac{1}{8}(1+r)(1+s)(1-t)v_4 + \frac{1}{8}(1-r)(1-s)(1+t)v_5 + \frac{1}{8}(1+r)(1-s)(1+t)v_6 + \\ & \frac{1}{8}(1-r)(1+s)(1+t)v_7 + \frac{1}{8}(1+r)(1+s)(1+t)v_8 \end{aligned}$$

and

$$\begin{aligned} w(x,y,z) = {} & \frac{1}{8}(1-r)(1-s)(1-t)w_1 + \frac{1}{8}(1+r)(1-s)(1-t)w_2 + \frac{1}{8}(1-r)(1+s)(1-t)w_3 + \\ & \frac{1}{8}(1+r)(1+s)(1-t)w_4 + \frac{1}{8}(1-r)(1-s)(1+t)w_5 + \frac{1}{8}(1+r)(1-s)(1+t)w_6 + \\ & \frac{1}{8}(1-r)(1+s)(1+t)w_7 + \frac{1}{8}(1+r)(1+s)(1+t)w_8 \end{aligned} \tag{3.36}$$

Hence, the shape function corresponding to node 1 is given by

$$[N_1]=\begin{bmatrix} \frac{1}{8}(1-r)(1-s)(1-t) & 0 & 0 \\ 0 & \frac{1}{8}(1-r)(1-s)(1-t) & 0 \\ 0 & 0 & \frac{1}{8}(1-r)(1-s)(1-t) \end{bmatrix} \quad (3.37)$$

$$=\begin{bmatrix} 1 & 0 & 0 \\ 0 & 1 & 0 \\ 0 & 0 & 1 \end{bmatrix}\frac{1}{8}(1-r)(1-s)(1-t) \quad (3.38)$$

In matrix notation, it can be written as, $[N_1] = [I]N_1$ (3.39)

Similarly,

$$[N_2] = [I]N_2,\ [N_3] = [I]N_3,\ \ldots\ldots\ldots\ldots\ldots [N_8] = [I]N_8 \quad (3.40)$$

Now, the shape functions are expressed as

$$[N_1] = \frac{1}{8}(1-r)(1-s)(1-t) \quad (3.41)$$

$$[N_2] = \frac{1}{8}(1+r)(1-s)(1-t) \quad (3.42)$$

$$[N_3] = \frac{1}{8}(1-r)(1+s)(1-t) \quad (3.43)$$

$$[N_4] = \frac{1}{8}(1+r)(1+s)(1-t) \quad (3.44)$$

$$[N_5] = \frac{1}{8}(1-r)(1-s)(1+t) \quad (3.45)$$

$$[N_6] = \frac{1}{8}(1+r)(1-s)(1+t) \quad (3.46)$$

$$[N_7] = \frac{1}{8}(1-r)(1+s)(1+t) \quad (3.47)$$

$$[N_8] = \frac{1}{8}(1+r)(1+s)(1+t) \quad (3.48)$$

The relationship between the local natural and global coordinate system can be computed by using the chain rule of the partial differentiation and are given below:

$$\frac{\partial u}{\partial r} = \frac{\partial u}{\partial x}.\frac{\partial x}{\partial r} + \frac{\partial u}{\partial y}.\frac{\partial y}{\partial r} + \frac{\partial u}{\partial z}.\frac{\partial z}{\partial r} \tag{3.49}$$

$$\frac{\partial u}{\partial s} = \frac{\partial u}{\partial x}.\frac{\partial x}{\partial s} + \frac{\partial u}{\partial y}.\frac{\partial y}{\partial s} + \frac{\partial u}{\partial z}.\frac{\partial z}{\partial s} \tag{3.50}$$

$$\frac{\partial u}{\partial t} = \frac{\partial u}{\partial x}.\frac{\partial x}{\partial t} + \frac{\partial u}{\partial y}.\frac{\partial y}{\partial t} + \frac{\partial u}{\partial z}.\frac{\partial z}{\partial t} \tag{3.51}$$

or

$$\begin{Bmatrix} \frac{\partial u}{\partial r} \\ \frac{\partial u}{\partial s} \\ \frac{\partial u}{\partial t} \end{Bmatrix} = [J] \begin{Bmatrix} \frac{\partial u}{\partial x} \\ \frac{\partial u}{\partial y} \\ \frac{\partial u}{\partial z} \end{Bmatrix} \tag{3.52}$$

where $[J]$ is called Jacobian and given by, $[J] = \begin{bmatrix} \frac{\partial x}{\partial r} & \frac{\partial y}{\partial r} & \frac{\partial z}{\partial r} \\ \frac{\partial x}{\partial s} & \frac{\partial y}{\partial s} & \frac{\partial z}{\partial s} \\ \frac{\partial x}{\partial t} & \frac{\partial y}{\partial t} & \frac{\partial z}{\partial t} \end{bmatrix}$ (3.53)

Substituting Eq. (3.34) for x, y and z in Eq. (3.53),

$$[J] = \sum_{i=1}^{8} \begin{bmatrix} x_i \frac{\partial N_i}{\partial r} & y_i \frac{\partial N_i}{\partial r} & z_i \frac{\partial N_i}{\partial r} \\ x_i \frac{\partial N_i}{\partial s} & y_i \frac{\partial N_i}{\partial s} & z_i \frac{\partial N_i}{\partial s} \\ x_i \frac{\partial N_i}{\partial t} & y_i \frac{\partial N_i}{\partial t} & z_i \frac{\partial N_i}{\partial t} \end{bmatrix} \tag{3.54}$$

The inverse of the above matrix can be written as

$$[J]^{-1} = \begin{bmatrix} \overset{*}{J}_{11} & \overset{*}{J}_{12} & \overset{*}{J}_{13} \\ \overset{*}{J}_{21} & \overset{*}{J}_{22} & \overset{*}{J}_{23} \\ \overset{*}{J}_{31} & \overset{*}{J}_{32} & \overset{*}{J}_{33} \end{bmatrix} \tag{3.55}$$

Now, the strain displacement relation is given by

$$\{\varepsilon\} = [B]\{a^e\} \tag{3.56}$$

where

$$\{a^e\}^T = [(u_1 v_1 w_1),(u_2 v_2 w_3),.....(u_8 v_8 w_8)] \tag{3.57}$$

Equation (3.56) becomes

$$\{\varepsilon\} = \sum_{i=1}^{8} [B_i]\{a_i\} \tag{3.58}$$

where nodal displacement is given by

$$\{a_i\}^T = [u_i \quad v_i \quad w_i] \tag{3.59}$$

The strain vector at any point within the element can be defined by its six components which contribute to internal work. Thus,

$$\{\varepsilon\} = \begin{Bmatrix} \varepsilon_x \\ \varepsilon_y \\ \varepsilon_z \\ \gamma_{yz} \\ \gamma_{xz} \\ \gamma_{xy} \end{Bmatrix} \tag{3.60}$$

In order to evaluate the derivative of displacements in global coordinates, the displacements have been differentiated in natural coordinates. Thus, differentiating Eq. (3.38) with respect to r, s and t, the following expression is obtained.

$$\begin{bmatrix} \frac{\partial u}{\partial r} & \frac{\partial v}{\partial r} & \frac{\partial w}{\partial r} \\ \frac{\partial u}{\partial s} & \frac{\partial v}{\partial s} & \frac{\partial w}{\partial s} \\ \frac{\partial u}{\partial t} & \frac{\partial v}{\partial t} & \frac{\partial w}{\partial t} \end{bmatrix} = \sum_{i=1}^{8} \begin{bmatrix} u_i \frac{\partial N_i}{\partial r} & v_i \frac{\partial N_i}{\partial r} & w_i \frac{\partial N_i}{\partial r} \\ u_i \frac{\partial N_i}{\partial s} & v_i \frac{\partial N_i}{\partial s} & w_i \frac{\partial N_i}{\partial s} \\ u_i \frac{\partial N_i}{\partial t} & v_i \frac{\partial N_i}{\partial t} & w_i \frac{\partial N_i}{\partial t} \end{bmatrix} \tag{3.61}$$

Hence,

$$\begin{bmatrix} \frac{\partial u}{\partial x} & \frac{\partial v}{\partial x} & \frac{\partial w}{\partial x} \\ \frac{\partial u}{\partial y} & \frac{\partial v}{\partial y} & \frac{\partial w}{\partial y} \\ \frac{\partial u}{\partial z} & \frac{\partial v}{\partial z} & \frac{\partial w}{\partial z} \end{bmatrix} = \begin{bmatrix} \overset{*}{J}_{11} & \overset{*}{J}_{12} & \overset{*}{J}_{13} \\ \overset{*}{J}_{21} & \overset{*}{J}_{22} & \overset{*}{J}_{23} \\ \overset{*}{J}_{31} & \overset{*}{J}_{32} & \overset{*}{J}_{33} \end{bmatrix} \begin{bmatrix} \frac{\partial u}{\partial r} & \frac{\partial v}{\partial r} & \frac{\partial w}{\partial r} \\ \frac{\partial u}{\partial s} & \frac{\partial v}{\partial s} & \frac{\partial w}{\partial s} \\ \frac{\partial u}{\partial t} & \frac{\partial v}{\partial t} & \frac{\partial w}{\partial t} \end{bmatrix} \tag{3.62}$$

On expansion the above equation yields,

$$\frac{\partial u}{\partial x} = \overset{*}{J}_{11}\frac{\partial u}{\partial r} + \overset{*}{J}_{12}\frac{\partial u}{\partial s} + \overset{*}{J}_{13}\frac{\partial u}{\partial t} \tag{3.63}$$

Substituting u of Eq. (3.35) in the above equation,

$$\frac{\partial u}{\partial x} = \sum_{i=1}^{8}\left(\overset{*}{J}_{11}\frac{\partial N_i}{\partial r} + \overset{*}{J}_{12}\frac{\partial N_i}{\partial s} + \overset{*}{J}_{13}\frac{\partial N_i}{\partial t}\right)u_i \tag{3.64}$$

or

$$\frac{\partial u}{\partial x} = \sum_{i=1}^{8}\frac{\partial N_i}{\partial x}u_i \tag{3.65}$$

Similarly, the remaining differentiations of displacements with respect to the Cartesian coordinate system can be derived and are given below.

$$\frac{\partial v}{\partial x} = \sum_{i=1}^{8}\frac{\partial N_i}{\partial x}v_i, \text{ and } \frac{\partial w}{\partial x} = \sum_{i=1}^{8}\frac{\partial N_i}{\partial x}w_i \tag{3.66}$$

Similarly,

$$\frac{\partial u}{\partial y} = \sum_{i=1}^{8}\frac{\partial N_i}{\partial y}u_i,\ \frac{\partial v}{\partial y} = \sum_{i=1}^{8}\frac{\partial N_i}{\partial y}v_i, \text{ and } \frac{\partial w}{\partial y} = \sum_{i=1}^{8}\frac{\partial N_i}{\partial y}w_i \tag{3.67}$$

$$\frac{\partial u}{\partial z} = \sum_{i=1}^{8}\frac{\partial N_i}{\partial z}u_i,\ \frac{\partial v}{\partial z} = \sum_{i=1}^{8}\frac{\partial N_i}{\partial z}v_i, \text{ and } \frac{\partial w}{\partial z} = \sum_{i=1}^{8}\frac{\partial N_i}{\partial z}w_i \tag{3.68}$$

Using Eqs. (3.65-3.68), $[B_i]$ can be obtained as

$$[B_i] = \begin{bmatrix} \frac{\partial N_i}{\partial x} & 0 & 0 \\ 0 & \frac{\partial N_i}{\partial y} & 0 \\ 0 & 0 & \frac{\partial N_i}{\partial z} \\ \frac{\partial N_i}{\partial y} & \frac{\partial N_i}{\partial x} & 0 \\ 0 & \frac{\partial N_i}{\partial z} & \frac{\partial N_i}{\partial y} \\ \frac{\partial N_i}{\partial z} & 0 & \frac{\partial N_i}{\partial x} \end{bmatrix} \tag{3.69}$$

Now, the matrix $[B]$ of Eq. (3.56) can be written as

$$[B] = [[B_1][B_2][B_3][B_4][B_5][B_6][B_7][B_8]] \tag{3.70}$$

with usual computation as outlined above. Assuming general linear elastic behaviour, the stress-strain relationship is of the form

$$\{\sigma\} = [\bar{Q}]\{\varepsilon\} \tag{3.71}$$

where $[\bar{Q}]$ = elastic matrix containing the appropriate material properties. The matrix $[\bar{Q}]$ will be formed as in Eqs. (3.21) and (3.26) for specially orthotropic and generally orthotropic laminates, respectively. Following the principle of virtual work, the element stiffness matrix is evaluated by assuming general linear elastic behaviour and the stress-strain relationship as given in Eq. (3.21) may be used for orthotropic FRP composite laminates. Following the principle of virtual work, the element stiffness matrix is evaluated as

$$[k^e] = \iiint_V [B]^T [\bar{Q}][B] dV \tag{3.72}$$

where $[\bar{Q}]$ is elastic matrix containing the appropriate material properties. The derivation of above Eq. (3.72) is given below.

To make the nodal forces statically equivalent to the actual boundary, the simplest procedure is to impose arbitrary (virtual) nodal displacements and to equate the external and internal work done by various forces and stresses during that displacement. Let the solid undergo such an arbitrary virtual displacement pattern $\{\delta a^e\}$ at the nodes, which results in strains $\{\delta\varepsilon\}$ and internal displacements $\{\delta\bar{u}\}$. The normal finite element discretization procedure leads to the following expressions:

$$\{\delta\bar{u}\} = [N]\{\delta a^e\}, \text{ and} \tag{3.73}$$

$$\{\delta\varepsilon\} = [B]\{\delta a^e\} \tag{3.74}$$

Then, by principle of virtual work

$$\iiint_V \{\sigma\}\{\delta\varepsilon\}^T dV - \{\delta a^e\}\{q^e\} = 0 \tag{3.75}$$

where $\{q^e\}$ is the nodal vector. On substitution of Eq. (3.56) in Eq. (3.71) and on further simplification, we get

$$\{q^e\} = [k^e]\{a^e\} \tag{3.76}$$

in which the element stiffness matrix is given by

$$[k]^e = \iiint_V [B]^T [\bar{Q}][B] dV \tag{3.77}$$

for a finite element with generally orthotropic material characteristics.

Finally the assembly of the individual element stiffness matrices has been made to form the global stiffness matrix and assembly of equilibrium equations. As the conditions of overall equilibrium are already satisfied within an element, all that is necessary is to establish equilibrium conditions at the nodes of whole domain of

analysis. After inserting the appropriate boundary conditions in the form of constraints, the resulting set of linear equations have been solved to yield the displacements. Stresses in the elements have been computed after a back-substitution of the displacements and the strain quantities as defined in Eqs. (3.71) and (3.56).

3.5 Solution procedure

Since the basic criterion of the finite element formulation in the study is that of displacements, final assembly equations are of the form

$$[K]\{r\} = [R] \tag{3.78}$$

where $[K]$, $\{r\}$ and $[R]$ are the elastic stiffness matrix, vector of nodal displacements, and vector of nodal loads, respectively for the entire assemblage. Accordingly, a large number of simultaneous equations result from the pre-processing phase. In any finite element program a large percentage of the total computation time is generally spent on the solution of stiffness equations. Therefore, the success depends on availability of an efficient means of solving the system of simultaneous equations. The first one is a direct elimination procedure where the matrix is transformed to a triangular form, which can be solved directly for the unknowns. The second one is an iterative procedure where a series of successive corrections to an original estimate of unknowns are made until the size of correction reaches an acceptable limit. In the present work a direct elimination process popularly known as "Wave Frontal Solution Technique" is employed. This method consists of assembling the finite element stiffnesses and nodal forces into a global stiffness matrix and load vector, and solving for the unknowns by means of a Gaussian elimination and back substitution process. The main idea is to assemble the equations and eliminate the variables at the same time. As the total system of equations are assembled from the element matrices, the equations for the nodal point which occur for the last time are algebraically solved in terms of remaining unknowns and are eliminated from the assembled matrix by Gaussian elimination procedure. The equations for a nodal point that occur for the first time are added to the assembled matrix as the solution progresses. The assembled matrix expands and contracts as the nodal points make their last and first appearances in the element specification. The varying size of the active matrix is the instantaneous wave front size. When several elements are connected to the same node, the degrees of freedom associated with these elements remain active in core until the wave front passes all the connected elements of that node. The arithmetic operations in this method are fewer than with other methods. Another advantage of the frontal

technique is that the nodal numbering is irrelevant whereas the ordering of the element is important.

3.6 Finite elements used for modelling of bonded joints

3.6.1 Isoparametric solid brick element (SOLID 45)

In the present Thesis, SOLID 45 is used for the 3D modelling of the adhesive layer. The SOLID 45 element is defined by its eight nodes and the orthotropic material properties. These elements possess three translational degrees of freedom at each node in x, y and z directions. This element also supports uniform reduced integration, and is very much essential for dealing with the non-linear analyses of bonded joints. A more versatile and generalised form of SOLID 45 is the layered volume element (SOLID 46) with capabilities of orthotropic layer material properties. This is described in the following Section.

3.6.2 Layered volume element (SOLID 46)

SOLID 46 is a layered version of the eight node structural solid (SOLID 45) element as shown in Fig. 3.4, designed to model layered thick shells or solids. These elements are most suitable for modelling of laminated FRP composites not only for minimizing the computational time but also for obtaining accurate results. The element has three degrees of freedom at each node: translations in the nodal x, y, and z directions.

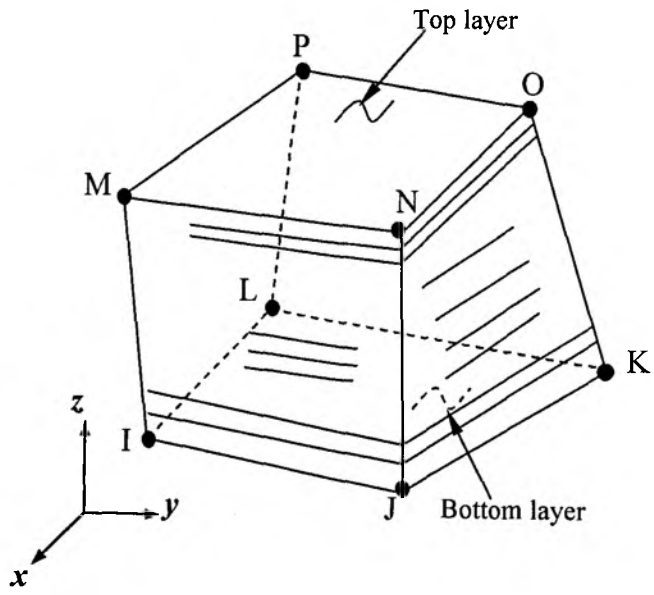

Figure 3.4 Three-dimensional layered element (SOLID 46).

The shape functions defining the geometry of element as well as the variation of displacement within the element are given by

$$[N_i] = \frac{1}{8}(1+rr_i)(1+ss_i)(1+tt_i),\ i = 1, 2, 3, \ldots\ldots 8. \tag{3.79}$$

where r, s and t are the natural coordinates and r_i, s_i and t_i are the natural coordinates for the node i. The main causes of inaccuracies of eight node solid element is its inability to represent the simple stress gradient and the displacement function given by

$$\{u\} = \sum_{i=1}^{8} N_i \{u_i\} \tag{3.80}$$

is incomplete, as it does not contain all the quadratic terms of the shape functions given by Eq. (3.79) [130, 132]. In order to improve the performance of the element in flexural mode, incompatible modes proposed by Wilson et al. [133] and Taylor et al. [134] are added to the shape function of the element. The incompatible modes are represented by shape functions of the type as given below:

$$[P_1] = (1-r^2),\ [P_2] = (1-s^2) \text{ and } [P_3] = (1-t^2) \tag{3.81}$$

The displacement variation of the eight nodded element with incompatible modes are given by

$$\{u\} = \sum_{i=1}^{8} N_i \{u_i\} + [P]\{\delta\} \tag{3.82}$$

$$\text{where } [P] = \begin{bmatrix} P_1 & P_2 & P_3 & 0 & 0 & 0 & 0 & 0 & 0 \\ 0 & 0 & 0 & P_1 & P_2 & P_3 & 0 & 0 & 0 \\ 0 & 0 & 0 & 0 & 0 & 0 & P_1 & P_2 & P_3 \end{bmatrix} \tag{3.83}$$

$$\text{and, } [\delta]^T = [\delta_1 \quad \delta_2 \quad \delta_3 \quad \delta_4 \quad \delta_5 \quad \delta_6 \quad \delta_7 \quad \delta_8 \quad \delta_9] \tag{3.84}$$

The strain at any point in the element can be written as

$$\{\varepsilon\} = [\varepsilon_1 \quad \varepsilon_2 \quad \varepsilon_3 \quad \gamma_{12} \quad \gamma_{23} \quad \gamma_{31}]^T \tag{3.85}$$

and the strain displacement relation can be written as

$$\{\varepsilon\} = [B]\{d\} \tag{3.86}$$

where

$$\{d\}^T = [u_1 \quad v_1 \quad w_1 \quad . \quad . \quad . \quad u_8 \quad v_8 \quad w_8 \quad \delta_1 \quad \delta_2 \quad . \quad . \quad . \quad \delta_8 \quad \delta_9] \tag{3.87}$$

This can be written as

$$\{\varepsilon\} = \sum_{i=1}^{8}[B_i]\{d_i\} + \sum_{j=1}^{8}[P_j']\{\delta\} \tag{3.88}$$

or $$\{\varepsilon\} = [B_a]\{d\} + [P']\{\alpha\} \tag{3.89}$$

where

$$[\delta]^T = [\delta_1 \quad \delta_2 \quad \delta_3 \quad \delta_4 \quad \delta_5 \quad \delta_6 \quad \delta_7 \quad \delta_8 \quad \delta_9],$$

$\{d\}^T = [u_1 \quad v_1 \quad w_1 \quad . \quad . \quad . \quad u_8 \quad v_8 \quad w_8]$ and $[P']$ represent the derivative of $[P]$ with respect to the global coordinates x, y, z.
Hence,

$$[B_i] = \begin{bmatrix} \frac{\partial N_i}{\partial x} & 0 & 0 \\ 0 & \frac{\partial N_i}{\partial y} & 0 \\ 0 & 0 & \frac{\partial N_i}{\partial z} \\ \frac{\partial N_i}{\partial y} & \frac{\partial N_i}{\partial x} & 0 \\ 0 & \frac{\partial N_i}{\partial z} & \frac{\partial N_i}{\partial y} \\ \frac{\partial N_i}{\partial z} & 0 & \frac{\partial N_i}{\partial x} \end{bmatrix} \text{ for } i = 1, 2, \ldots\ldots 8 \tag{3.90}$$

$$[P_j'] = \begin{bmatrix} \frac{\partial P_j}{\partial x} & 0 & 0 \\ 0 & \frac{\partial P_j}{\partial y} & 0 \\ 0 & 0 & \frac{\partial P_j}{\partial z} \\ \frac{\partial P_j}{\partial y} & \frac{\partial P_j}{\partial x} & 0 \\ 0 & \frac{\partial P_j}{\partial z} & \frac{\partial P_j}{\partial y} \\ \frac{\partial P_j}{\partial z} & 0 & \frac{\partial P_j}{\partial x} \end{bmatrix} \text{ for } j = 1, 2, 3 \tag{3.91}$$

Now $[P']$ can be written as

$$[P'] = [[P_1'][P_2'][P_3']] \tag{3.92}$$

and, hence

$$[B] = [B_1][B_2][B_3][B_4].....[B_8][P_1'][P_2'][P_3'] \tag{3.93}$$

The mass and stiffness matrix for the element are given as

$$[m] = \int_{-1}^{+1}\int_{-1}^{+1}\int_{-1}^{+1}[N]^T \rho[N]\det[J]drdsdt \tag{3.94}$$

and

$$[k^e] = \int_{-1}^{+1}\int_{-1}^{+1}\int_{-1}^{+1}[B]^T[\bar{Q}][B]\det[J]drdsdt \tag{3.95}$$

where $[N] = [[N_1][N_2][N_3][N_4].....[N_8]]$ (3.96)

and, the Jacobian $[J]$ can be defined as

$$[J] = \begin{bmatrix} \frac{\partial x}{\partial r} & \frac{\partial y}{\partial r} & \frac{\partial z}{\partial r} \\ \frac{\partial x}{\partial s} & \frac{\partial y}{\partial s} & \frac{\partial z}{\partial s} \\ \frac{\partial x}{\partial t} & \frac{\partial y}{\partial t} & \frac{\partial z}{\partial t} \end{bmatrix} \tag{3.97}$$

In evaluating the mass and stiffness matrix for this element, the density ρ and the elasticity matrix $[\bar{Q}]$ depend upon the material properties and the fiber orientation of the layers through-the-thickness of the element. So, numerical integrations for these

elements have been carried out from layer to layer through-the-thickness using Gaussian Quadrature Integration Technique. In this way, several layers are grouped together into one element. The mass matrix of this element given by Eq. (3.94) is a consistent mass matrix since same displacement functions are used to formulate stiffness and mass matrix of the element. The stiffness matrix of Eq. (3.95) is of size 33×33 and contains coefficients pertaining to incompatible modes. However, these terms are eliminated using static condensation technique and the condensed matrix will be of the order of 24×24 pertaining to the nodal degrees of freedom.

3.6.3 Multi-Point Constraint element (MPC 184)

MPC184 comprises a general class of Multi-Point Constraint element that implements kinematic constraints using Lagrange multipliers. These elements as shown in Fig. 3.5 are commonly known as constraint elements (Appendix I) and are used in situations to impose some kind of constraint to meet certain requirements. The MPC elements consist of 3-nodes. One of the node *k* is called as slave node which allows to slide on a line joining the other two nodes *i* and *j* designated as master nodes.

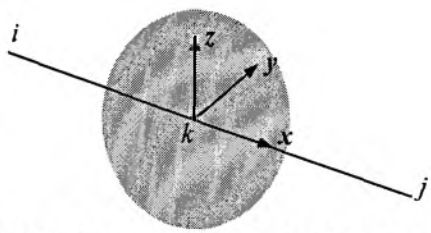

Figure 3.5 Geometry of MPC 184 element.

3.6.4 Contact or gap element (CONTA 178)

Figure 3.6 shows contact element CONTA 178 (Appendix II) to prevent the interpenetration of delaminated layers with implementing relevant interlayer contact stiffness between the adjacent layers. The force deflection relationships for the contact element can be separated into the normal and tangential (sliding) directions. The orientation of the interface is defined by the respective interlaminar node locations (*i* and *j*). Alternately this can be achieved by a user specified contact normal direction algorithm. The interface is assumed to be perpendicular to the *i-j* line or to the specified gap direction. The element has the capability to model such features as contact and sliding between any two nodes of any types of elements. The element has two nodes with three degrees of freedom at each node with translations in the *x*, *y*, and *z* directions. The element is capable of supporting compression in the contact

normal direction and Coulomb friction in the tangential direction. The element may be initially preloaded in the normal direction or it may be given a gap specification. The solid model data is transferred to FE model data by operation option. The damping capability is used for modal, harmonic or transient analyses.

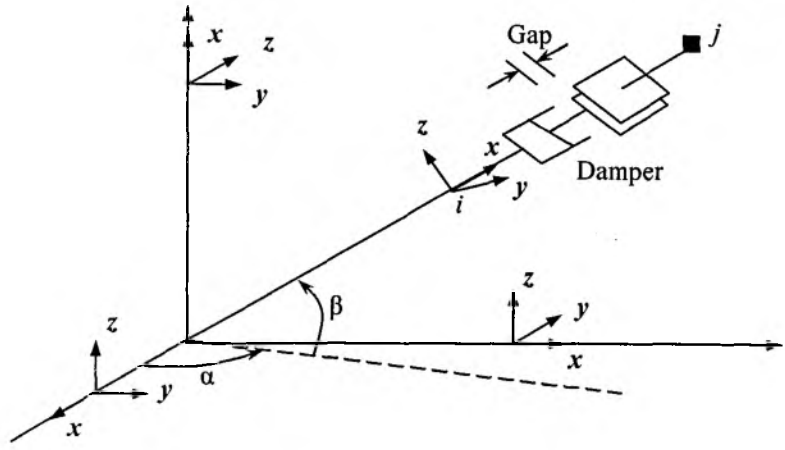

Figure 3.6 Node to node contact element (CONTA 178).

3.7 Mechanics of adhesion failure and delamination damages in bonded joints of laminated FRP composites

In this section, failure modes pertaining to the adhesion failure which usually initiates at the stress singularity points and propagates along the interfacial surfaces of the joint and the delamination induced damages (responsible for adherend failure) of various types of joints viz. SLJ, LSJ, DLJ and SWJ have been addressed in detail. A quite good number of research works have been existing addressing the cohesive failure which is confined to the adhesive layer and hence not included in the present study. Some typical failure modes and their propagation for DLJ and SLJ have been shown in Fig. 3.7. The most important failure modes in an adhesively bonded joint are due to the failure of laminated adherends. Due to the laminated nature of the FRP composite members and the relative weakness in the through-the-thickness direction, the failure mechanism of adhesively bonded joints become the focus of research. Figure 3.8 shows two typical failure modes such as net section fracture and delamination induced damages for an adhesively bonded joint. The failure due to delamination induced damages in an adhesively bonded joint have been shown in Fig. 3.9, which indicates that the joint may fail with two possibilities; (i) due to the

surface ply fracture and, (ii) due to the propagation of delamination damages in the adherend.

There is a fundamental difference between the mechanics of delamination damages in FRP composites and the mechanics of damages in isotropic materials like metals or their alloys. In metals, the largest damage in the form of a crack existing in the component has been assumed to control the strength. Failure of an adhesively bonded structure may be directly related, by the material's fracture toughness, to catastrophic propagation of this crack. However, delamination in laminated adherend subjected to in-plane loading is a subcritical failure mode whose effect may be (i) a stiffness loss that is benign in terms of the structural failure, (ii) a local tensile strain concentration in the load bearing plies that causes tensile failure, or (iii) a local instability that causes further growth which ends in compressive failure. In the latter two cases the delamination leads to a redistribution of structural load paths which, in turn, precipitates structural failure. Hence, delamination is indirectly responsible for the final failure of a composite bonded joint structure, whereas crack propagation in a metal is directly responsible for structural failure.

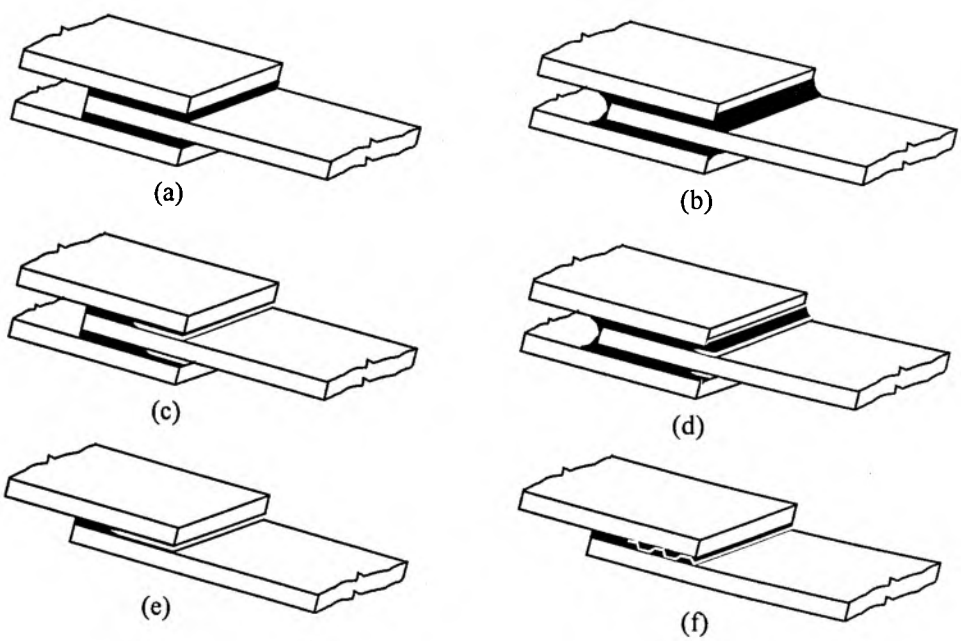

Figure 3.7 Different types of failure modes and their propagation paths in adhesive bonded joints; (a) DLJ without fillet, (b) DLJ with fillet, (c) possible adhesion failure

initiation and propagation path in a DLJ (without fillet), (d) possible adhesion failure initiation and propagation path in a DLJ (with fillet), (e) cohesion failure propagation path in an SLJ and (f) wavy failure propagation path along the two interfacial surfaces in an SLJ.

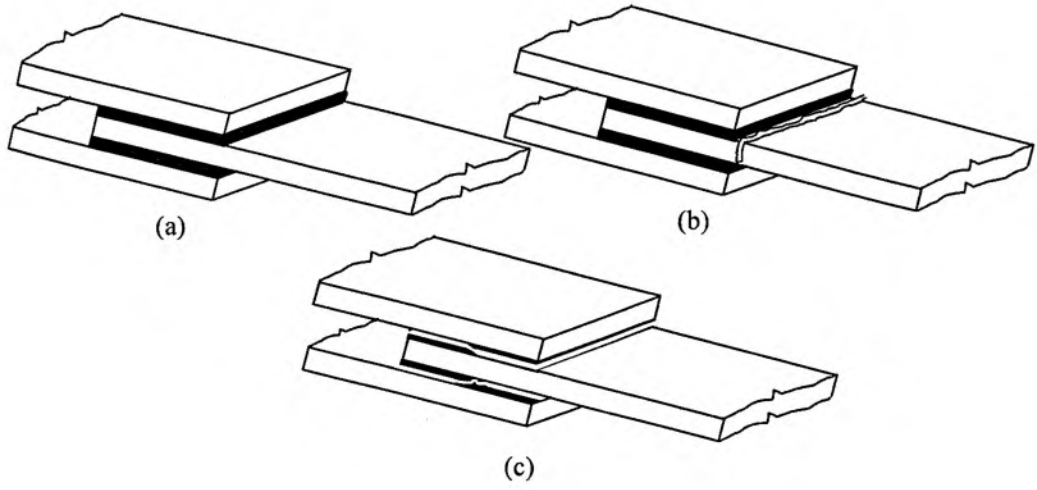

Figure 3.8 Typical failure modes in adhesive bonded DLJ; (a) intact joint, (b) net-section adherend failure and (c) failure due to adhesion failure.

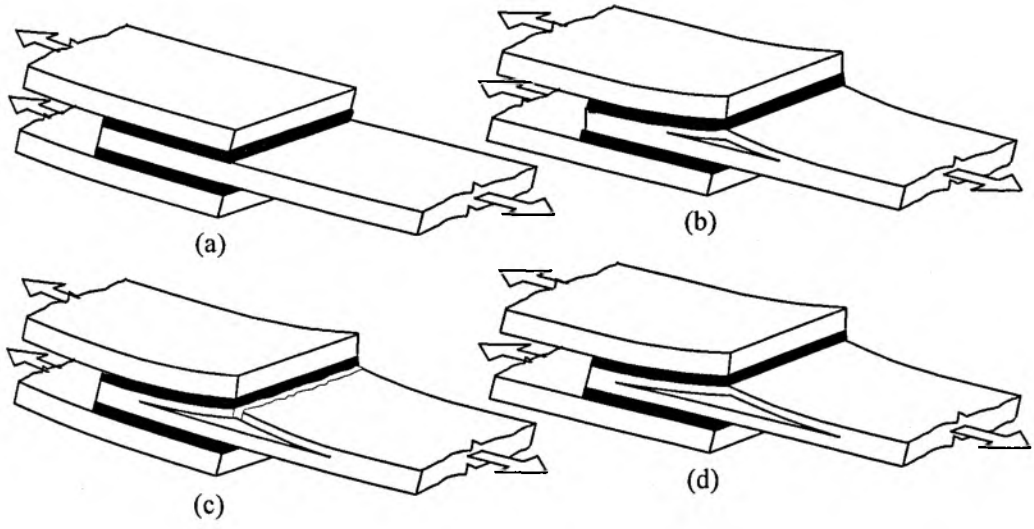

Figure 3.9 Peel stress induced delamination damages in DLJ; (a) DLJ without damage, (b) onset of delamination induced damage in the FRP composite adherend,

(c) failure of DLJ due to surface ply fracture and (d) joint failure due to propagation of delamination damage.

Consequently, interlaminar fracture toughness for composite delamination does not have the same significance to design as fracture toughness does for a metal. The designer must be able to determine the consequence of the delamination in terms of structural load redistribution and relate this to some appropriate structural failure criterion. Nevertheless, fracture mechanics is a useful tool for understanding the mechanics of delamination, to determine the variables that control when delaminations form and grow, and for characterizing the inherent delamination resistance of the composite.

3.8 Adhesion failure and delamination damage onset criterion

Accurate prediction of adhesively bonded joint strength and service life has been of the challenging tasks for assessing the structural integrity of any bonded structures. There is lack of complete understanding of failure mechanisms in various types of adhesively bonded joints. Joint failure mechanism includes the onset of initial failure, followed by stable failure propagation and finally the catastrophic damage propagation and this phenomenon becomes complex and much involved when the adherends are laminated FRP composites. There are a large number of failure criteria available that have been used for the prediction of onset of damages in the adhesively bonded joints. Two approaches have been used for prediction of location of onset of damages. One of them is based on mechanics of materials approach and the other follows the fracture mechanics procedures.

Failure criteria developed for isotropic materials have been utilized to predict the cohesive failure which occurs in the adhesive layer of adhesively bonded structures. Raghava et al. [135] have proposed a parabolic yield criterion as given below and this has been used for prediction of location of cohesive failure initiation in an adhesively bonded joint.

$$(\sigma_1-\sigma_2)^2+(\sigma_2-\sigma_3)^2+(\sigma_3-\sigma_1)^2+2(|Y_C|-Y_T)(\sigma_1+\sigma_2+\sigma_3)=2|Y_C|Y_T \qquad (3.98)$$

where σ_1, σ_2 and σ_3 are the allowable principal stresses causing yield and $|Y_C|$ and Y_T are the absolute values of the compressive and tensile yield stresses, commonly

known as strengths. It may be noted that when $|Y_C|$ and Y_T are equal, the above yield criterion reduces to the most familiar von Mises cylindrical criterion.

The interfacial failure also known as adhesion failure initiates from the stress singularity points of adhesively bonded structures. Also, delamination induced damages in the laminated FRP composite adherends have been considered as adhesion failure. For laminated composite adherends, adherend failure can occur due to high bending moment in the overlap zone of an adhesively bonded joint. The interlaminar delamination damages (as shown in Figs. 3.8 and 3.9) occur due to the high peel stress and low interlaminar shear strength. Thus, the onset of failures due to adhesion failures or the delamination damages has been predicted using Tsai-Wu's coupled stress failure criterion depending on the failure index values e_a and e_d. Accordingly, e_a and e_d, denote the failure indices due to the adhesion failure and the delamination induced damage, respectively over the bondline interfacial surfaces and below the surface ply adjacent to the adhesive layer of the bonded joint. The failure surface in the stress space can be represented in the following scalar form:

$$f(\sigma_k) = F_i\sigma_i + F_{ij}\sigma_i\sigma_j = 1 \tag{3.99}$$

where $i, j, k = 1, 2, \ldots\ldots 6$. F_i and F_{ij} are strength tensor.

Generally, the interlaminar or out-of-plane stresses are responsible for the initiation of adhesion and delamination failures and, hence, these stress components only have been used in Eq. (3.99) to determine the failure index values e and are given by

(i) Delamination in tension, for $\sigma_z > 0$;

$$\left(\frac{\sigma_z}{Z_T}\right)^2 + \left(\frac{\tau_{xz}}{S_{xz}}\right)^2 + \left(\frac{\tau_{yz}}{S_{yz}}\right)^2 = e^2 \begin{cases} e \geq 1, \text{ failure} \\ e < 1, \text{ no failure} \end{cases} \tag{3.100}$$

(ii) Delamination in compression, for $\sigma_z < 0$;

$$\left(\frac{\sigma_z}{Z_C}\right)^2 + \left(\frac{\tau_{xz}}{S_{xz}}\right)^2 + \left(\frac{\tau_{yz}}{S_{yz}}\right)^2 = e^2 \begin{cases} e \geq 1, \text{ failure} \\ e < 1, \text{ no failure} \end{cases} \tag{3.101}$$

3.9 Modelling and simulation of adhesion failure and delamination damages

Damages in bonded joints of laminated FRP composites are a function of orientation, aspect ratio, local volume fraction of the constituents, reinforcement direction and distribution, residual stresses, stacking sequence, ply overlap/ply drop, the

mechanical properties of the components as well as the configurations of joints. These macro-structural and micro-structural parameters scatter considerably, inducing spatial fluctuations in the mechanical properties. The damage process occurring inside the composite adherends can also be different from location to location and their growth and propagation also may be in different direction involving several complex phenomena. Delamination mode of failure is especially of insidious nature. It may easily escape detection since they are frequently embedded within the composite structure. They may arise out of low-velocity impact damage or manufacturing defects or sometimes may be service induced/operational malfunctioning.

In some specific cases, delamination may be strongly dominated by one mode with the other modes playing a negligible role. In such cases direct comparison can be made between the strain energy release rate and toughness parameter for the dominant mode. However, in general, consideration must be given to mixed mode loading and growth. In mixed mode cases, the failure condition for each mode cannot be regarded as independent of the energy release rate of the other. Hence an interactive criterion is to be used to find threshold or critical state of delamination for the stability and service-fit considerations of the structure. The purpose of this study is to understand the fracture behaviour in FRP composite laminates having different bonded joint configurations with embedded adhesion failure and/or delamination damages emanating from the critical locations and subjected to various kinds of mechanical loadings leading thereby to mixed mode failure conditions.

In this study, the modified crack-closure integral method based on Irwin's virtual crack extension concept is employed to calculate the values of strain energy release rate (SERR) viz, G_I, G_{II} and G_{III}. The SERR associated with crack extension is equal to the work required to close the incremental crack. The SERR procedures have been universally accepted as an indicator of delamination growth and propagation behaviour. The individual mode of SERR is calculated as the product of nodal forces at the crack front and corresponding displacements behind the crack front. Referring to Fig. 3.10, the double nodes created to simulate the crack growth at A and D are constrained before crack propagation. Nodal forces F_x and F_y keep the nodes together and work is done against these forces for the Δa propagation or crack closure along the interface. Δu and Δv are the respective displacements behind the crack front along x and y directions.

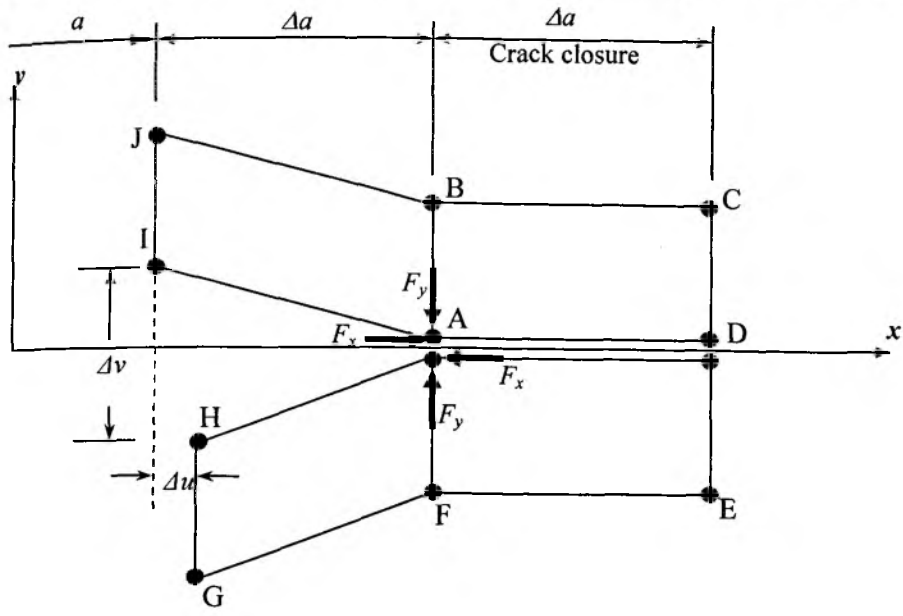

Figure 3.10 Representation of nodal forces at crack tip and displacements behind it.

3.9.1 Modelling approach

Modelling of bonded joint damages possesses the problem of material heterogeneity and anisotropy along the interface. Crack tip elements are being used for modelling square root tip singularity in cracked components [136]. Ingraffea et al. [137] have modelled the delamination boundary by using prismatic elements formed by collapsing one face of the solid/brick element as the case may be, and moving the nodes on the other adjacent four edges of the element to their quarter length, thereby satisfying the inverse square root singularity characteristic of linear fracture mechanics. These singular elements account for the square root singularity only, but not the oscillatory behaviour of the stresses as the crack front is approached in bimaterial interface. Again at the interface of a composite sublaminate the assumption of square root singularity is not strictly true. Shell and plate elements have been advantageously used due to its computational efficiency in incorporating laminate characteristics for delamination modelling. Interlaminar fracture behaviour was implemented by conducting a global-local analysis of delamination front [138-140].

The modelling approach requires prior identification of interply or bondline regions where delamination is expected to be critical to the response. In these regions, the structure is modelled as sublaminates separated by the bond or the interface resin layer containing the embedded delamination of various shapes/sizes. As shown in Fig. 3.11 the bondline itself is modelled by multi-point constraints connecting nodes

on opposite sides of the bond. Alternatively zero thickness interface elements can also be used to model the resin rich region. For simplicity of computation, it is assumed that nodes located on opposite sides of the bond fall upon the same normal vector. No offset in the plane of the bond is permitted between the endpoints of the springs. The interlayer is modelled as two separate layers, having identical isotropic properties, located above and below the delamination plane. Inside the delamination zone compatible contact/gap elements are used to prevent the interpenetration of top and bottom layer, which otherwise would make the analysis physically unrealistic.

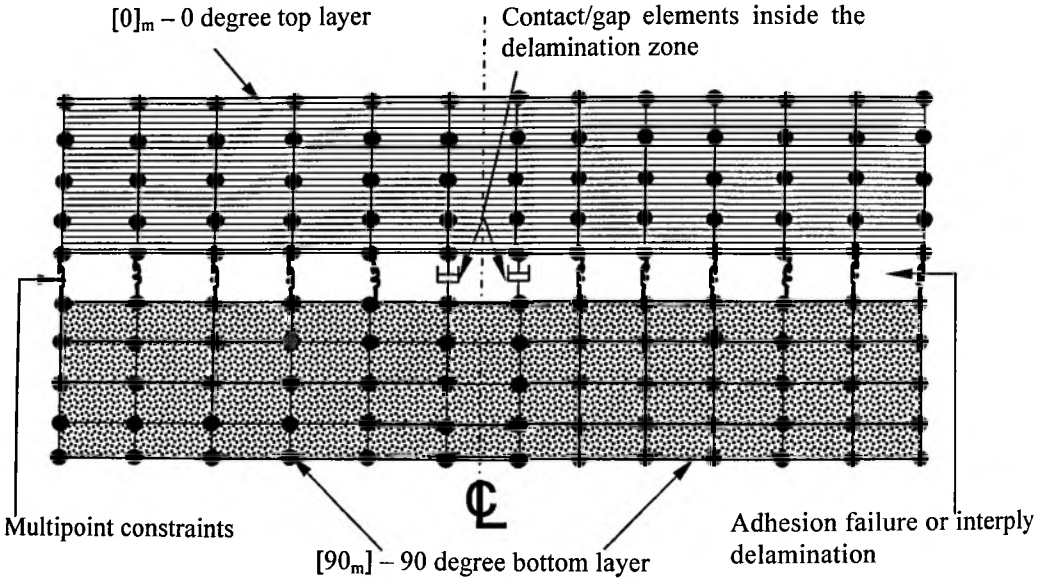

Figure 3.11 Schematic representation of modelling of interply delamination in cross-ply laminate.

3.9.2 Modelling of adhesion failure and delamination damages using sublaminate technique

One of the main problems remaining with application of the 3D finite element method to delaminations is that a very fine mesh is normally required in the region of the crack front. This presents both a theoretical and practical difficulty. The theoretical concern commonly raised is that the element size in the region of the crack front often has to be selected so small as to be very much on the scale at which the material cannot be treated as homogenous. This issue is, justifiably, the subject of debate in the research community. However, it is apparent that it does not, in itself; impose a significant restriction on the utility of the method as a tool for engineering approximation. A schematic three-dimensional representation of laminate stacking

sequences in the composite laminate has been displayed in Fig. 3.12 with respect to *xy* mid-plane. Figure 3.13 shows sublaminate modelling technique used for laminated composite SLJ embedded with through-the-width interlaminar delamination damage. Initially, the template of FE meshing of the delamination plane is made and it is repeated along the third direction to obtain the discretization of the whole domain of the single lap joint. Eight node SOLID 46 layered elements incorporated in ANSYS 10.0 FE software have been used for modelling the analysis domain.

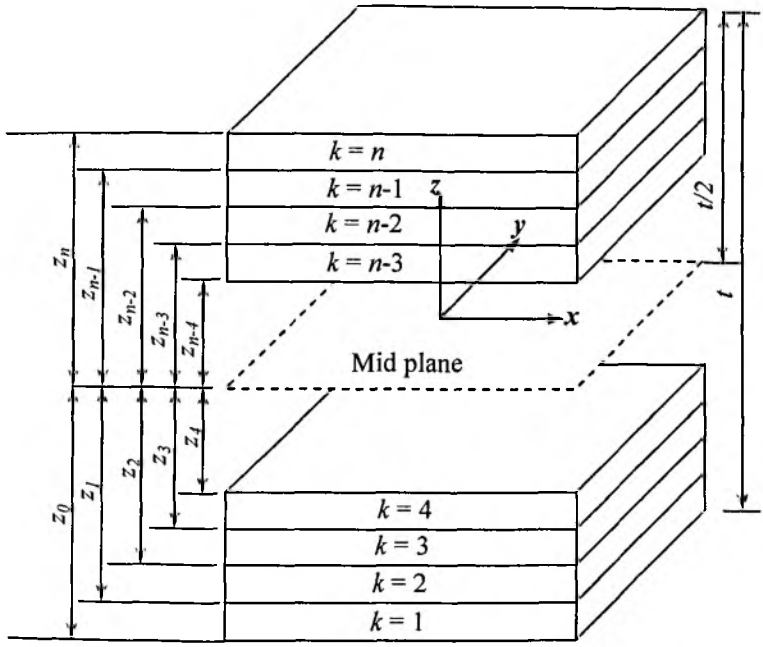

Figure 3.12 Three-dimensional representation of laminate stacking sequence.

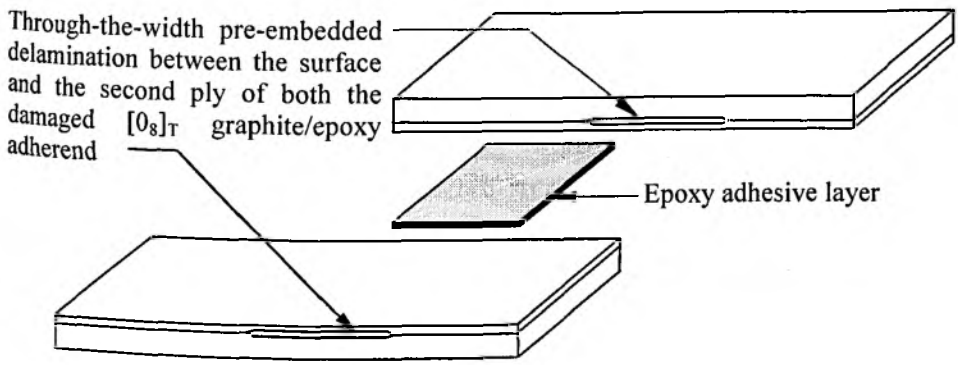

Figure 3.13 Sublaminates of laminated composite SLJ embedded with through-the-width delaminations.

3.10 Adhesion failure and delamination damage studies with Strain Energy Release Rate (SERR) approach

The structural integrity of adhesively bonded structure made of laminated FRP composite material is greatly hampered due to the presence of interlaminar embedded delaminations. For delamination studies, Classical laminated plate theories cannot be applied, as in this case the stresses σ_z, τ_{yz}, τ_{xz} are not zero, and rather they govern progressive propagation of delamination front. So the studies of interlaminar stresses become important for proper characterization of delamination failure. These interlaminar stresses are due to the mismatch of Poisson's ratio and influence coefficients between two consecutive layers. Classical lamination theory assumes a plane stress state involving σ_x, σ_y and τ_{xy}, but the existence of interlaminar stresses have been recognized for many years.

Early studies have shown that interlaminar shear stresses exist and that these stresses reach a maximum near the free edges. Subsequent works revealed that interlaminar normal stresses can also be generated and affect the composite behaviour. Even for a simple tensile loading on an angle ply laminate as τ_{xy} is zero at the free edge, for moment equilibrium another stress must exist to balance. So, the classical lamination theory holds at the center of an intact laminate only [141-144]. The complex stress-state occurring at free edges are difficult to model and analyze. The role of interlaminar stresses with respect to damage initiation and progression have been numerically investigated with finite element technique and strain energy release rate as the characterizing parameter of delamination mode of failure. This has been compared to some existing semi-analytical models. For delamination fracture studies, both stress intensity factor approach and strain energy release rate procedures may be adopted. But fracture toughness as the critical stress intensity factor, K_c, depends upon material and lay up. As such for each combination of material and lay up, testing is to be done to determine K_c, which would be prohibitively expensive. This leads to as a priori the calculation of individual modes of strain energy release rates for studying the delamination growth behaviour in adhesively bonded joints of laminated FRP composites.

3.10.1 Computation of Strain Energy Release Rate (SERR)

For a proper understanding of stable and unstable crack growth at different crack lengths, evaluation of energy release rates are necessary. Mixed mode critical energy release rate ratio is indicative of stable continuous crack growth through the laminate

specimen [145]. Hong and Liu [146] identified that the delamination area per unit impact energy in low velocity impact is similar to the critical strain energy release rate at the delamination front. Hence for a proper characterization of interlaminar fracture in composite laminates, analysis of strain energy release rates at the delamination front should be conducted. Strain energy release rate formulae were being predominantly used to characterize the interlaminar fracture in delamination and debonding analysis of composite structural members [147-149]. Calculations of energy release rate components are based on Irwin's theory of Crack Closure Technique [108]. Energy release rate procedure is robust as it is based on a sound energy balance principle and mode separation of SERR is possible. This can be easily incorporated into an analytical formulation and compared with critical fracture energy values for the efficient prediction of delamination growth and propagation.

The behaviour of an existing pre-embedded delamination is modelled as being governed by the values of three modes of SERR around the delamination front. However in composite laminates, due to their inherent complications, exact closed form expressions for the energy release rates are not possible. This leads to the finite element evaluation of energy release rates based on the principles of Linear Elastic Fracture Mechanics (LEFM). Estimation of the strain energy release rates G_I, G_{II} and G_{III} is the central notion of a delamination analysis. This interlaminar fracture energy release rate calculations depend primarily on the nature of the applied stress state and the crack geometry. Analytical solutions are available only for some simple stress states and geometries. However practical utility of such straightforward analytical solutions are limited. The implementation of the fracture mechanics approach relies on estimation (typically by analytical or numerical techniques) of the applied strain energy release rate. Behaviour of straight free edge problem can be analyzed as a two-dimensional problem. However the behaviour around a curved free edge or corner is inherently a three-dimensional problem. The energy release rate, denoted by G is defined for virtual crack extension in the same plane as

$$G = \frac{dW}{da} - \frac{dU}{da} \tag{3.102}$$

where W is the work done by the external traction per unit thickness, U is the strain energy of the body per unit thickness and a is the crack length.

The physical significance of the energy release rate corresponds to the rate of change of energy of the system per unit area of crack growth. For studies on delamination onset and growth, this value is compared with the toughness parameter G_c (material tests). It is convenient, in simplifying both analysis and test requirements, to decompose the applied strain energy release rate and the toughness into parameters corresponding to three possible modes of cracking. A damage may be stressed in four different modes, these modes acting independently or together (Figs. 1.10 and 1.11). Three strain energy release rates (G_I, G_{II} and G_{III}) and three material property parameters (G_{IC}, G_{IIC} and G_{IIIC}) are defined as corresponding to cracking modes *I*, *II* and *III* i.e. opening, shearing and tearing, respectively. The three critical SERR parameters G_{IC}, G_{IIC} and G_{IIIC} can be related to three fracture toughness parameters K_{IC}, K_{IIC} and K_{IIIC}. Thus, after evaluation of G_I, G_{II} and G_{III}, a comprehensive idea of the structural integrity of the structure is available. Failure mode studies of FRP composites are quite complex and involve a lot many data due to the anisotropic material properties. However, analysis of failure of composite laminates can be conducted in three ways as follows

- Empirical
- Analytical
- Numerical

The experimental results can subsequently be compared with the above methodologies to have a qualitative understanding of failure phenomena in FRP composites. However, difficulties in exact modelling of fractured laminate and simulation of crack growth in experimental setups sometimes restrict the analysis validation. The analysis techniques followed can be broadly categorized as follows.

- Stress Intensity Factor (SIF) calculations
- Evaluation of Strain Energy Release Rates (SERR)

There are basically two approaches in designing to take account of delamination characteristics. The first is mechanics of materials approach [150] in which, the interlaminar stress state over a critical distance from a free edge is calculated. This stress state is then compared with a failure criterion, which may be simply the transverse tensile strength or a more complex three-dimensional criterion. Brewer and Lagace [151] proposed a quadratic stress criterion as follows to predict delamination initiation.

$$e = \left[\frac{\overline{\sigma_z}}{Z}\right]^2 + \left[\frac{\overline{\tau_{yz}}}{S_{yz}}\right]^2 + \left[\frac{\overline{\tau_{xz}}}{S_{xz}}\right]^2 \tag{3.103}$$

with,

$$\left[\overline{\sigma_z}, \overline{\tau_{yz}}, \overline{\tau_{xz}}\right] = \frac{1}{x_c}\left[\int_0^{x_c} \sigma_z, \tau_{yz}, \tau_{xz}\right] dx \tag{3.104}$$

where, $\overline{\sigma_z}, \overline{\tau_{yz}}, \overline{\tau_{xz}}$ are the average interlaminar stresses along the delamination front and Z, S_{yz}, and S_{xz} are tensile strengths across the thickness, longitudinal shear strength and lateral shear strength, respectively, x_c is the critical distance over which the interlaminar stresses are averaged. If $e \geq 1$, then delamination initiation occurs; If $e < 1$, no delamination initiation is there. Once the critical distance over which the stresses are to be averaged has been established, this type of analysis may be integrated into a program for either a parametric design study or dimensioning optimization of the structures.

The second approach is based on a fracture mechanics methodology. Delamination is an example of the fracture mechanics for studying the behaviour of an orthotropic material. Two distinct parameters either a stress intensity (K) criterion or an energy release rate (G) criterion is invoked to evaluate the damage/crack growth behaviour of a laminate. For studying the potential of a defect, in the former case, the crack tip stress intensity factor K is compared with critical stress intensity factor K_c. However in composite materials the crack tip stress geometry function relating K to the stress σ and defect dimension a is not the standard isotropic factor and therefore most delamination studies and tests have been developed using the energy criterion. The energy criterion, first proposed by Griffith [94] for brittle materials, relates the energy necessary for unit area of crack propagation to the energy supplied to the stressed body. Thus crack extension to begin to occur when,

$$\frac{dW}{dA} - \frac{dU}{dA} > \frac{dU'}{dA} + \gamma \tag{3.105}$$

or $$G > G_C . \tag{3.106}$$

The left hand side of the above equation represents the difference between the applied work (W) and the global elastic strain energy (U), while the right hand side includes the irreversible (dissipated) strain energy (U') and the energy required to form new crack surface (γ). Thus, for material showing some ductility, crack propagation will occur when the crack driving energy release rate exceeds a critical value G_C. This criterion has the following two meaningful assumptions.

- The crack propagates in a self-similar manner and, in the same plane.
- The damage zone is small relative to the size of the specimen.

Thus, the Mode *I*, Mode *II*, and Mode *III* critical strain energy release rates G_{IC}, G_{IIC} and G_{IIIC} characterize the fracture behaviour of the material, respectively.

3.11 FE modelling and simulation of adhesion failure and delamination damage propagation

For most general geometries and loadings encountered in practice, numerical techniques are being commonly used to calculate the strain energy release rates. Finite element method is the most widely accepted procedure followed in the numerical analysis [152]. The advantage of the finite element method is that it imposes no inherent restriction on geometry, applied stress state and material behaviour. The approach to estimating strain energy release rates using finite element methods is initially to evaluate the (W-U) term in equation (3.102) for two models, one with an existing crack and the second considering an incremental growth in crack surface area. Though this approach is useful in certain cases but possesses difficulty in general applications. The main problem being that a G value for the structure as a whole is obtained with no information on its distribution along the crack front nor on the relative magnitude of the individual modes. Hence, except in some specific cases, it is not possible to apply the results in a failure criterion requiring direct comparison of strain energy release rate with material toughness. An alternative approach, still in reasonably common use, is to calculate G by integration of energy along a contour around crack front, i.e. determination of the J-integral. This has the benefit of allowing estimation of a local strain energy release rate and evaluation for each model. However, this requires the use of special collapsed elements at the crack front and this can add significantly to mesh and hence model complexity. A further problem is that it is not strictly applicable to cases where dissimilar materials on opposing sides of the crack tip give rise to an oscillating singularity, thereby requiring a three-dimensional analysis. In response to the above difficulties, several alternative

approaches have been developed in application of the finite element method. One of the most useful is the Virtual Crack Closure Technique (VCCT). In literature it is also sometimes addressed as Modified Crack Closure Integral (MCCI).

3.11.1 Modified Crack Closure Integral (MCCI)

For a straight edged crack front, the curvature plane and normal are constant everywhere. So mode definition is intuitive and constant for the entire front. Individual modes are well defined along the crack front. Mode *I* is caused by the out-of-plane crack opening, Mode *II* by the shear perpendicular to the straight delamination/crack front and Mode *III* by the shear component tangential to the front. Advantage is that a single model can be used for estimating strain energy release rates along the delamination/crack front. A major benefit of the method is that it allows accurate estimation of strain energy release rate while using a relatively simple mesh (although a fine mesh may still be needed at the crack tip). Furthermore, it allows separation of individual modes of SERRs G_I, G_{II} and G_{III} by isolating the relevant stresses and displacements for inclusion in the integrations. Further benefits include (i) the calculation of these values on an element-by-element basis and provision of results on a node-by-node basis and (ii) straight forward treatments of oscillatory singularities in stress. However this makes some assumptions regarding possible changes in the stress state for an incremental closure of the crack. Numerical analyses are conducted to evaluate the stress and displacement fields ahead of the delamination front. Fig. 3.14 shows the schematic of self-similar delamination crack front propagation of Δa crack length.

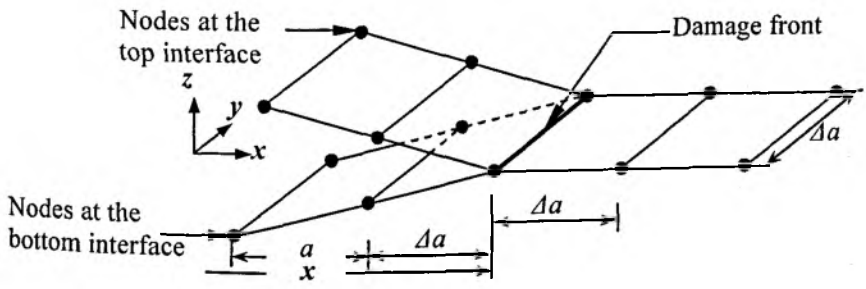

Figure 3.14 Schematic of propagation of damage front in 3D analyses.

Consider a 3D finite element idealization with finite elements symmetric about the damage front as shown in Fig. 3.15. If the adhesion failure propagates from a to $(a+\Delta a)$, for infinitesimal small values of Δa, the opening displacement behind the new damage front will be approximately the same as that behind the original one. Then the work required for propagation of damage length from a to $(a+\Delta a)$ is the same as that necessary to close the virtually opened damage length $(a+\Delta a)$ to damage length a. Irwin [108] computed this work as:

$$W = \frac{1}{2}\int_0^{\Delta a}\left[\sigma_z(\Delta a - x,0)\times w(x,0) + \tau_{xz}(\Delta a - x,0)\times u(x,0) + \tau_{yz}(\Delta a - x,0)\times v(x,0)\right]\times dx \tag{3.107}$$

where $w(x,0)$, $u(x,0)$ and $v(x,0)$ are the damage opening displacements in modes *I*, *II* and *III* at a distance $(\Delta a\text{-}x)$ behind the damage front and $\sigma_z(\Delta a\text{-}x,0)$, $\tau_{zx}(\Delta a\text{-}x,0)$ and $\tau_{yz}(\Delta a\text{-}x,0)$ are the corresponding stress components.

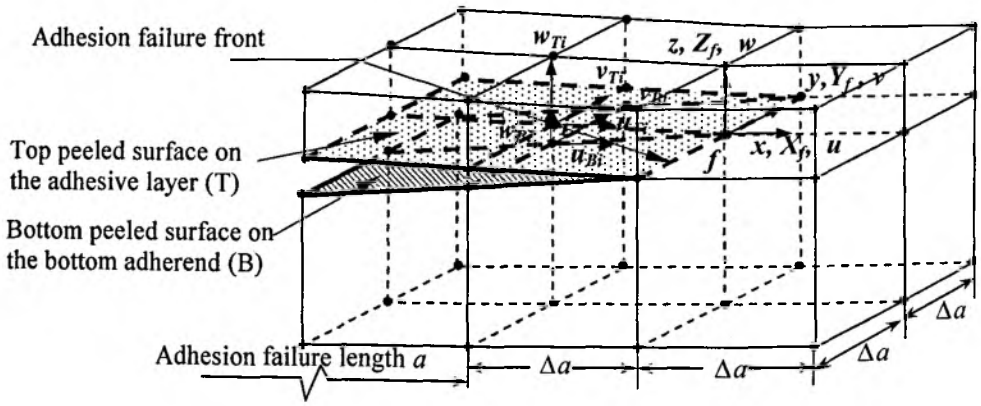

Figure 3.15 MCCI applied to the SLJ for propagation of adhesion failure length a at the interface between the bottom adherend and adhesive layer.

Irwin [108] conceptualized that stress field ahead of the crack due to an infinitesimal small crack extension could be made equal to that behind it due to the crack closure, when the crack was assumed to propagate in the same plane. Rybicki and Kanninen [13] discussed the advantage of the method of Modified Crack Closure Integral (MCCI) based on the postulates of Irwin's theory of crack field solution for

calculating the individual modes of strain energy release rates for cracks in bi-material interface. The SERR (G) is given by:

$$G = \lim_{\Delta a \to 0} \frac{W}{\Delta A}$$
$$= G_I + G_{II} + G_{III} \tag{3.108}$$

Another advantage of this MCCI method is that it is not very sensitive to mesh design [111, 153]. Using the modified crack closure integral the three individual modes of energy release rates can be expressed as follows:

$$G_I = \lim_{\Delta a \to 0} \frac{1}{2\Delta A} \int_{a}^{a+\Delta a} \int_{-\Delta a/2}^{\Delta a/2} \sigma_z(x,y) \times [w_T(x-\Delta a, y) - w_B(x-\Delta a, y)] dx dy \tag{3.109}$$

$$G_{II} = \lim_{\Delta a \to 0} \frac{1}{2\Delta A} \int_{a}^{a+\Delta a} \int_{-\Delta a/2}^{\Delta a/2} \tau_{xz}(x,y) \times [u_T(x-\Delta a, y) - u_B(x-\Delta a, y)] dx dy \tag{3.110}$$

$$G_{III} = \lim_{\Delta a \to 0} \frac{1}{2\Delta A} \int_{a}^{a+\Delta a} \int_{-\Delta a/2}^{\Delta a/2} \tau_{yz}(x,y) \times [v_T(x-\Delta a, y) - v_B(x-\Delta a, y)] dx dy \tag{3.111}$$

where T and B represent the top and bottom sublaminate parameters, respectively and a is the existing crack length, Δa is virtual crack extension length due to the external loads and Δa is also the width of the crack as shown in Figs. 3.14 and 3.15. The displacement parameters [u_T, v_T, w_T] and [u_B, v_B, w_B] are the corresponding values for the nodes at the top and bottom interface, respectively just behind the propagated crack front, and σ_z, τ_{zx} and τ_{zy} are the stresses required to close the progressive crack front. Though MCCI has the advantage of mode separation of strain energy release rates, but it requires specific meshing techniques. The practical difficulties associated with the need for a very fine mesh include the following.

- Models can be time consuming to generate.
- Analysis tends to be highly computationally intensive.
- Convergence studies are usually needed to verify that the mesh is adequate and these are in themselves time consuming.

Proper understanding of the characteristics of delamination and debonding at the interlaminar region is essential in any delamination analysis. The adhesion failure and delamination induced damage analyses of different types of bonded joints have been carried out as a part of the ongoing research work. It has been observed that the

bonding phenomena at the interface between adjacent plies affect severely the structural integrity and load carrying capacity of bonded joints of laminated Fiber Reinforced Polymeric (FRP) composites. Significant differences between the correlated results were observed by comparing strain energy release rate values with and without using contact elements between the delaminated surfaces. Also the influence of coefficient of friction on fracture energy was found to be significant for relatively small delamination configuration. Therefore in this work both contact and friction parameters have been judiciously chosen in the finite element modelling of the adhesion failure and the delamination propagation [154-156].

3.11.2 Virtual Crack Closure Technique (VCCT)

In the Rybicki and Kanninen's [13] method of VCCT implementation in the finite element analysis, the stress based Eqs. (3.109) to (3.111) takes the form of simple multiplication of corresponding nodal forces at the finite element nodes on the damage plane ahead of the failure front and the damage face displacements behind the damage front. Because of this, the finite element mesh needs to satisfy certain conditions [12, 13]. These are: (i) the finite element mesh should be symmetric on the damage plane as well as about the damage front, (ii) the element size Δa at the damage front should be small, and (iii) the normality of the finite element mesh should be maintained near the damage front.

For the three-dimensional specimen, the damage length a is represented by two adjacent surfaces with configuration of nodes as shown in Fig 3.15. The nodes at the top and bottom surfaces of the discontinuities have identical coordinates and are connected with each other by suitable gap elements to prevent interpenetration of the damaged surfaces. The damage front and subsequent undamaged portions are modelled using pairs of nodes with identical coordinates coupled through Multi-Point Constraint (MPC) elements to simulate the propagation of adhesion failure. The MPC elements along the damage front are activated during the FE simulations for self-similar failure propagation. The other MPC elements ahead of the damage front are passive. These passive MPC elements are activated in turn by incremental crack front displacement Δa to simulate the damage front propagation.

The mode *I*, mode *II* and mode *III* components of SERR, i.e., G_I, G_{II} and G_{III}, are computed accordingly and are given by

$$G_I = \frac{1}{2\Delta A} Z_f \left(w_{Ti} - w_{Bi} \right) \tag{3.112}$$

$$G_{II} = \frac{1}{2\Delta A} X_f \left(u_{Ti} - u_{Bi}\right) \tag{3.113}$$

$$G_{III} = \frac{1}{2\Delta A} Y_f \left(v_{Ti} - v_{Bi}\right) \tag{3.114}$$

where $\Delta A = \Delta a \times \Delta a$ is the area virtually closed. Referring to Fig. 3.15, Z_f, Y_f and X_f, the opening, tearing and sliding mode forces, respectively, are required to hold the nodes at the damage front (at the node *f*) together to prevent it from opening and its subsequent propagation. The corresponding displacements behind the damage front at the top peeled surface of the adhesive layer (T) nodes are denoted by $u_{Ti,}$ v_{Ti} and w_{Ti} and at the bottom peeled surface on the bottom adherend (B) nodes denoted by $u_{Bi,}$ v_{Bi} and w_{Bi}. All forces and displacements are obtained from the finite element analysis with respect to the global coordinate system.

The MPC element at the damage front helps in determining the values of the forces and the gap elements used behind the damage front give the values of the displacements of the upper and lower surfaces created due to the adhesion failure. Thus, G_I and G_{II} at any point on the damage front are determined by releasing in turn the MPC elements for simulating the damage propagation.

4

Three-Dimensional Finite Element analyses of Adhesively Bonded Single Lap Joint

4.1 Introduction

Adhesively bonded Single Lap Joint (SLJ) with laminated FRP composite plays a significant role in many structural applications especially in space, aircraft and automobile industries. However, designing the composite SLJ is quite complex, because their performance is limited by the characteristics of the laminated composite adherends and bi-material interface which usually have low interlaminar strengths. The interlaminar stresses induced in the vicinity of the bondline leading edges of joints can cause delamination in the laminated adherends. Also, cohesive and adhesion failures are major threats to the adhesively bonded joint. Thus, accurate 3D analysis is essential for understanding the joint stress fields, damage initiation and its propagation in practical applications.

The damage study of adhesively bonded SLJ problem is typically approached in one of the two ways; with finite element analysis or through analytical modelling. Accurate analyses of adhesively bonded joints using Finite Element Method are the most demanding tasks [31, 157] and there is a specific need for the analysis that can provide accurate and better results. Examples of finite element investigations of adhesively bonded composite joints include research works of Kairouz and Matthews [37], Tsai et al. [158], Tong [21, 35], Li et al. [82], Krüeger et al. [159] and others. The literature shows that standard finite element codes can analyze the adhesively bonded joints with or without damages under arbitrary loading conditions. In design and sizing, many different joint configurations must be analyzed quickly, and each finite element model can take hours or even days to properly carry out the pre- and post-processing. Second, because the stress gradients for bonded joints are very steep especially at the re-entrant corners, the accuracy of the method can be highly dependent on mesh refinement.

Analytical approaches to bonded joint analysis employ simplifying assumptions in terms of the joint geometry, loading, and boundary conditions in order to formulate efficient closed-form elasticity solutions for the local fields in the joint

region. The advantage of analytically modelling the bonded joints is that each joint configuration can be analyzed quickly although with lot of embedded assumptions. These approaches have roots in classical shear-lag analysis of Volkersen [15] and the work of Goland and Reissner [16], who accounted for bending in the analysis of a bonded single lap joint. Hart-Smith [17] extended these solutions to account for the inelastic behaviour of the adhesive and considered many different joint configurations. However, these formulations have traditionally been limited by the types of applied loading considered and by the 1-D treatment of the adherends with an effective stiffness in the joint direction. Delale et al. [160] developed a closed-form solution for lap-shear joints with orthotropic adherends using classical plate theory. Oplinger [19] developed a layered beam analysis, which includes large deflections. The above analytical methods mainly focus on obtaining the adhesive stresses with many assumptions [25] for simplification of the problems, while generally ignoring out-of-plane stresses at the interface of the joint, which are known to be the key contributors to failure of the joint.

More recently, Mortensen [85] presented a unified analytical approach to analyze an array of common bonded joint configurations for more general loading conditions. Mortensen's treatment also considers arbitrary laminate adherends (based on classical lamination theory) and solves for the distributions of the normal and shear force and moment resultants along the joint in both adherends as well as peel and shear stress distributions in the adhesive. Further, through the application of an efficient solution algorithm, convergence issues that sometimes arise in Hart-Smith's formulation have been overcome.

Adam and Peppiatt [72] noticed the 3-dimensional natures of stresses in a SLJ by an approximate numerical analysis assuming that normal stresses are constant along the width of the joint and neglecting the edge bending moment and adhesive peel stress. Wang and Rose [161] have developed analytical solution for two normal stresses, parallel and perpendicular to the joint due to the constraint imparted by the adherends. Although extensive studies have been devoted to the stress analysis of SLJs both analytically and numerically, in almost all the work published so far, only two stress components (shear stress and transverse peel stress) have been considered. However, there is a very little work in the literature regarding the complete triaxial stress state, damage prediction and its propagation in regard to the SLJ. In the present studies, SLJs are considered as specimens for a complete evaluation of the triaxial

stress fields and in particular the interlaminar stresses which play the dominant role of damage initiation and propagation.

The adherends are laminated FRP composites which are vulnerable for various types of failures viz. interlaminar failure [27, 35, 37] and delaminations, etc. besides the conventional failures like cohesive failure and adhesion failures [21]. Fracture mechanics parameters such as SERR, J-integral and SIF can be used to characterize the propagation of such failures or damages. Although lots of literatures are available for the damage prediction and its propagation in the laminated FRP composites, only a few have been devoted to adhesively bonded SLJ. Also, the literatures contain very limited research on the calculation of SERR which is the key parameter for the present studies. Raju et al. [162] emphasized on SERR for the problem with skin stiffener debonding. The importance of SERR to characterize the delamination damages and its growth including the modelling aspects using Multi-Point Constraint (MPC) elements are discussed in detail by Pradhan et al. [11, 163-165].

This Chapter presents a new capability for the analysis of bonded joints using FEM consisting of layered brick elements for the adhesive and adherends. The effects of free rotation of the joint overlap and adherend have been considered. However, the secondary bending moment has been neglected. The objectives of this Chapter are:

- to discuss the 3-dimensional issues for the SLJ specimen due to the eccentricity of the loading path with a special importance to the interlaminar stresses.
- to identify the location of the damage initiation in the joint based on mechanics of materials approach.
- to discuss in detail about the various types of failures/damages in an adhesively bonded joint with FRP composite adherends.
- to determine the SERRs, which are responsible for the propagation of damages.

Based on the observations, suitable design recommendations have been suggested.

4.2 Finite element analyses of the SLJ

The geometry, configuration, loading and boundary conditions of the SLJ specimen analyzed are shown in Fig. 4.1. Two $[0/90]_s$ laminated FRP composite plates are used as adherends. The material properties along with their strength values for adhesive and adherends are given in Table 4.1. A three-dimensional finite element analysis is

performed to calculate the out-of-plane stress distributions in the overlap region. The zoomed view of the finite element mesh of the overlap region is shown in Fig. 4.2.

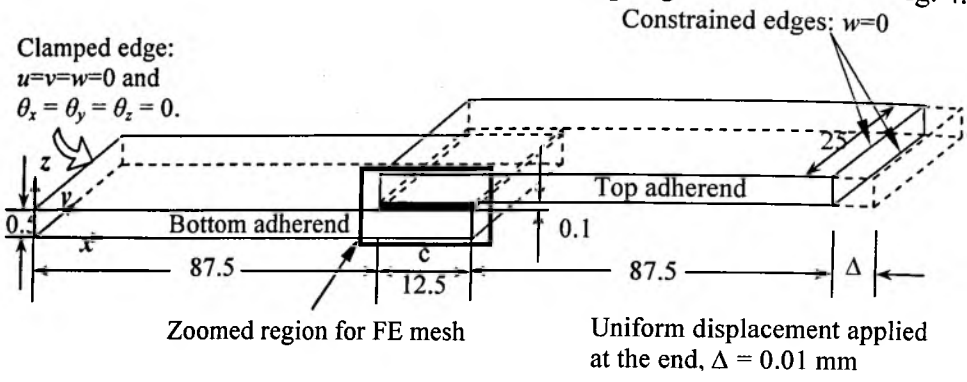

Figure 4.1 The SLJ specimen. (All dimensions are in mm)

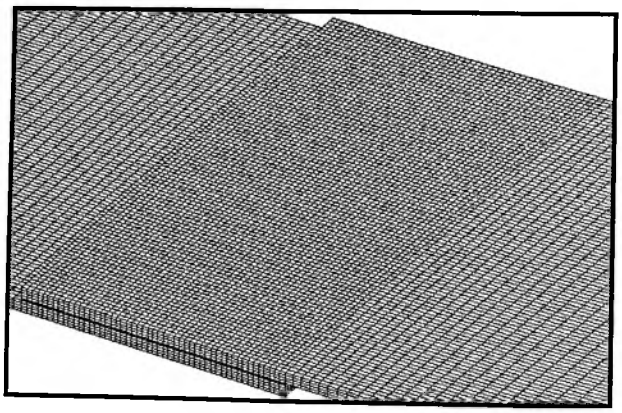

Figure 4.2 Zoomed view of finite element mesh of the overlap region.

Table 4.1 Graphite/epoxy FRP composite lamina and epoxy adhesive material properties [20, 21].

T300/934 graphite/epoxy FRP composite adherend:	Material constants: E_x = 127.5 GPa, E_y = 9 GPa, E_z = 4.8 GPa $\nu_{xy} = \nu_{xz}$ = 0.28, ν_{yz} = 0.41 $G_{xy} = G_{xz}$ = 4.8 GPa, G_{yz} = 2.55 GPa	Strengths: X_T = 1586 MPa, X_C =1517MPa $Y_T = Y_C$ = 80 MPa, Z = 49 MPa S = 2.55 MPa
Epoxy adhesive:	E = 2.8 GPa, ν = 0.4	Y_T = 65 MPa, Y_C = 84.5 MPa

Each layer of the adherend is modelled individually. SOLID 45 and SOLID 46 elements of ANSYS FE package are used for modelling the epoxy adhesive layer and the FRP composite adherends, respectively. A very fine mesh is adopted to take care of high stress gradients at the free edges of the joint over the overlap portion of the joint. The element size in the overlap region is (0.25 mm × 0.25 mm × 0.125 mm) for the adherend and (0.25 mm × 0.25 mm × 0.05 mm) for the adhesive layer. The secondary bending moment which usually occurs in the joint due to free rotation about the y-axis is considered to be zero. Due to the complicated behaviour of the SLJ, the numerical calculations necessitate more iterations, which in turn is more time consuming and computationally costly especially to capture the 3-dimensional effects. The three surfaces (i) the interface of the bottom adherend and the adhesive layer, (ii) the mid- surface of the adhesive layer and (iii) the interface of the top adherend and the adhesive layer in the overlap region of the joint are the critical locations of interest of the present investigation. The out-of-plane stress distributions over such surfaces are plotted in Figs. 4.3-4.5. The overlap distance c is measured from the left end of the adhesive layer while presenting the results in these figures. Some important 3-dimensional issues as observed from the results have been discussed in Sec. 4.2.1.

4.2.1 Three-dimensional issues

The three-dimensional effects are due to the free edge, differential elasticity and coupling between the rotation, stretching and bending. Free edge effect is due to the discontinuities of materials, loading and geometry; whereas the mismatch of Poisson's ratios particularly at the interfaces of the joint gives rise to shear coupling effects. Further, there will be a definite coupling between stretching, bending and twisting. Due to the above factors, clear 3-dimensional effects are illustrated in Figs. 4.3-4.5. The effect of above factors can not be neglected in the initiation of damage and its growth.

The free edge effect is basically due to the mismatch of elastics properties of the joint materials. The state of stress in the vicinity of the free edge of the joint is fully three-dimensional which has not been taken into account in any classical theory so far. Due to the mismatch of Poisson's ratios, the upper and lower surfaces of the adherend deform in a convex (concave) manner in one direction and concave (convex) in the perpendicular direction when the joint is subjected to bending [166]. When this deformation is constrained by an adhesive bond, complex 3-dimensional stress states are developed at the interfaces of the joint [167]. Also, the lamination

constitutional relationships and coupling effect due to bending, twisting and stretching give rise to three-dimensional state of stress at the overlap region.

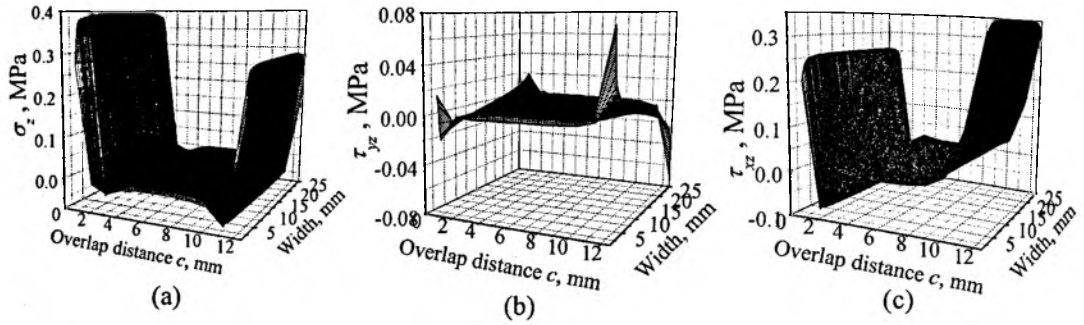

Figure 4.3 Out-of-plane stress distributions along the interface of the bottom adherend and the adhesive layer.

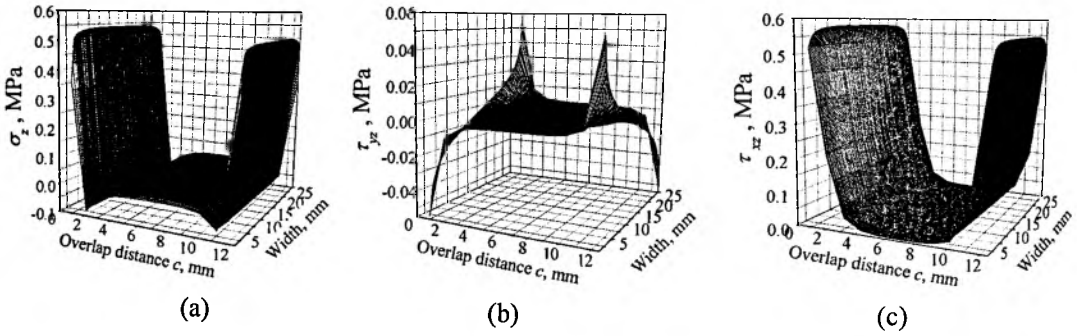

Figure 4.4 Out-of-plane stress distributions along the mid surface of the adhesive layer.

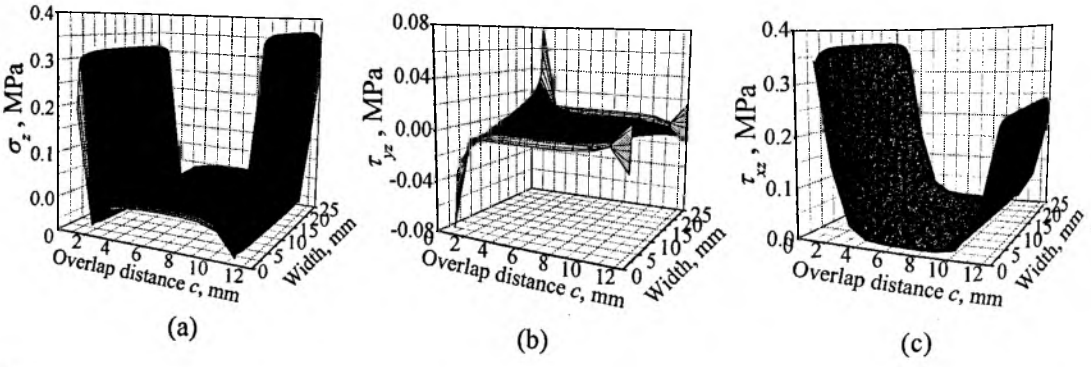

Figure 4.5 Out-of-plane stress distributions along the interface of the top adherend and the adhesive layer.

4.3 Failure studies of the SLJ

The adhesively bonded joint experiences two important modes of mechanical failure: (i) Interfacial failure also known as the adhesion failure which occurs between the adhesive and the adherend and (ii) Cohesive failure within the adhesive apart from the failure or damage due to delamination in the composite adherends. Dattaguru et al. [168] studied the cohesive failure by geometrically non-linear analyses of adhesively bonded joints. This research is concerned with a detailed understanding of the mechanics of adhesion failure in the SLJ.

4.3.1 Adhesion failure criterion

After knowing the out-of-plane stresses from the stress analysis, which are responsible for the damages over the different surfaces in the overlap region, the next step is to use these data to compute the location of damage initiation. Under the three-dimensional stress states in the overlap region, the failure generally can be evaluated by the Quadratic failure criterion [4] which takes into account the interaction of all six stress components as given below:

$$\frac{\sigma_x^2}{X_T^2}+\frac{\sigma_y^2}{Y_T^2}+\frac{\sigma_z^2}{Z_T^2}+\frac{\tau_{xy}^2}{S_{xy}^2}+\frac{\tau_{yz}^2}{S_{yz}^2}+\frac{\tau_{xz}^2}{S_{xz}^2}+\sigma_x\left(\frac{1}{X_T}-\frac{1}{X_C}\right)+\sigma_y\left(\frac{1}{Y_T}-\frac{1}{Y_C}\right)+$$
$$\sigma_z\left(\frac{1}{Z_T}-\frac{1}{Z_C}\right)+f_{xy}\sigma_x\sigma_y+f_{yz}\sigma_y\sigma_z+f_{xz}\sigma_x\sigma_z=e^2\begin{cases}e\geq 1, \text{ failure}\\ e<1, \text{ no failure}\end{cases} \quad (4.1)$$

where X_T, Y_T and Z_T are the allowable tensile strengths in the three principal material directions, X_C , Y_C and Z_C are the allowable compressive strengths in the three principal material directions, and S_{xy} , S_{yz} and S_{xz} are the shearing strengths of the orthotropic layer in various coupling modes. The coupling coefficients reflecting the interaction between x, y and z directions are given by f_{xy}, f_{yz} and f_{xz}, respectively.

In this Chapter, the adhesion failure is considered as a delamination damage which is mainly attributed to the interlaminar stress effects, so only the interlaminar shear stresses (τ_{xz} and τ_{yz}) and through-the-thickness normal stress (σ_z) are required to be used to predict the damage initiation. Therefore, the Tsai-Wu criterion as given in Eq. (4.1) can be simplified as;

$$\left(\frac{\sigma_z}{Z}\right)^2+\left(\frac{\tau_{yz}}{S_{yz}}\right)^2+\left(\frac{\tau_{xz}}{S_{xz}}\right)^2=e^2\begin{cases}e\geq 1, \text{ failure}\\ e<1, \text{ no failure}\end{cases} \quad (4.2)$$

where, Z is the interlaminar normal strength and S is the inter-laminar shear strengths which are considered to be equal i.e. $S_{yz} = S_{xz} = S$.

Similarly, the failure index of SLJ in the adhesive layer is formulated by a cohesive failure philosophy. As reported by Adams [27], parabolic yield criterion given in Eq. (3.98) is used for the isotropic adhesive layer. Using Eqs. (4.1), (4.2) and (3.98) with material properties given in Table 4.1, the failure indices are calculated over the overlap region at various points of different surfaces and thus, the variations of failure indices are plotted in Fig. 4.6. It is obvious from Fig. 4.6 that the possibility of damage initiation under a given loading, geometry and boundary conditions would be at the interface of the loaded adherend (top) and adhesive along the free edge. Once it is predicted, the next step in the analysis is to study the propagation of such damage by evaluation of SERR.

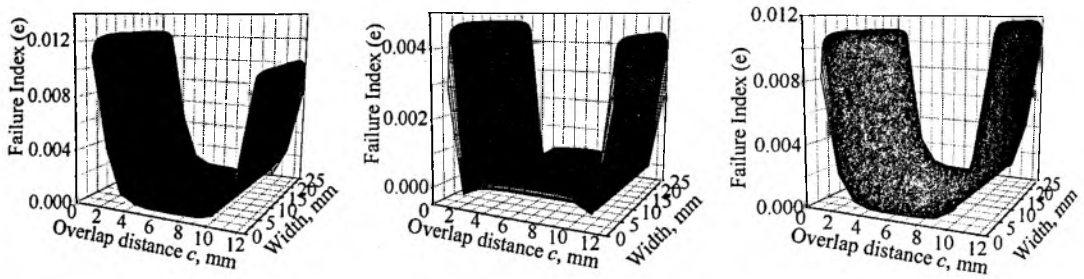

Figure 4.6 Variations of failure index (e): (a) at the interface of the bottom adherend and the adhesive layer, (b) at the adhesive layer (c) at the interface of the top adherend and the adhesive layer.

4.4 Damage analysis of SLJ with adhesion failure

The damage analysis is now performed for the SLJ specimen by simulating an embedded adhesion failure as shown in Fig. 4.7. The adhesion failure is embedded at the critical location as predicted in the failure analysis discussed in the earlier section. The SERR which is the driving parameter responsible for the propagation of adhesion failure is calculated using the Virtual Crack Closure Technique (VCCT). The individual values of SERR of different modes responsible for the propagation can be calculated from the results of the present analysis.

4.4.1 SERR computations

As shown in Fig. 4.7, adhesion failure of length a is present at the interface of the free edge of the loaded adherend along the width of the joint. Multi- Point Constraint (MPC) elements are used along the damage front to extract the nodal forces responsible to close the damage. These nodal forces are useful for the calculation of SERR using the Virtual Crack Closure Technique (VCCT).

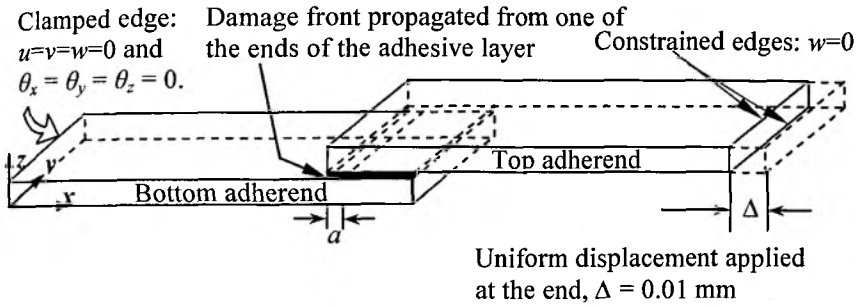

Figure 4.7 SLJ specimen with embedded adhesion failure.

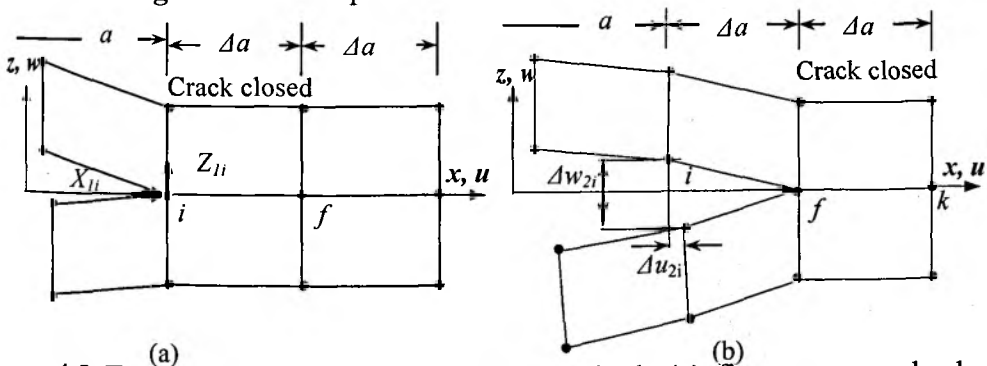

Figure 4.8 Two-dimensional crack closure method; (a) first step: crack closed (b) second step: crack extended.

The VCCT is based on the same assumptions as the Irwin's crack closure method [108] and Rybicki and Kanninen's method of implementation [13]. The method is based on the assumption that the energy ΔE released when the crack is extended by Δa from a (Fig. 4.8 (a)) to $a+\Delta a$ (Fig. 4.8 (b)) is identical to the energy required to close the crack between locations i and f. For a crack modelled with two-dimensional four nodded elements as shown in Fig. 4.8, the work ΔW required to close the crack along one element side can be calculated as

$$\Delta W = \frac{1}{2}\left(X_{1i}\Delta u_{2i} + Z_{1i}\Delta w_{2i}\right) \tag{4.3}$$

where X_{1i} and Z_{1i} are the shear and opening forces at nodal point i to be closed as shown in Fig. 4.8 (a) and Δu_{2i} and Δw_{2i} are the differences in shear and opening nodal displacements at node i as shown in Fig. 4.8 (b). This method establishes the original condition before the crack was extended. Therefore, the forces required to close the cracks are identical to the forces acting on the upper and lower surfaces of the closed crack. The forces X_{1i} and Z_{1i} may be obtained from a first finite element analysis where the crack is closed as shown in Fig. 4.8 (a). The displacements Δu_{2i} and Δw_{2i} are obtained from a second finite element analysis where the crack has been extended to length $a+\Delta a$ as in Fig. 4.8 (b).

Additionally, it is assumed that a crack extension of Δa from $a+\Delta a$ (node f) to $a+2\Delta a$ (node k) does not significantly alter the state at the crack tip. Therefore, the displacements behind the crack tip at node f are approximately equal to the displacements behind the original crack tip at node i. Further, the energy ΔE released when the crack is extended by Δa from $a+\Delta a$ to $a+2\Delta a$ is identical to the energy required to close the crack between location f and k. Thus, the work required to close the crack along one element side can be calculated using the Eq. (4.3). Thus, forces and displacements required to calculate the energy ΔW to close the crack may be obtained from one single finite element analysis. A portion of the SLJ specimen with adhesion failure is shown in Fig. 4.9 along with the finite element mesh consisting of one layer of 8 nodded three-dimensional solid elements (SOLID 46) representing the top adherend and adhesive layer.

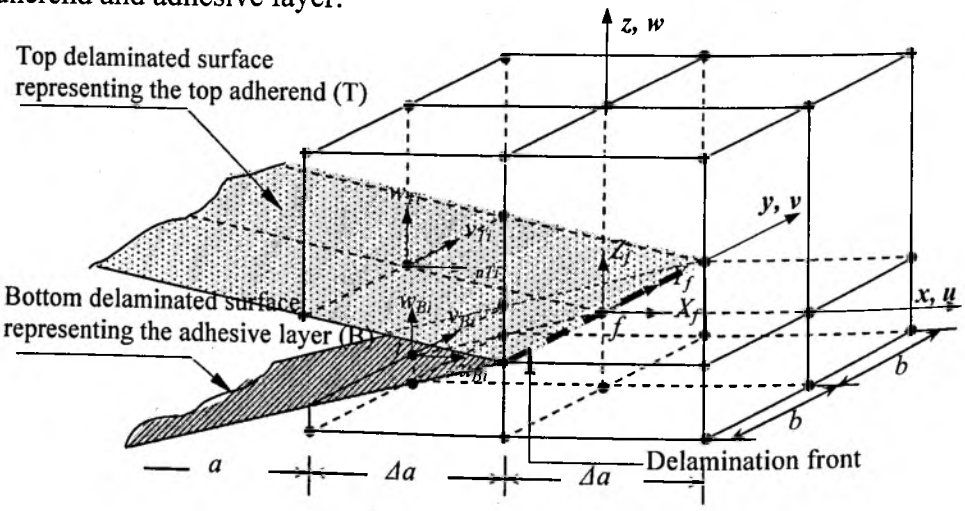

Figure 4.9 VCCT for the 3D damage study in SLJ with eight nodded solid elements.

The adhesion failure has been considered as a typical delamination damage existing at the interface of the adhesive layer and adherend. The length of

delamination is taken as a and represented as a two-dimensional discontinuity by two surfaces. The additional dimension allows calculating the distribution of the energy release rates along the delamination front and making it possible to obtain G_{III}, which is identical to zero for two-dimensional models. Nodes at the top surface and the bottom surface of the delaminated area have identical coordinates and are not connected with each other. The delamination front is represented by two rows of nodes coupled through the Multi-Point Constraint elements (MPC 184). The undamaged section where the joint is intact is modelled using single nodes.

Referring to Fig. 4.9, the mode *I*, mode *II* and mode *III* components of the SERR G_I, G_{II} and G_{III} at a point *f* in the delamination front are calculated as

$$G_I = \frac{1}{2\Delta A} Z_f \left(w_{Ti} - w_{Bi}\right) \tag{4.4}$$

$$G_{II} = \frac{1}{2\Delta A} X_f \left(u_{Ti} - u_{Bi}\right) \tag{4.5}$$

$$G_{III} = \frac{1}{2\Delta A} Y_f \left(v_{Ti} - v_{Bi}\right) \tag{4.6}$$

where $\Delta A = \Delta a \times b$ is the area virtually closed. Δa is the length of the element at the delamination front and b is the width of the elements. X_f, Y_f and Z_f denote the forces in the delamination front at the node *f* and the corresponding displacements behind the delamination front at the top delaminated surface representing the top adherend (T) nodes are denoted by u_{Ti}, v_{Ti} and w_{Ti} and at the bottom delaminated surface representing the adhesive layer (B) nodes denoted by u_{Bi}, v_{Bi} and w_{Bi}. All forces and displacements are obtained from the finite element analysis with respect to the global coordinate system.

Previous investigations have shown that care must be taken in interpreting the values for G_I, G_{II} and G_{III} obtained from the Eqs. (4.4-4.6) for interfacial damage between the bi-material interface [14, 112]. Mathematical solutions of the near crack tip fields indicated that the stresses are highly oscillating in the immediate vicinity of the tip when the crack growth occurs at the interfaces between materials with dissimilar properties. For the VCCT, the energy release rates are defined as the virtual crack closure integral over a finite crack closure length. This crack closure length corresponds to the lengths of the elements adjacent to the delamination front. This element length, Δa must be chosen small enough to assure a converged FE solution but large enough to avoid oscillating results. The FE work of Raju et al. [111] suggests that if the element size or characteristic length is chosen to be between 0.25

to 0.5 of the ply thickness, the components of SERR are well evaluated. The mesh design in the present Chapter has been adopted with the above philosophy and for this purpose an element size of one-fourth of each ply thickness has been used near the damage front. Using Eqs. (4.4-4.6) the SERRs G_I, G_{II} and G_{III} are calculated for different delamination lengths. Fig. 4.10 illustrates the variations of SERRs along the delamination front.

4.5 Results and discussion

4.5.1 Stress distributions in the SLJ

The out-of-plane normal and shear stress distributions along the mid-plane of the adhesive layer are shown in Fig. 4.4 for an in-plane axial extension of 0.01mm applied at the free end. Three-dimensional effects can be observed. Especially the peel stresses are largest at the center of the joint and decrease at the edges. Also it is noticed that the stress distributions are constant for most of the overlap portion except at the edges. This behaviour is in qualitative agreement with experimental and numerical results [29, 83]. This is due to the mismatch of elastic properties and bending effect of the adherends. Figures 4.3-4.5 (b) and (c) show the out-of-plane shear stress distributions. The three-dimensional effects are also observed. However τ_{yz} is more sensitive to the three-dimensional effect compared to other stresses (σ_z and τ_{xz}). These are similar to those observed by Tsai and Morton [70]. There is a strong stress concentration effect at the two corners of the free edges of the overlap, but the maximum values are not significant compared to the other stress components. These facts are same for the adhesive-adherend interfaces and adhesive layer.

It is interesting to note that the out-of-plane normal stress (known as peel stress) in the adhesive layer is maximum compared to adhesive-adherend interface. The shear stress (τ_{xz}) is also significant for 3-dimensional effects. Further, it may be noted that the peel stress is more at the bottom adherend-adhesive interface along the free edge of the loading end than the free end, while it is reverse at the interface of top adherend and adhesive. It is due to the fact that the stress concentration effect reduces from the loading edge to the free end of the adherend-adhesive interface. But the out-of-plane shear stress (τ_{xz}) is simply reverse and there is not such characteristic for the τ_{yz} component. It is evident from the stress analysis that there are large tensile peel stresses at the end of the overlap away from the free surface compared to other stress components. Therefore, it may be predicted that the out-of-plane peel stress

triggered failure by delamination of the bonded joint would be at the site away from the free surface but not at the edges.

4.5.2 Damage onset

It is apparent from the stress analysis that the location of the failure initiation can not be predicted with full conviction. There are three surfaces (two are at the adherend-adhesive interfaces and one is at the mid- surface of the adhesive layer) in the overlap region and are considered as critical ones for the initiation of failure. Using Eqs. (4.2) and (3.98), failure index (e) is calculated for the adherend-adhesive interface surface and the adhesive layer, respectively. Failure index (e) is defined as the parameter to assess the failure of the joint. When the value of $e \geq 1$, failure occurs else there is no failure. The distributions of failure index over the critical surfaces are shown in Fig. 4.6. Eventhough the out-of-plane stresses are maximum for the adhesive layer, the possibility of failure initiation would be from the interface of the top adherend-adhesive along the free edge, since the value of e is the highest here compared to any other locations.

4.5.3 Propagation of damage

Fig. 4.10 illustrates the variations of SERRs G_I, G_{II} and G_{III} in mode *I*, mode *II* and mode *III* along the damage front for different damage lengths a. It is observed that the energy release rate is almost constant along the damage front except near the edges. The G distributions obtained from the present analysis indicate that, as expected, mode *II* SERR (G_{II}) is the dominant mode. Away from the boundary region, mode *III* SERR (G_{III}) values are nearly zero. Mode *I* SERR (G_I)values are lower while mode *II* SERR (G_{II}) became larger in the central portion of the joint. The longer damage length showed similar trend, but gave lower SERR values. These results are in excellent agreement with the available literature [162]. Since mode *II* SERR (G_{II}) is mainly responsible for the propagation of damage due to adhesion failure, this explains why the adhesively bonded lap joints experience shearing failure. Also it is seen that the peak values of the G components occur in different locations for any damage length. This indicates that the damage propagation is not at the same rate along the width of the joint due to adhesion failure, though the SERRs are derived based on the assumption that the damage growth is self similar in nature and occurs in the same plane. The loci of the different damage fronts propagated in the present analysis are shown in Fig. 4.11. The damage front is curving near the free edge of the specimen during its propagation.

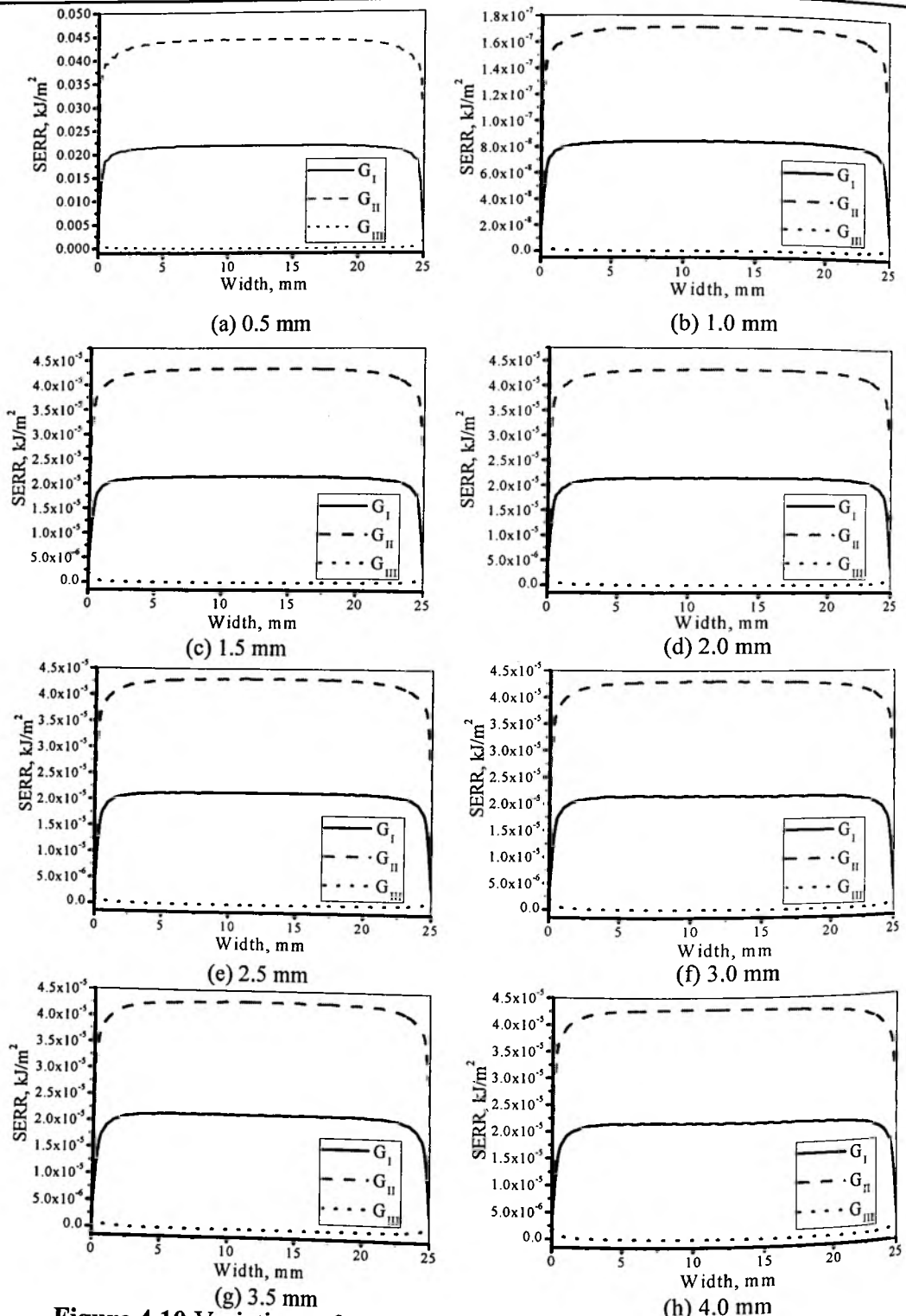

Figure 4.10 Variations of SERRs over various delamination lengths.

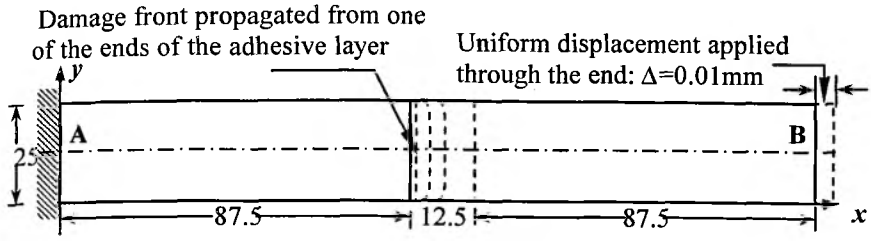

Figure 4.11 Loci of damage fronts during damage propagation in the SLJ specimen.

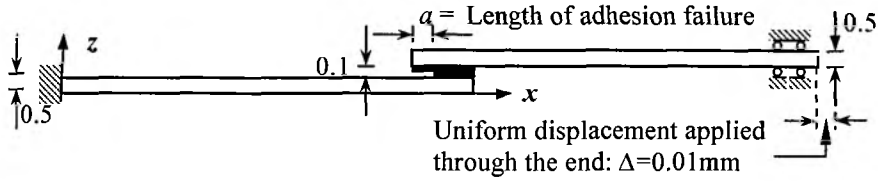

Figure 4.12 Specimen with adhesion failure.

In order to assess the effect of SERRs on damage front propagation, the mode *I* (G_I) and mode *II* (G_{II}) SERRs are calculated along two longitudinal sections of the SLJ, one along the *xz* plane through the free edge (Fig. 4.12) and the other through the central cross section along AB as shown in Fig. 4.11. The variations of individual modes of SERR for varying damage lengths are shown in Fig. 4.13. This helps to examine (i) delamination process in terms of stable damage growth characteristics and (ii) the SERR as a parameter for predicting the damage growth. Particularly, Fig. 4.13 (a) represents the trend of SERR variations over a large portion of the total width of the joint for different delamination damage lengths, whereas Fig. 4.13 (b) shows the results for the free edge. Several finite element calculations are made to examine whether the SLJ specimen has the existence of stable damage growth characteristics. The procedure involves the evaluation of the energy release rate G for various delamination lengths by keeping the applied load, joint geometry and boundary conditions constant. The results shown in Fig. 4.13 indicate that some stable delamination growth occurs. This is in good agreement with the analytical results and experimental observations reported by Rybicki et al. [169].The results given in Table 4.2 shows that the energy release rate decreases initially during the delamination propagation and remain constant after a particular damage length is reached. A

constant value of G during propagation indicates that it is a material property independent of geometry and is hence a candidate parameter for predicting the damage growth behaviour. Thus, based on these results, the energy release rate appears to warrant further investigation as a viable parameter for study of stable damage growth behaviour in the SLJ.

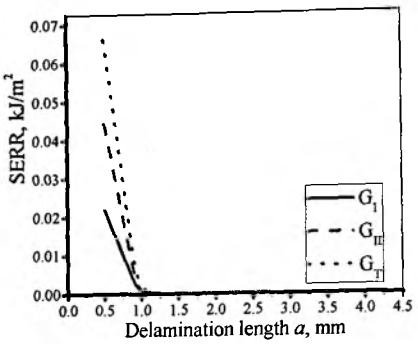

(a) Along the central cross section through AB (Fig. 4.11)

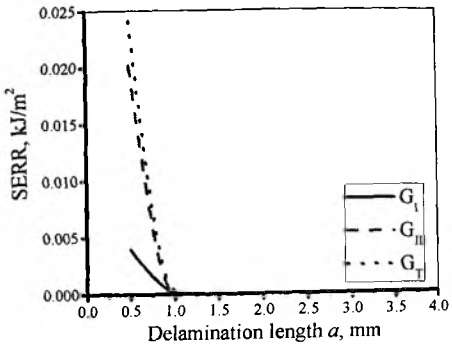

(b) Along the free edge, i.e. *xz* plane (Fig. 4.12)

Figure 4.13 Variations of SERR with different delamination lengths in various longitudinal cross sections.

Table 4.2 Magnitude of SERRs at the two considered cross sections (Figs. 4.11 and 4.12).

a (mm)	Along the central cross section through AB of the SLJ (Fig. 4.11)			Along the free edge of the SLJ i.e. *xz* plane (Fig. 4.12)		
	G_I, kJ/m² (×10⁻⁵)	G_{II}, kJ/m² (×10⁻⁵)	G_T, kJ/m² (×10⁻⁵)	G_I, kJ/m² (×10⁻⁵)	G_{II}, kJ/m² (×10⁻⁵)	G_T, kJ/m² (×10⁻⁵)
0.5	2179.9	4430.3	6610.2	393.9	2016	2409.9
0.75	1005.6	1998.8	3004.4	148.9	534.6	683.5
0.9	276.3	356.8	633.1	48.95	68.75	117.7
1.0	0.00842	0.0171	0.02552	0.00142	0.00772	0.00914
1.5	2.14	4.33	6.47	0.352	1.96	2.312
2.0	2.14	4.32	6.46	0.346	1.95	2.296
2.5	2.14	4.31	6.45	0.341	1.95	2.291
3.0	2.15	4.30	6.45	0.336	1.94	2.276
3.5	2.15	4.29	6.44	0.331	1.93	2.261
4.0	2.16	4.28	6.44	0.330	1.93	2.260

4.6 Conclusions

Three-dimensional stress distributions for the adhesive layer and adhesive-adherend interface of the overlap region have been determined by linear elastic three-dimensional finite element analyses. Special importance is given to the evaluation of out-of-plane stresses which play a key parameter for failure or damage of the joint. Strength of the joint in the overlap region is predicted in terms of the failure indices which are being evaluated based on the mechanics of materials approach. The locations for the damage initiation have been identified. The damage analysis of the SLJ is carried out by embedding an adhesion failure (which is considered as a manifestation of delamination damage). The delamination damage propagation is considered to be governed by the three components of Strain Energy Release Rate (SERR) based on fracture mechanics approach. The SERRs have been calculated using Virtual Crack Closure Technique (VCCT). Conclusions based on the observations from the present analysis are given below:

- Analytical solutions for the damage study of the SLJ of laminated FRP composites exist for simple geometry, loading and boundary conditions. In real applications of bonded joints involving complicated geometry, loading and boundary conditions, three-dimensional finite element analyses are essential to model all types of damage problems of bonded joints.
- The free ends of the adhesive-adherend overlap distinctly demonstrate the existence of a three-dimensional state of stress as compared to the interior regions. The validity of the commonly used two-dimensional plane-strain analysis seems to be accurate for predicting stress state only in the region away from the free surfaces. Detailed evaluation of 3D states of stresses in the free end regions of the overlap will enable an accurate prediction of the strength of the joint and damage propagation studies.
- The magnitudes of the out-of-plane normal stresses (known as peel stresses) are significantly higher compared to the shearing stresses in any of the surfaces among all critical surfaces in the overlap region and τ_{yz} is negligibly small except at the corners.
- The damage initiates from the free edge of the bottom adherend-adhesive interface in the SLJ under uniaxial tension.
- Delamination damage propagation due to adhesion failure is mainly due to the shearing mode. The opening and tearing mode SERRs G_I and G_{III} are much less compared to the shearing mode SERR G_{II}.

- The SERRs variations along the damage front are almost uniform along the width of the joint except at the free edge. Also, it is seen that G_{III} is zero except at the free edges. Thus, the non-uniform SERR distribution leads to a possibility of non-self similar delamination propagation characteristics. The rate of damage propagation in the central portion of the SLJ is at a higher rate than that along the free edge.
- There will be stable delamination damage propagation up to the length of delamination damage length of 1 mm beyond which the SERR remains constant indicating unstable damage propagation.

5

Damage Analyses of Adhesively Bonded Single Lap Joint due to Adhesion Failures

5.1 Introduction

Adhesive bonding has been one of the most important and evolving technologies for many structural applications in a great variety of industries over the past few decades. Compared to other joining methods like mechanical fastening, welding, brazing and soldering, adhesive bonding can offer improved performance and substantial economic advantages. The ability to join dissimilar materials (like laminated composites), joining of thin sheets and joining of materials with complex geometrical configurations has made the adhesive bonding more attractive over other methods of joining. A smoother load transfer between the connecting members helps in lowering the localized stress concentrations as compared to mechanical fasteners. The increasing use of adhesive bonding methods in many applications such as space, aircraft and automotive industries, etc. has placed considerable demand for more accurate analyses and design methods keeping in mind the field conditions. Failure analyses and appropriate design recommendations would always make these joints worthy of acceptance in such important applications. Besides typical failures like interlaminar or interply delaminations in the adherends, an adhesively bonded joint can fail by different modes as shown in Fig. 5.1 (a) and listed as below:

- Adhesion failure at the adherend-adhesive interfaces caused by excessive peel and shear stresses at critical locations.
- Cohesive failure within the adhesive layer.
- Out-of-plane adherend failure in laminated FRP composite adherends caused by interlaminar stresses.

The failure of both isotropic and anisotropic adherends due to bending, tension or compression can be predicted using the standard stress based mechanics of materials approach as well as the Tsai-Hill coupled failure criterion. Cohesive and out-of-plane adherend failure modes pertaining specifically to the failure of the adhesively bonded joints are discussed in detail by some researchers [67, 168]. However, there has been practically very little effort to analyze the adherend-adhesive

interface failure which is known as adhesion failure or delamination/debonding damages caused by interfacial peel and shear stresses. Such damages occur at the bi-material interfaces i.e. at the interface of the adherend and adhesive in case of bonded joints. Adhesion failure occurs on a macro-scale when surface preparation or material qualities are poor and, consequently, this mode of failure cannot be ignored. Though all joints are assumed to be manufactured to specifications, but due to the above-mentioned reasons, adhesion failures are expected to initiate from the edges of the stress singularity points and would propagate along the adherend-adhesive interfaces as shown in Fig. 5.1 (b). It is also shown both experimentally and numerically by Kelly [170] that the failure of bonded joints occurs with the fracture initiating from the toe of the adhesive fillet and propagating along the adherend-adhesive interfaces of the joint. Potter et al. [171] carried out an interesting study on the crack growth behaviour with adhesive fillets.

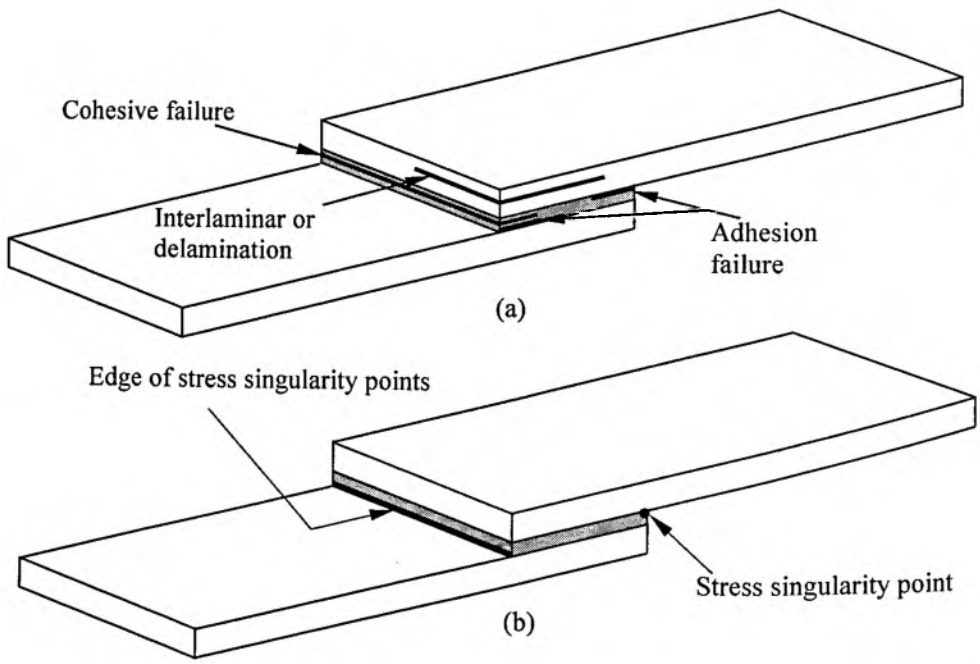

Figure 5.1 (a) Failure modes in an adhesively bonded single lap laminated FRP composite joint and (b) Initiation of adhesion failures from the stress singularity points.

5. Damage Analyses of Single Lap Joint due to Adhesion Failure

For a Single Lap Joint (SLJ), the occurrence of adhesion failures can be initiated from the stress singularity points at one or both ends of the adhesive layer. In a recent three-dimensional analysis of an SLJ by Panigrahi and Pradhan [172], the initiation of such failures was predicted using the mechanics of materials approach and was found to occur along the free edges of the overlap length. More precisely, the critical points for initiation of adhesion failures were found to be in the central portions of the free edges of the overlap length of the joint. Tsai and Morton [167] examined the three-dimensional nature of an SLJ using the finite element method. They concluded that the commonly used two-dimensional plane strain analysis was valid for predicting the stress, strength and the damage propagation due to adhesion failure.

Hart-Smith [17] and Adams [27] have indicated that only a bonded joint failure with minimum flexural deflection can be analyzed and failure loads can be predicted using simplistic analysis procedures and failure criteria. Adams and coworkers [20, 28, 31] have made significant contributions towards the failure analysis of adhesively bonded joints. In general, their approach for joint failure prediction has involved finite element analysis (FEA) considering plane strain assumption with geometric and material non-linearties and ignoring three-dimensional effects [172].

The basic phenomenon which makes bonded joint failure prediction very difficult is the presence of both geometric and material singularities at the ends of the joint [173]. Kayupuv and Dzenis [38] used finite element method to deal with the stress concentration which exists at the damage front and found that it had significant influence on stresses and strength of the joint. The accuracy with which the finite element solution predicts the stresses near the end of the overlap length of the joint will, therefore, depend heavily on the refinement of the finite element mesh. Groth [174] has used stress singularity parameter approach to predict the joint failure to overcome the singularity problem. Linear elastic finite element analyses were carried out by Quaresimin and Ricotta [175] to evaluate the generalized Stress Intensity Factor (SIF) and SERR for a single lap bonded joint in composite materials.

Considering the above discussions, the objective of this study is to analyze the effect of embedded adhesion failures at both ends of the adhesive layer and their propagation on the stress distributions, joint strength and SERR variations. The strength and performance of adhesively bonded joints in any structure will be affected by the propagation of these adhesion failures. The detailed methodology to determine

the strength of the joint taking into account the evaluation of the undamaged lengths along the adherend-adhesive interfaces and mid-surface of the adhesive layer of the considered SLJ specimen is dealt with in this Chapter. The interaction of adhesion failures emanating from either end of the adhesive layer has been studied in detail. The loci of adhesion failure propagation paths often follow along the adherend-adhesive interfaces as predicted by many researchers [20, 101, 170]. However, due to the presence of two adhesion failures at the two ends of the adhesive layer, the failure propagation behaviour for even the simplest single lap composite joint becomes very complex. At a first glance, one might feel that the adhesion failures propagated along the adherend-adhesive interfaces from either end of the adhesive layer would have identical effects and the same strain energy release rate. But it may not be so, because of loading eccentricity, joint material heterogeneity, rotation of free length of adherend, and different boundary conditions in the fixed and loaded ends [176] of the SLJ specimens.

Plane strain finite element solutions have been shown to be appropriate to analyze effectively the problems of bonded joints with damages by some researchers [21, 67] taking a longitudinal cross section along the central region of the SLJ and assuming self-similar adhesion failure propagation. The present Chapter deals with a more rigorous three-dimensional finite element analysis of an adhesively bonded SLJ and the results are presented for a longitudinal cross section taken through the central portion of the joint when the adhesion failures are embedded along the interfaces of adhesive and adherend at both ends of the adhesive layer. The geometric non-linear FEA using ANSYS on HP workstation has been carried out here with the following objectives:

- Computation of the peel and shear stresses along the mid-surface of the adhesive layer for varying adhesion failure lengths to find out the influence of adhesion failure lengths on the strength of the joint.
- Study of the effect of varying adhesion failure lengths on failure index.
- Evaluation of SERR for study of the propagation of adhesion failure lengths from both ends of the adhesive layer.

5.2 Finite element analyses

An adhesively bonded single lap laminated FRP composite joint, as shown in Fig. 5.2, clamped at one end and subjected to uniform extension of 0.1mm at the other end

is considered for the present analysis. The two adherends are identical with respect to free length, thickness, materials and lay-up scheme.

Three types of analyses exist for an SLJ viz. (i) linear analysis, (ii) non-linear analysis including large deformation only, and (iii) non-linear analysis including both large deformation and material non-linearity. The linear and non-linear analyses yield significant differences in the computed values of peel and shear stresses. It has been emphasized that the non-linear analysis procedure must be used for an SLJ in order to evaluate the stresses in the joint accurately. However, the effect of adhesive material non-linearity on peel stresses is insignificant [21]. Thus, three-dimensional finite element analyses with geometric non-linearties have been carried out for the SLJ to study the interaction of the adhesion failures propagating from both ends of the adhesive layer. These failures are found to initiate from the critical locations, i.e. from the stress singularity points as shown in Fig. 5.1 (b).

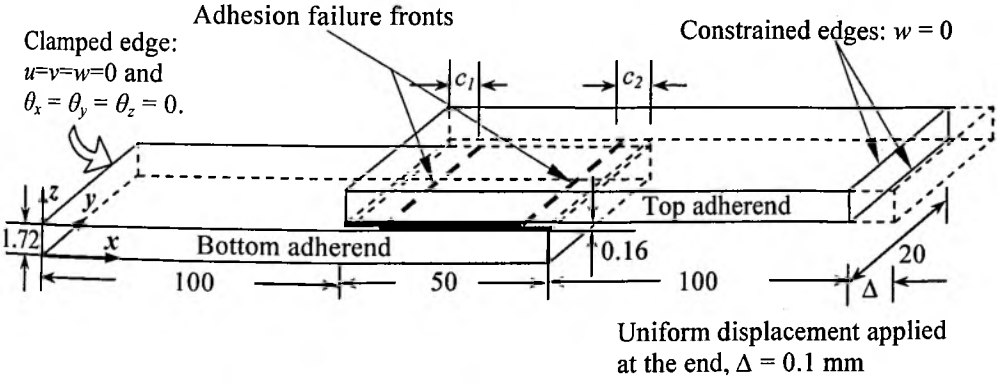

Figure 5.2 SLJ specimen with embedded adhesion failures of lengths c_1 and c_2 propagating from both ends of the adhesive layer. (All dimensions are in mm)

The adherend and adhesive layer of an SLJ can be modelled either with shell elements or three-dimensional brick elements [140, 177]. The 3D brick element models have been shown to be more accurate especially in separating the total strain energy release rate G into individual components G_I, G_{II} and G_{III} [178-180]. But using many layers of brick elements through-the-thickness to model the individual plies and adhesive layer, modelling and computational effort may become prohibitively large. Therefore, it is necessary to use a layered volume element for improving computational efficiency without compromising accuracy of the FE analysis. In the present analysis, isoparametric, three-dimensional eight-node layered

volume elements designated as SOLID 46 have been used to model the laminated adherend ply-by-ply and orthotropic material properties have been considered for each ply. The convergence of the solution has been ensured using appropriate mesh density of the elements near the adhesion failure front as suggested in references [111, 153]. The acceptable error limit has been set to be 0.001% of the converged result, i.e. of the dominant SERR mode G_{II}. For this purpose an element size of one-fourth of each ply thickness has been used near the damage front along with a graded coarse mesh in the remaining areas of the joint. For simulating self-similar propagation of linear adhesion failure front, the 3D model construction of the SLJ specimen has been simplified by generating a template of 2D mesh pattern. This pattern has been protruded in the transverse direction for the full 3D FE models. Experimental evidence by Wang [181] indicated that very thin resin-rich layers existed between the neighbouring plies in fiber reinforced composites and this interlaminar matrix region usually had a dimension of one-twentieth to one-tenth of an individual layer thickness. Such proposition is not required in the present analysis, since the adhesion failures propagate along the adherend-adhesive interface. At the interface duplicate nodes with identical coordinates have been defined between the adhesive layer and the adherends. In the undamaged region, the corresponding nodes of the top and bottom adherends are constrained using Multi-Point Constraint (MPC) elements so that the continuity condition prevails. By sequentially removing the constraints, progressive propagation of self-similar adhesion failure has been realized.

The specimen geometry and materials (Table 5.1) have been adopted from the works of Tong and Steven [21] and Tong [35]. The boundary conditions used in this analysis (shown in Fig. 5.2) are the same as those considered by Reddy and Roy [77]. The laminated FRP composite adherends were made of 8 plies of T300/934 plane woven prepregs manufactured by Feberite Corporation, Winona, Minnesota, USA by incorporating the Fiberite 934 epoxy resin in T300 plain woven fabric (Supplier product designation was HMF-5-332/34c). The prepregs had a fiber of 3000 filaments per tow at a curing temp of 177°C. Each ply had a nominal thickness of 0.215mm. Adhesion failures of different lengths (2mm, 4mm, 6mm, 8mm and 10 mm) with negligible thickness were considered for modelling the damaged specimen. The finite element meshing scheme used for modelling and simulating the adhesion failure growth was adopted in conformity to the requirements of accuracy and convergence as has been stated earlier in this section. The finite element mesh around the embedded adhesion failure regions at the two ends of the adhesive layer along with

the joint overlap region is shown in Fig. 5.3. The SLJ was fixed at the left end and subjected to uniform axial extension of $\Delta = 0.1$mm in 20 equal increments at the other end. The adhesion failure propagation was simulated using MCCI based on Linear Elastic Fracture Mechanics (LEFM) as recommended by Rybicki and Kanninen [13] for SERR calculations. The variation of SERR along the adhesion failure front for different embedded adhesion failure lengths was used to describe the location of adhesion failure propagation. For a complete understanding of the adhesion failure propagation behaviour, all three SERR components (G_I, G_{II} and G_{III}) need to be calculated. However, computations [172] have shown that the SERR in mode *III* (G_{III}) is very small along the adhesion failure front for the SLJ and has very little influence on the adhesion failure propagation.

Table 5.1 Graphite/epoxy FRP composite lamina and epoxy adhesive material properties [21]

T300/934 graphite/epoxy cloth ply FRP composite adherend:	Material constants: $E_x = E_y = 57.23$ GPa, $E_z = 4.8$ GPa $\nu_{xy} = 0.05$, $\nu_{xz} = \nu_{yz} = 0.28$ $G_{xy} = 4.48$ GPa, $G_{xz} = G_{yz} = 4.4$ GPa	Strengths: $X_T = 1586$ MPa, $X_C = 1517$MPa $Y_T = Y_C = 80$ MPa
Epoxy adhesive:	$E = 2.8$ GPa, $\nu = 0.32$	$Y_T = 65$ MPa, $Y_C = 84.5$ MPa

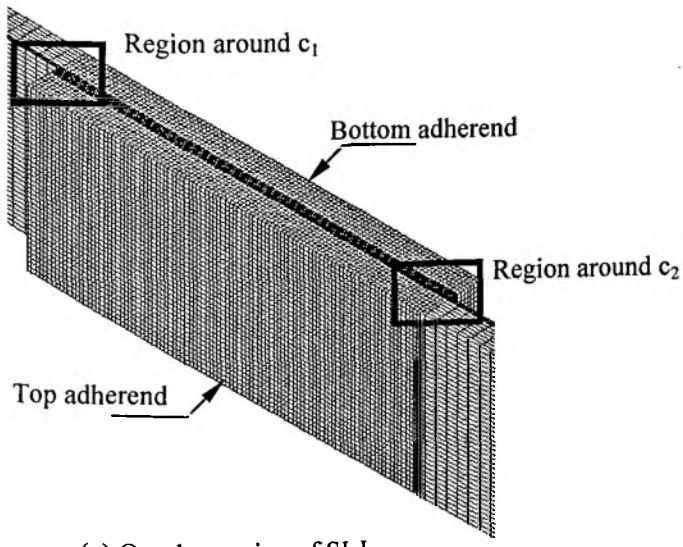

(a) Overlap region of SLJ

Figure 5.3 Finite element mesh of the overlap region of SLJ along with zoomed views of regions around the embedded adhesion failures at both ends of the adhesive layer.

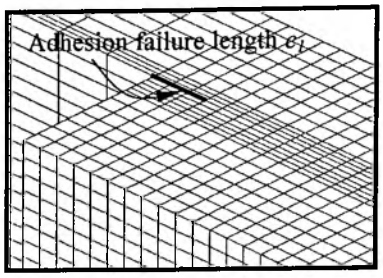

(b) Zoomed view of region around c_1

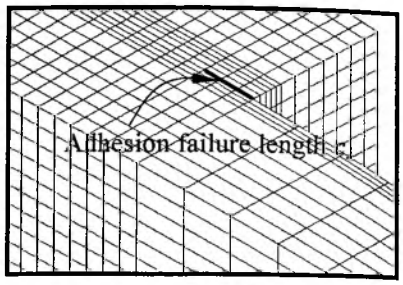

(c) Zoomed view of region around c_2

Figure 5.3 Continued.

5.3 Computation of SERR

Consider the 2D specimen with adhesion failure length a as shown in Fig. 5.4. The SERR, G, for self-similar failure front propagation under load is defined as

$$G = \frac{dW}{da} - \frac{dU}{da} \tag{5.1}$$

where W is the work done by the external load per unit thickness, U is the total strain energy of the composite specimen and a is the adhesion failure length. For a mixed mode situation, the SERR can be calculated for the given configuration by calculating the work required to close the virtually opened damage length ($a+\Delta a$) to damage length a and the opening mode (G_I), shearing mode (G_{II}) and tearing mode (G_{III}) components of SERR at any location on the damage front are given by Eqs. (3.109) to (3.111). The relative damaged face displacements behind the damage front are denoted by $w(\Delta a\text{-}x,0)$ and $u(\Delta a\text{-}x,0)$, respectively and, σ_z and τ_{zx} are the peel and shear stresses at the damage front of the adhesion failure as shown in Fig. 5.5.

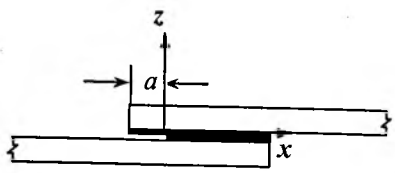

(a) SLJ specimen with adhesion failure length a

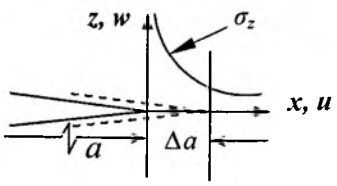

(b) MCCI applied to the tip of the adhesion failure length a

Figure 5.4 MCCI applied to the SLJ with adhesion failure length a at the adherend-adhesive interface.

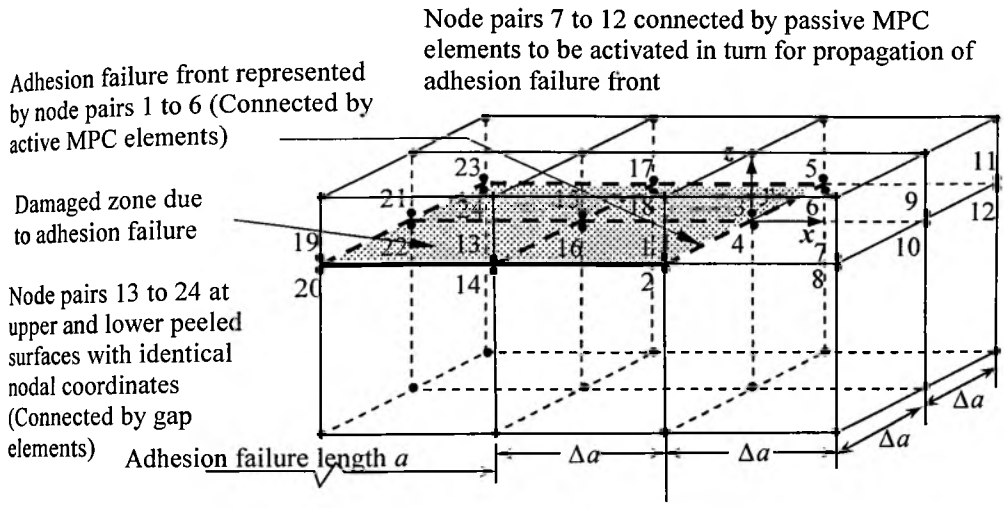

Figure 5.5 3D Finite element discretization of the SLJ having adhesion failure length a used for computation of SERR by MCCI.

For a bonded joint with adhesion failures, the stress field near the damage tip at the bi-material interface possesses oscillatory character and, as a result, the mode *I* and mode *II* components of SERR, i.e., G_I and G_{II}, do not converge in terms of crack closure integrals. This fact has also been observed by Sun and Jih [112] near the crack tip at the bi-material interface. The region of oscillatory perturbation of the stress field near the crack tip is very small and, therefore, if the element size near the crack tip i.e. the assumed crack tip extension is larger than this region, then the G_I and G_{II} components can be computed accurately. This aspect has been discussed in details in Sec. 4.4.

5.4 Results and discussion

Figure 5.6 shows the longitudinal cross section through the central region of the SLJ along which the variations of stress distribution, strength and SERR have been presented from the results of the three-dimensional FE analysis carried out and use of MCCI. The paths of propagation of adhesion failure lengths c_1 and c_2 from the two ends of the adhesive layer are represented by adherend-adhesive interfaces CD and AB, respectively.

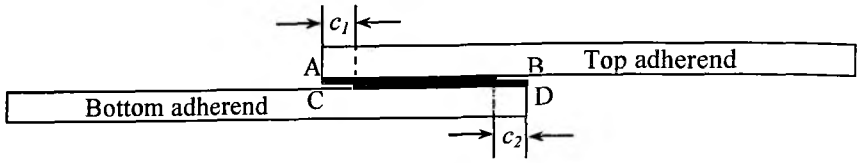

Figure 5.6 Longitudinal cross section through the central region of SLJ along which the variations of stress distribution and SERR have been presented (CD and AB are the paths of propagation of adhesion failure lengths c_1 and c_2 from both ends of the adhesive layer).

5.4.1 Stress distributions in the adhesive layer

The mid-surface of the adhesive layer is prone to cohesive failure due to both peel stress (σ_z) and shear stress (τ_{zx}). The peel and shear stress distributions along the mid-surface of the adhesive layer of the longitudinal cross section taken along the central region of the SLJ for varying adhesion failure lengths c_1 and c_2 from the two ends of the adhesive layer are shown in Figs. 5.7 and 5.8. The effects of varying c_1 on peel and shear stress distributions along the mid-surface of the adhesive layer are illustrated in Figs. 5.7 (a) and 5.8 (a), whereas Figs. 5.7 (b) and 5.8 (b) represent the effect of varying c_2.

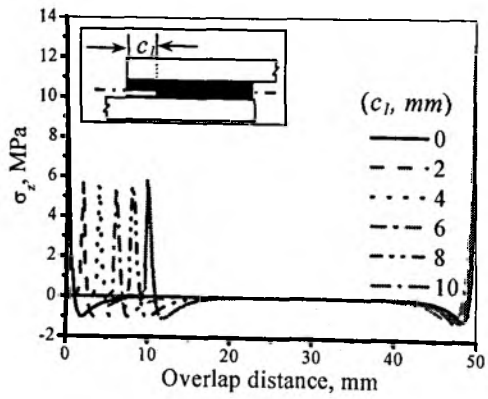

(a) Effect of variation of c_1

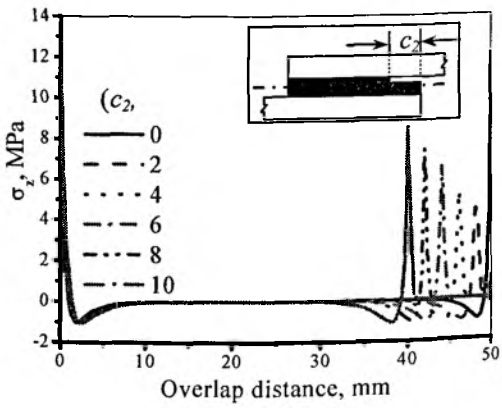

(b) Effect of variation of c_2

Figure 5.7 Peel stress (σ_z) distribution along the mid-surface of adhesive layer for varying adhesion failure lengths c_1 and c_2 from both ends of the adhesive layer.

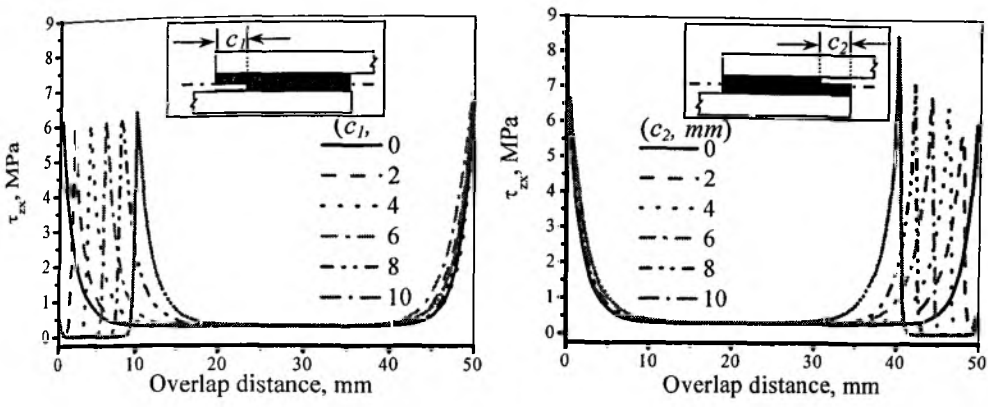

(a) Effect of variation of c_1 (b) Effect of variation of c_2

Figure 5.8 Shear stress (τ_{zx}) distribution along the mid-surface of adhesive layer for varying adhesion failure lengths c_1 and c_2 from both ends of the adhesive layer.

It is observed that in both cases the peel and shear stresses become almost zero in the regions away from the adhesion failure tip. There is only a marginal increase of peak peel and shear stresses when the adhesion failure length c_1 increases, whereas there is significant increase of both peel and shear stresses with increasing value of c_2. The peel or shear stresses are maximum when the values of c_1 or c_2 are equal to 10mm. It is observed that such peak values of the peel or shear stresses are increased due to the presence of adhesion failures, whereas the joint with no adhesion failure has the lowest peak peel or shear stress at the overlap end. From Figs. 5.7 and 5.8, it is also seen that secondary peak values of peel and shear stresses exist in the adhesive layer close to the adhesion failure tip and the values of secondary peak stresses increase significantly when the adhesion failure length c_2 propagates. The peel and shear stresses in the damaged model obtained from the present FE analysis have similar trends of distributions as observed by earlier researchers [21, 36, 88].

Thus, from the stress analysis it may be concluded that the effect of propagation of adhesion failure length c_2 is more prominent compared to that of c_1 on failure of the joint occurring in the adhesive layer.

5.4.2 Joint strength

The load carrying capacity of the SLJ largely depends on the undamaged portion along the adherend-adhesive interfaces i.e. AB and CD as shown in Fig. 5.6. This fact

necessitates the determination of the failure index along AB and CD for different values of c_1 with varying adhesion failure length c_2. Failure index e may be defined as the parameter which characterizes the failure initiation and this corresponds to the location having a higher value of e in the 3D parabolic failure criterion given by Raghava et al. [135] as expressed in Eq. (3.98). Using Eq. (3.98) along with the material properties given in Table 5.1, the failure indices have been calculated along the adherend-adhesive interfaces of undamaged portions of the overlap region of the SLJ.

Figure 5.9 shows the effects of varying the failure lengths c_1 (0 to 10mm) and c_2 (0 to 10mm) on the failure index e along the mid-surface of the adhesive layer. Further, Fig. 5.10 shows the effects of varying the adhesion failure lengths c_1 and c_2 on the failure index e along the top interface AB of the SLJ (ref. to Fig. 5.6). Similarly, Fig. 5.11 shows the effects of varying the failure lengths c_1 and c_2 on the failure index e of the bottom interface CD of the SLJ.

The maximum value of failure index e along the mid-surface of the adhesive layer is smaller compared to that along the interfaces irrespective of the magnitudes of the adhesion failure lengths c_1 and c_2, which indicates that a cohesive failure would not occur due to the presence of adhesion failure as long as the path of propagation is along the adherend-adhesive interfaces. Figures 5.9-5.11 also indicate that the maximum value of e is at the point of discontinuity, i.e. the tip of adhesion failure front and is largest for c_1=10mm. There is no specific trend in the variation of the value of e at the tip of adhesion failure length c_2 except for c_1=0. The e value remains constant at the damage front of c_2 for all values of failure lengths c_2. The distribution of e along the top interface as shown in Fig. 5.10 indicates that the maximum value of e is at the failure front c_1 for c_1=0 as shown in Fig. 5.10 (a) and there is an increase in the maximum value of e at the failure front c_2 and is highest for c_2=10mm as shown in Fig. 5.10 (f). Similarly, the variation of e along the bottom interface as shown in Fig. 5.11 indicates that the e value for c_1=0 is minimum for any failure length c_2 and there is a marginal increase in e value at the failure front c_2 and is highest for c_2=10mm as shown in Fig. 5.11 (f). These results, in general, indicate the reduction of failure load in a damaged specimen of the embedded adhesion failures by increasing either of the adhesion failure lengths c_1 or c_2, rather than the case of two adhesion failures simultaneously initiating from the two ends of the adhesive layer and propagating to cause the final failure of the joint.

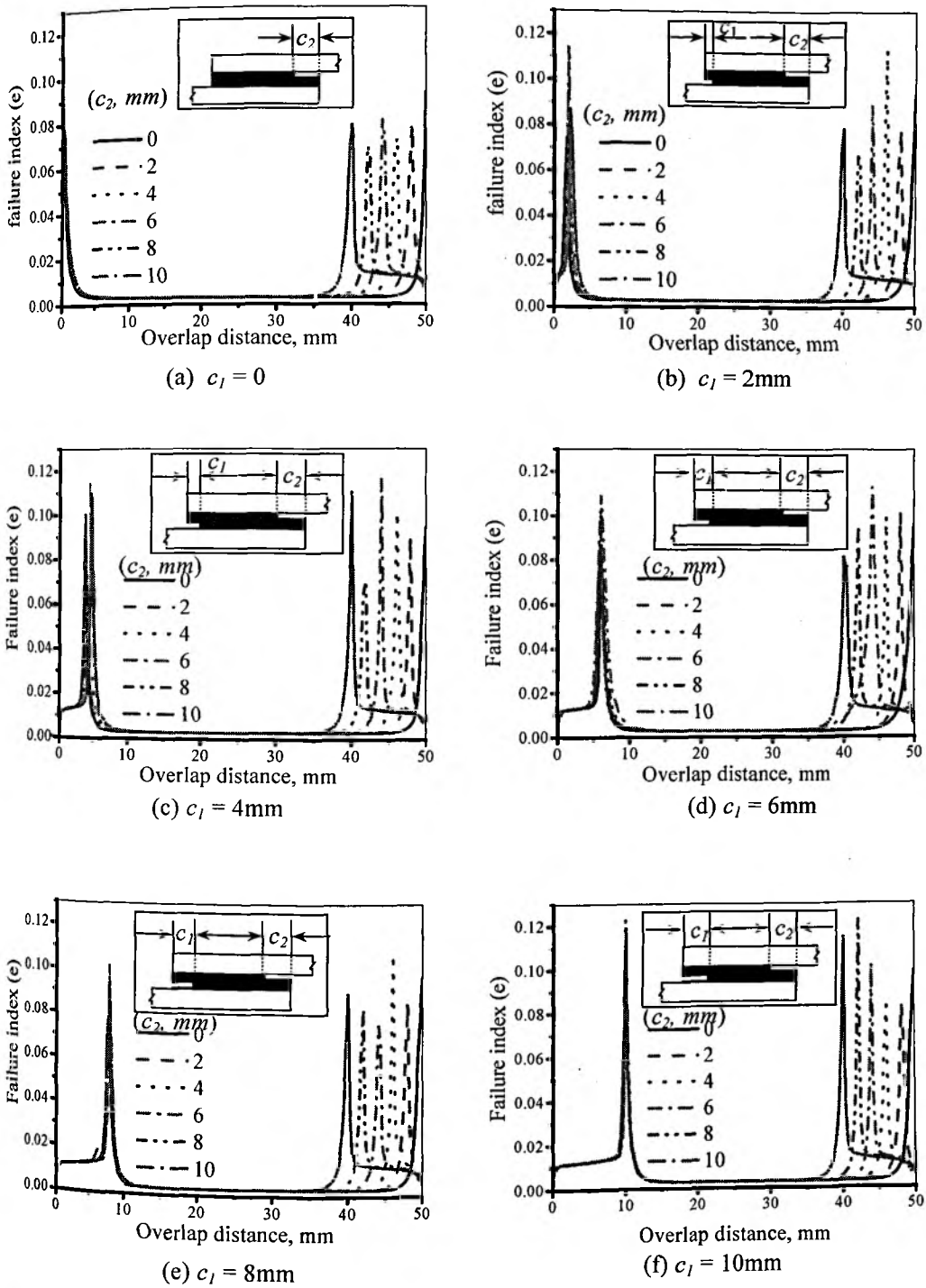

Figure 5.9 Effects of varying the adhesion failure lengths c_1 and c_2 on the failure index (e) along the mid-surface of adhesive layer.

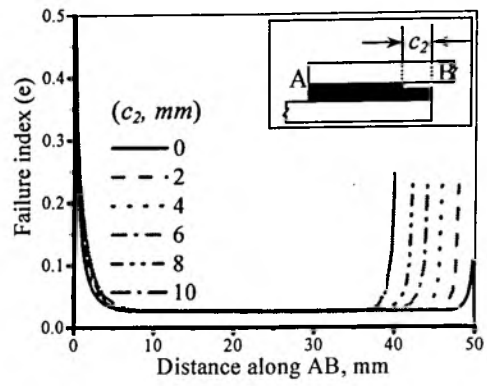

(a) $c_1 = 0$

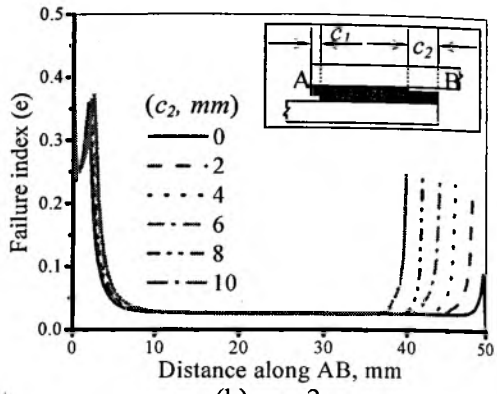

(b) $c_1 = 2$mm

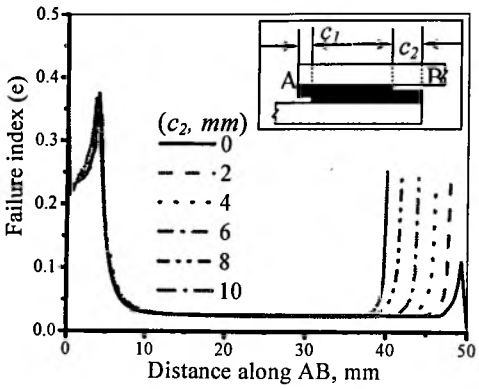

(c) $c_1 = 4$mm

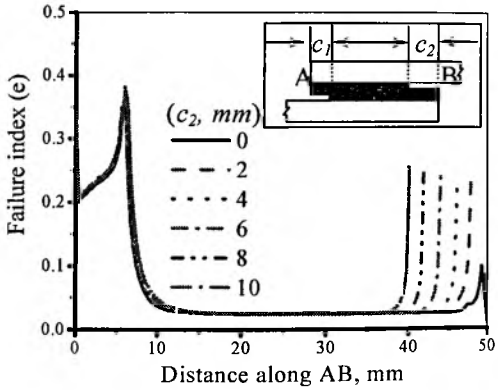

(d) $c_1 = 6$mm

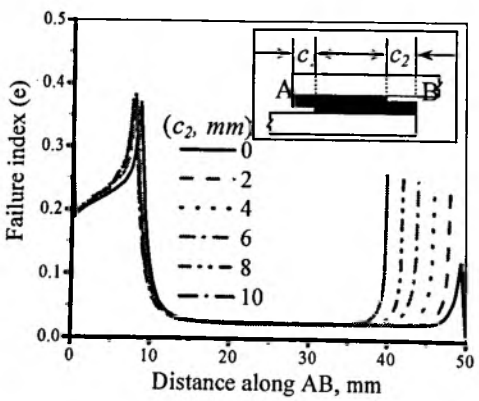

(e) $c_1 = 8$mm

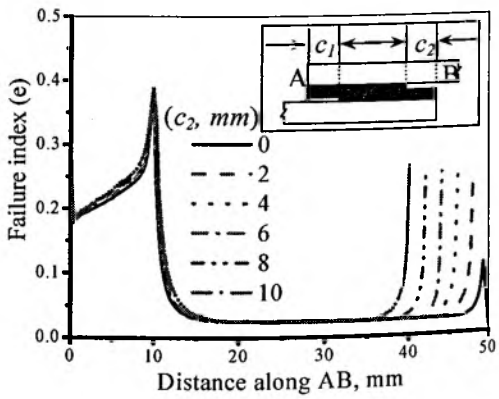

(f) $c_1 = 10$mm

Figure 5.10 Effects of varying the adhesion failure lengths c_1 and c_2 on the failure index (e) along the top interface (AB).

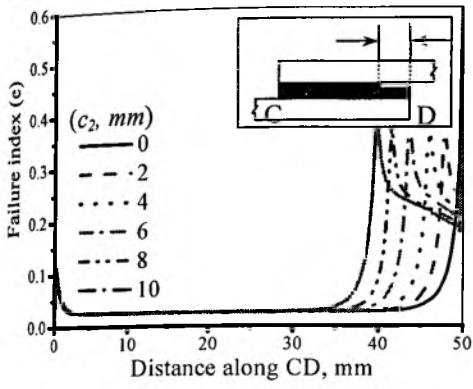

(a) c_1 = 0mm

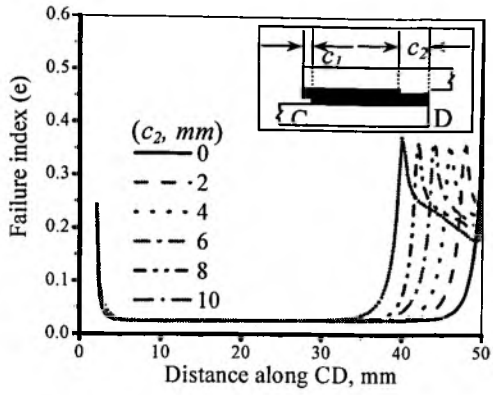

(b) c_1 = 2mm

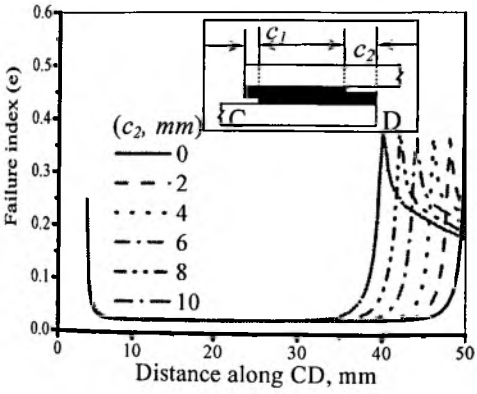

(c) c_1 = 4mm

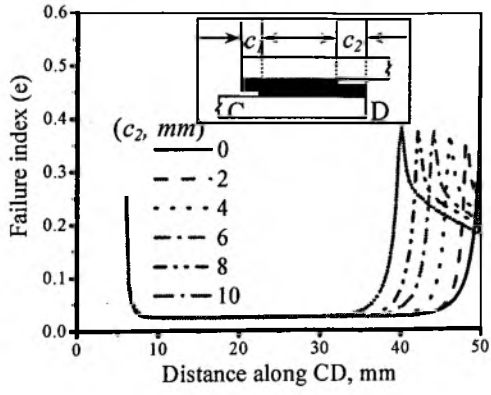

(d) c_1 = 6mm

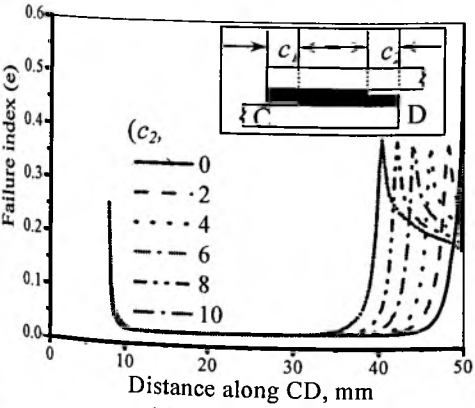

(e) c_1 = 8mm

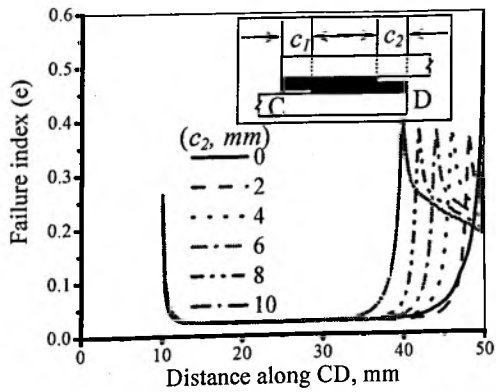

(f) c_1 = 10mm

Figure 5.11 Effects of varying the adhesion failure lengths c_1 and c_2 on the failure index (e) along the bottom interface (CD).

5.4.3 SERR variations due to adhesion failure propagation

The mode *I* SERR (G_I) and the mode *II* SERR (G_{II}) at the fronts of the adhesion failure lengths were determined using Eqs. (3.109) and (3.110) and have been presented in Figs. 5.12 and 5.13 for varying adhesion failure lengths c_1 and c_2 from the two ends of the adhesive layer. Figure 5.12 (a) represents the variation of SERR in mode *I* (G_I) when adhesion failure of length c_1 propagates with pre-embedded adhesion failure length c_2 (0.21mm, 1mm and 1.5mm). Similarly G_I has been plotted in Fig. 5.12 (b) by varying the value of c_2 for pre-embedded adhesion failure length c_1 (0.21mm, 1mm and 1.5mm). Figure 5.13 shows the variation of mode *II* SERR (G_{II}) for varying adhesion failure lengths c_1 and c_2 from the two ends of the adhesive layer.

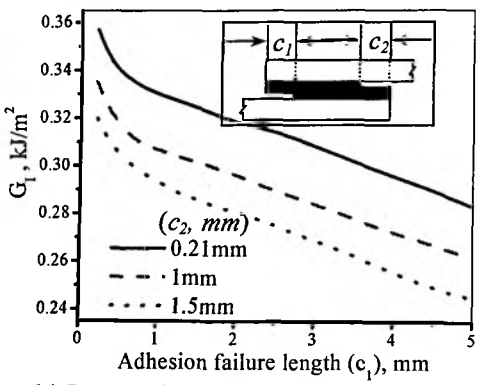

(a) Propagation of c_1 with pre-embedded adhesion failure length c_2

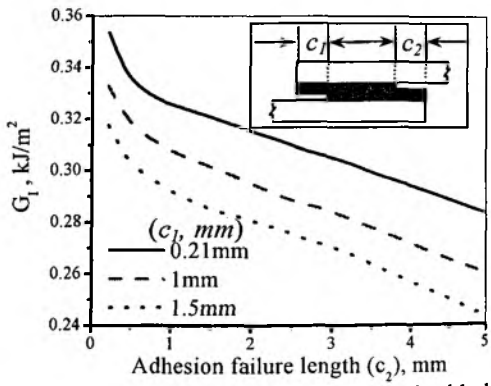

(b) Propagation of c_2 with pre-embedded adhesion failure length c_1

Figure 5.12 Variation of SERR (G_I) for varying adhesion failure lengths c_1 and c_2 from both ends of the adhesive layer.

Figure 5.12 illustrates that the mode *I* SERR (G_I) at the adhesion failure front decreases as the adhesion failure propagates, i.e. the smaller the adhesion failure length c_1 or c_2, the larger is the SERR value. This indicates that the resistance to initiation of adhesion failure propagation in mode *I* is high for joints having small adhesion failure lengths and gets even smaller as the adhesion failure length propagates. The joints with large embedded adhesion failure lengths at both ends of the adhesive layer have low SERR values. This means that the resistance to failure initiation and its subsequent propagation is less. It is seen that mode *I* SERR, i.e., G_I value decreases at a faster rate up to c_1 or c_2 = 1mm and beyond this, the decrease is relatively slow. Thus, it may be concluded that composite SLJ's with smaller

adhesion failure lengths at both ends of the adhesive layer are more damage tolerant in mode *I* compared to the joints having larger adhesion failure lengths.

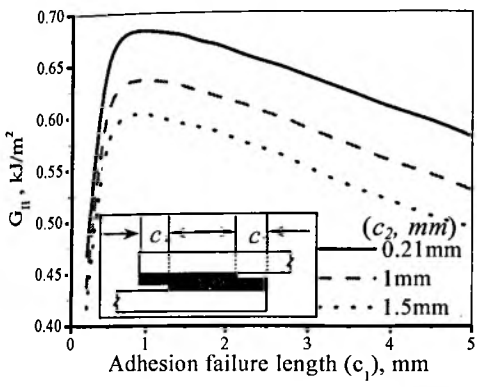

(a) Propagation of c_1 with pre-embedded adhesion failure length c_2

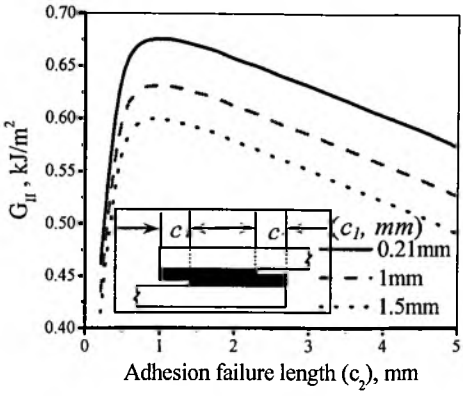

(b) Propagation of c_2 with pre-embedded adhesion failure length c_1

Figure 5.13 Variation of SERR (G_{II}) for varying adhesion failure lengths c_1 and c_2 from both ends of the adhesive layer.

Figure 5.13 illustrates that the SERR in mode *II* (G_{II}) increases almost linearly up to the value of c_1 or c_2 = 0.5mm. It has been seen that when the embedded adhesion failure length c_1 or c_2 propagates up to 0.5mm, the difference in G_{II} values is insignificant for any pre-existing adhesion failure at both the ends. This indicates that resistance to failure propagation up to 0.5mm under mode *II* is not affected by the embedded adhesion failures. However, referring to Figs. 5.13 (a) and 5.13 (b), G_{II} value is the highest when c_1 and c_2 propagate up to 0.8mm and 1mm, respectively and beyond which it decreases. This indicates that the resistance to adhesion failure propagation is the highest until the failure propagates up to 0.8mm for c_1 and 1mm for c_2 under mode *II* and beyond which it decreases for all lengths of embedded adhesion failures. Further, it is observed that for smaller values of adhesion failure lengths c_1 or c_2, SERR in mode *II* is larger and is independent of failure propagation path. For all values of adhesion failure lengths, SERR in mode *II* (G_{II}) is larger than SERR in mode *I* (G_I) which indicates that SERR in mode *II* is more responsible for propagation of adhesion failure.

5.5 Conclusions

Geometric non-linear finite element analyses utilizing the MCCI approach have been used to study the behaviour of adhesion failure propagation in an adhesively bonded single lap laminated FRP composite joint with embedded adhesion failures. Some of the observations and conclusions are given below:

- The adhesion failures propagating along the adherend-adhesive interfaces from the two ends of the adhesive layer of the SLJ have dissimilar effects.
- In addition to the peak stresses at the overlap ends, there exist secondary peak peel and shear stresses in the adhesive layer close to the adhesion failure front and the secondary peak peel stresses increase significantly when the adhesion failure length c_2 propagates. But the increase is only marginal in case of propagation of c_1.
- The presence of adhesion failure eliminates the possibility of initiation of cohesive failure in the SLJ. Adhesion failure will initiate from one of the ends of the adhesive layer and propagate until the final failure of the joint rather than two adhesion failures simultaneously initiating from the two ends of the adhesive layer.
- The interaction of adhesion failures initiating at both ends of the adhesive layer and their subsequent propagation reduces the load carrying capacity of the joint significantly. The failure index is high at the tips of adhesion failures and is the highest for the adhesion failure length of 10mm.
- Variations of SERR for varying adhesion failure lengths indicate that the smaller is the adhesion failure length, the higher will be the SERR value. Therefore, SLJs having smaller adhesion failure lengths offer higher resistance for the initiation of adhesion failure propagation compared to those having larger failure lengths. Irrespective of the size of the adhesion failure length c_1 or c_2, the shear mode i.e. mode *II* is the dominant mode for adhesion failure propagation in an SLJ.

6

Delamination Damage Analyses of Single Lap Joint for Varied Positions of Through-the-Width Pre-embedded Delaminations

6.1 Introduction

Adhesive bonding in laminated FRP composites is being increasingly used in many applications especially in space, aircraft and automobile industries because of its well known advantages over the other joining methods such as mechanical fastening, welding, brazing and soldering, etc. A good number of research investigations relating to adhesively bonded joints in FRP composites have included the single lap joint configurations amongst the wide variety of geometries being analyzed. Notably among them, Volkersen [15], Goland and Reissner [16], Hart-Smith [18] and Adams et al. [20, 27, 28, 182] provided considerable elucidations of qualitative behaviour of loaded adhesively bonded single lap joints. Their analyses are limited to isotropic metallic adherends and are based on certain simplified assumptions as highlighted by Carpenter [25] in order to achieve tractable results and the consequent quantitative agreement with experiments has hitherto been less than adequate to form a basis for the designer without empirical modifications. The factors considered for these analyses include adhesive plasticity, adherend stiffness imbalance, nature of loadings and other influencing parameters like spew geometry, thickness of the adherends and the adhesive layer, overlap lengths, etc. With optimized values of those influencing parameters along with valid assumptions, extensive research efforts have been put forward by Tong [21, 35, 64, 97], Adams et al. [20, 27, 28, 182], Renton and Vinson [80] and Jena [183], etc. for laminated FRP composite adherends using analytical and numerical techniques. The potential problems of coupled anisotropy and material heterogeneity associated with the use of laminated composite adherends always require a relook for further research. In addition to the existing complexities due to the material heterogeneity and discontinuities of loading and geometry giving rise to stress concentration effect, the various modes of failures such as delaminations, fiber

breakage and interlaminar cracking make the joint analyses more complex and involved.

Interlaminar or interply delamination is a major failure mode in the adherends of a FRP composite bonded joint [37, 40, 182]. As a result of this, the structures having bonded joints reduce their strengths and stiffness and thus the lives of the structures are limited. Due to the low transverse tensile strength, the SLJ experiences peel loading, and so the adherends are likely to fail in transverse tension before the adhesive layer fails. Like the shear stresses, the values of the peel stresses are the highest at the overlap ends and hence can induce adherend failures due to the low tensile strength in the transverse direction (through-the-thickness). Also, the severity of joint failure would be enhanced due to loading eccentricity in case of SLJ. In such cases, eventhough the remote loading is of in-plane type, the local loading effect near the discontinuities prevailing around the overlap portions of the joint may be out-of-plane type. Although a lot of work has been done to understand and predict the failure behaviour of laminated FRP SLJ [34, 42, 167, 168, 172, 184], no appreciable effort has been devoted to understand the effect of presence of through-the-width delamination when embedded in the adherends on delamination propagation parameters such as interlaminar stresses (σ_z, τ_{yz} and τ_{xz}) and the three individual modes of Strain Energy Release Rates (SERR).

The present Chapter deals with the study of the effect of embedded delamination positions on stress distributions in the adhesive layer, interlaminar stress distributions and SERR variations on delamination fronts, when they are present in either of the laminated adherends for the considered SLJ as shown in Fig. 6.1. The analytical solutions [16, 18, 28, 161, 185] indicate that the peel stress and shear stress distributions in the adhesive layer are maximum at the overlap ends. Thus, it necessitates to study the effects of through-the-width embedded delamination, located beneath the surface ply of either adherends adjacent to the adhesive layer and closer to the overlap ends of the joint, on stress distributions in the adhesive layer, interlaminar stress variations and different modes of SERR (G_I, G_{II} and G_{III}). Figure 6.1 (a) represents the geometry and configuration of the laminated FRP composite SLJ when through-the-width delamination is embedded in the bottom adherend and similarly Fig. 6.1 (b) shows the delamination damage location in the top adherend. Non-linear finite element analyses have been carried out for varying delamination locations by embedding them at either a distance d_1 or d_2 equal to $0.4c$, $0.5c$ and $0.6c$ in either of the adherends. Here, d_1 or d_2 is the distance between the center of the

embedded delamination and the mid point of the overlap length c of the bottom or the top adherend of the joint, respectively. The stress states are much different at the two overlap ends because of loading eccentricity prevailing in the joint and hence analyses have been performed separately for the two cases corresponding to Figs. 6.1 (a) and 6.1 (b).

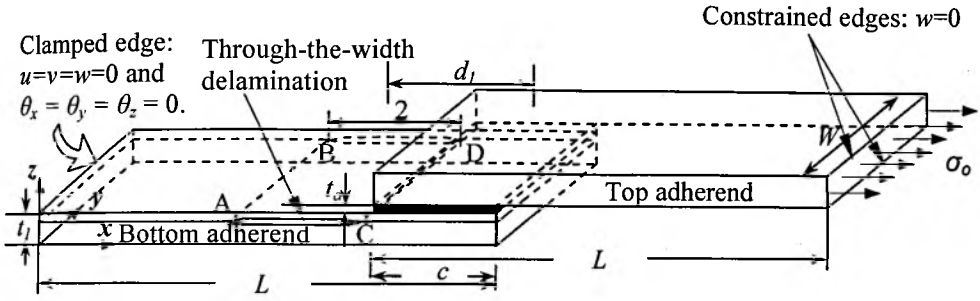

d_1 = Distance between center of delamination embedded in the bottom adherend and mid point of the overlap length

(a) Bottom adherend showing two delamination fronts AB and CD

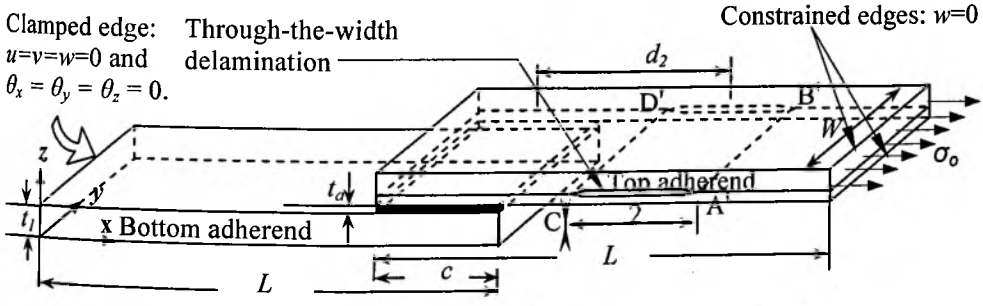

d_2 = Distance between center of delamination embedded in the top adherend and mid point of the overlap length

(b) Top adherend showing two delamination fronts A'B' and C'D'

Figure 6.1 Single lap laminated FRP composite joint showing delamination damages embedded in either of the adherends near the overlap ends beneath the surface ply adjacent to the overlap region.

6.2 Joint geometry and material constants

The laminated FRP composite SLJ specimen is shown in Fig.6.1 and has length L = 95mm, width W =20mm, overlap length c = 15mm and adhesive layer thickness t_a = 0.26mm. The top and bottom adherends are of $[0]_8$ graphite/epoxy FRP composite laminates whose material constants are given in Table 6.1. Each ply thickness is taken to be 0.125mm. The through-the-width delaminations of length 2mm each have been presumed to be pre-embedded as shown in Figs. 6.1 (a) and 6.1 (b), respectively. Non-linear finite element analyses have been carried out for the SLJ with embedded delaminations at three specified locations; (i) when the delamination is completely within the overlap region of the SLJ, i.e. d_1 or d_2=0.4c, (ii) when the mid point of the delamination is exactly aligned with the overlap end, i.e. d_1 or d_2=0.5c and (iii) when the delamination is completely outside the overlap region of the SLJ, i.e. d_1 or d_2=0.6c. One end of the SLJ is clamped and the other end is uniformly loaded as shown in Fig. 6.1. A total of 20kN load has been uniformly distributed to be applied through this end. Stresses have been evaluated in the adhesive layer and on the delamination fronts using finite element software ANSYS 10.0 in a high speed IBM platform. The components of Strain Energy Release Rate (SERR), G_I, G_{II} and G_{III} corresponding to opening, shearing and tearing modes of fracture have been computed to characterize the delamination propagation characteristics in respect to varied positions of the embedded delaminations.

Table 6.1 Graphite/epoxy FRP composite lamina and epoxy adhesive material properties [165]

Graphite/epoxy FRP composite adherend:	Material constants: E_x = 181 GPa, $E_y = E_z$ = 10.3 GPa $\nu_{xy} = \nu_{xz}$ = 0.28, ν_{yz} = 0.3 $G_{xy} = G_{xz}$ = 7.17GPa, G_{yz} = 4 GPa
Epoxy adhesive:	E = 2.8 GPa, ν = 0.4

6.3 Finite element analyses of SLJ with pre-embedded delaminations

The bonded joint analysis becomes more involved and complex due to the presence of delamination even with straight delamination front. Usually Linear Elastic Fracture Mechanics (LEFM) procedures have been adopted for studying the delamination propagation characteristics in SLJ of laminated FRP composites. Either a stress intensity factor (K) criterion or strain energy release rate (G) criterion is considered to

establish the delamination damage propagation characteristics. In the former case, the delamination front stress intensity factor K is compared with the critical stress intensity factor K_c of the material. However, in composite materials the crack tip stress geometry function relating K to the stress σ and defect dimension is not the standard isotropic factor, and therefore, most delamination studies and tests have been developed using the strain energy release rate criterion. Strain energy release rate is a material parameter independent of geometry and hence has been considered to be a candid parameter for predicting the damage growth [186]. Thus, the delamination induced damaged composite material is characterized by the modes *I*, *II*, and *III* critical strain energy release rates G_{Ic}, G_{IIc}, and G_{IIIc}, respectively. The three components of strain energy release rate are being used to characterize the interlaminar fracture in delamination and debonding analyses of composite structural members [147-149]. Therefore, to characterize the interfacial delamination behaviour in FRP composite joints, three-dimensional finite element analyses are required to be conducted [186, 187] to evaluate the SERRs along the delamination fronts. Calculations of energy release rate components are based on Irwin's theory of Crack Closure Technique [108]. It is hypothesized that for an infinitesimal increment in crack length Δa, the crack opening displacement $\delta(x-\Delta a)$ for the crack of length a can be considered equal to the crack opening displacement δx along the delamination front. By this method, the displacement field ahead of the delamination front is approximated to be the same as that one behind it. The significant advantage of this method is that only one finite element run is required instead of two to evaluate the values of individual modes of SERR [188].

Interlaminar stresses are responsible for the initiation and further propagation of delamination. Since the stress state is inherently three-dimensional [186], this aspect necessitates for a full three-dimensional damage analysis for obtaining complete information on the delamination front. The 3D brick element models are known to be more accurate especially in dividing the strain energy release rate into individual modes [189]. Though, brick elements are more accurate for SERR computations, but by using many layers of brick elements through-the-thickness to model the individual plies, the modelling and computational effort may become prohibitively large [11, 140, 165]. Therefore, in the present analysis, three-dimensional eight-node layered volume elements (SOLID 46) with layerwise material constants have been used to model the different sublaminates of laminated composite adherends and SOLID 45 elements have been used for the adhesive layer. The

through-the-width delaminations are presumed to be embedded in either of the adherends between the surface and second plies and each has been modelled as a sublaminate as shown in Fig. 6.2. Figures 6.2 (a) and (b) demonstrate the sublaminates of bottom and top adherends, respectively, to be used for finite element meshing and subsequent evaluation of the individual modes of strain energy release rates on the delamination fronts. The 3D finite element meshes of the overlap region of the SLJ specimens embedded with through-the-width delaminations in either of the adherends are shown in Fig. 6.3. The zoomed views of the finite element mesh of the bottom and the top adherends embedded with through-the-width delaminations have been displayed in Figs. 6.4 (a) and (b).

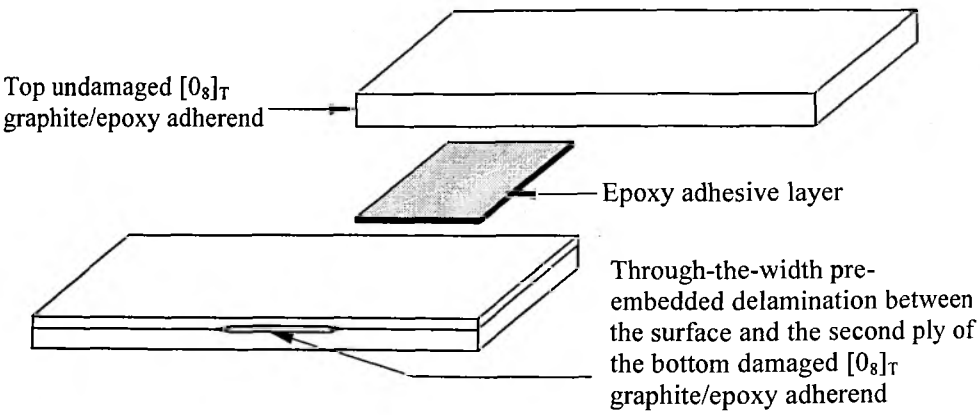

(a) Sublaminates of the SLJ shown in Fig. 6.1 (a)

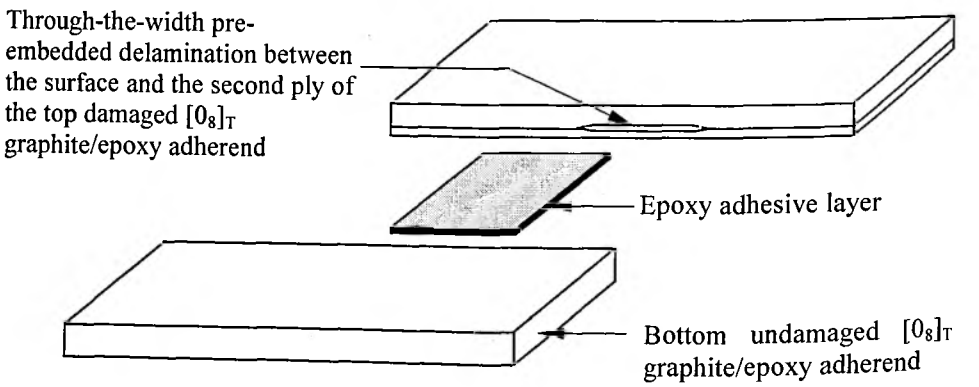

(b) Sublaminates of the SLJ shown in Fig. 6.1 (b)

Figure 6.2 Sublaminates of laminated composite SLJ embedded with delamination damage.

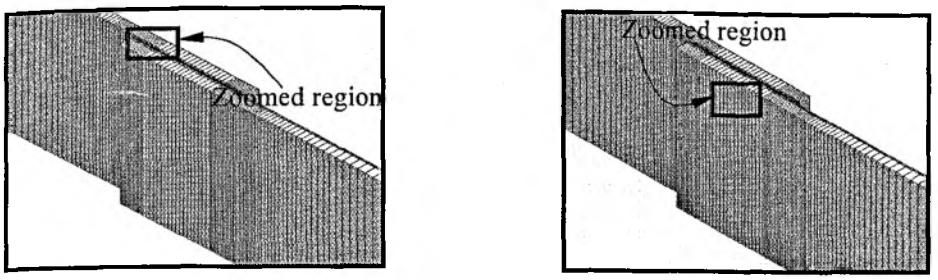

(a) Embedded delamination in bottom adherend (b) Embedded delamination in top adherend

Figure 6.3 Finite element meshes showing the overlap region of the SLJ specimens embedded with delaminations in either of the adherends. (Cases: Fig. 6.1 (a) and Fig. 6.1 (b)).

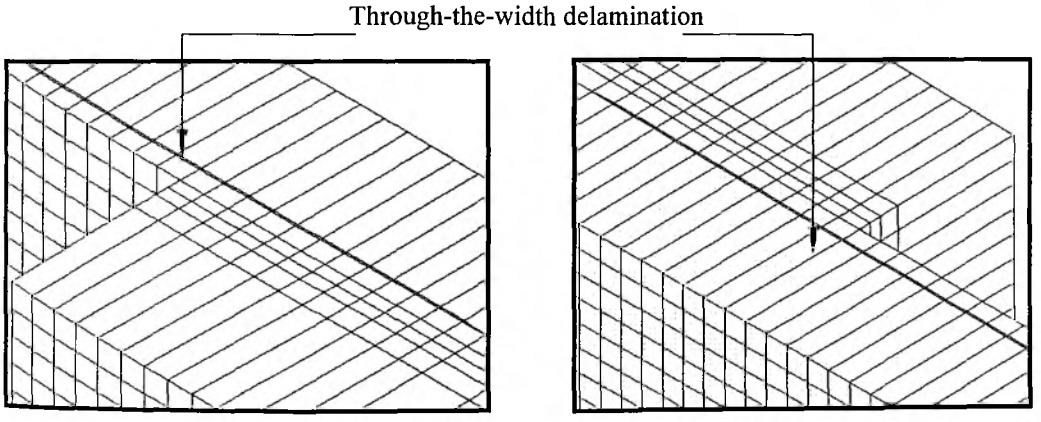

(a) Embedded delamination in bottom adherend (b) Embedded delamination in top adherend

Figure 6.4 Zoomed view of the finite element meshes.

The propagation of delamination front is assumed to be self-similar and occur in the same plane. The delamination propagation characteristics are quite complex and thus the FE analyses should have rigorous error analysis and convergence requirements with judicious mesh grading and appropriate element size near the delamination front. This is needed to avoid the oscillatory nature of the stress field very near to the delamination front and also to accurately evaluate the delamination propagation characteristics. This has been duly carried out during computational stages to achieve the required level of accuracy. The element size has been taken as one fourth of the ply thickness as suggested [11, 140, 147-149] near the delamination zone and has been found to be satisfactory for the convergence requirements. Except over the delaminated region, Multi-Point Constraints are imposed on the nodes along

the delamination boundary and contact elements are used within the delaminated region to prevent mutual interpenetration of the top and bottom delaminated surfaces. This contact processor always maintains a positive value of displacement difference along the z-direction between the pair of nodes inside the delaminated zone of the top and bottom delaminated surfaces. Furthermore, it has been assumed that the delamination plane is the weakest and the delamination will propagate parallel to the *xy* plane. Thus, the possibility of out-of-plane propagation is ignored. The three components of strain energy release rate viz. G_I, G_{II}, and G_{III} have been evaluated using Modified Crack Closure Integral (MCCI) and have been used as parameters for assessing the delamination growth characteristics.

6.4 Computation of SERR

Figure 6.5 shows the model for evaluation of MCCI applied to the SLJ for computation of SERR along the delamination front CD when through-the-width delamination of length a is embedded beneath the surface ply in the bottom adherend. The strain energy released by the propagation of a delamination of length a to $a+\Delta a$ is given by

$$W = \frac{1}{2}\int_{a}^{a+\Delta a}\int_{-\Delta a/2}^{\Delta a/2}\sigma(x,y)\times\delta(x-\Delta a,y)\,dx\,dy \tag{6.1}$$

where $\delta(x-\Delta a,y)$ is the crack opening displacement between the top and bottom delaminated surfaces and $\sigma(x,y)$ is the stress at any point on the delamination front CD required to close the delaminated area.
Then the strain energy release rate (G) is obtained as

$$G = \lim_{\Delta a\to 0}\frac{W}{\Delta A} \tag{6.2}$$

where ΔA represents the delamination propagated area and equals to one element area in xy plane i.e. $\Delta a\times\Delta a$ for the present case. The MCCI has the advantage of mode separation of strain energy release rate. This will help for a qualitative analysis of delamination damage propagation behaviour. Accordingly, the three components of strain energy release rates G_I, G_{II} and G_{III} for modes *I*, *II*, and *III* can be expressed as given in Eqs.(3.109-3.111).

While implementing these Equations to evaluate the three components of SERR for delamination damage analyses of Single Lap Joint for varied positions of through-the-width pre-embedded delaminations, the subscripts T and B represent the top and bottom delaminated sublaminates, respectively. The existing delamination length is denoted by a and Δa is considered to be the virtual delamination growth. [u_T, v_T, w_T] and [u_B, v_B, w_B] represent the displacements corresponding to the nodes at the top and bottom delaminated surfaces, respectively, behind the delamination front and σ_z, τ_{zx} and τ_{zy} are the stresses required to close the delamination front.

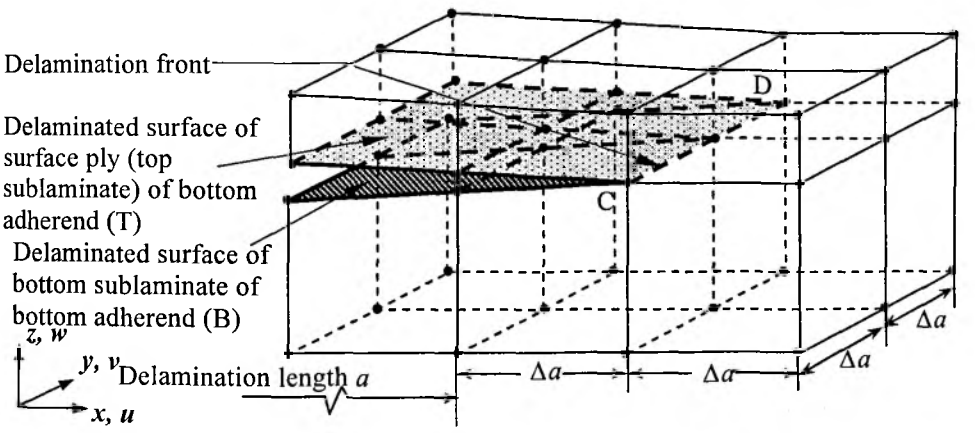

Figure 6.5 MCCI applied to the SLJ for computation of SERR along the delamination front CD when delamination is embedded in the bottom adherend (Case Fig. 6.1 (a)).

6.5 Results and discussion

6.5.1 Effect of delamination positions on out-of-plane stress distributions in the adhesive layer

The stress magnitude in the adhesive layer is always an important factor of the bonded joint analysis. The out-of-plane stresses (σ_z, τ_{xz} and τ_{yz}) are shown in Figs. 6.6-6.12 when through-the-width delamination is embedded in the bottom and the top adherends with varying delamination positions. The stress distributions in the

adhesive layer without delamination damage are shown in Fig. 6.6 and are similar to that given in the literatures [20, 21, 161, 172]. Figures 6.7 and 6.8 indicate that the out-of plane normal stress (σ_z) becomes compressive in the region close to the delamination fronts when embedded in both the adherends and located completely inside the overlap region i.e. d_1 or d_2=0.4c. When the center of delamination front is exactly aligned with the overlap end of the SLJ i.e. d_1 or d_2=0.5c, it is seen that secondary peak of out-of-plane stress components (σ_z, τ_{xz} and τ_{yz}) appear at locations closer to the overlap end of the SLJ as shown in Figs. 6.9 and 6.10. However, secondary peak value of peel stress (σ_z) is higher for the bottom delaminated adherend as shown in Fig. 6.9. This condition may enhance the possibility of fiber breakage at the surface ply of the delaminated adherend as predicted experimentally by Tong [35]. On the other hand, there is not much change in the magnitude of the two other stress components (τ_{yz} and τ_{xz}) when embedded in both the adherends. Figures 6.11 and 6.12 illustrate that there is not much influence on out-of-plane stress components when the delamination is located completely outside the overlap region i.e. d_1 or d_2=0.6c.

In general, the stress magnitudes in the overlap region remain more or less same along the width except at the free edges. Figures 6.6-6.12 depict clearly the three-dimensional nature of stresses and it can be emphasized here that the analysis involving composite SLJ must be carried out by three-dimensional finite element modelling.

6.5.2 Effect of delamination positions on interlaminar stress variations

Figures 6.13-6.16 represent the variations of interlaminar stresses (σ_z, τ_{xz} and τ_{yz}) along the delamination fronts AB, CD and A'B', C'D' when the through-the-width delaminations are embedded in the bottom and the top adherend, respectively, with varying delamination positions. Except for τ_{yz} stress components, there is marginal change in the stress distributions of σ_z and τ_{xz} over the middle portion of the joint irrespective of the delamination positions. Compared to the magnitude of the normal stress (σ_z), the magnitudes of the two shear stress components (τ_{xz} and τ_{yz}) are small. Thus, it indicates that the mode *I* i.e. the opening mode is predominant for the delamination propagation. It may be observed from Figs. 6.13 and 6.14 that σ_z values are significantly high when delamination is embedded completely within the overlap region of either of the adherends i.e. for d_1 or d_2 = 0.4c and is largest for the bottom delaminated adherend. This indicates that the delamination front closer to the overlap end is more sensitive to propagation of delamination damage. Figures 6.15 and 6.16

show that the σ_z value is high when the center of the delamination is exactly aligned with the overlap end of the SLJ for both the adherends compared to other positions of the delamination and is highest for the bottom delaminated adherend.

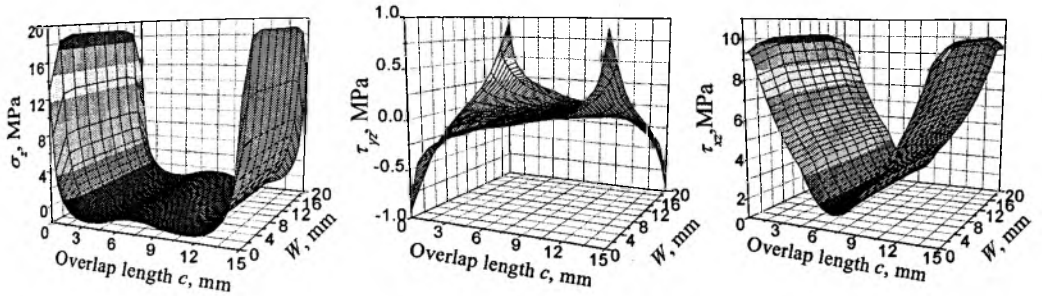

Figure 6.6 Out-of-plane stress (σ_z, τ_{yz} and τ_{xz}) variations in the mid-surface of the adhesive layer of the SLJ without delamination.

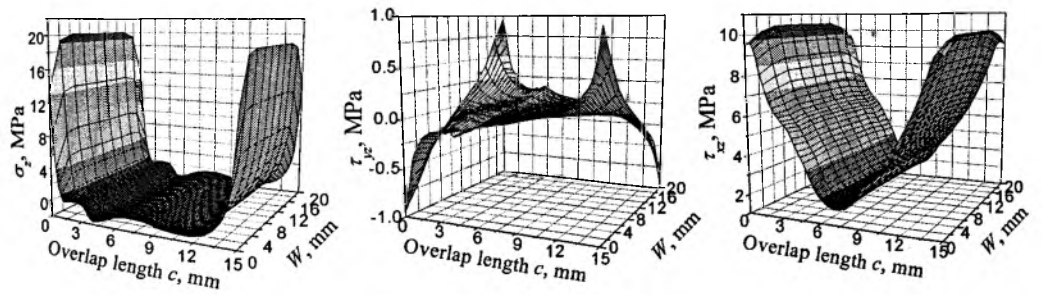

Figure 6.7 Out-of-plane stress (σ_z, τ_{yz} and τ_{xz}) variations in the mid-surface of the adhesive layer when delamination is embedded within the overlap region ($d_1 = 0.4c$) of the bottom adherend.

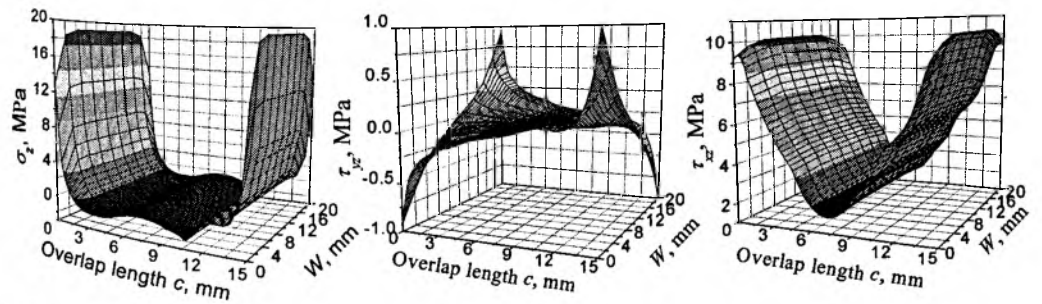

Figure 6.8 Out-of-plane stress (σ_z, τ_{yz} and τ_{xz}) variations in the mid-surface of the adhesive layer when delamination is embedded within the overlap region ($d_2 = 0.4c$) of the top adherend.

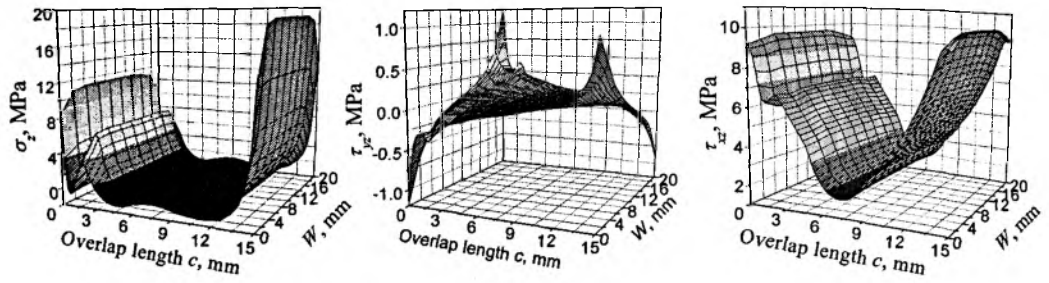

Figure 6.9 Out-of-plane stress (σ_z, τ_{yz} and τ_{xz}) variations in the mid-surface of the adhesive layer when the center of the delamination is exactly aligned with the overlap end ($d_1 = 0.5c$) of the bottom adherend.

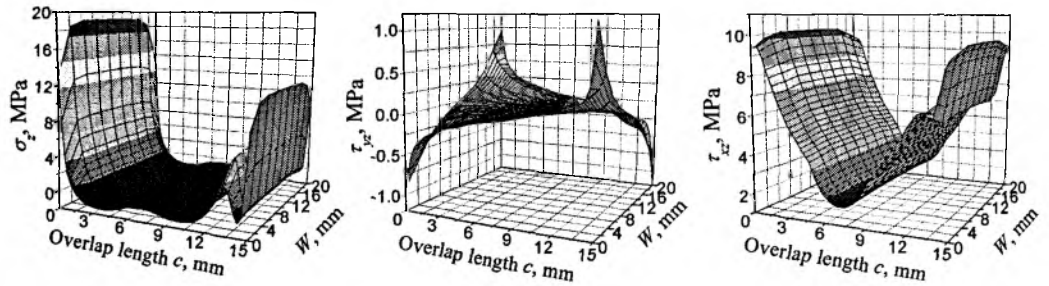

Figure 6.10 Out-of-plane stress (σ_z, τ_{yz} and τ_{xz}) variations in the mid-surface of the adhesive layer when the center of delamination is exactly aligned with the overlap end ($d_2 = 0.5c$) of the top adherend.

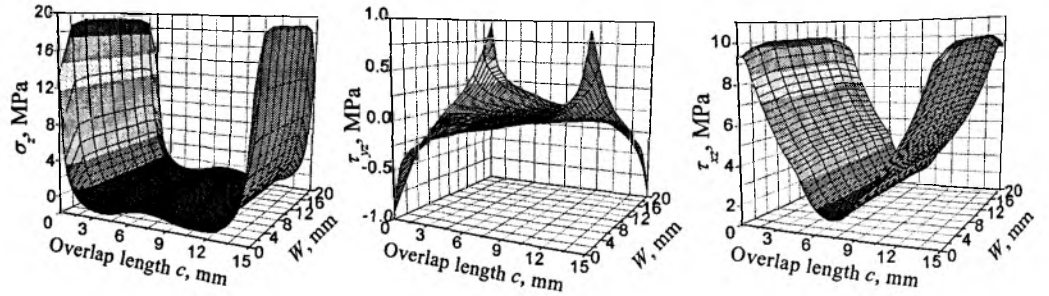

Figure 6.11 Out-of-plane stress (σ_z, τ_{yz} and τ_{xz}) variations in the mid-surface of the adhesive layer when the center of delamination is embedded outside the overlap end ($d_1 = 0.6c$) of the bottom adherend.

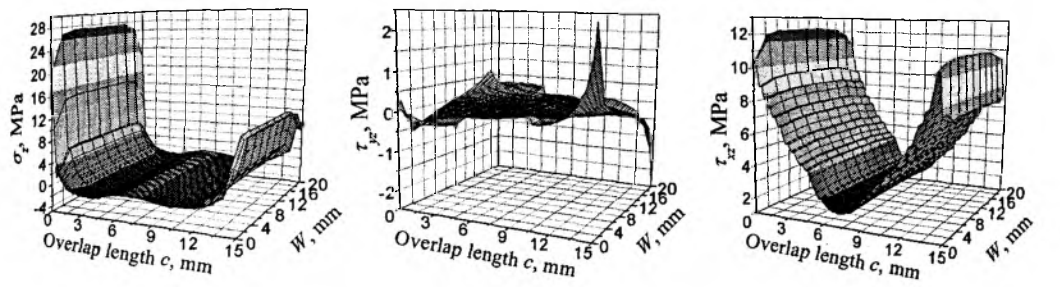

Figure 6.12 Out-of-plane stress (σ_z, τ_{yz} and τ_{xz}) variations in the mid-surface of the adhesive layer when the center of delamination is embedded outside the overlap end ($d_2 = 0.6c$) of the top adherend.

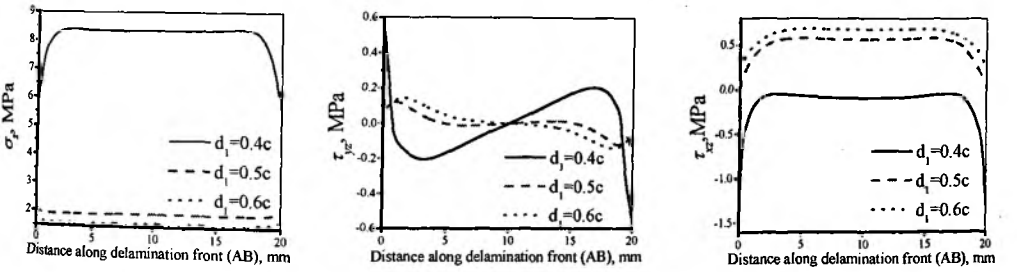

Figure 6.13 Interlaminar stress variations along the delamination front (AB) when embedded in the bottom adherend for varying delamination positions.

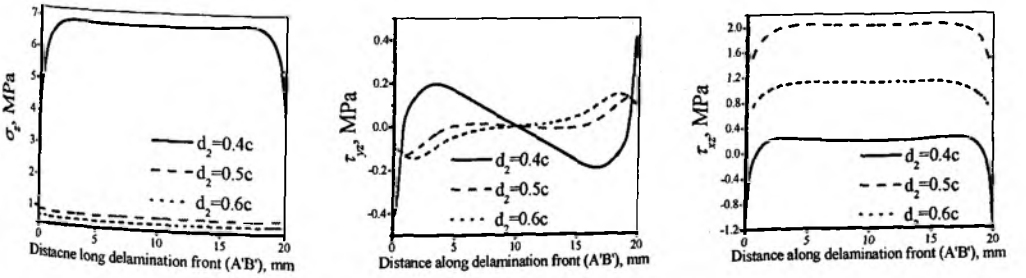

Figure 6.14 Interlaminar stress variations along the delamination front (A'B') when embedded in the top adherend for varying delamination positions.

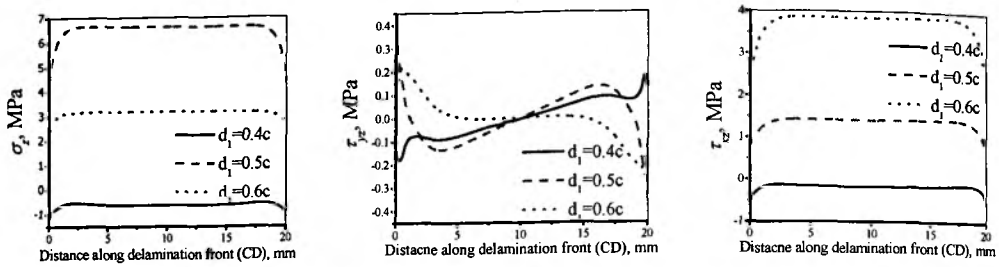

Figure 6.15 Interlaminar stress variations along the delamination front (CD) when embedded in the bottom adherend for varying delamination positions.

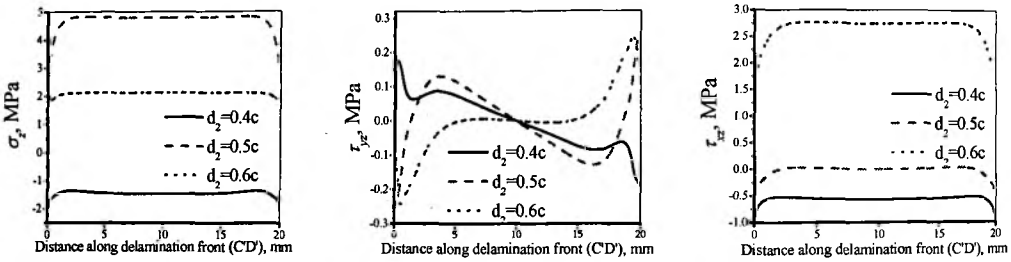

Figure 6.16 Interlaminar stress variations along the delamination front (C'D') when embedded in the top adherend for varying delamination positions.

The unequal interlaminar stress magnitudes along the delamination fronts AB, CD and A'B', C'D' (Figs. 6.13-6.16) indicate that the delamination propagation rates would be different from its both fronts when the delamination is embedded in either of the adherends. Although the τ_{yz} values are smaller, the natures are different as shown in Figs. 6.13-6.16. This may be due to the fact that, the bottom and top adherends of the SLJ are subjected to a bending moment of different nature caused by the loading eccentricity.

6.5.3 Effect of delamination positions on SERR variations

Individual modes of SERR (G_I, G_{II} and G_{III}) distributions along the delamination fronts AB, CD and A'B', C'D' are shown in Figs. 6.17-6.20 when through-the-width delaminations have been embedded in the bottom and the top adherends for varying delamination positions. It is observed that the magnitude of G_I is comparatively higher than G_{II} and G_{III} for all positions of the embedded delaminations in either of the adherends. This indicates that the delamination will propagate predominantly

under mode *I*, as has been predicted from the stress analyses discussed in the earlier section.

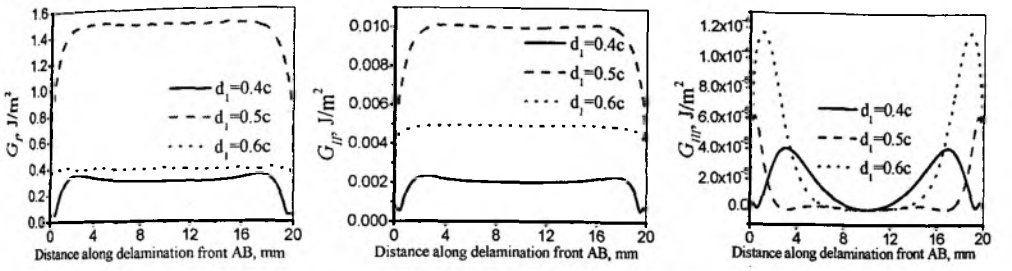

Figure 6.17 SERR variations along the delamination front AB when embedded in the bottom adherend for varying delamination positions.

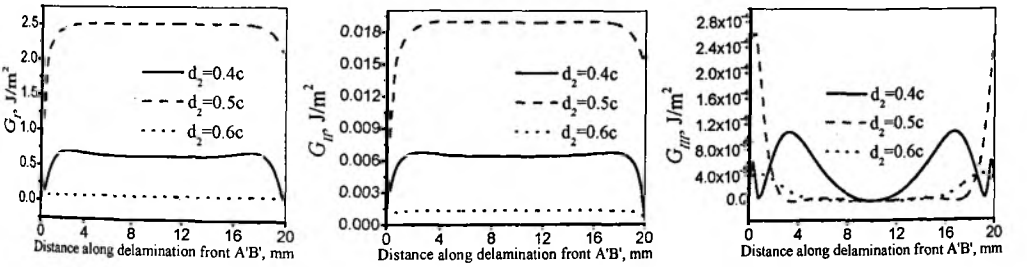

Figure 6.18 SERR variations along the delamination front A'B' when embedded in the top adherend for varying delamination positions.

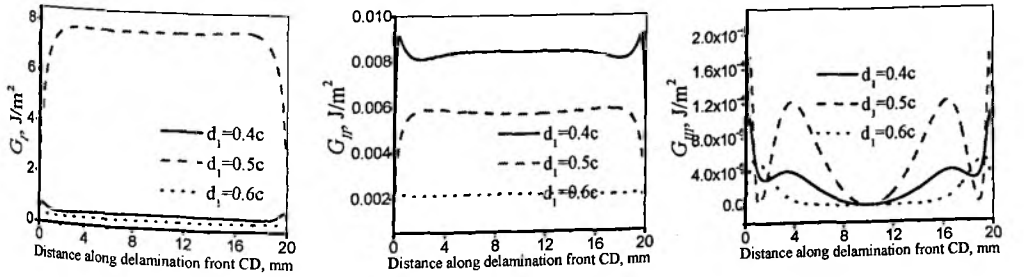

Figure 6.19 SERR variations along the delamination front CD when embedded in the bottom adherend for varying delamination positions.

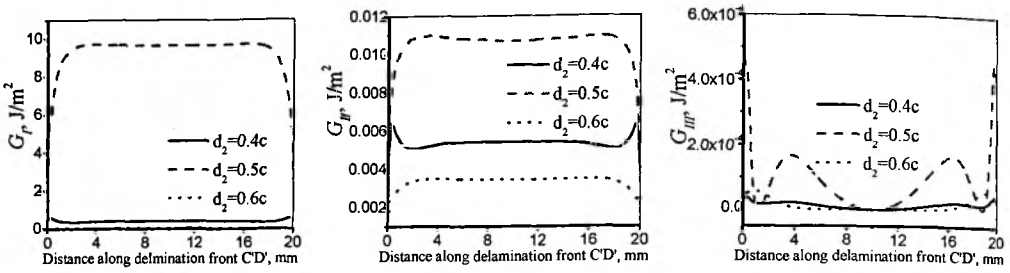

Figure 6.20 SERR variations along the delamination front C'D' when embedded in the top adherend for varying delamination positions.

The values of G_I along the delamination fronts A'B' or C'D' are higher compared to that along the fronts AB or CD, when the delamination is present in the top adherend and located at d_1 or d_2 = 0.5c. This indicates a faster rate of delamination propagation compared to the other locations of the delaminations. Figure 6.20 shows that G_I is the largest for C'D' for the same position i.e. d_2 = 0.5c. Thus, it can be concluded that the delamination front lying within the overlap region of the joint will propagate at a faster rate compared to the other fronts when the center of the delamination is exactly aligned with the overlap end of the joint. The out-of-plane peel stresses (σ_z) are higher along the said front and have been responsible for mode *I* delamination propagation.

On the other hand G_{II} values are the highest along the delamination front A'B' when the center of the delamination is exactly aligned with the overlap end as shown in Fig. 6.18. It is seen that irrespective of any position of the embedded delamination in either of the adherends, the G_{III} values are insignificant.

Thus, since the magnitudes of G_I, G_{II} and G_{III} along the two delamination fronts are different as shown in Figs. 6.17-6.20, the rates of delamination damage propagations are different at the two fronts. It is also observed that, when the delamination is located outside the overlap region i.e. d_1 or d_2 = 0.6c in either of the adherends, the SERR values at both of its fronts are very small and insignificant.

6.6 Conclusions

Three-dimensional non-linear finite element analyses have been carried out to study the effects of through-the-width delaminations pre-embedded in laminated FRP composite adherends on delamination damage propagation characteristics of adhesively bonded single lap joints. It is seen that the locations of through-the-width delaminations play significant role on the delamination damage propagation

behaviour and on the performance of the joint. The out-of-plane stress distributions in the adhesive layer, interlaminar stress distributions along the delamination fronts and the variations of SERR components G_I, G_{II} and G_{III} have been evaluated. Based on the above, the conclusions derived are as follows:

- The locations of the embedded delaminations in either of the laminated FRP composite adherends influence significantly the values of the peak out-of-plane peel stresses (σ_z) in the adhesive layer, whereas it is not so for the other two stress components τ_{yz} and τ_{xz}. The peak value of σ_z is the largest for the bottom delaminated adherend, when the center of the delamination is exactly aligned with the overlap end of the SLJ.
- The interlaminar stresses σ_z and τ_{xz} remain same along the delamination front in the central region of the width of the joint except at the free edges. But the shear stress τ_{yz} varies significantly across the width. This is due to the loading eccentricity prevailing in the joint area of the SLJ. The unequal interlaminar stress magnitudes along the two delamination fronts induce dissimilar delamination damage propagations in the two adherends.
- The SERR in opening mode (G_I) is relatively of higher magnitude than the SERR values in shearing (G_{II}) and tearing (G_{III}) modes. Hence the opening mode SERR predominantly governs the propagation of delamination damage for all positions of the pre-embedded delaminations in the SLJ.
- The non-uniform variations of SERR along the delamination fronts indicate non-uniform delamination propagation growths irrespective of the location of the delaminations.

7

Delamination Damage Analyses of Adhesively Bonded FRP Composite Lap Shear Joint

7.1 Introduction

Various lap joint theories [25, 35, 95] have been developed for the linear elastic solution of adhesively bonded lap shear joints of laminated FRP composite plates subjected to in-plane loading. The existing stress and strain solutions are either analytical or numerical depending on the complexities of the bonded joint problems. Analytical solutions [167, 184, 190] have given explicit relationships between joint stresses and deformations, but with many simplified assumptions. Among the numerical methods, Finite Element Analyses (FEA) have been extensively used by many researchers [182, 191]. A variety of important aspects, such as complex geometry, material non-linearity and large deformations may be taken into account in the FEA. Hart-Smith [18], Adams and Peppiatt [10] are amongst those who first employed FEA to determine the stress distributions in adhesively bonded joints.

A good number of literatures [31, 192, 193] are available based on plane stress or plane strain assumptions for bonded joint stress analysis. Adams and Peppiatt [72] examined the three-dimensional nature of Single Lap Joint (SLJ) by performing numerical analysis, assuming that width wise normal stress is constant through-the-thickness of the adherends and neglecting the important factors such as edge moments and adhesive peel stresses. Pindera and Wang [194] characterized the three-dimensional phenomena using optical isodyne techniques. Tsai and Morton [167] have analyzed the three-dimensional deformations in the SLJ specimen. Panigrahi and Pradhan [172] carried out a three-dimensional failure analysis and predicted the location of the damage initiation using Tsai-Hill coupled failure criterion and emphasized for the three-dimensional modelling of the damaged region of the composite SLJ. FRP composite Lap Shear Joints (LSJ) are widely used in many structural applications. But the delamination damage analyses for these joints are not available in the literature. The existence of singular stresses due to geometric and material discontinuities at the interface corners poses the real problems in the lap shear joints. The pre-existed delamination if any around the joint area and its

propagation further complicates the analysis procedures. This requires an appropriate three-dimensional finite element analysis to evaluate the peel and interlaminar shear stresses in the delamination zones. Structural integrity of the composite LSJ in the presence of delaminations and their subsequent propagations can be ascertained by evaluation of strain energy release rate components.

The objective of the present research is to investigate the effect of pre-embedded delamination in the resin rich layer between the first and second plies of the strap adherend of the LSJ and its propagation on (i) the out-of-plane stress (σ_z, τ_{yz} and τ_{xz}) distributions in the adhesive layer between the lap and strap adherends, (ii) the interlaminar stress (σ_z, τ_{yz} and τ_{xz}) variations along the delamination fronts and (iii) the variation of Strain Energy Release Rate (SERR) components along the delamination fronts. Thus, the structural integrity of the LSJ can be established.

7.2 Delamination damages in FRP composite LSJ: An overview

Delamination is one of the possible failure modes in laminated FRP composite lap shear joints in addition to the normal bonded joint failures which occur in the adhesive layer and at the bondline interfaces. The presence of delamination in composite LSJs leads to loss in overall stiffness of the joint, increases stress concentration effects and finally may cause local instabilities. Thus, the delamination induced damages may accelerate the final failure of the joint. Hence, delamination damage is considered to be one of the most influencing modes of failure in laminated FRP composite joints. The joints in the presence of pre-existed delaminations or joints prone to delamination initiation and subsequent propagation need to be properly analyzed and accordingly, the techniques for prevention or delay of delamination propagation are needed to be developed. Some of the approaches for the prevention of delamination propagation being considered are: (i) improvement in the quality of the resins, (ii) adhesive interleaving, (iii) braiding, (iv) 3D weaving, (v) through-the-thickness stitching and (vi) novel designs such as proper fiber orientation and laminate sequencing to reduce interlaminar stresses.

Basically delaminations may result from the interlaminar stresses developed by impact induced loads, eccentric load paths or from the structural discontinuities because of material anisotropy and heterogeneity of laminated FRP composite adherends. Interlaminar stresses are greatly influenced due to the mismatch in Poisson's ratios and coefficients of mutual influence in addition to the mismatch in the elastic and shear moduli between the layers [2]. A few sources which may induce

local out-of-plane loads leading to interlaminar stresses are; (i) straight or curved (near the holes or cut-outs) free edges (ii) ply terminations or ply drops and (iii) bonded joints, etc.

Interlaminar stresses arising out of the above discussed reasons lead to delamination in the strap adherends of the composite LSJ and have significant influence in the strength and the stiffness of the joint. The presence of delamination redistributes the stresses which may influence the life of the bonded joint and lead to early failure of the structure. The extensive studies of adhesively bonded joints by researchers [34, 175, 195] demonstrated that the location and size of the delamination like flaws in the overlap region may affect the joint strengths significantly. If the flaw lies away from the free edges, it may have insignificant influence on the performance of the joint. But if it occurs near the free edges of the joint, the critical locations of peak stresses are shifted to a location adjacent to the flaw. In this situation, the stress distribution shows peculiarly very high values and substantial loss of joint strength occurs.

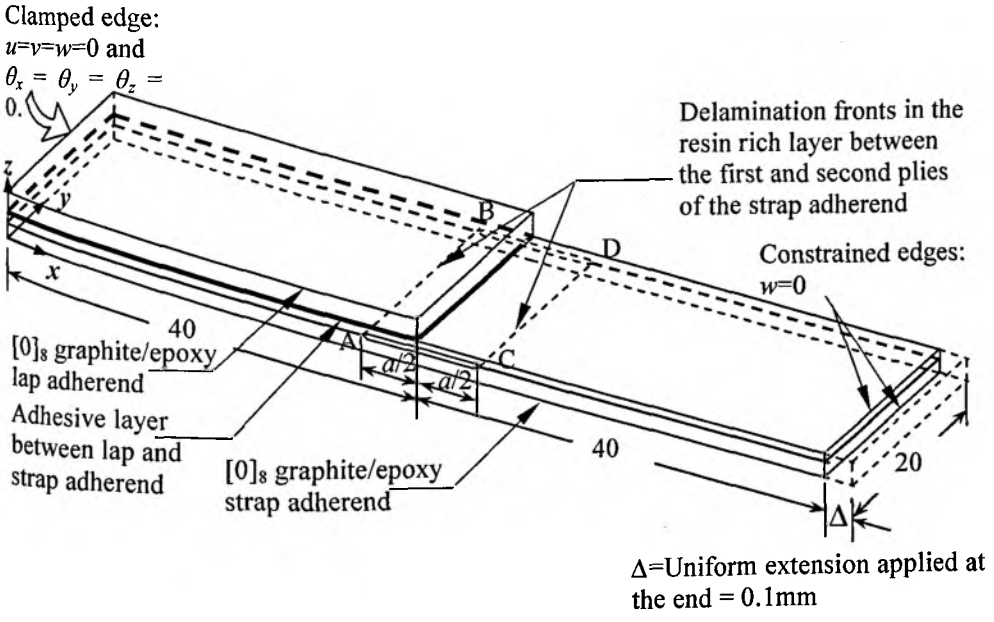

Figure 7.1 FRP composite LSJ specimen (All dimensions are in mm).

7.3 FEA of delamination damage in FRP composite LSJ

Figure 7.1 shows the geometry, loading and boundary conditions of the FRP composite LSJ. The lap and the strap adherends are of $[0]_8$ graphite/epoxy FRP composite laminates whose material properties are given in Table 6.1 of Chapter 6, which includes also the material properties of the adhesive isotropic epoxy resin. Each ply thickness is taken to be 0.125mm. Referring to Fig. 7.1, the through-the-width delamination of thickness 0.02mm has been presumed to be pre-embedded in the resin rich layer of 0.02mm thick between the first and second plies of the strap adherend, whose centre is exactly aligned with the overlap end of the joint. Different delamination lengths a = 2, 5, 8 and 10mm have been considered in the present analysis. One end of the LSJ is clamped and the other end is uniformly loaded in terms of uniform extension Δ = 0.1mm applied in 100 equal substeps. This far end has been constrained as shown in Fig. 7.1 in z-direction to simulate in-plane loading. The out-of-plane stresses in the adhesive layer between the lap and strap adherends and the interlaminar stresses on delamination fronts of pre-embedded delamination in the resin rich layer between the first and second plies of the strap adherend have been evaluated using finite element software ANSYS 10 in a high speed IBM platform. The components of SERR, G_I, G_{II} and G_{III} have been computed to characterize the delamination propagation characteristics in respect to varied positions of the embedded delamination.

The bonded joint analysis becomes more involved and complex due to the presence of delamination even with straight delamination front. In view of this, Linear Elastic Fracture Mechanics (LEFM) procedures are usually adopted for studying the delamination propagation behaviour in adhesively bonded LSJ in laminated FRP composites. Either a stress intensity factor (K) criterion or strain energy release rate (G) criterion is considered to establish the delamination damage propagation characteristics. In the former case, the delamination front stress intensity factor K is compared to the critical stress intensity factor K_c of the material. However, in composite materials the crack tip stress geometry function relating K to the stress σ and defect dimension is not the standard isotropic factor, and therefore, most delamination studies and tests have been developed using the strain energy release rate criterion. Strain energy release rate is a material parameter independent of geometry and hence has been considered to be a candid parameter for predicting the damage growth [186]. Thus, the delamination induced damaged composite material is characterized by the modes *I*, *II*, and *III* critical strain energy release rates G_{Ic}, G_{IIc},

and G_{IIIc}, respectively. The three components of strain energy release rate are used to characterize the interlaminar fracture behaviour for delamination and debonding analyses of FRP composite structural members [147, 149, 165]. Therefore, to characterize the interfacial delamination behaviour in FRP composite joints, three-dimensional finite element analyses are required to be conducted [187] to evaluate the SERRs along the delamination fronts. Calculations of energy release rate components are based on Irwin's theory of Crack Closure Technique [108]. It is hypothesized that for an infinitesimal increment in crack length Δa, the crack opening displacement $\delta(x-\Delta a)$ for the crack of length a can be considered equal to the crack opening displacement δx along the delamination front. By this method, the displacement field ahead of the delamination front is approximated to be same as that one behind it. The significant advantage of this method is that only one finite element run is required instead of two to evaluate the values of individual modes of SERR [188].

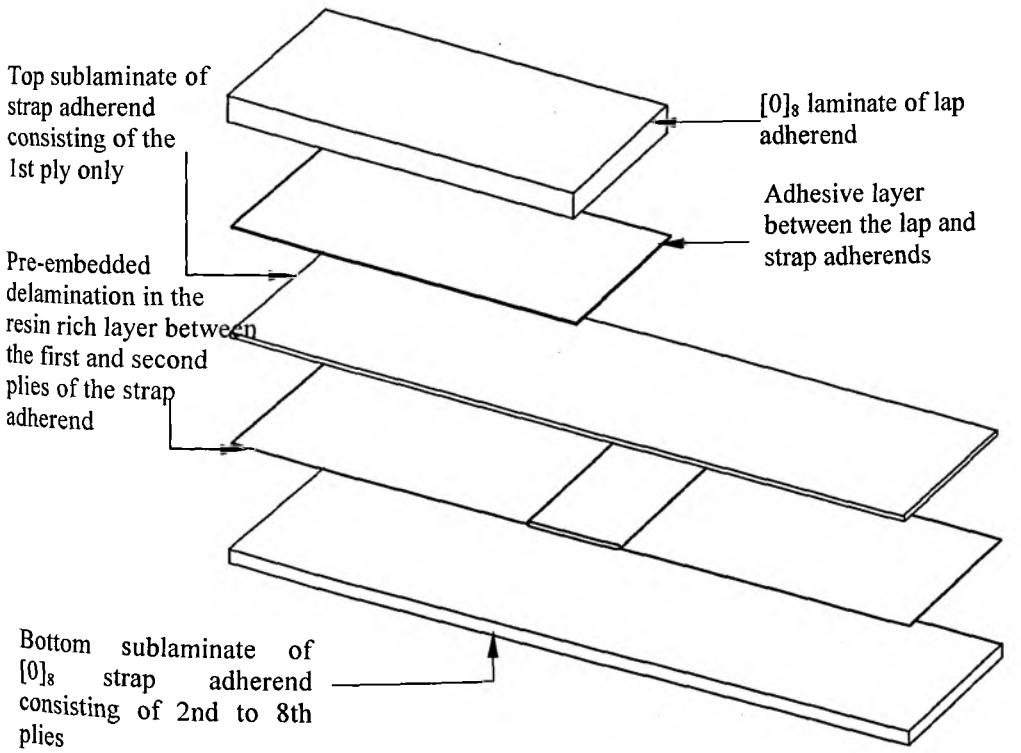

Figure 7.2 Sublaminate modelling of FRP composite LSJ specimen.

7.4 FE modelling of FRP composite LSJ with pre-embedded delaminations

Interlaminar stresses along the delamination fronts are responsible for the initiation and subsequent propagation, where the stress state is inherently three-dimensional [186]. This aspect necessitates for a full three-dimensional damage analysis for obtaining complete information of stress and deformation field at and near the delamination front. The 3D brick element models are known to be very accurate especially in dividing the strain energy release rate into individual modes [189]. Though brick elements are more accurate for SERR computations, but by using many layers of brick elements through-the-thickness to model the individual plies, the modelling and computational effort becomes prohibitively large. Therefore, the composite LSJ is often being modelled using sublaminate technique. The sublaminate modelling of FRP composite LSJ specimen is shown in Fig. 7.2. In this technique, the lap adherend, the adhesive layer between the lap and strap adherend, the delaminated strap adherend have been modelled as separate sublaminates. The strap adherend consists of three sublaminates such as (i) top sublaminate of strap adherend consisting of the 1st ply only, (ii) pre-embedded delamination in the resin rich layer between the first and second plies of the strap adherend and (iii) bottom sublaminate strap adherend consisting of 2nd to 8th plies.

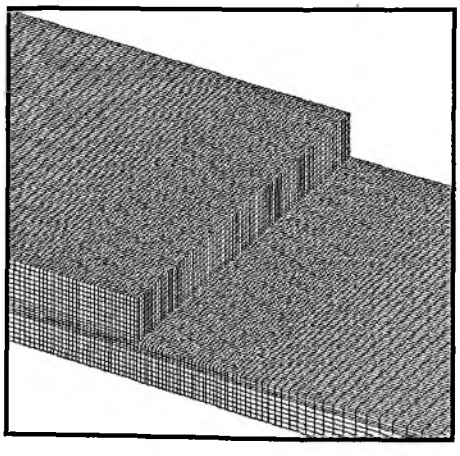

Figure 7.3 Zoomed view of sub-modelled finite element mesh of LSJ around the delamination region.

In the present analysis, three-dimensional eight-node layered volume elements (SOLID 46) with appropriate material properties (Table 6.1) have been used to model the different sublaminates of lap and strap composite adherends and SOLID 45

elements are used for the adhesive layer. The zoomed view of sub-modelled finite element mesh of the LSJ around the delamination region existing in the thin resin rich layer between the 1st and 2nd plies of the strap adherend is shown in Fig. 7.3. The centre of such through-the-width embedded delaminations of varied lengths is presumed to be exactly aligned with the overlap end of the lap adherend. Experimental evidence indicates that a thin resin-rich layer exists between the neighbouring plies, in which the imperfections such as delaminations were found to exist [149, 165, 188] and the propagation of delamination fronts are assumed to be planar and self-similar. Since the delamination propagation characteristics are quite complex, the FE analyses should incorporate rigorous error analysis procedures and convergence requirements with judicious mesh grading and appropriate element size in the vicinity of the delamination front. This is needed to avoid the oscillatory nature of the stress field very near to the delamination front and also to accurately evaluate the delamination propagation characteristics. This has been duly carried out during computational stages to achieve the required level of accuracy. The element size taken as one fourth of ply thickness [147, 164, 165] near the delamination zone has been found to be satisfactory for the accuracy and convergence requirements. Except over the delaminated region, Multi-Point Constraints are imposed on the nodes along the delamination boundary and contact elements are used within the delaminated region to prevent mutual interpenetration of the delaminated surfaces. This contact processor always maintains a positive value of the displacement difference along the z-direction between the pairs of nodes inside the delaminated zone of the top and bottom delaminated surfaces. Furthermore, it has been assumed that the delamination plane is the weakest and the delamination will propagate parallel to the xy plane. Thus, the possibility of out-of-plane propagation of the delamination has been carefully excluded. The three components of strain energy release rate viz. G_I, G_{II}, and G_{III} have been evaluated using Modified Crack Closure Integral (MCCI) and they have been used as parameters for assessing the delamination growth characteristics.

7.5 Computation of SERR

Figure 7.4 shows the configuration for evaluation of MCCI applied to the lap shear joint for computation of SERR along the delamination front CD when delamination of length a is embedded in the resin rich layer between the first and the second plies of the strap adherend.

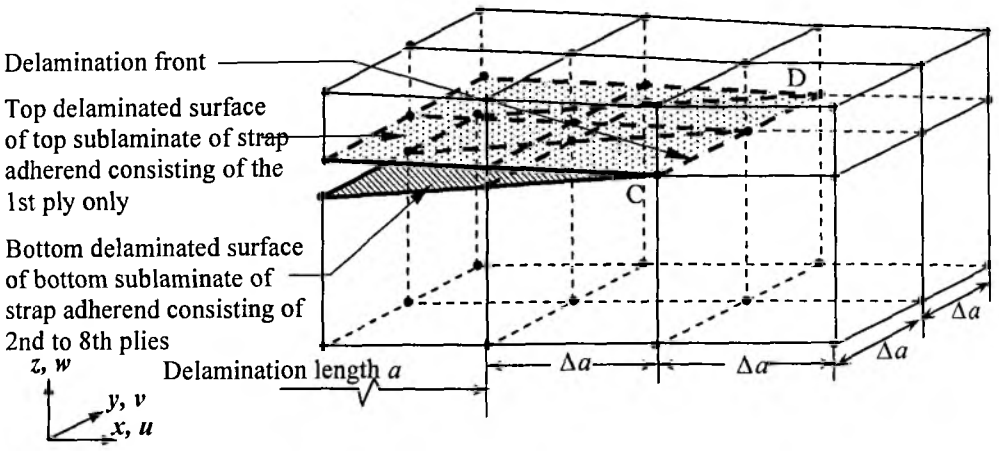

Figure 7.4 MCCI applied to the LSJ for computation of SERR along the delamination front CD.

The strain energy released by the propagation of a delamination of length a to $a+\Delta a$ is given by

$$W = \frac{1}{2}\int_{a}^{a+\Delta a}\int_{-\Delta a/2}^{\Delta a/2}\sigma(x,y)\times\delta(x-\Delta a,y)dxdy \tag{7.1}$$

where $\delta(x-\Delta a,y)$ is the crack opening displacement between the top and bottom delaminated surfaces and $\sigma(x,y)$ is the stress at any point on the delamination front CD required to close the delaminated area. Then, the strain energy release rate (G) is obtained as

$$G = \lim_{\Delta a\to 0}\frac{W}{\Delta A} \tag{7.2}$$

where ΔA represents the delamination propagated area and equals to one element area in xy plane i.e. $\Delta a\times\Delta a$ for the present case. The MCCI has the advantage of mode separation of strain energy release rate. This will help for a qualitative analysis of delamination damage propagation behaviour. Accordingly, the three components of strain energy release rates G_I, G_{II} and G_{III} for modes *I*, *II*, and *III* can be expressed as given in Eqs. (3.109 - 3.111).

While implementing these Equations to evaluate the three components of SERR for delamination damage analyses of Adhesively Bonded Lap Shear Joint, the subscripts T and B represent the top and bottom delaminated sublaminates, respectively. The existing delamination length is denoted by a, and Δa is the virtual delamination length due to the external loads. Here, $[u_T, v_T, w_T]$ and $[u_B, v_B, w_B]$ represent the displacements corresponding to the nodes at the top and bottom delaminated surfaces, respectively, behind the delamination front and, σ_z, τ_{zx} and τ_{zy} are the stresses required to close the delaminated surfaces.

7.6 Results and discussion

7.6.1 Out-of-plane stress distributions in the adhesive layer existing between the lap and strap adherends

The out-of-plane stress distributions in the adhesive layer existing between the lap and the strap adherend of the LSJ is always an important concern in bonded joint analysis due to the simple reason that the adhesive layer is comparatively of lower strength than the adherends. Figure 7.5 shows the peel stress (σ_z) and shear stress (τ_{yz} and τ_{xz}) distributions in the mid-surface of the adhesive layer between the lap and strap adherends for varying embedded delamination lengths existing in the resin rich layer between the first and second plies of the strap adherend. The results are compared with the undamaged LSJ. It is seen that stress distributions of the damaged specimen are different from the undamaged one. The peel and shear stresses become zero at the region away from the delamination front towards the clamped end for all damaged and undamaged specimen indicating joint failure would not occur at any locations away from the delamination front. A secondary peak of out-of-plane stress components near to the delamination front appear due to the presence of delamination. The secondary peak values for delamination of length 2mm is the lowest as shown in Fig. 7.5 (b) and the increase in peak values are insignificant as the delamination propagates. Also, it is observed that the magnitude of out-of-plane stresses at the overlap end of the damaged specimen is small compared to the undamaged one as shown in Fig. 7.5 (a). It indicates that the composite LSJ with no delamination may fail in net-sectional fracture and damaged specimen will fail by the propagation of delaminations.

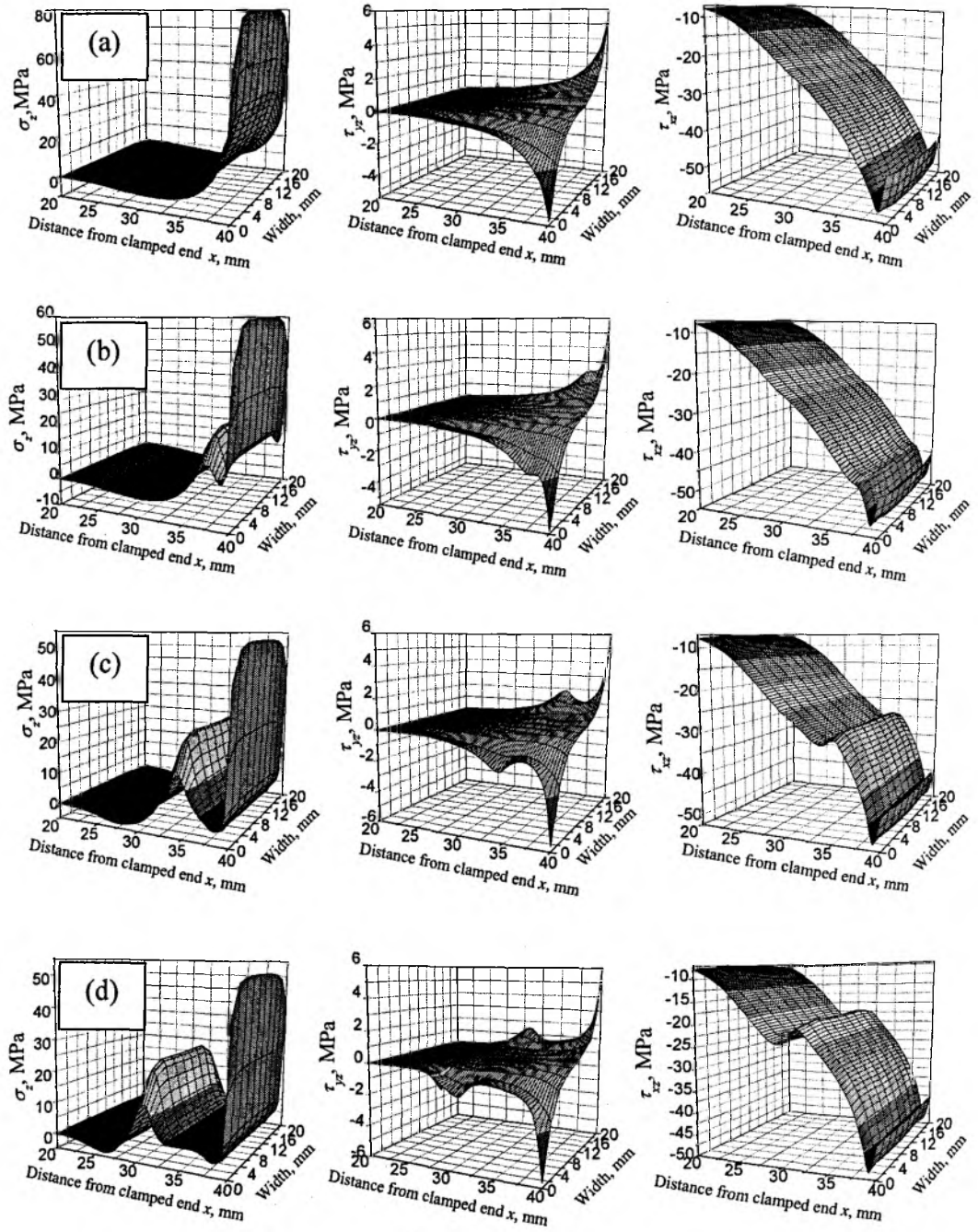

Figure 7.5 Distributions of out-of-plane stresses (σ_z, τ_{yz} and τ_{xz}) in the adhesive layer existing between the lap and the strap adherend of LSJ for varying delamination lengths in the resin rich layer between the top and the bottom sublaminate of strap adherend; (a) no delamination, (b) a = 2mm, (c) a = 5mm, (d) a = 8mm and (e) a = 10mm.

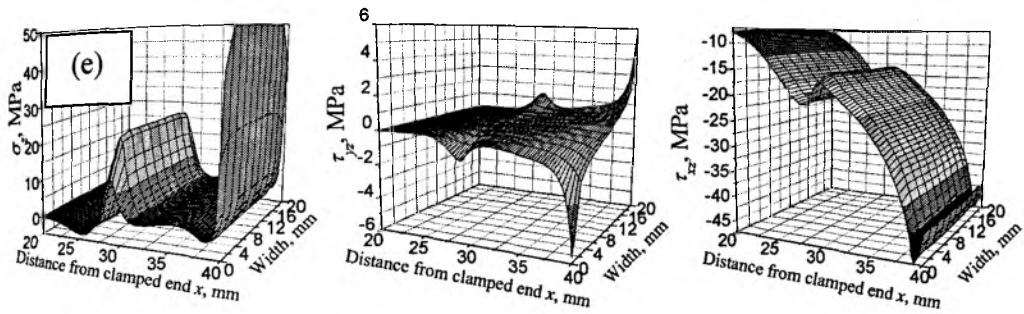

Figure 7.5 Continued.

The magnitude of the shear stress τ_{xz} of the damaged specimen is larger in the region between the damage front and clamped end compared to the undamaged joint, whereas the τ_{yz} values remain unchanged. Like peel stress, there is also a secondary peak shear stress and it appears to be located close to the delamination front. The value of secondary peak shear stress decreases as the delamination propagates. This means that the damaged joint having smallest delamination length has the highest value of secondary peak shear stress value. The magnitudes of shear stress for the region between the delamination front and overlap end are smaller compared to the undamaged joints. The results obtained from the present analysis are in good agreement with the plane strain analytical and experimental stress analysis of Cheuk and Tong [36]. From the stress distributions of both damaged and undamaged joint, it is observed that peel stresses (σ_z) are the highest towards the central region of the joint, whereas τ_{yz} is the highest at the free edge and τ_{xz} remain uniform along the width.

7.6.2 Interlaminar stress variations along the delamination fronts

Interlaminar stresses (σ_z, τ_{xz} and τ_{yz}) play a key role for characterization of delamination damage propagation. Figure 7.6 illustrates the variation of interlaminar stresses along the delamination fronts AB and CD, when the pre-embedded delamination propagates in the resin rich layer existing between the 1st and 2nd plies of the strap adherend. Referring to Fig. 7.6 (a), σ_z stress component along the delamination front AB is significantly high compared to that along CD as shown in Fig. 7.6 (b) for all delamination lengths. It shows that the possibility of delamination propagation would be through the front AB rather than CD, especially in the opening mode. It is interesting to note that σ_z values along AB are the lowest when the delamination propagates upto a maximum value i.e. for a = 10mm and the highest for delamination length a = 5mm to 8 mm. It indicates that as the delamination

propagates, the surface ply of the strap adherend of the composite LSJ may get fractured thus reducing the σ_z value further and becomes lowest for the highest value of delamination length i.e. for a = 10mm. Also, it is seen that there is a significant difference in σ_z values along the front AB between the central region and free edge of the joint but the difference is negligibly small along the delamination front CD.

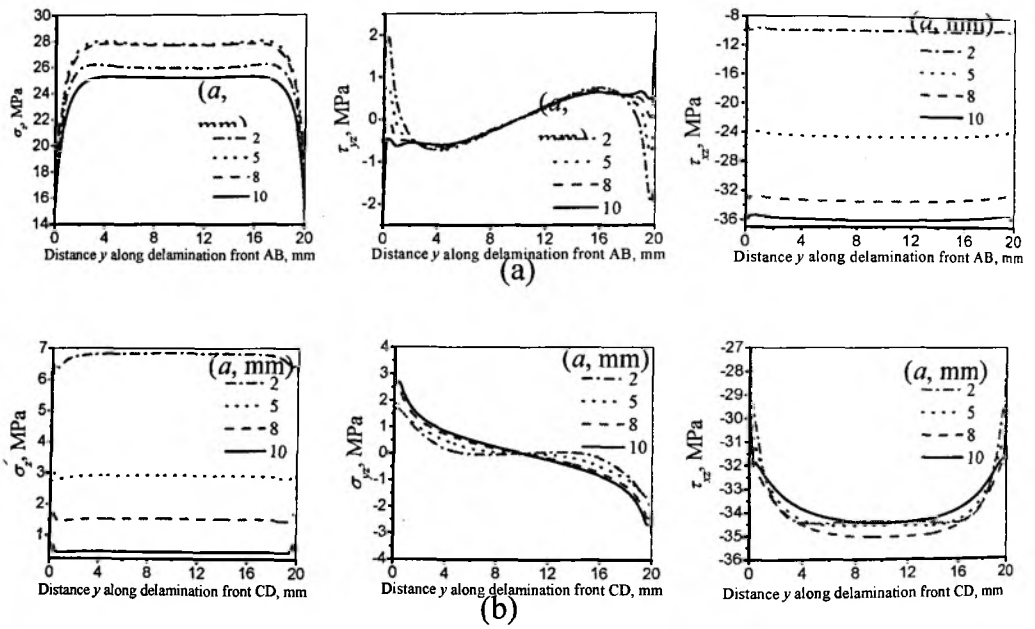

Figure 7.6 Interlaminar stresses along the delamination fronts (delamination pre-embedded in the resin rich layer between the first and second plies of the strap adherend) AB and CD for different delamination lengths.

The changes in shear stress components (τ_{xz} and τ_{yz}) along the delamination fronts CD are insignificant as shown in Fig. 7.6 (b). But the effect of delamination propagation on τ_{xz} along the delamination front AB can not be ignored and is insensitive on τ_{yz} except at the free edge.

The initial values of interlaminar stresses (σ_z, τ_{xz} and τ_{yz}) along the delamination fronts AB and CD at one of the free edges are given in Table 7.1 for different propagated delamination lengths. The values of σ_z at the free edges decrease and τ_{xz}, τ_{yz} values increase for the delamination front CD. Along the delamination front AB, σ_z values increase till the delamination propagates up to 8 mm and beyond which it decreases, whereas τ_{xz} and τ_{yz} components increase.

Table 7.1 Interlaminar stresses (σ_z, τ_{yz} *and* τ_{xz}) at one of the free edges along the delamination fronts (delamination pre-embedded in the resin rich layer between the first and second plies of the strap adherend) AB and CD.

Delamination fronts	AB				CD			
a (mm)	2	5	8	10	2	5	8	10
σ_z (MPa)	14.86	16.82	16.94	15.1	5.47	2.05	1.126	0.49
τ_{yz} (MPa)	0.945	-0.52	-1.06	-2.03	1.76	2.28	2.89	3.06
τ_{xz} (MPa)	-9.01	-23.9	-32.62	-35.54	-27.32	-28.13	-29.51	-29.6

7.6.3 SERR variations along the delamination fronts

Modified Crack Closure Technique (MCCI) discussed in the Sec. 7.5 has been used to evaluate the individual modes of SERR (G_I, G_{II} and G_{III}) along the delamination fronts AB and CD, when the pre-embedded delamination propagates in the resin rich layer existing between the first and second plies of the strap adherend and the distributions have been shown in Figs. 7.7 (a) and (b). The interlaminar stresses (σ_z, τ_{xz} and τ_{yz}) have been used to evaluate G_I, G_{II} and G_{III}, respectively.

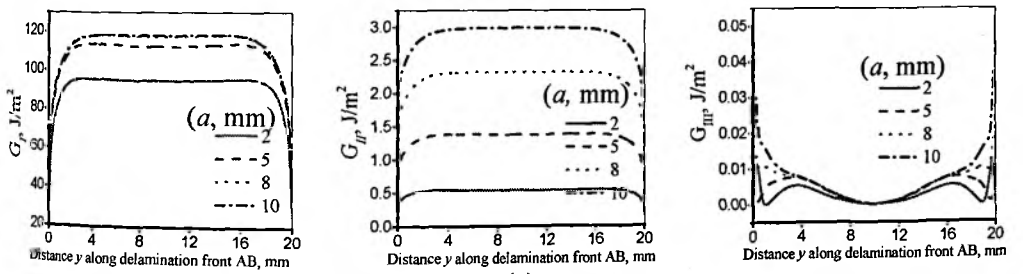

(a)

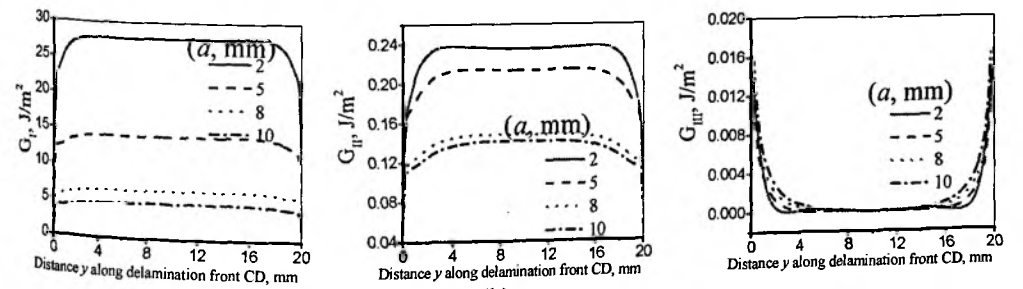

(b)

Figure 7.7 Variation of SERRs (G_I, G_{II} and G_{III}) along the delamination fronts AB and CD (delamination pre-embedded in the resin rich layer between the first and second plies of the strap adherend) for different delamination lengths.

It is observed that G_I and G_{II} values along the delamination front AB are significantly larger compared to the other front CD for all delamination lengths. Along the width of the joint, SERR values are almost constant except at the free edges. Further, it may be noticed in Fig. 7.7 that, G_I and G_{II} values in the central region are higher compared to the free edges, whereas G_{III} values are less at the central region of the joint. This indicates the straight delamination front may be curved as the delamination propagates. The contribution of G_{III} for delamination damage propagation at the free edge is quite high compared to the central region of the joint. This may be due to the simple reason that τ_{yz} at the free edge is high. Thus, individual components of SERR has significant magnitudes at the free edges of the joint indicating the delamination propagates due to mixed mode conditions as shown in Fig. 7.7. For all delamination lengths, the G_I values are significantly higher compared to the other two components of SERR G_{II} and G_{III}, indicating the predominance of Mode *I* contribution for the propagation of delamination.

In reference to Fig. 7.7 (a), G_I values along the delamination front AB reduce drastically as the delamination propagates. On the other hand, G_I values along the front CD are the highest for smaller delamination length i.e. for a = 2mm as shown in Fig. 7.7 (b). Thus, it is interesting to note that, SERR values at both of its delamination fronts are not equal for all delamination lengths. This influences the delamination propagation at both of its fronts not to be at the same rate and similar manner. Similar observations are also highlighted by Tong [192], for a single lap joint experimentally and analytically. Table 7.2 enlists the values of SERR at one of the free edges over the delamination fronts AB and CD.

Table 7.2 SERR components (G_I, G_{II} and G_{III}) at one of the free edges along the delamination fronts (delamination pre-embedded in the resin rich layer between the first and second plies of the strap adherend) AB and CD.

Delamination fronts	AB				CD			
a (mm)	2	5	8	10	2	5	8	10
G_I (J/m^2)	25.6	31.43	33.75	33.93	9.83	4.96	2.14	1.45
G_{II} (J/m^2)	0.15	0.46	0.82	1.07	0.08	0.075	0.051	0.048
G_{III} (J/m^2)	0.002	0.005	0.028	0.046	0.013	0.0148	0.014	0.0145

The critical delamination length can not be determined by knowing the SERR variations along the delamination fronts. Figure 7.8 illustrates the effect of initial pre-embedded delamination lengths on maximum value of SERRs (G_I, G_{II} and G_{III}) along the delamination fronts AB and CD. It has been proposed that [188], the delamination

would be propagated from the point having higher G value, since SERR is considered as the driving force for delamination propagation. Accordingly, the maximum values of SERR components along both the delamination fronts AB and CD have been extracted from the three-dimensional finite element analyses. The present three-dimension solutions of SERR values establish the delamination propagation behaviour. Further it is noticed from Fig. 7.8 that, G_I, G_{II} and G_{III} values along the delamination front AB increase, while G_I and G_{II} values decrease along the delamination front CD as the delamination propagates.

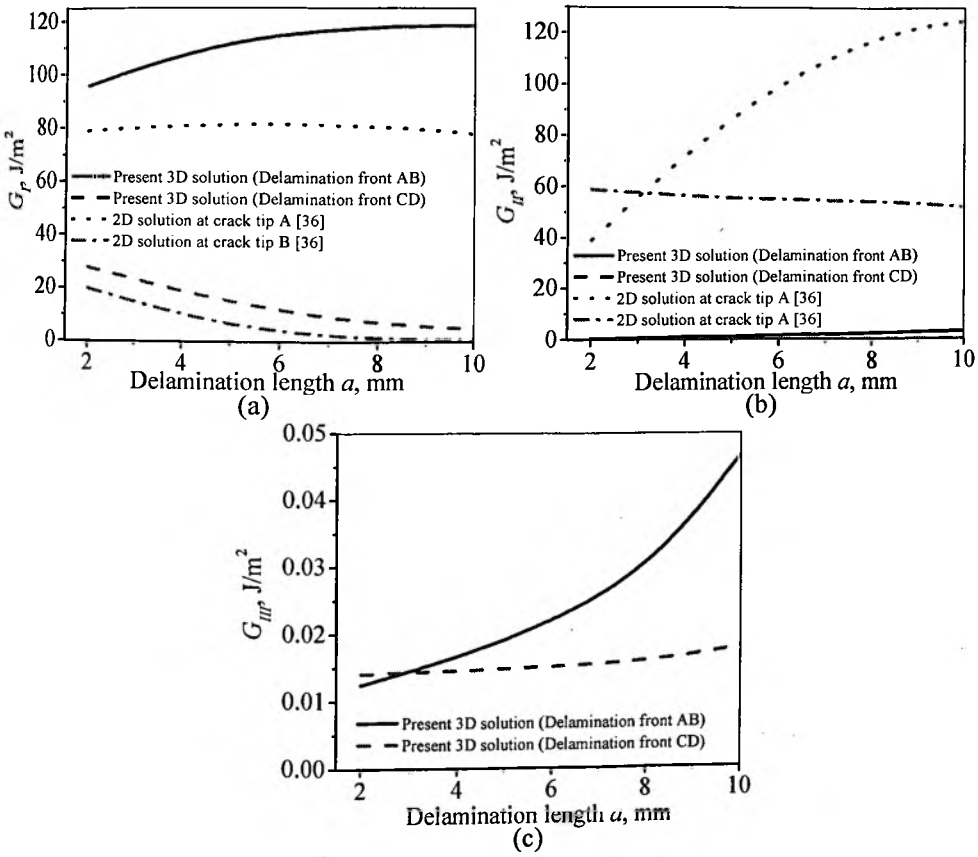

Figure 7.8 Effect of pre-embedded delamination lengths on maximum values of SERRs (G_I, G_{II} and G_{III}) along the delamination fronts AB and CD.

The SERR values obtained from the present three-dimensional analyses have been compared with the experimental, analytical and numerical solutions of Cheuk and Tong [36] which are based on two-dimensional plane strain assumptions. Figures 7.8 (a) and (b) show the comparison of G_I and G_{II} values obtained form the present

3D solutions and the trends are found to be in excellent agreement with the literature [36]. But, there is a difference between the magnitudes of SERR values. This may be so, because, their analyses are based on assumptions such as; (i) plane strain conditions, (ii) delamination was assumed as a crack and (iii) no contact analysis was performed (interpenetrations of damaged surfaces are inevitable if proper precautions are not considered in the modelling).

7.7 Conclusions

Embedded delamination damage propagation behaviour of adhesively bonded LSJ in laminated FRP composites have been studied using non-linear finite element analyses. The effects of embedded delamination lengths on the out-of-plane stress distributions in the adhesive layer existing between the lap and the strap adherend of LSJ for varying delamination propagations, the interlaminar stresses and the SERR variations along the delamination fronts AB and CD of pre-embedded delamination in the resin rich layer between the first and second plies of the strap adherend for different pre-embedded delamination lengths have been studied. Conclusions obtained from the present analyses are summarized as follows:

- The out-of-plane stress distributions of mid-surface of the adhesive layer existing between the lap and the strap adherend distinctly demonstrate the existence of a three-dimensional state of stress. The validity of two-dimensional analysis seems to be somewhat accurate for predicting stress state only in the region towards the central portion of the joint. Otherwise a full three-dimensional finite element analysis is required to evaluate the structural integrity of the LSJ.
- There is significant reduction (up to 30%) of maximum value of peel stress σ_z for the damaged LSJ compared to the undamaged one, whereas the reduction is negligible for the other two out-of-plane stress components (τ_{yz} and τ_{xz}). It indicates that the LSJ with no delamination may fail in net-sectional fracture and the damaged LSJ will fail by the propagation of delaminations.
- There is a significant difference in the magnitude and nature of interlaminar stress components between the edge and central portion of the joint. This necessitates the importance of performing 3-dimensional analysis. Thus, the assumption of delamination as a crack for a composite lap shear joint and to carry out the analysis with 2-dimensional plane strain or plane stress approach

as is done by other researchers is an oversimplification and may lead to errors in evaluation.

- Unequal distributions of SERR over the delamination fronts indicate that straight delamination front grow into curved front as the delamination propagates. G_I is significantly higher compared to the other two modes G_{II} and G_{III}. Thus, the influence of opening mode is the highest compared to the other two modes for delamination damage propagation.
- The SERR values along the delamination front inside the overlap region are higher compared to the other front which lies outside the overlap region. This indicates that the delamination damage propagates from the delamination front trapped inside the overlap region.

8

Delamination Damage Analyses of Adhesively Bonded Double Lap Joint

8.1 Introduction

Joining of composite structures using adhesive bonding in the form of Double Lap Joint (DLJ) remains a problem of renewed research interest because performance and structural integrity of the joint are severely influenced by the characteristics of laminated FRP composite adherends, which usually have low interlaminar strengths. Interlaminar stresses in forms of out-of-plane stresses are induced in the vicinity of the singular regions in case of the DLJ as shown in Fig. 8.1. These stresses can cause damages such as adhesion failure, cohesive failure and delamination damages or combination of these failures. The adhesion failure initiates from the stress singularity regions and propagates along the bondline interfaces due to peeling or shearing. These failures occur on a macro-scale when surface preparation or material qualities are poor and, consequently, this mode of failure cannot be ignored.

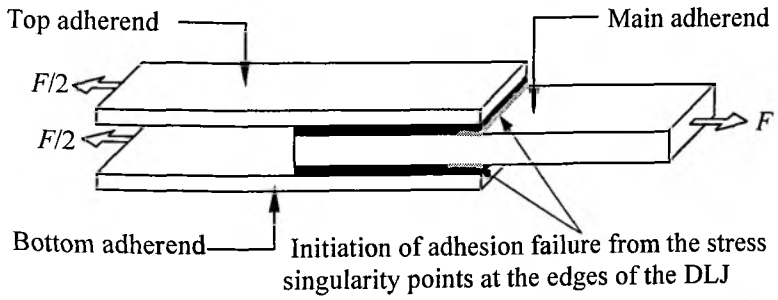

Figure 8.1 Peel stress induced adhesion failure in laminated FRP composite DLJ.

Though all joints are assumed to be manufactured to specifications, but due to the above-mentioned reasons, adhesion failures are expected to initiate from the edges of the stress singularity points. It is also shown both experimentally and numerically by Kelly [170] that the failure of bonded joints occurs with the fracture initiating from the toe end of the adhesive fillet and propagating along the adherend-adhesive interfaces in case of a Single Lap Joint (SLJ). Potter et al. [171] have carried out an interesting experimental study on the crack growth behaviour for an SLJ with

adhesive fillets. Cohesive failures occur in the adhesive layer due to shear yielding of adhesives and as expected such failures mostly are governed by the properties of the resin. Failures due to delamination induced damages occur in the laminated FRP composite adherends by the transverse or interlaminar stresses. This is so, because the interlaminar strengths of FRP composites are of the same order or lower than that of the matrix. Bonded joints experience peel loadings and so it may fail due to delamination induced damages in FRP composite adherends before the adhesive fails. Laminated FRP composite adherends will fail by interlaminar tension (in conjunction with a negative influence from the concurrent interlaminar shear) for a given load level at which the adhesive peel stress exceeds the interlaminar strength. Thus, the failure due to delamination will initiate at the overlap end of the joint between the first and second layers of fibers adjacent to the adhesive layer as shown in Fig. 8.2.

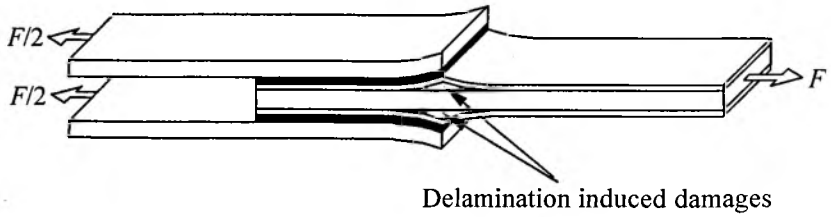

Figure 8.2 Peel stress induced delamination damage beneath the surface ply adjacent to the adhesive layer of the main adherend of the laminated FRP composite DLJ.

The DLJs are considered to be very important in bonded joint construction methods in FRP composites since the adhesive peel stresses are of low magnitude as compared to the SLJ and the adhesive fails in shear mode only. There is no net bending effect on a symmetrical DLJ as it exists in case of an SLJ and the joint does not experience any rotation. However, peel stresses are expected to be the highest at the overlap ends. Their influence on onset and growth of delamination induced failure in the laminated FRP composite adherends due to the low transverse tensile strength was recognized by Adams et al. [20]. The main composite adherend splits apart locally due to the peel stresses, thereby destroying the load transfer capacity between the top and bottom adherends as shown in Fig. 8.2. Because of no overall joint rotation in a DLJ, large deformations are not present and the analysis domain is treated as moderately geometrically non-linear and failure study pertaining to the onset and growth of adhesion failure and delamination induced damage have been performed using LEFM approaches. Components of SERR are considered to be the governing parameters to characterize the above mentioned damages in laminated FRP

composite DLJ. Structural integrity of the laminated FRP composite DLJs with damages and can be ascertained by evaluation of SERR components and further by studying the damage propagations.

A good number of literatures [21, 37, 76, 168, 196] on stress and failure analyses for SLJ configurations are available based on plane stress or plane strain assumptions using either FEA or experimental data. Altus [33] presented a 3-dimensional numerical analysis of DLJ specimen and concluded that both plane strain and plane stress solutions give higher bounds for the critical loads and emphasized the importance of 3-dimensional analysis. He has presented a profound discussion on several important issues for a better understanding of DLJ problems. Among those are: specific features of 3D state of stress variations; double edge effects at the corner points and inability of capturing it by 2D analyzes; parametric effects, application of failure and fracture criteria, etc. However, some observations and findings concerning to stress singularities have not been sufficiently justified. Adams and Peppiatt [72] have examined the three-dimensional nature of Single Lap Joint (SLJ) by performing numerical analysis, assuming that widthwise normal stress is constant through-the-thickness of the adherends and neglecting the important factors such as edge moments and adhesive peel stresses. Pindera and Wang [194] characterized the three-dimensional phenomena using optical isodyne techniques. Tsai and Morton [167] have analyzed the three-dimensional deformations in the SLJ specimen. Panigrahi and Pradhan [172] have carried out a three-dimensional failure analysis and predicted the location of the damage initiation using Tsai-Hill coupled failure criterion and emphasized for the three-dimensional modelling of the damaged region of the composite SLJ. Some important issues like free edge effects and bending-twisting coupling effects for an SLJ have been discussed in Refs.[84, 161, 172]. These issues related to DLJ are very important and till date have not been addressed satisfactorily.

The adhesively bonded joint problems are approached in one of the following two ways; (i) through analytical methods and (ii) with finite element analyses. Notably among many researchers, Kayupov and Dzenis [38], Adams and co-authors [31, 32], Tong et al. [92], Krüeger et al. [177], and Panigrahi and Pradhan [34] have performed extensive research on bonded joints using FEA. On the contrary, analytical approaches employ many simplifying assumptions in terms of joint geometry, loading, boundary conditions, etc. [25] in order to formulate a closed form solution for bonded joint analyses. Pioneering contributions have been made by Volkersen [15] and Goland and Reissner [16] and Hart-Smith [17], etc. towards the stress

analyses of bonded joints using analytical methods. Their analyses mainly focused on obtaining adhesive stresses, while ignoring the stresses in the adherends, particularly interlaminar stresses, which are known to be the key factors to the onset and growth of damages in laminated FRP composite adherends.

The 3D states of stress and failure prediction of bonded joints are difficult to deal analytically. An adequate solution has to account for the geometrical discontinuities; loading eccentricity and material property variations, anisotropy and laminated construction of the adherends, etc. Thus, accurate three-dimensional finite element analyses are essential for understanding the onset and subsequent growth of damages due to the adhesion failure and the delamination induced damage in laminated FRP composite DLJ. Locations of damage initiation are identified by strength criterion proposed by Tsai and Wu [197] and individual components of SERR are computed using MCCI to study the damage propagation.

8.2 Finite element analyses of laminated FRP composite DLJ

Three types of analyses may be carried out for a DLJ viz. (I) linear analysis, (ii) non-linear analysis including large deformation only, and (iii) non-linear analysis including both large deformation and material non-linearity. The linear and non-linear analyses yield significant differences in the computed values of peel and shear stresses. It has been emphasized that the non-linear analysis procedure must be used for a DLJ in order to evaluate the stresses in the joint accurately. However, the effect of adhesive material non-linearity on peel stresses is insignificant [21]. Thus, three-dimensional finite element analyses with geometric non-linearties have been carried out for the DLJ to predict the location of initiation of damages due to adhesion failure and delamination.

8.2.1 DLJ specimen configuration

The laminated FRP composite DLJ specimen is shown in Fig. 8.3 and the dimensions adopted [32] are as follows:

Joint length L = 230mm, Thickness of the main adherend h_2 = 4mm Thickness of the top and bottom adherends h_1 = 2mm, Bondline thickness a_t = 0.5mm, Width W = 20mm and overlap length c = 50mm.

The top, the main and the bottom adherends consist of $[0]_8$, $[0]_{16}$ and $[0]_8$ graphite/epoxy FRP composite laminates, respectively. The thickness of each ply is taken as 0.215mm. The layerwise orthotropic material properties [198] of the adherends and isotropic material properties of the adhesives along with their strength

values are given in Table 8.1. A total load F equal to 10kN has been applied to the DLJ specimen in 100 equal sub-steps in terms of uniformly applied load through the ends.

Table 8.1 Graphite/epoxy FRP composite lamina and epoxy adhesive material properties of the DLJ [198].

(HTA/6376) Graphite/epoxy adherend:	Material constants: E_x = 141 GPa, E_y = 10 GPa, E_z = 11 GPa ν_{xy} = 0.3, $\nu_{xz} = \nu_{yz}$ = 0.5 $G_{xy} = G_{xz}$ = 5.2 GPa, G_{yz} = 3.9 GPa	Strengths: Z_T = 94 MPa, Z_C = 290 MPa S_{xy} = 98 MPa, S_{yz} = 30 MPa S_{xz} = 98 MPa
Epoxy adhesive:	E = 2.8 GPa, ν = 0.32	Y_T = 65 MPa, Y_C = 84.5 MPa

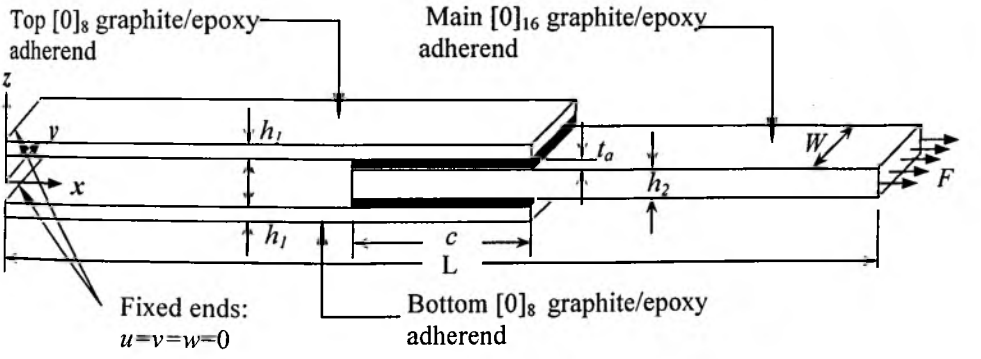

Figure 8.3 Laminated FRP composite DLJ specimen.

The adherends and adhesive layer of DLJ can be modelled either with shell elements or three-dimensional brick elements. The 3D brick element models have been shown to be more accurate especially in separating the total strain energy release rate G into individual components G_I, G_{II} and G_{III} [10, 165, 188]. But using many layers of brick elements through-the-thickness to model the individual plies and adhesive layer, modelling and computational effort may become prohibitively large. Therefore, it is necessary to use a layered volume element for improving computational efficiency without compromising accuracy of the FE analysis. In the present analysis, isoparametric, three-dimensional eight-node layered volume elements designated as SOLID 46 of FE software ANSYS-10 have been used to model the laminated FRP composite adherend ply-by-ply and orthotropic material properties have been considered for each ply. The convergence of the solution has been ensured using appropriate mesh density of the elements near the adhesion failure

front as suggested in references [9, 165, 199]. For this purpose an element size of one-fourth of each ply thickness has been used near the damage front along with a graded coarse mesh in the remaining areas of the joint.

Because of symmetry, only upper half of the DLJ specimen is considered for the analysis purposes. Mid-plane symmetry constraints on plane z=0 have been applied for the analysis domain comprising of the upper half of the DLJ. The displacement boundary conditions, accordingly, are given as

(i) $u = v = w = 0$, for all nodes at $x = 0$,

(ii) $w = 0$, for all nodes at $z = 0$ (due to mid-plane symmetry) and

(iii) $w = 0$, for all nodes at $z = 2.5$ and 4.5mm within the region $0 \leq x \leq$ 25mm and at $z = 2$mm within the region 205mm $\leq x \leq$ 230 mm. This has been so taken to prevent any rotation of the adherends at $x = 0$ and 230mm.

In the above, u, v and w are the displacements along the x, y and z directions, respectively. The finite element meshing scheme used for modelling and simulating damages in a DLJ is shown in Fig. 8.4.

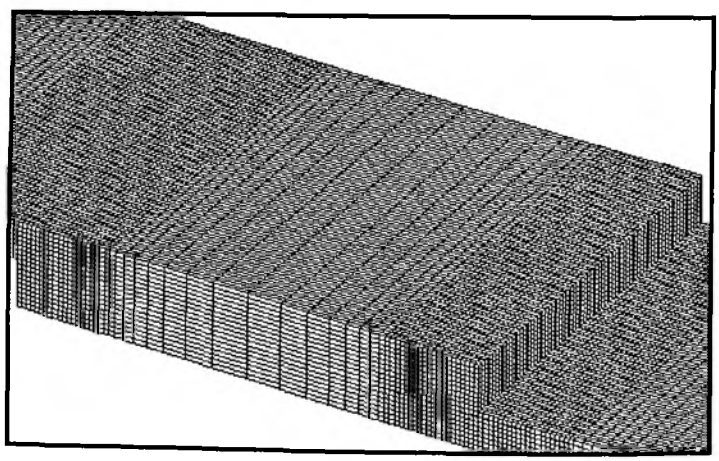

Figure 8.4 Zoomed view of the FE mesh of the symmetric upper half of the DLJ.

8.3 Criterion for onset of adhesion failure and delamination damage

One of the major concerns in the analyses of laminated FRP composite DLJ is the prediction of location of damage initiation due to the prevailing triaxial states of stresses which have to be accurately evaluated by three-dimensional FEA. Only two types of failures; (i) adhesion failures and (ii) delamination damages are considered in

the present analysis. Tsai and Wu [197] coupled failure criterion is used to determine the adhesion and delamination failure indices, represented as e_a and e_d, respectively over the bondline interfacial surfaces and below the surface ply adjacent to the adhesive layer of the main adherend of the DLJ. Accordingly, a failure surface in the stress space is represented in the following form:

$$f(\sigma_k) = F_i\sigma_i + F_{ij}\sigma_i\sigma_j = 1 \tag{8.1}$$

where $i, j, k = 1, 2, \ldots\ldots 6$ and F_i and F_{ij} are the strength tensors.

Interlaminar or out-of-plane stresses are responsible for initiation of adhesion and delamination failures and, hence, these stress components only are used in Eq. (8.1) to determine the failure indices e_a and e_d and are given by

(i) Delamination in tension, for $\sigma_z > 0$;

$$\left(\frac{\sigma_z}{Z_T}\right)^2 + \left(\frac{\tau_{xz}}{S_{xz}}\right)^2 + \left(\frac{\tau_{yz}}{S_{yz}}\right)^2 = e_a{}^2 (or = e_d{}^2), \begin{cases} e_a \text{ (or } e_d) \geq 1, \text{ failure} \\ e_a \text{ (or } e_d) < 1, \text{ no failure} \end{cases} \tag{8.2}$$

(ii) Delamination in compression, for $\sigma_z < 0$;

$$\left(\frac{\sigma_z}{Z_C}\right)^2 + \left(\frac{\tau_{xz}}{S_{xz}}\right)^2 + \left(\frac{\tau_{yz}}{S_{yz}}\right)^2 = e_a{}^2 (or = e_d{}^2) \begin{cases} e_a \text{ (or } e_d) \geq 1, \text{ failure} \\ e_a \text{ (or } e_d) < 1, \text{ no failure} \end{cases} \tag{8.3}$$

Thus, based on the magnitudes of e_a and e_d, the critical locations for onset of damage due to the adhesion failure and the delamination damage in the laminated FRP composite DLJ have been identified. Subsequently, the damage propagation has been studied using the individual modes of strain energy release rates (G_I, G_{II} and G_{III}).

8.4 Computation of SERR and damage propagation studies

The damage propagation behaviour due to the adhesion and the delamination failures emanating from the critical locations have been modelled and their propagations are governed by the individual modes of SERR along the damage front for the considered laminated FRP composite DLJ. In the laminated FRP composite adherends of DLJ, due to their inherent geometrical, loading and material properties complexities, exact closed form expressions for the strain energy release rates are not possible. The singularity of damage front stress field in an orthotropic media is quite different from that of the conventional square root singularity at the crack tip in homogeneous isotropic material system. This leads to the evaluation of interlaminar fracture energy released due to the propagation of the existing delamination by a very small amount

[14]. Strain energy release rate procedure is suitable for assessing damage propagation behaviour due to the reason that it is based on a sound energy balance principle implying its robustness, and also mode separation of SERR is possible. Irwin's theory of crack closure [108] has been followed for evaluating individual modes of strain energy release rates. This aspect is very important, as in most of the cases, the fracture mechanism is a mixed mode phenomenon in multi-directional laminated FRP composites.

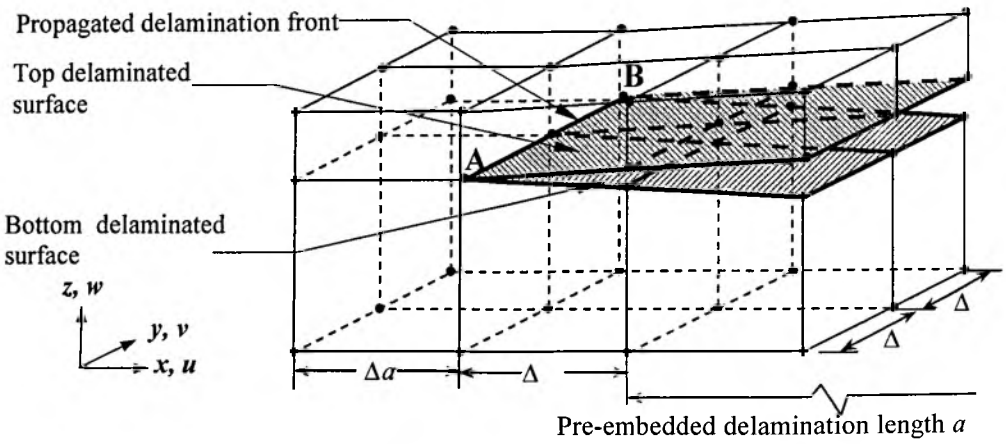

Figure 8.5 MCCI applied to the laminated FRP composite DLJ for computation of SERR along the delamination front AB.

Figure 8.5 shows the configuration for evaluation of MCCI applied to the laminated FRP composite DLJ for computation of SERR along the delamination damage front AB of length a existing below the surface ply of the main adherend adjacent to the adhesive layer. Except over the damaged region, Multi-Point Constraints are imposed on the nodes along the damage boundary and contact elements are used within the damaged region to prevent mutual interpenetration of the top and bottom damaged surfaces. This contact processor always maintains a positive value of displacement difference along the z-direction between the pair of nodes inside the damaged zone of the top and bottom damaged surfaces. Furthermore, it has been assumed that the damaged plane is the weakest and the damages will propagate parallel to the xy plane. Thus, the possibility of out-of-plane propagation is ignored. The three components of strain energy release rate viz. G_I, G_{II}, and G_{III} have been evaluated using Modified Crack Closure Integral (MCCI) and have been used as parameters for assessing the damage propagation characteristics. Evaluation of

interlaminar stresses σ_z, τ_{xz} and τ_{yz} along the damage front and the displacement fields around it is the central point of focus of any strain energy release rate analysis. Then the strain energy release rates along the damage front can be calculated from those stresses and displacement fields using Irwin's theory of crack closure. The strain energy released by the propagation of a delamination of length a to $a+\Delta a$ is given by

$$W = \frac{1}{2}\int_{a}^{a+\Delta a}\int_{-\Delta a/2}^{\Delta a/2}\sigma(x,y)\times\delta(x-\Delta a,y)dxdy \tag{8.4}$$

where $\delta(x-\Delta a,\ y)$ is the crack opening displacement between the top and bottom delaminated surfaces and $\sigma(x,y)$ is the stress at any point on the delamination front AB required to close the delaminated area. Then, the strain energy release rate (G) is obtained as

$$G = \lim_{\Delta a\to 0}\frac{W}{\Delta A} \tag{8.5}$$

where ΔA represents the delamination propagated area and equals to one element area in xy plane i.e. $\Delta a\times\Delta a$ for the present case. The MCCI has the advantage of mode separation of strain energy release rate, which will help for a qualitative analysis of delamination damage propagation behaviour. Accordingly, the three components of strain energy release rates G_I, G_{II} and G_{III} for Modes *I*, *II*, and *III* can be expressed given in Eqs. (3.109 – 3.111).

While implementing these Equations to evaluate the three components of SERR for delamination damage analyses of Adhesively Bonded Double Lap Joint the subscripts T and B represent the top and bottom delaminated surfaces, respectively. The existing damage length is denoted by a, and Δa is the virtual damage length due to the external loads. Here, $[u_T,\ v_T,\ w_T]$ and $[u_B,\ v_B,\ w_B]$ represent the displacements corresponding to the nodes at the top and bottom delaminated surfaces, respectively behind the delamination front and, σ_z, τ_{zx} and τ_{zy} are the stresses required to close the delaminated surfaces.

8.5 Results and discussion

8.5.1 Stress distributions

The peel and shear stresses distributions along the line passing through the middle of the adhesive layer of the DLJ are shown in Fig. 8.6 for comparison with the existing analytical solutions [17, 102]. The present 3D solutions pertaining to the adhesive peel stress is found to be in good agreement and validates the FE mesh used for modelling the laminated FRP composite DLJ specimen. However, there are some differences in shear stress values and it may be due to some simplified assumptions such as that the adhesive shear stress is constant, so that the peel stress solutions may be decoupled from the shear stresses.

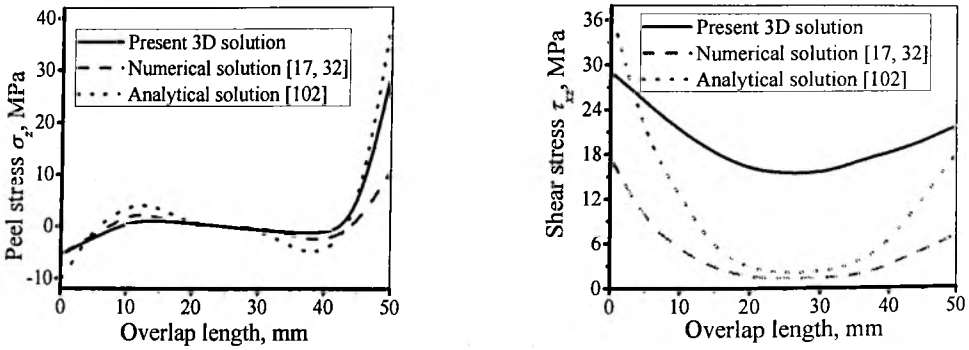

Figure 8.6 Comparison of peel and shear stresses in the adhesive layer of laminated FRP composite DLJ.

The 3-dimensional nature of the stress field on different interfacial surfaces i.e. (i) the top adherend and the adhesive layer, (ii) the main adherend and the adhesive layer and (iii) the first and second plies of the main adherend adjacent to the adhesive layer of the joint have been shown in Figs. 8.7-8.9. These have been used for finding out the region for the initiation of failures in the joint. It is observed that the peak values of out-of-plane stress components (σ_z, τ_{yz} and τ_{xz}) on the interfacial surface between the main adherend and the adhesive layer are the highest and the lowest on the interfacial surface between the top adherend and the adhesive layer. Comparing the stress distributions among the above interfacial surfaces, it is seen that at the interfacial surfaces between the main adherend and the adhesive layer and that between the first and second plies of the main adherend are more susceptible for onset of adhesion failure and delamination damage, respectively as shown in Figs. 8.7-8.9. Also, the present 3D stress analyses depict the exact location of the damage initiation i.e. the stress singularity points at the edges of the DLJ and exactly below the overlap

end of the main adherend due to the adhesion failure and the delamination damage, respectively.

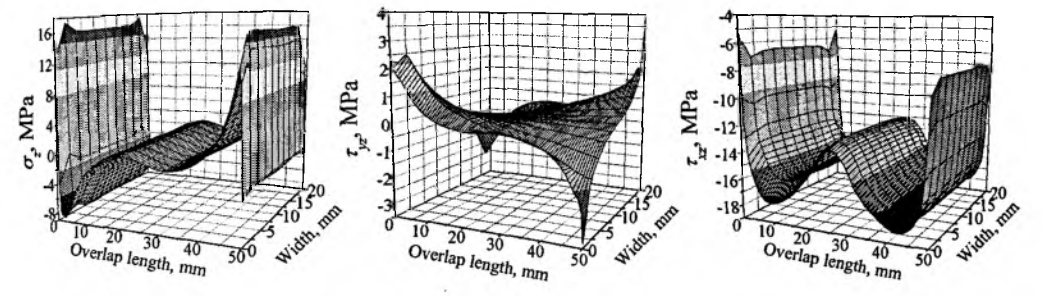

Figure 8.7 Out-of-plane stress variations on the interfacial surface between the top adherend and the adhesive layer of the laminated FRP composite DLJ.

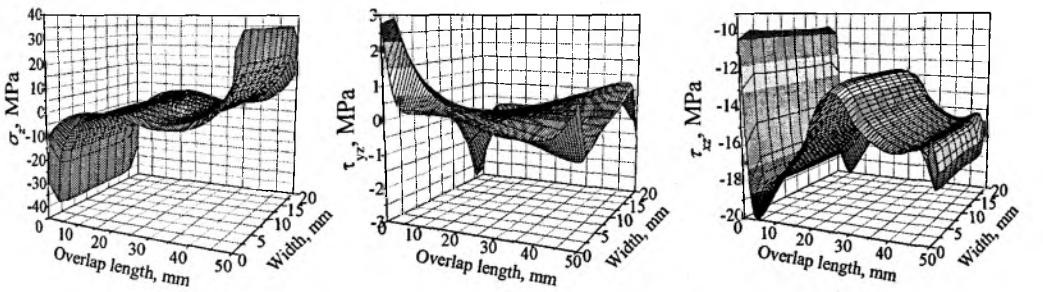

Figure 8.8 Out-of-plane stress variations on the interfacial surface between the main adherend and the adhesive layer of the laminated FRP composite DLJ.

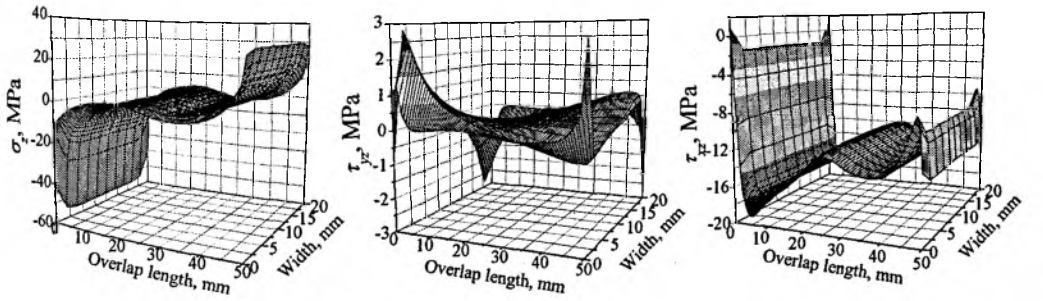

Figure 8.9 Interlaminar stress distributions on the surface below the surface ply adjacent to the adhesive layer of the main adherend of the laminated FRP composite DLJ.

8.5.2 Evaluation of failure criterion parameters and onset of adhesion failure and delamination damage

The failure indices e_a and e_d which represent the adhesion failure and the delamination damage initiation parameters, respectively, have been computed using Tsai-Wu's coupled stress failure criterion (Eqs. (8.2) & (8.3)) as given in Sec. 8.3 and the variations have been shown in Fig. 8.10. It is seen that e_a values are the highest at the stress singularity points at the overlap edges of the DLJ, followed by e_d values at exactly below the overlap end of the main adherend.

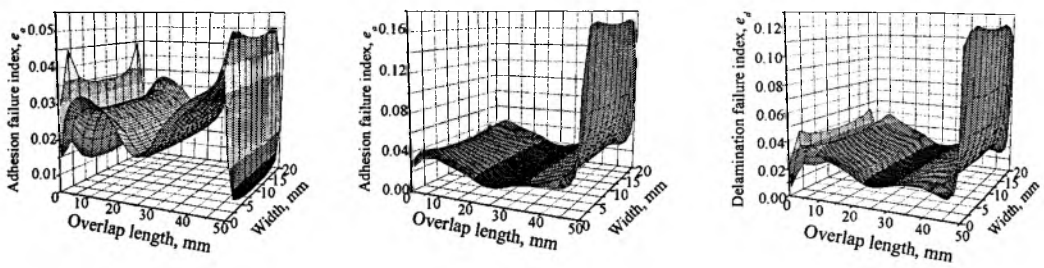

(a) (b) (c)

Figure 8.10 Adhesion failure and delamination damages in terms of failure indices e_a and e_d, respectively, in laminated FRP composite DLJ on different interfacial surfaces between; (a) the top adherend and the adhesive layer, (b) the main adherend and the adhesive layer and (c) second and surface plies adjacent to the adhesive layer of the main adherend.

8.5.3 Delamination damage propagation

The stress and failure analyses indicate the critical locations for the onset of the adhesion failure and the delamination damage. The propagation of damages due to the adhesion failure and the delamination have been studied by pre-embedding the damages at the critical locations of the DLJ as shown in Fig. 8.11 by three-dimensional finite element analyses with varied damage lengths a. Individual modes of the SERR, G_I, G_{II} and G_{III} considered as the fracture parameters governing the propagation of damages, have been computed using MCCI along the damage fronts and their variations have been shown in Figs.8.12-8.14 with varied damage lengths.

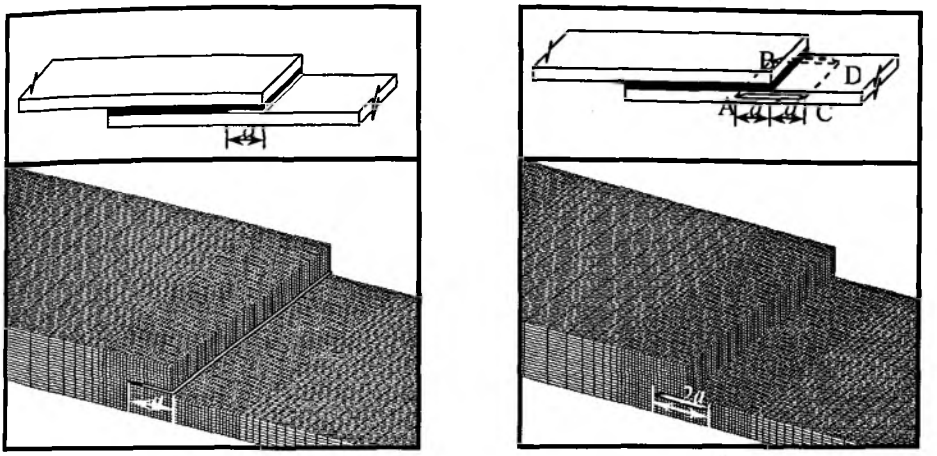

Figure 8.11 FE simulation for varied damage propagation lengths a due to; (a) adhesion failure initiated from the edges of stress singularity points and (b) delamination damage initiated beneath the surface ply of the main adherend adjacent to the adhesive layer.

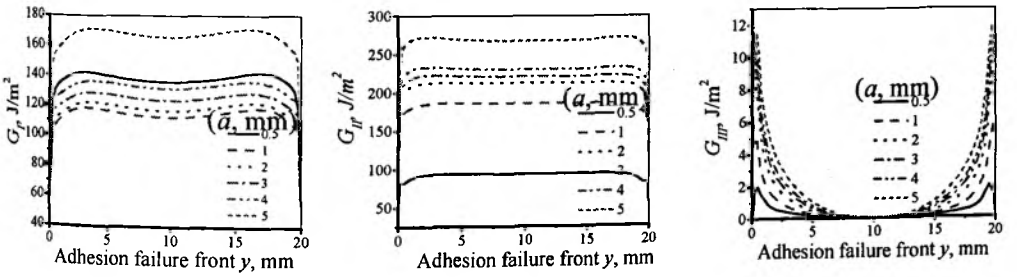

Figure 8.12 Variations of individual modes of SERR (G_I, G_{II} and G_{III}) along the adhesion failure front for varied adhesion failure lengths a between the main adherend and the adhesive layer (Ref. 8.11 (a)).

Figure 8.12 shows the SERR variations along the damage front existing in case of adhesion failure and Figs. 8.13 and 8.14 show the SERR variations along AB and CD which represent the two delamination fronts at the left and right ends of the embedded delamination. It is seen that SERR values remain uniform along the width of the joint except for the G_{III} component. Near the free edges i.e. at $y = 0$ and 20mm, the SERR values are significantly less compared to the SERR values in the central portion. This trend is similar to the double cantilever beam and similar specimens

taken by Raju et al. [200]. Comparing the individual modes of SERR values along the adhesion failure front, it is seen in Fig. 8.12 that G_{II} i.e. shearing mode (Mode *II*) is the highest and this parameter governs the propagation of adhesion failure. But the contributions of G_I and G_{III} in adhesion failure propagation can not be outrightly ignored. Therefore, it can be said that the adhesion failure propagates under mixed mode condition.

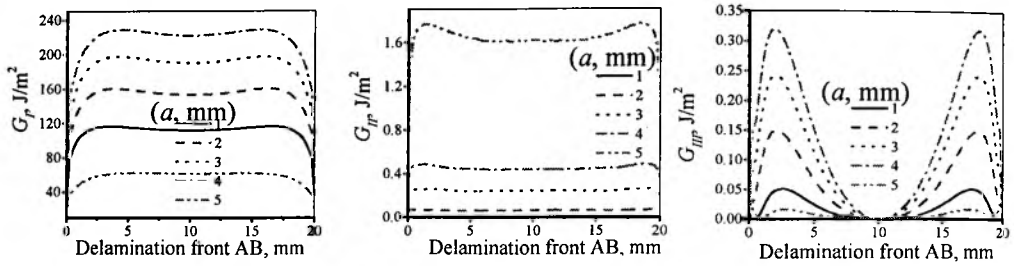

Figure 8.13 Variations of individual modes of SERR (G_I, G_{II} and G_{III}) along the delamination front AB for varied pre-embedded delamination damage lengths *a* beneath the surface ply of the main adherend (Ref. Fig. 8.11 (b)).

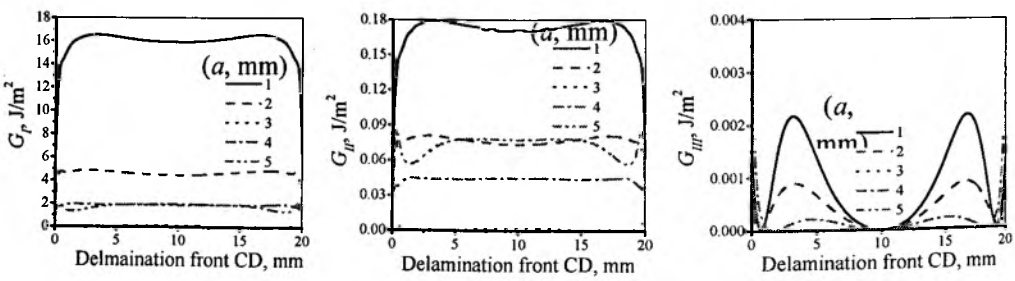

Figure 8.14 Variations of individual modes of SERR (G_I, G_{II} and G_{III}) along the delamination front CD for varied pre-embedded delamination damage lengths *a* beneath the surface ply of the main adherend (Ref. 8.11 (b)).

In regards to the delamination induced damage propagation at locations beneath the surface ply of the main adherend near the adhesive layer, it is observed that the SERR values along the delamination front AB are significantly higher compared to those along the delamination front CD as shown in Figs. 8.13 and 8.14, respectively. The unequal magnitudes of SERR components along these two delamination fronts depict the unequal rates of propagation of delamination damages.

The delamination will propagate more vigorously from the delamination front AB till the joint fails. This is due to the significantly higher values of the components of SERR. It can be concluded that the delamination front existing in the main adherend lying within the overlap region of the joint is more influential for propagation of the delamination damage. Similar observations have been made by Tong [35] for an SLJ specimen. Another important observation is that G_I values are quite high compared to the G_{II} and G_{III} values. It indicates that the opening mode i.e. Mode *I* is the predominant mode for propagation of the delamination damage. Whereas, the shearing mode i.e. Mode *II* dominates the propagation of the adhesion failure. The G_{II} and G_{III} values in the second case considered are negligibly small. Hence, the contribution of Mode *II* and Mode *III* SERR towards delamination propagation is marginal.

On comparison of the two cases i.e. the adhesion failure (Fig. 8.11 (a)) and the delamination damage propagation (Fig. 8.11(b)), G_{II} values along the adhesion failure front are comparatively higher than the G_I values along the delamination front for all values of damage lengths a. Therefore, it can be concluded that the adhesion failure is more detrimental than the delamination damages for the failure of DLJ when the DLJ is embedded with both types of damages.

8.6 Conclusions

Three-dimensional non-linear finite element analyses of laminated FRP composite DLJ have been carried out to study the onset and growth of adhesion failure and delamination induced damages. Out-of-plane stress distributions have been evaluated at different interfacial surfaces of the joint, and also the interlaminar stresses between the first and second plies of the main adherend adjacent to the adhesive layer within the overlap region have been evaluated for failure analyses to identify the critical locations for the onset of the adhesion failure and the delamination induced damage. The individual modes of SERR along the damage fronts have been evaluated using MCCI for varied embedded lengths of adhesion failure and delamination induced damage. The conclusions, based on the results and observations on the variations of the different components of the SERR, are as follows:

- The out-of-plane stress components are the highest on the interfacial surface between the main adherend and the adhesive layer of the DLJ.
- The adhesion failure initiates from the stress singularity points at the edges of the DLJ i.e. from the overlap end of the joint.

- Adhesion failure propagation is due to mixed mode SERR whereas the delamination damage propagates primarily due to Mode *I*.
- Non-uniform and non-equal SERR variations along the delamination damage fronts depict unequal rates of propagation of delamination damages. This may cause the straight damage front to grow into a curved damage front.
- Delamination front lying inside the overlap region is more detrimental for the propagation of pre-embedded delamination compared to the ones lying outside the overlap region of the DLJ.
- The adhesion failure is more detrimental compared to the delamination induces damages for the failure of DLJ when the DLJ is embedded with both types of damages.

9

Design and Development of Load Coupler Profiles of Spar Wingskin Joints for Integral Structural Construction of Aircraft Wings

9.1 Introduction

The Spar Wingskin Joint (SWJ) consists of a thin spar which overlaps and is co-cured to a thick wingskin. The SWJs are mostly used in integral modular wing fabrication of aircraft structures with laminated GFRP composites as shown in Fig. 9.1 and are intended for transferring and sharing the wing load and fluid pressure. The space between the wingskin flanges and the spar called the core is filled up with some suitable adhesive or bonding material called as the load coupler. These joints are subjected to out-of-plane loads. Analysis and determination of design data adopted in the integrated modular wing concept of fabrication technique is relatively a much newer and useful step for the SWJ subjected to out-of-plane loads.

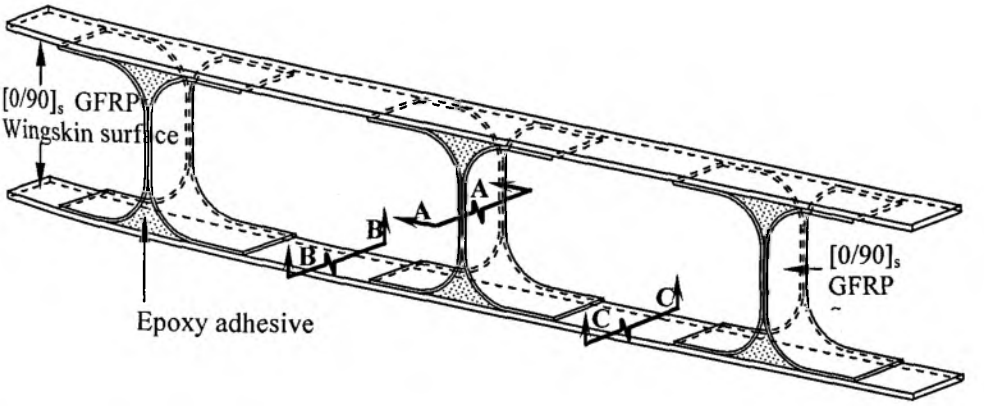

Figure 9.1 GFRP composite SWJ used in integral structural construction of aircraft wings showing the spar and wingskin surfaces (The portion of the structure between sectional planes AA, BB and CC comprises of the analysis domain of the SWJ).

The SWJ with complicated configurations and non-planar loadings are remaining so far intractable, complex and much involved. Also, the analytical or continuum mechanics based solutions are not possible for the failure analyses of the SWJ. The methodology to determine the stresses and subsequently to predict the

onset of delamination induced damage and its propagation in the SWJ is not yet known. The relevant literatures in the analysis of the SWJ do not exist as the analysis is only at its nascent stage even today. The complicated shape, loading, boundary conditions and orthotropic material properties of the joint components are the formidable obstacles for the closed form solutions. Some attempts in experimental as well as finite element analyses have been taken to study the behaviour and to predict the strength of the joint. Lackman et al. [104] developed a method for strengthening bonded structures to cover joints to withstand the combination of structural loads and fuel pressure which generates peeling forces at the end of the spar base flanges. Gillespie and Pipes [105] conducted experiments and finite element analyses on integral composite joints with Titanium and Graphite/Epoxy inserters in the SWJ. Copes and Pipes [106, 107] have analyzed SWJ with different load coupler profiles viz. triangular and circular shape using FEA to predict the ultimate load using Tsai-Wu and maximum stress failure criteria. There is no literature available related to the three-dimensional stress analysis and onset of the delamination induced damage with varied load coupler profiles and aspect ratios defined as the ratio of the base width (b) to the height (h) of the load coupler.

This Chapter encompasses rigorous non-linear three-dimensional finite element analyses of laminated FRP composite SWJ with different load coupler profiles of varied aspect ratios. Tsai-Wu coupled stress failure criteria are used to predict the locations of delamination damage onset for varied load coupler profiles. Based on the stress and failure analyses, suitable geometry and configuration of the SWJ have been recommended. Based on the stress analysis, Jena [183] recommended the suitability of modified elliptical adhesive core profile of SWJ using FEA and experimental study. The failure analyses of SWJ with modified elliptical adhesive load coupler profile of aspect ratio equal to 1.5 have been carried out. The delamination damage propagation in the SWJ has been evaluated using individual Modes of SERR which are computed by Modified Crack Closure Integral (MCCI) based on Linear Elastic Fracture Mechanics (LEFM) as recommended by Rybicki and Kanninen [13].

9.2 Developments of SWJ

In the integral modular concept of fabrication technique, the SWJ connects in a co-cured manner the lower cover skin (wingskin) to the top substructure through a number of spars as shown in Fig. 9.1. Conventional I beams were being used as the

substructure for the spar during the initial designs towards the development of SWJ. By using the I-beams, either stitching or spar-to-cover metallic barbed pins were adopted for reinforcing the substructure i.e. to connect the spar with the wingskin. However, metallic pinning or stitching concept was inefficient especially under fatigue loading as the pin holes are supposed to be the potential stress raisers. This method was ineffective because of local damages induced while manufacturing thereby inducing high stress concentrations. Hence, further development was necessitated to achieve the required design goal. The next development was accomplished by the load coupler concept and this helped in providing a smooth transfer of wingskin load to the spar, thereby reducing the peel forces considerably. The load coupler can have different geometrical profiles viz. triangular, circular, elliptical, modified elliptical, etc. and it stands sandwiched between the wingskin and the bifurcated flanges of the spar. Subsequently, the SWJ with circular or elliptical corner fillets with a filled adhesive core were developed and Figs. 9.2 (b-d) show the typical examples of the SWJ and are the obvious choices for better and smooth load transfers.

9.2.1 SWJ with varying load coupler profiles

Only triangular and circular load coupler profiles were chosen for investigation by Copes and Pipes [107] and Jena [183]. The adhesive has been used to fill the void created at the base of the spar between the overlap and the wingskin. The SWJ employed with different load coupler profiles under study are shown in Fig. 9.2.

The SWJ with triangular adhesive core (concept I) utilizing the load coupler concept is a moderate development to facilitate smooth and efficient transfer of wingskin loads to the substructure member spar as shown in Fig. 9.2 (a). The connection of the spar and the wingskin through concept I is simpler and convenient from fabrication point of view, but higher stress concentration problems are posed because of the existence of the sharp corners. These could be smoothened by providing circular (concept II) or elliptical adhesive core (concept III) profiles as shown in Figs. 9.2 (b) and (c) and reductions in stress concentrations can be achieved. For an improved form, the circular adhesive core profile is replaced by an elliptical profile as shown in Fig. 9.2 (c). In this, it is possible to increase the base width of the adhesive core without increasing its height. This will further enhance the joint strengths. The SWJ employed with modified elliptical adhesive core profile as shown in Fig. 9.2 (d), strengthens the stiffness of the rib portion of the spar. Also, the height and thickness of the adhesive core are increased by slight modification of the

elliptical core in order to resist lateral buckling of the spar under the structural load and fluid pressure. There are significant influences of the geometric and material parameters on the performance of the FRP composite SWJ. This Chapter emphasizes the effects of varying the aspect ratios (base to height) of the load coupler on the variations of stresses, identification of locations for the delamination damage initiations for different concepts as described above, leading to a recommendation for the suitable profile of the SWJ for improved performance.

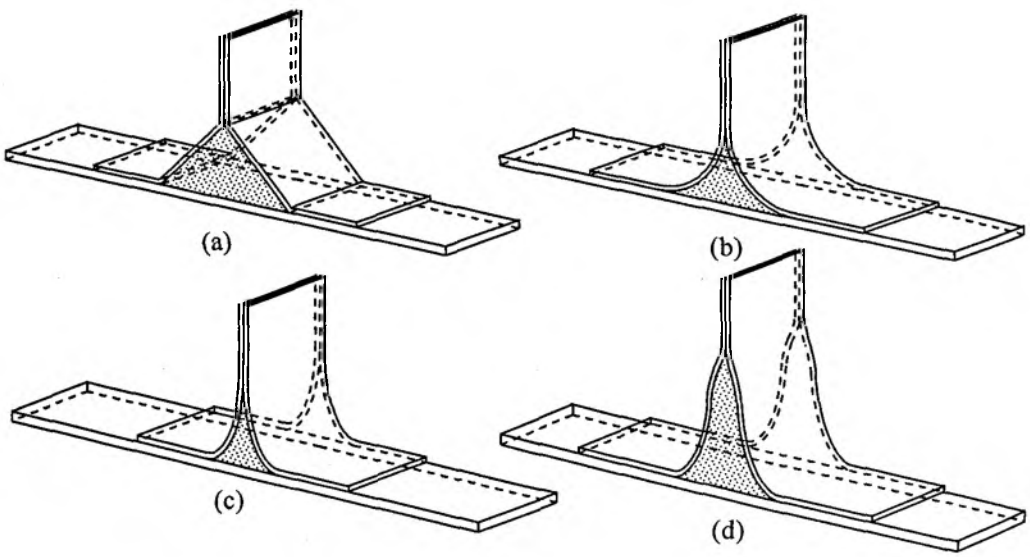

Figure 9.2 Adhesively bonded laminated FRP composite Spar Wingskin Joints (SWJ) with various load coupler profiles; (a) Triangular, (b) Circular, (c) Elliptical and (d) Modified elliptical.

9.3 Finite element analyses of the SWJ

FRP composite SWJs with circular and modified elliptical adhesive core profiles are shown in Figs. 9.3 (a) and 9.4 (a), respectively. The symmetric half section model of the SWJ as shown in Figs. 9.3 (b) and 9.4 (b) are used for the finite element analyses. The dimensions of the FRP composite SWJ are as follows;

Half span length L = 60 mm, Thickness of the spar t_1 = 1 mm,

Thickness of the wingskin t_2 = 2 mm, Width of the SWJ W= 25 mm,

Spar overlap length c= 15 mm, A = 8 mm and B = 2 mm.

The spar and the wingskin are made of $[0/90]_s$ Graphite Fiber Reinforced Polymeric (GFRP) composite laminates of ply thicknesses 0.125mm and 0.5mm,

respectively. The material properties and strength values of HTA/6376 GFRP lamina and the epoxy adhesive properties are given in Table 9.1. The portion of the SWJ structure between sectional planes AA, BB and CC (Fig. 9.1) comprises of the analysis domain. Figures 9.5 and 9.6 show the finite element meshes for the symmetric half sections of the SWJ along with the loadings and the symmetric displacement boundary conditions. A uniformly distributed transverse load of 40N/mm in 100 equal increments has been applied along the width of the wingskin near the free end of the SWJ. Similar FE modelling procedures have been adopted for the SWJ of other concepts (concept I and concept III).

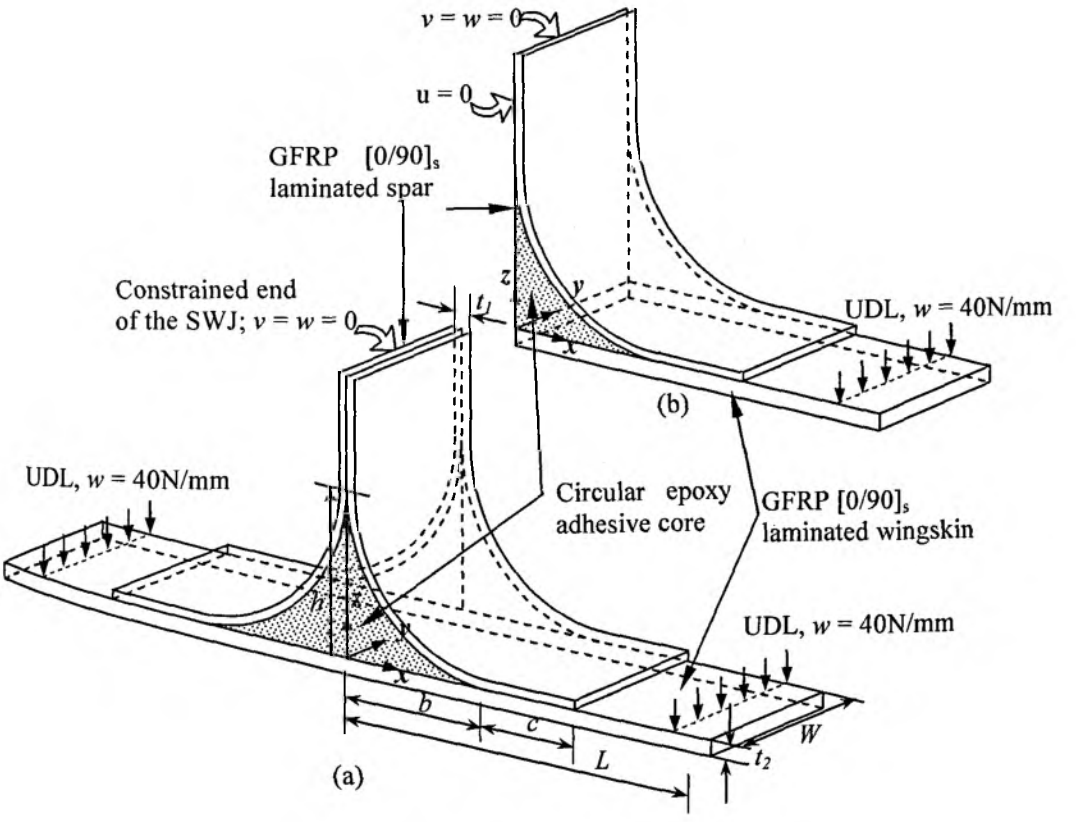

Figure 9.3 (a) SWJ with circular load coupler profile and (b) Symmetric half section model of SWJ for FEA.

The linear and non-linear analyses yield significant differences in the computed values of peel and shear stresses. It has been emphasized that the non-linear analysis procedure must be used for an SWJ in order to evaluate the stresses in the

joint accurately. Thus, three-dimensional finite element analyses with geometric non-linearities have been carried out for the SWJ.

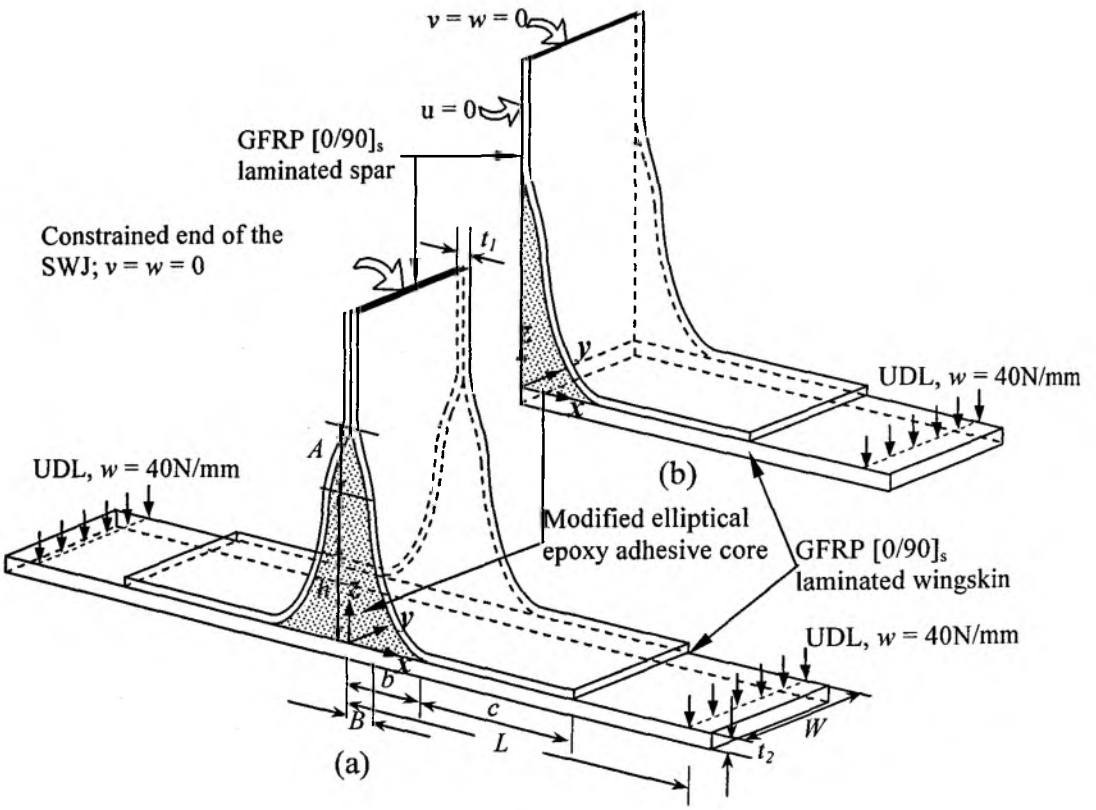

Figure 9.4 (a) SWJ with modified elliptical load coupler profile and (b) Symmetric half section model of SWJ for FEA.

Table 9.1 GFRP Lamina and epoxy adhesive core material properties [198].

(HTA/6376) Graphite/epoxy Spar/Wingskin:	Material constants: E_x = 141 GPa, E_y = 10 GPa, E_z = 11 GPa ν_{xy} = 0.3, ν_{xz} = ν_{yz} = 0.5 G_{xy} = G_{xz} = 5.2 GPa, G_{yz} = 3.9 GPa	Strengths: Z_T = 94 MPa, Z_C = 290 MPa S_{xy} = 98 MPa, S_{yz} = 30 MPa S_{xz} = 98 MPa
Epoxy adhesive:	E = 2.8 GPa, ν = 0.32	Y_T = 65 MPa, Y_C = 84.5 MPa

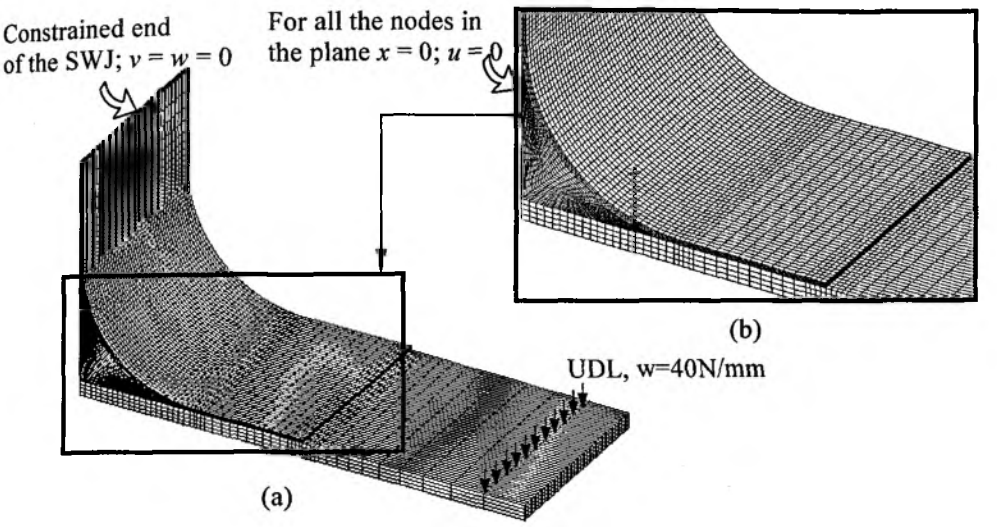

Figure 9.5 FE meshes: (a) Symmetric half section of the SWJ with circular load coupler profile and (b) Zoomed view of the toe-end of the spar flange.

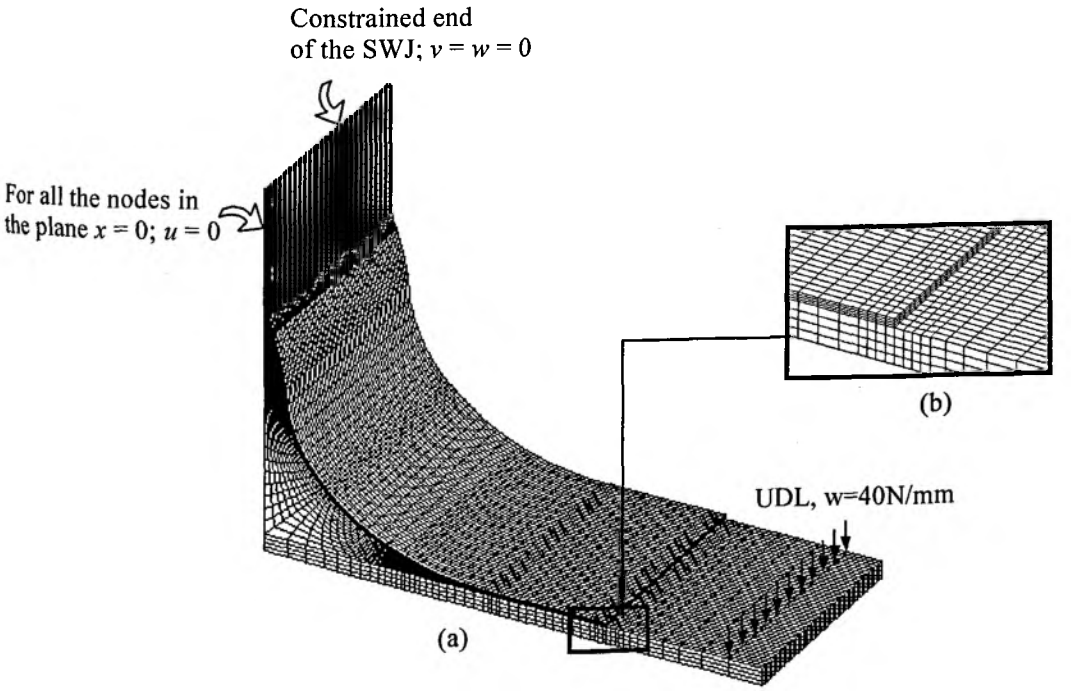

Figure 9.6 FE meshes: (a) Symmetric half section of the SWJ with modified elliptical load coupler profile and (b) Zoomed view of the toe-end of the spar flange.

9.3.1 Finite element modelling

The spar and wingskin of an SWJ can be modelled either with shell elements or three-dimensional brick elements. The 3D brick element models have been shown to be more accurate especially in separating the total strain energy release rate G into individual components G_I, G_{II} and G_{III} [34, 179, 199]. But, using many layers of brick elements through-the-thickness to model the individual plies, modelling and computational effort may become prohibitively large. Therefore, it is necessary to use a layered volume element for improving computational efficiency without compromising the accuracy of the FE analysis. In the present FE analysis, isoparametric, three-dimensional eight-node layered volume elements designated as SOLID 46 of ANSYS-10 have been used to model the laminated FRP composite spar and the wingskin. Layerwise orthotropic material properties as given in Table 9.1 have been considered for each ply. The 3D model construction of the SWJ specimen has been simplified by first generating a template of 2D mesh pattern in xz plane, and then this pattern has been protruded in the y-direction for the full 3D FE models.

Traditionally, components of SERR G_I, G_{II} and G_{III} are being used to analyze the interfacial delaminations between two orthotropic solids using Virtual Crack Closure Technique (VCCT) [110-112]. However, the stress field solutions of the near crack tip field indicated that stresses started to oscillate in the immediate vicinity of the tip, when crack growth occurred at the interfaces between materials with dissimilar properties. Oscillatory stress fields were observed by Rice [201] at the interface. Interface crack growth studies in orthotropic media are quite complex in nature due to the mismatch of material properties at the interface. The singularities of the stress field at the tip of the delamination are generally more complex than those associated with cracks in homogeneous medium.

The convergence of the solution has been ensured by increasing the mesh density of the elements near the damage front as suggested in references [111, 153]. In the SERR method of damage propagation studies, it is not necessary to emphasize much about the values of the stresses exactly at the delamination front. The stresses and the displacements over the damaged area are evaluated and these values are used for evaluating G_I, G_{II} and G_{III}. Further, it is not required to use a very refined mesh in this region as per Tay et al. [153]. They have discussed the adequacy of the local near-tip mesh in greater details. They also observed that an extreme fine mesh could result in non convergence when the region enters the zone of oscillatory stress fields. The FE work of Raju et al. [111] suggests that if the element size or characteristic

length is chosen to be between 0.25 to 0.5 of the ply thickness, the components of SERR are well evaluated. The mesh design in the present Chapter has been adopted with the above philosophy and for this purpose an element size of one-fourth of each ply thickness has been used near the damage front.

9.4 Damage onset

It is customary for the joint designer to predict the failure initiation in SWJ with known material properties, geometries and loading. Compared to the failure in metal joints a large number of failure modes can be identified for composites due to their anisotropic nature. The laminated FRP composites used for the spar and the wingskin develop local failures or exhibit local damage such as matrix cracks, fiber failure, fiber-matrix shear-outs and delaminations. The most important failure mode in FRP composites is due to the delamination damages. Thus, the ability to identify the location of initiation and growth of delamination induced damage is essential for assessing the performance of the joint either experimentally or numerically.

Stress analyses have been performed by most models using 2D linear or non-linear finite element analyses. However, in case of the SWJ, the stress states at the point of discontinuities are three-dimensional and depend on many complex parameters which can not be considered by the 2D model. Thus, after the computation of stresses from the three-dimensional non-linear finite element analyses, stress based failure criteria for laminated FRP composites can be carried out as given in the literatures [197, 202]. Tsai-Wu's [197] coupled stress failure criteria have been used to predict the locations for delamination induced damages. Accordingly, the interlaminar stress components (σ_z, τ_{yz} *and* τ_{zx}) responsible for initiation of delamination damages have been considered in the Tsai-Wu's coupled stress failure criterion. The failure criteria are given as follows:

(i) Delamination with $\sigma_z > 0$;

$$\left(\frac{\sigma_z}{Z_T}\right)^2 + \left(\frac{\tau_{xz}}{S_{xz}}\right)^2 + \left(\frac{\tau_{yz}}{S_{yz}}\right)^2 = e_d^{\,2} \quad , \begin{cases} e_d \geq 1, \text{ failure} \\ e_d < 1, \text{ no failure} \end{cases} \tag{9.1}$$

(ii) Delamination with $\sigma_z < 0$;

$$\left(\frac{\sigma_z}{Z_C}\right)^2 + \left(\frac{\tau_{xz}}{S_{xz}}\right)^2 + \left(\frac{\tau_{yz}}{S_{yz}}\right)^2 = e_d^{\,2}, \quad \begin{cases} e_d \geq 1, \text{ failure} \\ e_d < 1, \text{ no failure} \end{cases} \tag{9.2}$$

The notations of the quantities appearing in the above failure criterion refer to the local coordinate system. In this system, the x- and y- axes are parallel and transverse to the fibers, respectively, while, the z-axis coincides to the normal direction. The quantities in the denominators are the strengths in the corresponding directions. Suffixes T and C in Eqs. (9.1) and (9.2) denote the strength values under tension and compression, respectively. Locations of delamination induced damage initiations in the SWJ are predicted in terms of failure index e_d using Eqs. (9.1) and (9.2) and material properties given in Table 9.1. The delamination damage index (e_d) over the interfacial surface of the spar and the wingskin for varying b/h ratios have been computed. Based on the magnitudes of e_d, the critical locations for delamination damage initiations in the SWJ have been identified.

9.4.1 Computation of SERR

Figure 9.7 shows the model for evaluation of MCCI applied to the SWJ for computation of SERR along the delamination front when delamination of length a is embedded at the critical location i.e. at the toe end of the spar flanges in contact with the wingskin. The strain energy released by the propagation of a delamination of length a to $a+\Delta a$ is given by

$$W = \frac{1}{2}\int_{a}^{a+\Delta a}\int_{-\Delta a/2}^{\Delta a/2}\sigma(x,y)\times\delta(x-\Delta a,y)\,dx\,dy \tag{9.3}$$

where $\delta(x-\Delta a, y)$ is the crack opening displacement between the top and bottom delaminated surfaces of spar and wingskin, respectively and $\sigma(x,y)$ is the stress at any point on the delamination front required to close the delaminated area. Then the strain energy release rate (G) is obtained as

$$G = \lim_{\Delta a\to 0}\frac{W}{\Delta A} \tag{9.4}$$

where ΔA represents the delamination propagated area and equals to one element area in xy plane i.e. $\Delta a\times\Delta a$ for the present case.

The MCCI has the advantage of mode separation of strain energy release rate. This will help for a qualitative analysis of delamination damage propagation

behaviour. Accordingly, the three components of strain energy release rates G_I, G_{II} and G_{III} for Modes *I*, *II*, and *III* can be expressed as in Eqs. (3.109 – 3.111).

While implementing these Equations to evaluate the three components of SERR for delamination damage analyses of Spar Wingskin Joint, the subscripts *T* and *B* represent the top and bottom delaminated surfaces of spar and wingskin, respectively. The existing delamination length is denoted by a and Δa is considered to be the virtual delamination growth. The quantities $[u_T, v_T, w_T]$ and $[u_B, v_B, w_B]$ represent the displacements corresponding to the nodes at the top and bottom delaminated surfaces, respectively, behind the delamination front and σ_z, τ_{zx} and τ_{zy} are the stresses required to close the delamination front.

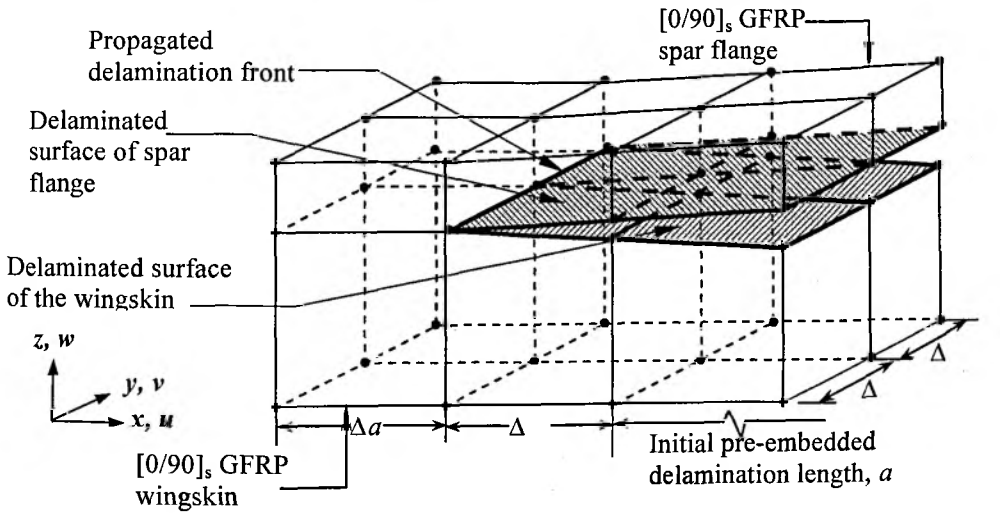

Figure 9.7 MCCI applied to the SWJ for computation of SERR along the interfacial delamination front existing at the toe-end of the spar flanges and the top surface of the wingskin.

9.5 Load coupler profiles with improved performance for integral structural construction of aircraft wings

9.5.1 Effect of load coupler profiles on stress variations in the SWJ

Normal and shear stresses (σ_x, σ_y, σ_z, τ_{xy}, τ_{yz} *and* τ_{zx}) have been determined from the 3D non-linear FEA for various load coupler profiles of SWJ and have been presented along the central symmetrical longitudinal cross-section of the SWJ. The results have been compared with the experimental values of Jena [183] for the SWJ of triangular and circular load coupler profiles as shown in Figure 9.8 and the trend of the normal stress (σ_x) variation over the bottom and the top surfaces of the wingskin are seen to be in good agreement. Referring to Fig. 9.8 (a), the normal stresses σ_x have been normalized by dividing with σ_b, which is equal to the maximum bending stress occurring in a simply supported beam identical in all respect to that of the wingskin member of the SWJ

i.e. $$\sigma_b = \frac{6M_{max}}{Wt_2^2}.$$

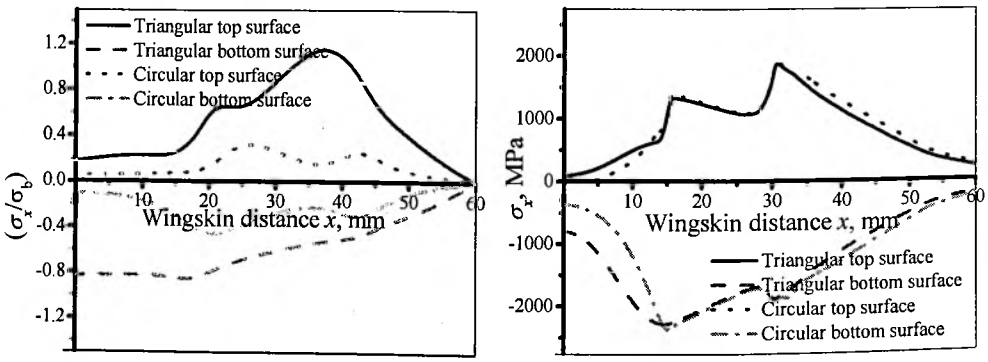

(a) (b)

Figure 9.8 Normal stress (σ_x) variations over the top and the bottom surface of the wingskin of the SWJ having triangular and circular adhesive core profiles; (a) experimental [183] and (b) present FEA.

The 3D state of stress components (σ_x, σ_y, σ_z, τ_{xy}, τ_{yz} *and* τ_{zx}) over the bottom and the top surfaces of the wingskin of the SWJ having four different concepts (concept I: triangular, concept II: circular, concept III: elliptical and concept IV: modified elliptical) for varied aspect ratios (b/h= 0.5, 1.0 and 1.5) have been evaluated and the stress variations are presented in Figs. 9.9-9.14. It is seen that the shear stress components (τ_{xy} and τ_{yz}) are negligibly small compared to the other stress

components for all concepts of SWJ. It is also observed that the magnitudes of the stresses (σ_x, σ_y, σ_z *and* τ_{zx}) are found to have two peak values, one is at the location just below the point where the inclined and horizontal portions of the spar intersect and the other is at the point which is common to the overlap end of the spar and the top surface of the wingskin, the latter being the highest. For the bottom surface of the wingskin all stress components are compressive in nature as shown in Figs. 9.9-9.11 and the stresses are tensile in nature on the top surface of the wingskin as shown in Figs.9.12-9.14. The magnitude of peel stress (σ_z) is negligibly small throughout the interfacial surface of the spar and the wingskin except at the toe-end of the spar overlapping flange where the stress magnitude is very high along with a very steep gradient as shown in Figs. 9.9-9.14 (c).

Figures 9.9-9.14 indicate the significant effects of the geometry of the load coupler profiles on the stress variations of the SWJ. The SWJ with triangular adhesive core is the worst and the SWJ having modified elliptical adhesive core is the best among the four concepts considered. Accordingly, the SWJ with modified elliptical adhesive core is preferred for better load carrying capacity. The use of modified elliptical adhesive core profile not only smoothens the sharp corners of the joint existing in case of triangular adhesive core profile, but also reduces the stress concentrations and adds to the stiffness of the rib portion of the spar.

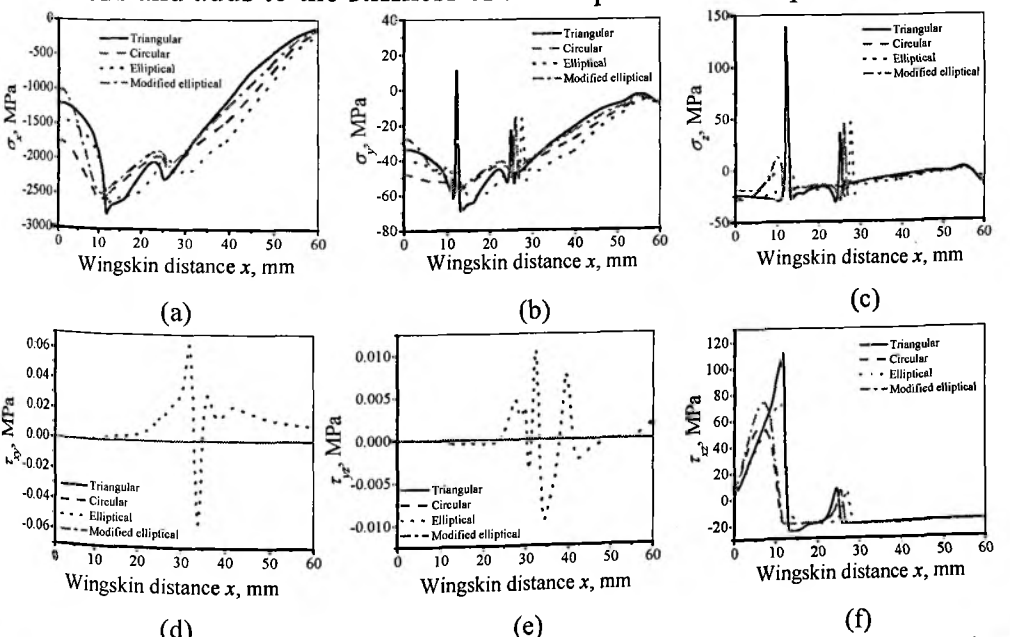

Figure 9.9 Normal and shear stress variations on the bottom surface of the wingskin of the SWJ having different adhesive core profiles with $b/h = 0.5$.

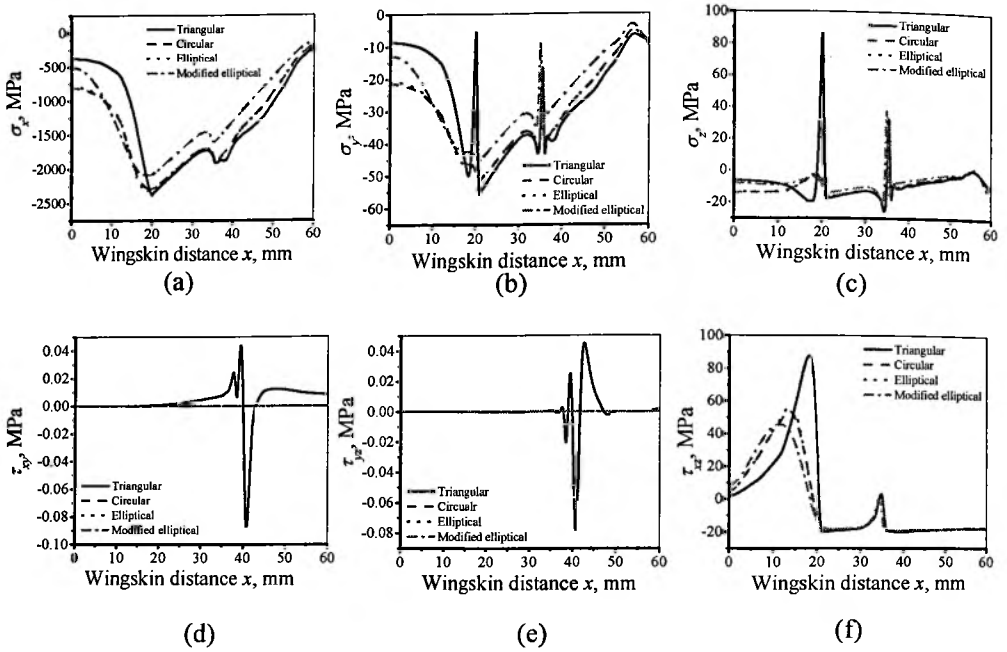

Figure 9.10 Normal and shear stress variations on the bottom surface of the wingskin of the SWJ having different adhesive core profiles with b/h = 1.0.

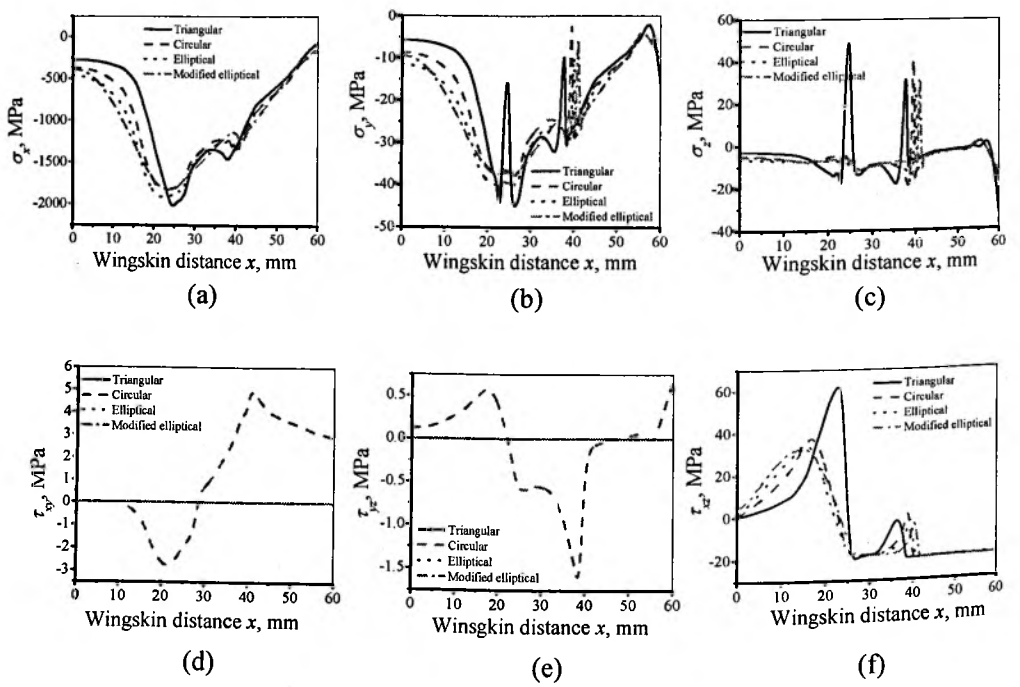

Figure 9.11 Normal and shear stress variations on the bottom surface of the wingskin of the SWJ having different adhesive core profiles with b/h = 1.5.

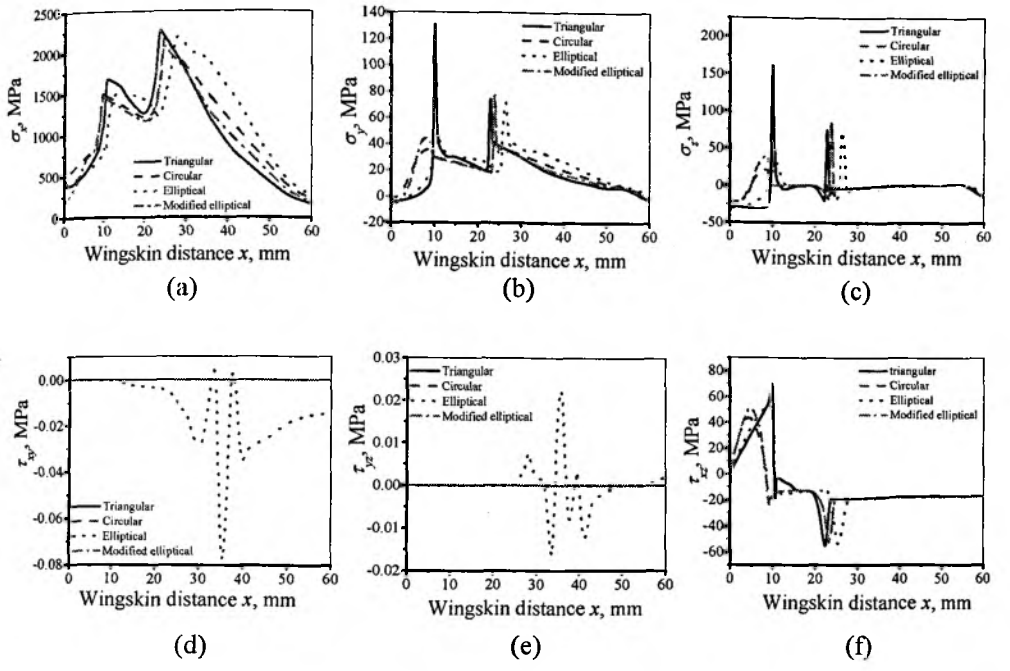

Figure 9.12 Normal and shear stress variations on the top surface of the wingskin of the SWJ having different adhesive core profiles with $b/h = 0.5$.

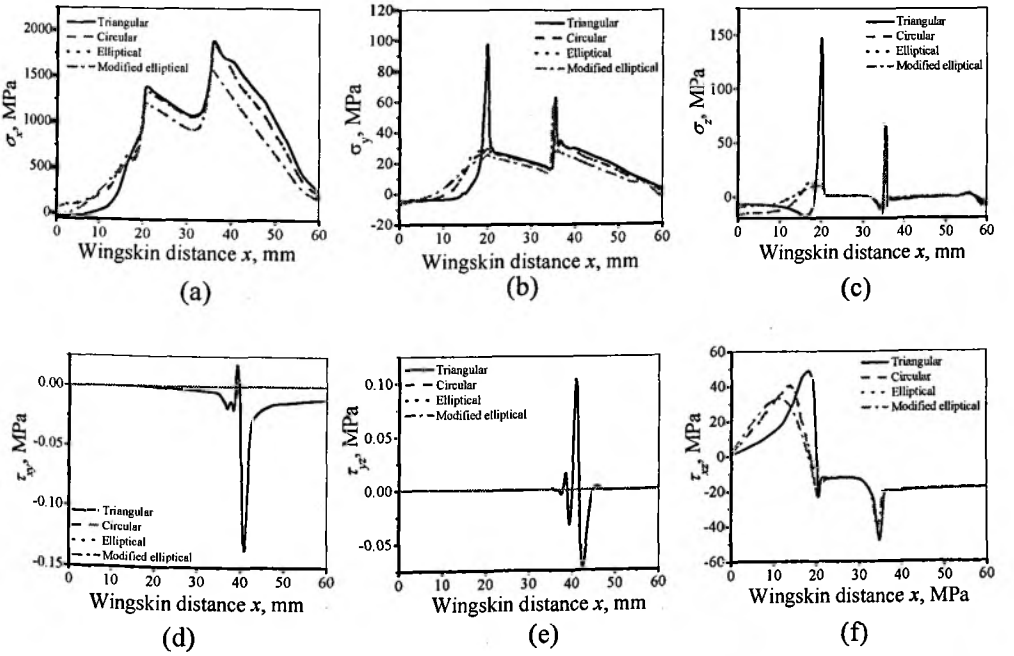

Figure 9.13 Normal and shear stress variations on the top surface of the wingskin of the SWJ having different adhesive core profiles with $b/h = 1.0$.

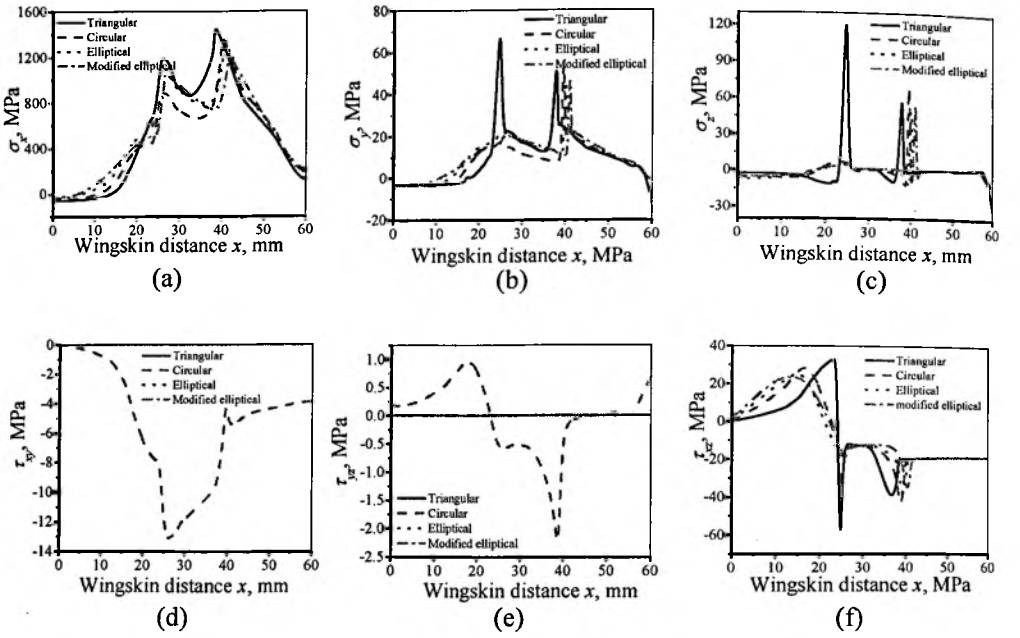

Figure 9.14 Normal and shear stress variations on the top surface of the wingskin of the SWJ having different adhesive core profiles with $b/h = 1.5$.

9.5.2 Effect of load coupler profiles on the onset of delamination damage

Tsai-Wu coupled stress failure criterion, as given in Eqs. (9.1) and (9.2), are used to predict the locations of onset of delamination induced damages in the SWJ of different concepts of load coupler profiles for varied aspect ratios (b/h). The term e_d represents the delamination damage initiation index. The variations of e_d over the top interfacial surface of the wingskin for different b/h ratios of the SWJ are shown in Fig. 9.15. The e_d values are seen to be critical in the wingskin at the toe-end of the spar overlap and at the transition point where the spar changes its orientation from horizontal to inclined. For the SWJ of triangular adhesive core (concept I), the e_d values are the highest and it is the lowest for the SWJ of modified elliptical adhesive core profile. Hence, the modified elliptical adhesive core profiles are preferred for all values of aspect ratios of the SWJ. It is recommended not to use triangular profiles and to never use triangular profiles with $b/h \leq 1.0$. SWJs with circular or elliptical profiles of the adhesive core are preferred over the triangular profiles. Also it is recommended that the SWJ with modified elliptical adhesive core profile with $b/h =$ 1.5 is the most suitable profile.

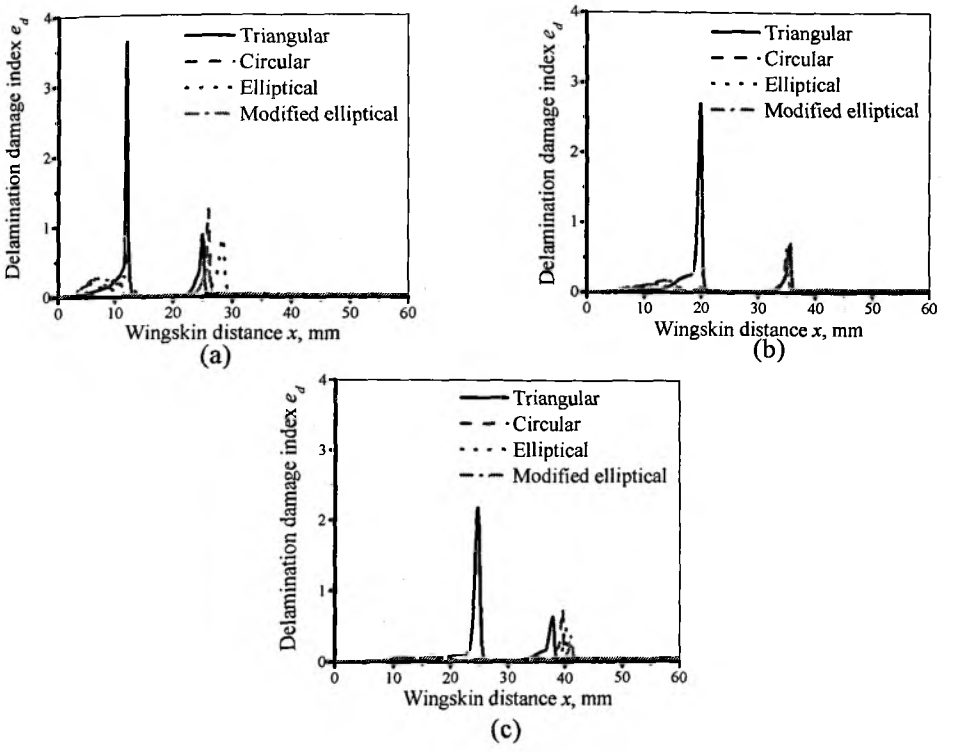

Figure 9.15 Variation of the delamination damage index e_d on the interracial surface of the spar and the wingskin of the SWJ having different load coupler profiles of varied aspect ratios (b/h): (a) b/h = 0.5, (b) b/h = 1.0 and (c) b/h = 1.5.

9.6 Delamination damage analyses of the SWJ with modified elliptical load coupler profile

9.6.1 SERR variations

The delamination would propagate from the critical location which has been depicted from the failure analyses as discussed in the previous section. It is found to occur at the toe-end of the spar flanges in contact with the wingskin. The delamination propagation has been studied by embedding a straight delamination front along the width at the toe-end of the spar flanges of the SWJ for b/h ratio equal to 1.5. Finite element mesh of the delaminated specimen of the SWJ for varied pre-embedded delamination damage lengths, a = 0.5, 1.0, 2.0, 3.0 and 5.0mm, are shown in Fig. 9.16. The individual Modes of SERR i.e. Mode *I* component G_I due to interlaminar tension, the Mode *II* component G_{II} due to interlaminar shear and the Mode *III* component G_{III} due to interlaminar scissoring shear are computed from the three-

dimensional non-linear finite element analyses using MCCI technique. The influence of pre-embedded delamination damage lengths on computed SERR values has been studied in details. The variations of individual Modes of SERR (G_I, G_{II} and G_{III}) along with total SERR (G_T) along the width of the SWJ have been presented in Fig. 9.17.

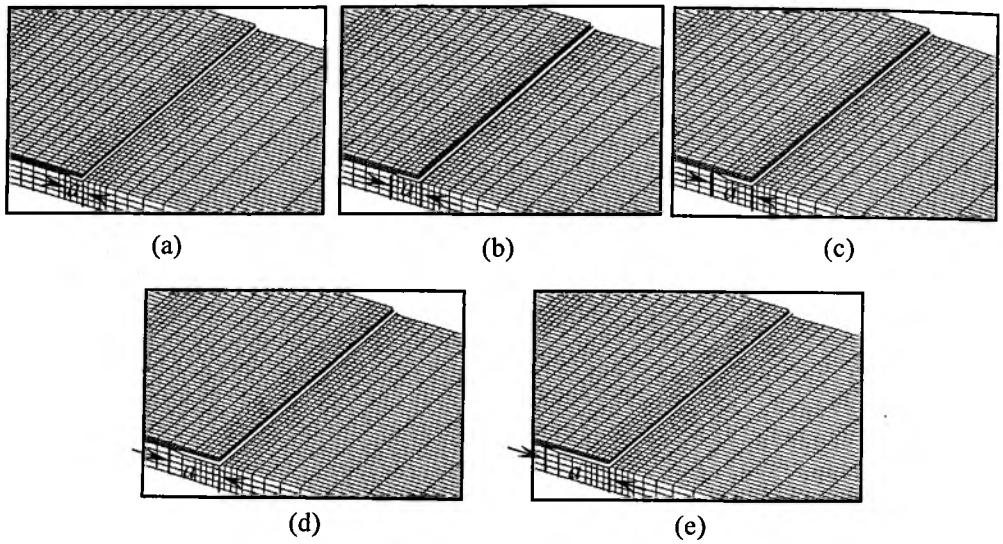

Figure 9.16 Finite element mesh of damaged specimen of SWJ for varying pre-embedded delamination damage lengths (a); (a) 0.5mm, (b) 1mm, (c) 2mm, (d) 3mm and (e) 5mm. (a = delamination damage length measured from the toe-end of the spar).

It is seen that individual and total SERR variations are not uniform in the central part of the SWJ specimen. For all the pre-embedded delamination damage lengths, G_I, G_{II} and G_T values progressively reduce from the peak value at the center towards the edges causing the straight delamination front to grow into a curved delamination front. Similar observations are also noticed by earlier researchers for crack propagation in case of a double cantilever beam specimen [34, 116, 203]. But G_{III} contribution is almost zero in the central portion of the SWJ specimen. The magnitudes of G_{II} *and* G_{III} are very small and therefore, it can be said that the SERR in Mode *I* predominantly governs the delamination damage propagation. G_I values across the width of the SWJ increase as the delamination propagates, whereas G_{II} values decrease as shown in Fig. 9.17 (a-b). Referring to Fig. 9.17 (c), G_{III} values are negligibly small for nearly 90% of the width of the joint for delamination length a = 0.5mm whereas it reduces further as the delamination propagates. Values of individual Modes (G_I, G_{II} and G_{III}) and total (G_T) SERR of the SWJ along the

delamination front existing at the toe-end of the spar flanges (at y = 0 and 25mm) are presented in Table 9.2 for pre-embedded delamination lengths varying from 0.5mm to 5mm.

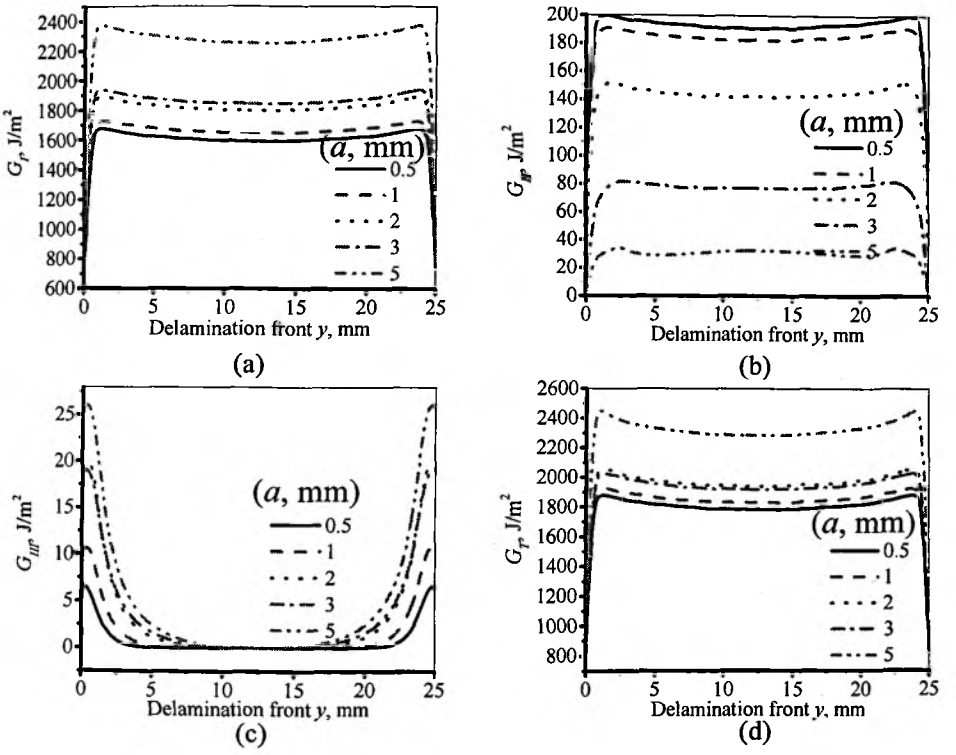

Figure 9.17 Variations of SERR along the delamination front for varying delamination lengths a: (a) G_I, (b) G_{II}, (c) G_{III} and (d) G_T.

Table 9.2 Individual modes (G_I, G_{II} and G_{III}) and total (G_T) Strain Energy Release Rates of the SWJ along the interfacial delamination front existing at the toe-end of the spar flanges and the top surface of the wingskin (at y = 0 and 25mm).

SERR, J/m^2	Pre-embedded delamination lengths (a), mm				
	a = 0.5	a = 1.0	a = 2.0	a = 3.0	a = 5.0
G_I	748.8	781.9	834.21	854.7	1029.14
G_{II}	80	72.9	31.98	1.11	0.98
G_{III}	6.88	10.4	18.82	19	26
G_T	835.68	865.4	885	874.83	1055.14

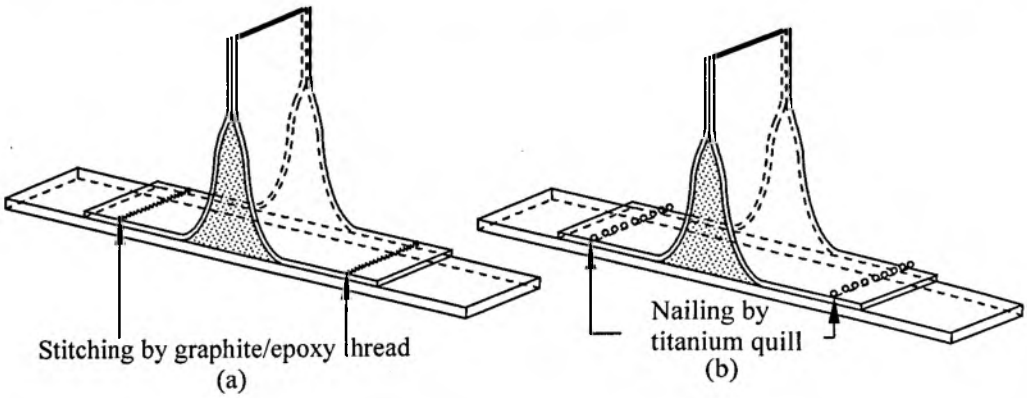

Figure 9.18 Recommended arresting mechanism of delamination damage propagation initiated from the toe-end of the spar of the SWJ; (a) stitching concept and (b) nailing concept.

It may now be concluded that the SWJ would fail due to the propagation of the pre-embedded delamination initiated from the toe-end of the spar-wingskin interfacial surface. To arrest or eliminate the delamination induced damage propagation, suitable concept such as stitching with graphite/epoxy thread or nailing with titanium quills should be used across the width of the composite SWJ at the toe-end of the spar flanges as illustrated in Fig. 9.18.

9.7 Conclusions

Three-dimensional non-linear FEA have been carried out to evaluate the stresses and subsequently to predict the onset of delamination induced damage for the recommendation of suitable geometry and configuration of the SWJ. Both in-plane and out-of-plane stress variations on the different surfaces of the wingskin have been determined. Coupled stress failure criteria have been used to determine the locations of onset of delamination induced damages. Delamination damage propagation has been studied by calculating individual and total Mode of SERRs for the SWJ with a modified elliptical adhesive core with $b/h = 1.5$. The conclusions based on the present FEA are as follows:

- Stresses developed in the adhesive core are quite less and hence, epoxy resin with no reinforcements can be used as the core material in the integral manufacture of SWJ for aircraft wings.
- Normal stresses are significantly higher compared to the shear stresses in the SWJ. Critical values of these tensile stresses occur in the interfacial surfaces

between the spar and the wingskin at the toe-ends of the spar flanges. The peel stresses (σ_z) are found to be the highest at the toe-end of the spar flanges in contact with the wingskin. This would induce onset of failure and delamination induced damages.

- It is recommended not to use triangular adhesive core profiles in the SWJ and never to use triangular adhesive core profiles with aspect ratio $b/h \leq 1.0$. SWJs with circular or elliptical profiles of the adhesive core are preferred over the triangular profiles.
- For the SWJ with modified elliptical adhesive core, the peak values of normal stresses decrease by increasing the base width b of the adhesive core and is the lowest for $b/h = 1.5$. The possibility of delamination damage initiation is the highest at the toe-end of the spar flanges. The recommended base width of the adhesive core is $2b = 3h$ for the SWJ with modified elliptical adhesive core profile.
- Non-uniform distributions of SERR across the width of the SWJ indicate that straight delamination front would grow into a curved delamination front. Delamination onset and growth is predominantly governed by the Mode I SERR (G_I).
- To avoid delamination induced failure, suitable concept such as stitching with graphite/epoxy thread or nailing with titanium quills should be used across the width of the composite SWJ at the toe-end of the spar flanges.

10

Conclusions and Scope for Further Work

This Thesis deals with the analyses of various types of damages in different types of adhesively bonded joint configurations viz. Single Lap Joint (SLJ), Lap Shear Joint (LSJ), Double Lap Joint (DLJ) and Spar Wingskin Joint (SWJ) of laminated FRP composite adherends under mechanical loading. Three-dimensional finite element analyses have been carried out to determine the critical locations of onset of damages in adhesively bonded joints considering the geometric non-linearity. Analyses have also been performed to investigate the suitability of adhesive core profiles used for the SWJ based on three-dimensional stress and failure analyses. Appropriate damage arresting mechanisms have been suggested for a SWJ with modified elliptical adhesive core profile by studying the damage propagation behaviour using the Strain Energy Release Rates (SERR) which have been evaluated using the Linear Elastic Fracture Mechanics Approach (LEFM). This Chapter outlines the contribution of the present work with some concluding remarks, which will help in a judicious establishment of design philosophy for adhesively bonded joints of laminated FRP composite structures.

10.1 Summary

Full three-dimensional finite element analyses have been conducted to calculate the stresses at different interfacial surfaces including the adhesive layer of an adhesively bonded joint. Displacements and interlaminar stresses at the damage front responsible for the damage onset and growth have also been determined. Modified Crack Closure Integral (MCCI) vis-a-vis Virtual Crack Closure Techniques (VCCT) based on the concepts of fracture mechanics are employed to evaluate the individual modes of strain energy release rates during the damage propagation. The interlaminar matrix region of one-twentieth to one-tenth of the individual fiber layer thickness has been assumed to be present to model the delamination damages. To account for the possibility of bending-stretching coupling in the sublaminates above and below the delaminated interface, full-scale models of the laminate geometry instead of quarter/half symmetry models are considered. The effects of the delamination positions on the out-of-plane stresses and the mode of failure have been studied.

Following general conclusions have been summarized from the present research work.

- The validity of the commonly used two-dimensional plane strain or plane stress analysis seems to be accurate for predicting stress state only in the region away from the free surfaces. Accurate evaluation of 3D state of stress in the free end regions of the overlap will enable an accurate prediction of strength of the joint and subsequent damage propagation studies due to the anisotropy and heterogeneity of composite material, loading eccentricity and geometrical discontinuities.
- The variation of the out-of-plane stresses, the interlaminar stresses and the SERR values along the width of the joint are constant except at the free edges.
- Due to the presence of damages, there exist secondary peak peel and shear stresses in the adhesive layer close to the damage front in addition to the peak stresses at the overlap ends. The peak values of the secondary peak peel stresses increase significantly due to the propagation of the damages.
- The effect of interlaminar shear stresses is to impart sliding between the neighbouring laminae of the laminated FRP composite adherends, whereas the normal tensile interlaminar stresses (peel stresses) tend to separate the constituting plies from each other.
- For in-plane loading of bonded joints, G_{III} is very small implying the dominance of mode *I* and mode *II*. In transverse loading, as in case of the SWJ, the contribution of all three modes of SERR are significant for the propagation of delamination induced damages particularly at the free edges of the joint implying the mixed mode delamination fracture behaviour.
- Non-uniform and non-equal SERR variations along the delamination damage fronts depict unequal rates of propagation of delamination damages. This may cause the straight damage front to grow into a curved damage front.
- Delamination front lying inside the overlap region is more detrimental for the propagation of pre-embedded delamination compared to the ones lying outside the overlap region of the joint.

10.2 Specific conclusions

10.2.1 Single Lap Joint (SLJ)

- The magnitudes of the out-of-plane normal stresses (known as peel stresses) are significantly higher compared to the shearing stresses in any surfaces in

the overlap region and the out-of-plane shear stress components are negligibly small except at the corners.

- The damage initiates from the stress singularity points of i.e. from the free edge of the SLJ.
- Delamination damage propagation due to adhesion failure is mainly in shearing mode rather than opening or tearing, as SERR in mode *II* (G_{II}) is larger than G_I and G_{III}.
- Presence of two adhesion failures and their propagation along the adherend-adhesive interfaces from the two ends of the adhesive layer of the SLJ have dissimilar effects.
- The presence of adhesion failure eliminates the possibility of initiation of cohesive failure in the SLJ implying that the adhesion failure will initiate from one of the ends of the adhesive layer and propagate until the final failure of the joint rather than two adhesion failures simultaneously initiating from the two ends of the adhesive layer.
- The locations of the embedded delaminations in either of the laminated FRP composite adherends of an SLJ influence significantly the values of the peak out-of-plane peel stresses (σ_z) in the adhesive layer, whereas it is not so for the other two stress components τ_{yz} and τ_{xz}. The peak value of σ_z is the largest for the bottom delaminated adherend, when the center of the delamination is exactly aligned with the overlap end of the SLJ.
- The interlaminar stresses σ_z and τ_{xz} remain same along the delamination front in the central region of the width of the joint except at the free edges. But the shear stress τ_{yz} varies significantly across the width. This is due to the loading eccentricity prevailing in the joint area of the SLJ. The unequal interlaminar stress magnitudes along the two delamination fronts induce dissimilar delamination damage propagations in the two adherends.
- The SERR in opening mode (G_I) is relatively of higher magnitude than the SERR values in shearing (G_{II}) and tearing (G_{III}) modes. Hence the opening mode SERR predominantly governs the propagation of delamination damage for all positions of the pre-embedded delaminations in the SLJ.

10.2.2 Lap Shear Joint (LSJ)

- There is significant reduction (up to 30%) of maximum value of peel stress σ_z for the damaged LSJ compared to the undamaged one, whereas the reduction is negligible for the other two out-of-plane stress components (τ_{yz} and τ_{xz}). It

indicates that the LSJ with no delamination may fail in net-sectional fracture and the damaged LSJ will fail by the propagation of delaminations.

- The SERR in mode *I*, G_I is significantly higher compared to the other two modes of SERR G_{II} and G_{III}. Thus, the contribution of opening mode is the highest compared to the other two modes for delamination damage propagation.
- The SERR values along the delamination front inside the overlap region are higher compared to the other front which lies outside the overlap region. This indicates that the delamination damage propagates from the delamination front trapped inside the overlap region.

10.2.3 Double Lap Joint (DLJ)

- The out-of-plane stress components are the highest on the interfacial surface between the main adherend and the adhesive layer of the DLJ.
- Adhesion failure propagation is due to mixed mode SERR whereas the delamination damage propagates primarily due to Mode *I*.
- The adhesion failure is more detrimental compared to the delamination induces damages for the failure of DLJ when the DLJ is embedded with both types of damages.

10.2.4 Spar Wingskin Joint (SWJ)

- Stresses developed in the adhesive core are quite less and hence, epoxy resin with no reinforcements can be used as the core material in the integral manufacture of SWJ for aircraft wings.
- It is recommended not to use triangular adhesive core profiles in the SWJ and never to use triangular adhesive core profiles with aspect ratio $b/h \leq 1.0$. SWJs with circular or elliptical profiles of the adhesive core are preferred over the triangular profiles.
- For the SWJ with modified elliptical adhesive core, the peak values of normal stresses decrease by increasing the base width b of the adhesive core and is the lowest for $b/h = 1.5$. The possibility of delamination damage initiation is the highest at the toe-end of the spar flanges. The recommended base width of the adhesive core is $2b = 3h$ for the SWJ with modified elliptical adhesive core profile.

- To avoid delamination induced failure, suitable concept such as stitching with graphite/epoxy thread or nailing with titanium quills should be used across the width of the composite SWJ at the toe-end of the spar flanges.

10.3 Scope for further work

The last two decades have observed a revolutionary attempt in modifying and implementing new methodologies and design concepts resulting in enhanced and successful implementation of laminated FRP composites in almost all areas, thereby gradually substituting traditional monolithic materials. Still, there are several inhibiting factors, which have delayed the widespread use of composites in aircrafts, military armaments and spaceships, where the potential for weight reduction is at a premium. This is ascribed to the complex multi-mode failures in composites and the inherent anisotropic unpredictability, damage tolerance, sensitivity to 3D stresses and out-of-plane short duration loadings.

Composites with inherent flaws, discontinuities and delaminations or cracks behave in a different way in comparison to metals or alloys. In addition to it, such environmental or manufacturing induced effects as hygrothermal or residual stresses have a pronounced effect on the damage characteristics of bonded joints in laminated FRP composite structures. The use of co-cured, co-bonded, or secondary bonded subcomponents and ease of manufacturing as a single component for critical dimensioned and shaped assembly parts not only offers the possibility of a significantly lighter structure but also reduces production costs. However, in spite of all these advantages, composites have relatively low through-the-thickness (out-of-plane transverse) strength and hence high shear or peeling stresses can cause delamination, which may subsequently propagate in an unstable fashion inflicting catastrophic failure of composite structural system.

Although there has been a significant increase in the use of advanced composite materials in lightweight bonded joint structures now-a-days, sometimes all the above considerations give a perception that as if the study of mechanics and damage mechanisms in bonded joints of FRP composite material system is at a natal stage. In retrospect, the application of composites are diversifying and has become so versatile at such pace, there is no denying of the fact that new areas of damage and structural design concepts are coming into picture. Therefore, there is no dearth of works yet to be done in those emerging fields, which nevertheless need to be tackled

efficiently. In considerations to all above, following future works related to the present investigation have been suggested for further study.

- Damage analyses for other types of adhesively bonded joints of laminated FRP composites.
- Study of hygroscopic and thermo-elastic effect on damages in the bonded joints.
- Onset and propagation of damages in the bonded joints subjected to impact and out-of-plane loading.
- Effect of stitching and nailing on delamination damage analysis of SWJ.
- Study of damage level, stacking sequence and material anisotropy in bonded joints of laminated FRP composites.

References

[1] Gay, D., Hoa, S. V. and Tsai, S. W., 2003, *Composite Materials: Design and Applications*, CRC Press, Unites States of America.

[2] Herakovich, C. T., 1998, *Mechanics of Fibrous Composites*, John Wiley & Sons, Unites States of America.

[3] Jones, R. M., 1999, *Mechanics of Composite Materials*, Taylor & Francis, London.

[4] Tsai, S. W. and Hahn, H. T., 1980, *Introduction to Composite Materials*, Technomic Publishing Company, Unites States of America.

[5] Chai, H. and Babcock, C. D., 1985, "Two-dimensional modelling of compressive failure in delaminated laminates," Journal of Composite Materials, **9**, pp. 67-98.

[6] Johanneson, T., Sjoblam, P. and Selden, R., 1984, "The detailed structure of delaminated surfaces in graphite/epoxy laminates," Journal of Material Science, **19**, pp. 1171-1177.

[7] O'Brien, T. K., 1982, *Characterization of delamination onset and growth in a composite laminate.* Damages in Composite Laminates, ASTM STP 775.

[8] Liu, S., 1993, "Delamination and matrix cracking of cross-ply laminates due to spherical indenter," Composite Structures, **25**, pp. 257-265.

[9] Krüeger, R. and Minguet, P. J., 2007, "Analysis of composite skin–stiffener debond specimens using a shell/3D modeling technique," Composite Structures, **81**, pp. 41-59.

[10] Panda, S. K., 2005, *Mixed-Mode Interlaminar Delamination Damage Evolution in Laminated FRP Composites*, Ph.D Thesis, Mechanical Engineering Department, Indian Institute of Technology, Khararagpur, India.

[11] Pradhan, B. and Chakraborty, D., 2000, "Fracture behaviour of FRP composite laminates with an embedded elliptical delamination at the interface," Journal of Reinforced Plastics and Composites, **19**, pp. 1004-1023.

[12] Raju, I. S., 1987, "Calculation of strain energy release rates with higher order and singular finite elements," Engineering Fracture Mechanics, **28**, pp. 252-274.

[13] Rybicki, E. F. and Kanninen, M. F., 1977, "A finite element calculation of stress intensity factors by a modified crack closure integral," Engineering Fracture Mechanics, **9**, pp. 931-938.

References

[14] Sun, C. T. and Manoharan, M. G., 1989, "Strain energy release rates of an interfacial crack between two orthotropic solids," Journal of Composite Materials, **23**, pp. 460-478.

[15] Volkersen, O., 1938, "Die niektraftverteiling in zugbeanspruchten mit konstanten laschenquerscritten," Luftfahrtforschung, **15**, pp. 41-47.

[16] Goland, M. and Reissner, E., 1944, "The stresses in cemented joints," ASME Transactions, Journal of Applied Mechanics, **7**, pp. A17-27.

[17] Hart-Smith, L. J., 1973, *Adhesive-Bonded Double Lap Joints*, NASA-CR-112235.

[18] Hart-Smith, L. J., 1973, *Adhesive-Bonded Single Lap Joints*, NASA-CR-112236.

[19] Oplinger, D. W., 1991, *A Layered Beam Theory for Single Lap Joints*, MTL TR91-23.

[20] Adams, R. D. and Wake, W. C., 1984, *Structural Adhesive Joints in Engineering*, Elsevier Science Publishing Company, United Kingdom.

[21] Tong, L. and Steven, G. P., 1999, *Analysis and Design of Structural Bonded Joints*, Kluwer Academic Publishers, Unites States of America.

[22] Kinloch, A. J., 1987, *Adhesion and Adhesives: Science and Technology*, Chapman and Hall, London.

[23] Matthews, F. L., Kilty, P. F. and Godwin, E. W., 1982, "A review in the strength of joints in fiber reinforced plastics," Composites, **13**, pp. 29-37.

[24] Fleck, N. A., Hutchinson, J. W. and Suo, Z., 1991, "Crack path selection in a brittle adhesive layer," International Journal of Solids and Structures, **27**, pp. 1683-1703.

[25] Carpenter, W. C., 1991, "A comparison of numerous lap joint theories for adhesively bonded joints," Journal of Adhesion, **35**, pp. 55-73.

[26] Zienkiewicz, O. C., 2002, *The Finite Element Method*, Tata McGraw Hill Publishing Company Limited, New Delhi.

[27] Adams, R. D., 1989, "Strength predictions for lap joints, especially with composite adherends: A review," Journal of Adhesion, **30**, pp. 219-242.

[28] Adams, R. D. and Harris, J. A., 1987, "The influence of local geometry on the strength of adhesive bonded joints," International Journal of Adhesion and Adhesives, **7**, pp. 69-80.

[29] Adams, R. D. and Mallick, V., 1992, "A method for the stress analysis of lap joints," Journal of Adhesion, **38**, pp. 199-217.

[30] Crocombe, A. D. and Adams, R. D., 1981, "Influence of the spew fillet and other parameters on the stress distribution in the single lap joint," Journal of Adhesion, **13**, pp. 141-155.

[31] Harris, J. A. and Adams, R. D., 1984, "Strength prediction of bonded single lap joints by non-linear finite element methods," International Journal of Adhesion and Adhesives, **4**, pp. 65-78.

[32] Silva, L. F. M. da and Adams, R. D., 2007, "Joint strength predictions for adhesive joints to be used over a wide temperature range," International Journal of Adhesion and Adhesives, **27**, pp. 362–379.

[33] Altus, E., 1985, "Three-dimensional singularities in double lap joints," Engineering Fracture Mechanics, **21**, pp. 1098-1112.

[34] Panigrahi, S. K. and Pradhan, B., 2007, "Adhesion failure propagation in adhesively bonded single lap laminated FRP composite joints," Journal of Adhesion Science and Technology, **21**, pp. 379-398.

[35] Tong, L., 1998, "Strength of adhesively bonded composite single lap joints with embedded cracks," AIAA Journal, **36**, pp. 448-456.

[36] Cheuk, P. T. and Tong, L., 2002, "Failure of adhesive bonded composite lap shear joints with embedded precrack," Composites Science and Technology, **62**, pp. 1079-1095.

[37] Kairouz, K. C. and Matthews, F. L., 1993, "Strength and failure modes of bonded single lap joints between cross-ply adherends," Composites, **24**, pp. 475-484.

[38] Kayupov, M. and Dzenis, Y. A., 2001, "Stress concentrations caused by bond cracks in single-lap adhesive composite joints," Composite Structures, **54**, pp. 215–220.

[39] Kim, K. S., Yoo, J. S., Yi, Y. M. and Kim, C. G., 2006, "Failure mode and strength of uni-directional composite single lap bonded joints with different bonding methods," Composite Structures, **72**, pp. 477-485.

[40] Qin, M. and Dzenis, Y., 2003, "Analysis of single-lap adhesive composite joints with delaminated adherends," Composites-Part B: Engineering **34**, pp. 167-173.

[41] Tsai, M. Y. and Morton, J., 1995, "The effect of a spew fillet on adhesive stress distributions in laminated composite single-lap joints," Composite Structures, **32**, pp. 123-131.

[42] Guild, F. J., Potter, K. D., Heinrich, J., Adams, R. D. and Wisnom, M. R., 2001, "Understanding and control of adhesive crack propagation in bonded joints between carbon fibre composite adherends, II. Finite element analysis," International Journal of Adhesion and Adhesives, **21**, pp. 445–453.

[43] Adams, R. D., 2005, *Adhesive Bonding: Science Technology and Applications*, CRC Press, England.

[44] Heslehurst, R. B., 1996, "Analysis and Modeling of Damage and Repair of Composite Materials in Aerospace," *Numerical Analysis and Modelling of Composite Materials*, Ed. J. W. Bull, Chapman and Hall, pp. 28-59.

[45] Chai, H., 1987, "A note on crack trajectory in an elastic strip bounded by rigid substrates," International Journal of Fracture, **32**, pp. 211-213.

[46] Hoskin, B. C. and Baker, A. A., 1986, *Joining Advanced Fiber Composites, Composite Materials for Aircraft Structures*, AIAA Education Series, Chapter 8, pp. 115-139.

[47] Tong, L., Sheppard, A., Kelly, D. and Chalkley, P., 1998, "Effect of joint flexibility in adhesively bonded composite panel-to-flange joints," Composites-Part B: Engineering, **29**, pp. 287-298.

[48] Talreja, R., 1985, "Transverse cracking and stiffness reduction in composite laminates," Journal of Composite Materials, **19**, pp. 355-375.

[49] Talreja, R., 1986, "Stiffness properties of composite laminates with matrix cracking and interior delamination," Engineering Fracture Mechanics, **25**, pp. 751-762.

[50] Stout, M. G., Koss, D. A., Liu, C. and Idasetima, J., 1999, "Damage development in carbon/epoxy laminates under quasi-static and dynamic loading," Composites Science and Technology, **59**, pp. 2339-2350.

[51] Hart-Smith, L. J., 1978, "Mechanically fastened joints for advanced composites: phenomenological considerations and simple analysis," 4th Conference on Fibrous Composites in Structural Design, San-Diego, California, pp. 543-573.

[52] Reddy, J. N., 1987, "A generalization of two-dimensional theories of laminated composite plates" Communications Applied Numerical Methods, **3**, pp. 173–180.

[53] Nosier, A., Kapania, R. K. and Reddy, J. N., 1994, "Low velocity impact of laminated composites using a layerwise theory," Computational Mechanics, **13**, pp. 360-379.

[54] Christoforou, A. P. and Swanson, S. R., 1991, "Analysis of impact response in composite laminates," International Journal of Solids and Structure, **27**, pp. 161-170.

[55] Qian, Y. and Swanson, S. R., 1990, "Experimental measurement of impact response in carbon/epoxy plates," AIAA Journal, pp. 1069-1074.

[56] Tong, J., Guild, F. J., Ogin, S. L. and Smith, P. A., 1997, "On matrix crack growth in quasi-isotropic laminates-I. Experimental investigation," Composites Science and Technology, **57**, pp. 1527-1536.

[57] Tong, J., Guild, F. J., Ogin, S. L. and Smith, P. A., 1997, "On matrix crack growth in quasi-isotropic laminates – II. Finite element analysis," Composites Science and Technology, **57**, pp. 1537-1545.

[58] Nairn, J. A., 2000, *Comprehensive Composite Materials: Volume 2-Polymer Matrix Composites*, Nairn, J. A., Elsevier, Amsterdam.

[59] Nairn, J. A. and Hu, S., 1994, *Damage Mechanics of Composite Materials*, Nairn, J. A. and Hu, S., Elsevier, Amsterdam.

[60] Lee, S. H., Noguchi, H. and Cheong, S. K., 2003, "Static behavior characteristics of hybrid composites with non-woven carbon tissues," Journal of Composite Materials, **37**, pp. 233-252.

[61] Qing, X., Chang, F. K. and Starnes, J., 2003, "Damage tolerance of notched composite laminates with reinforcing strips," Journal of Composite Materials, **37**, pp. 111-128.

[62] Zheng, S. F., Denda, M. and Weng, G. J., 2003, "Overall elastic and elasto-plastic behavior of a partially debonded fiber-reinforced composite," Journal of Composite Materials, **37**, pp. 741-758.

[63] Melin, L. G. and Schön, J., 2001, "Buckling behavior and delamination growth in impacted composite specimen under fatigue load: An experimental study," Composites Science and Technology, **61**, pp. 1841-1852.

[64] Tong, L., 1996, "Bond strength for adhesive-bonded single lap joints," Acta Mechanica, **117**, pp. 101-113.

[65] Beaumont, P. W. and Schultz, J. M., 1990, *Macroscopic fracture theories in failure analysis of composite materials, Delaware Composites Design Encyclopedia*, Technomic Publishing Company, United States of America.

[66] Hutchinson, J. W. and Suo, Z., 1992, "Mixed mode cracking in layered materials," Advances Applied Mechanics, **65**, pp. 44-53.

References

[67] Sheppard, A., Kelly, D. W. and Tong, L., 1998, "A damage zone model for the failure analysis of adhesively bonded joints," International Journal of Adhesion and Adhesives **18**, pp. 385-400.

[68] Erdogan, F. and Ratwani, M., 1971, "Stress distribution in bonded joints," Journal of Composite Materials, **5**, pp. 378-393.

[69] Wooley, G. R. and Carver, D. R., 1971, "Stress concentration factors for bonded lap joints," Journal of Aircraft, **8**, pp. 817-820.

[70] Tsai, M. Y. and Morton, J., 1994, "An evaluation of analytical and numerical solutions to the single lap joint," International Journal of Solids and Structures, **31**, pp. 2537-2563.

[71] Liu, A. T., 1976, *Linear elastic and elasto-plastic stress analysis for adhesive lap joints*, TAM Report no. 410.

[72] Adams, R. D. and Peppiatt, N. A., 1974, "Stress analysis of adhesively bonded lap joints," Journal of Strain Analysis, **9**, pp. 185-196.

[73] Humphreys, E. A., 1977, *Non-linear Analysis of Bonded Joints with Thermal Effects*, Virginia Polytechnic Institute, Virginia.

[74] Allman, D.J., 1977, "A theory for elastic stresses in adhesive bonded lap joints," Journal of Mechanics of Applied Mathematics, **30**, pp. 415-436.

[75] Hart-Smith, L. J., 1974, *Analysis and Design of Advanced Composite Bonded Joints*, NASA CR 2218

[76] Pickett, A. K. and Hollaway, L., 1985, "The analysis of elastic adhesive stresses in bonded lap joints in FRP structures," Composite Structures, **3**, pp. 55-79.

[77] Reddy, J. N. and Roy, S., 1988, "Non-linear analysis of adhesively bonded joints," International Journal of Non-Linear Mechanics, **23**, pp. 97-112.

[78] Jeandrau, J. P., 1993, "Adhesive bonding assembly of composite materials," 9th International Conference of Composite Materials, Madrid.

[79] Groth, H. L. and Nordulund, P., 1991, "Shape optimization of bonded joints," International Journal of Adhesion and Adhesives, **11**, pp. 204-211.

[80] Renton, W. J. and Vinson, J. R., 1975, "The efficient design of adhesive bonded joints," Journal of Adhesion, **7**, pp. 175-193.

[81] Sage, G. N., 1976, "Some aspects of bonded joint design in CFRP," Journal of Composite Materials, pp. 256-260.

[82] Li, G. and Lee-Sullivan, P., 2001, "Finite element and experimental studies on single-lap balanced joints in tension," International Journal of Adhesion and Adhesives, **21**, pp. 211-220.

[83] Andruet, R. H., Dillard, D. A. and Holzer, S. M., 2001, "Two and three dimensional geometrical non linear finite elements for analysis of adhesive Joints," International Journal of Adhesion and Adhesives, **21**, pp. 17-34.

[84] Pandey, P. C. and Narasimhan, S., 2001, "Three dimensional nonlinear analysis of adhesively bonded lap joints considering viscoplasticity in adhesives," Composite Structures, **79**, pp. 769-783.

[85] Mortensen, F. and Thomsen, O. T., 2002, "Analysis of adhesive bonded joints: A unified approach," Composites Science and Technology, **62**, pp. 1011-1031.

[86] Brussat, T. R., Chiu, S. T. and Mostovoy, S., 1977, *Fracture Mechanics for Structural Adhesive Bonds*, AFML TR 117-163.

[87] Johnson, W. S., 1987, "Stress analysis of the cracked lap shear specimen: an ASTM round robin," ASTM Journal of Testing and Evaluation, **6**, pp. 303-324.

[88] Edde, F. and Verreman, Y., 1992, "On the fracture parameters in a clamped cracked lap shear adhesive joint," International Journal of Adhesion and Adhesives, **12**, pp. 43-48.

[89] Lai, Y. H., Rakestraw, M. D. and Dillard, D. A., 1996, "The cracked lap shear specimen revisited-A closed form solution," International Journal of Solids and Structures, **33**, pp. 1725-1743.

[90] Lin, C. and Liechti, K. M., 1987, "Similarity concepts in the fatigue fracture of adhesive bonded joints," Journal of Adhesion, **21**, pp. 1-24.

[91] Chen, D. and Cheng, S., 1983, "An analysis of adhesive bonded single lap joints," ASME Transaction, Journal of Appllied Mechanics, **50**, pp. 109-115.

[92] Tong, L., Sheppard, A. and Kelly, D., 1994, "A numerical study of adhesively bonded composite panel-flange joints," Composite Structures, **28**, pp. 449-458.

[93] Kendall, K., 1975, "Crack propagation in lap shear joints," Journal of Physics, **8**, pp. 512-522.

[94] Griffiith, A. A., 1921, "Phenomenon of rupture and flow in solids," Phil. Transactions, Royal Society of London, **A221**, pp. 163.

[95] Wang, S. S. and Yau, J. F., 1982, "Interface cracks in adhesive bonded lap shear joints," International Journal of Fracture, **19**, pp. 295-309.

References

[96] (ESDU), Engineering Science Data Unit, 1979, *Inelastic shear stresses and strains in the adhesives bonding lap joints loaded in tension or shear*, Item no. 79016, London.

[97] Tong, L., 1994, "Bond shear strength for adhesive bonded double-lap joints," International Journal of Solids and Structures, **31**, pp. 2919-2931.

[98] Adams, R. D., Atkins, R. W., Harris, J. A. and Kinloch, A. J., 1986, "Stress analysis and failure properties of carbon fiber reinforced plastics/steel double lap joints," Journal of Adhesion, **20**, pp. 29-53.

[99] Tong, L., Sheppard, A. and Kelly, D., 1996, "The effect of adherend alignment on the behaviour of adhesively bonded double lap joints," International Journal of Adhesion and Adhesives, **16**, pp. 241-247.

[100] Tong, L., Sheppard, A. and Kelly, D., 1995, "Relationship between surface displacement and adhesive peel stress in bonded double lap joints," International Journal of Adhesion and Adhesives, **15**, pp. 43-48.

[101] Cheuk, P. T., Tong, L., Wang, C. H., Baker, A. and Chalkley, P., 2002, "Fatigue crack growth in adhesively bonded composite-metal double lap joints," Composite Structures, **57**, pp. 109-115.

[102] Keer, L. M. and Chantaramungkorn, K., 1975, "Stress analysis for a double lap joint," ASME Transactions, Journal of Applied Mechanics, pp. 353-357.

[103] Osnes, H. and McGeorge, D., 2005, "Analysis of overlaminated double lap joints," Composites-Part B: Engineering, **36**, pp. 544-558.

[104] Lackman, L. M., O'Brien, W. L. and Loyd, M. S., 1978, "Advanced composite integral structures meet the challenge of future aircraft systems," Proceedings of 4th Conference on Fibrous Composites in Structural Design, San-Diego, California, pp. 125-144.

[105] Gillespie, J. W. Jr. and Pipes, R. B., 1978, "Behaviour of integral composite joints-Finite element and experimental evaluation," Journal of Composite Materials, **12**, pp. 408-421.

[106] Cope, R. D. and Pipes, R. B., 1978, "Design of the spar-wingskin joint," Proceedings of 4th Conference on Fibrous Composites in Structural Design, San-Diego, California, pp. 603-617.

[107] Cope, R. D. and Pipes, R. B., 1982, "Design of the composite spar-wingskin joint," Composites, **13**, pp. 47-53.

[108] Irwin, G. R., 1957, "Analysis of stresses and strains near the end of a crack traversing a plate," ASME Transactions, Journal of Applied Mechanics, **24**, pp. 361-364.

[109] Hellen, T. K., 1975, "On the method of virtual crack extension," International Journal of Numerical Methods in Engineering, **9**, pp. 187-207.

[110] Hwu, C. and Hu, J., 1992, "Stress intensity factors and energy release rates of delaminations in composite laminates," Engineering Fracture Mechanics, **42**, pp. 977-988.

[111] Raju, I. S., Crews, J. H. and Aminpour, M. A., 1988, "Convergence of strain energy release rate components for edge-delaminated composite laminates," Engineering Fracture Mechanics, **30**, pp. 383-396.

[112] Sun, C. T. and Jih, C. J., 1987, "On Strain energy release rates for interfacial cracks in bi-material media," Engineering Fracture Mechanics, **28**, pp. 13-20.

[113] Beuth, J.L. and Narayan, S.H., 1997, *Separation of crack extension modes in composite delamination problems in Composite Materials: Fatigue and Fracture*, ASTM STP 1285, American Society for Testing and Materials, pp. 324-342.

[114] Huang, H. and Kardomateas, G. A., 2001, "Mixed-mode stress intensity factors for cracks located at or parallel to the interface in bimaterial half planes," International Journal of Solids and Structures, **38**, pp. 3719-3734.

[115] Sun, C. T. and Pandey, R. K., 1994, "Improved method for calculating strain energy release rate based on beam theory," AIAA Journal, **32**, pp. 184-189.

[116] Davidson, B. D., 1990, "An analytical investigation of delamination front curvature in double cantilever beam specimens," Journal of Composite Materials, **24**, pp. 1124-1137.

[117] Davidson, B. D., Krüeger, R. and König, M., 1996, "Effect of stacking sequence on energy release rate distributions in multidirectional DCB and ENF specimens," Engineering Fracture Mechanics, **55**, pp. 557-569.

[118] Davidson, B. D. and Schapery, R. A., 1988, "Effect of finite width on deflection and energy release rate of an orthotropic double cantilever specimen," Journal of Composite Materials, **22**, pp. 640-656.

[119] Nilsson, K. F., 1993, "On growth of crack fronts in the DCB-test" Composites Engineering, **3**, pp. 527-546

[120] Carpenter, W. C., 1995, "Insensitivity of the reciprocal work contour integral method to higher order eigenvectors," International Journal of Fracture, **73**, pp. 93-108.

[121] Qian, W. and Sun, C. T., 1997, "Calculation of stress intensity factors for interlaminar cracks in composite laminates," Composites Science and Technology, **57**, pp. 637-650

[122] Qian, W. and Sun, C. T., 1998, "Methods for calculating stress intensity factors for interfacial cracks between two orthotropic solids," International Journal of Solids and Structures, **35**, pp. 3317-3330.

[123] Boniface, V. and Simha, K.R.Y., 1999, "Re-examination of crack opening model of interface fracture," Engineering Fracture Mechanics, **64**, pp. 677-691

[124] Sun, C. T. and Qian, W., 1997, "The use of finite extension strain energy release rates in fracture of interfacial cracks," International Journal of Solids and Structures, **34**, pp. 2595-2609.

[125] Venkatesha, K. S., Dattaguru, B. and Ramamurthy, T.S., 1996, "Finite element analysis of an interface crack with large crack-tip contact zones," Engineering Fracture Mechanics, **54**, pp. 847-860.

[126] Venkatesha, K. S., Dattaguru, B. and Ramamurthy, T.S., 1996, "Generalized Modified Crack Closure Integral (GMCCI) and its application to interface crack problems," Composite Structures, **60**, pp. 665-676.

[127] Venkatesha, K. S., Ramamurthy, T. S. and Dattaguru, B., 1998, "A study of the behavior of subinterface cracks in bimaterial plates," Engineering Fracture Mechanics, **59**, pp. 241-252.

[128] Tian, Z. and Swanson, S. R., 1991, "The fracture behaviour of carbon/epoxy laminates containing internal cut fibers," Journal of Composite Materials, **25**, pp. 1427-1444.

[129] Reddy, J. N., 2003, *Mechanics of Laminated Composite Plates and Shells: Theory and Analysis*, CRC Press, United States of America.

[130] Cook, R. D., Malkus, D. S., Plesha, M. E. and Witt, R. J., 2001, *Concepts and Applications of Finite Element Analysis*, John Wiley & Sons, Inc, New York.

[131] Reddy, J. N., 1993, *An Introduction to the finite Element Method*, Tata Mc Graw Hill Publishing Company Limited, New Delhi.

[132] Bathe, K. J., 1982, *Finite Element Procedures in Engineering Analysis*, Prentice Hall, Englewood Cliffs, N. J.

[133] Wilson, K. J., Taylor, R. L., Doherty, W. P. and Ghaboussi, J., 1973, *Incompatible displacement models*, Numerical and Computer Methods in Structural Mechanics, Academic Press, pp. 43-57.

[134] Taylor, R. L., Beresford, P. J. and Wilson, E. L., 1976, "A non-conforming element for stress analysis," International Journal of Numerical Methods in Engineering, **10**, pp. 1211-1219.

[135] Raghava, R. S., Cadell, R. M. and Yeh, G. S., 1973, "The macroscopic yield behaviour of polymers," Journal of Material Science, **8**, pp. 225-232.

[136] Barosum, R. S., 1977, "Triangular quarter-point elements as elastic and perfectly-plastic crack tip elements," International Journal of Numerical Methods in Engineering, **11**, pp. 85-98.

[137] Ingraffea, A. R. and Hahn, H. T., 1980, "Stress intensity factor computation in three dimensions with quarter-point elements," International Journal of Numerical Methods in Engineering, **15**, pp. 1427-1445.

[138] Klüg, J., Wu, X. X. and Sun, C. T., 1996, "Efficient modeling of postbuckling delamination growth in composite laminates using plate elements," AIAA Journal, **34**, pp. 178-184.

[139] Krüeger, R., Minguet, P. J. and O'Brien, T. K., 2003, "Implementation of interlaminar fracture mechanics in design: An overview," Proceedings of 14th International Conference on Composite Materials (ICCM-14) San Diego, SME Technical Paper EM 03-384.

[140] Krüeger, R. and O'Brien, T. K., 2001, "A shell/3D modeling technique for the analysis of delaminated composite laminates," Composites-Part A: Applied Science and Manufacturing, **32**, pp. 25-44.

[141] Erdogan, F. and Gupta, G. D., 1971, "Layered composites with an interface flaw," International Journal of Solids and Structure **2**, pp. 1089 – 1107.

[142] Pagano, N. J. and Pipes, R. B., 1971, "The influence of stacking sequence on laminate strength," Journal of Composite Materials, **5**, pp. 50-57.

[143] Pipes, R. B. and Pagano, N. J., 1970, "Interlaminar stresses in composite laminates under uniform axial extension," Journal of Composite Materials, **4**, pp. 538-548.

[144] Sih, G. C., Chen, E. P., Huang, S. L. and Mcquillen, E. J., 1975, "Material characterization on the fracture of filament-reinforced composites," Journal of Composite Materials, **9**, pp. 167-186.

[145] Williams, J. G., 1988, "On the calculation of energy release rates for cracked laminates," International Jounal of Fracture, **36**, pp. 101-119.

[146] Hong, S. and Liu, D., 1989, "On the relationship between impact energy and delamination area," Experimental Mechanics, **29**, pp. 115-120.

[147] Dattaguru, B., Ramamurthy, T. S. Venkatesha and Buchholz, F. G., 1994, "Finite element estimates of strain energy release rate components at the tip of an interface crack under Mode I loading," Engineering Fracture Mechanics, **49**, pp. 211-228.

[148] Sankar, B. V. and Sonik, V., 1995, "Point-wise energy release rate in delaminated plates," AIAA Journal, **33**, pp. 1312–1318.

[149] Wang, J. T. and Raju, I. S., 1996, "Strain energy release rate formulae for skin-stiffener debond modeled with plate elements," Engineering Fracture Mechanics, **54**, pp. 211-228.

[150] Kim, R. Y. and Soni, S. R., 1984, "Experimental and analytical studies on the onset of delamination in laminated composites," Journal of Composite Materials, **18**, pp. 70-80.

[151] Brewer, J. C. and Lagace, P. A., 1988, "Quadratic stress criterion for initiation of delamination," Journal of Composite Materials, **22**, pp. 1141-1155.

[152] Miravete, A. and Jimenez, M. A., 2002, "Application of the finite element method to prediction of onset of delamination growth," ASME Transactions, Journal of Applied Mechanics Review, **55**, pp. 89-106.

[153] Tay, T. E., Shen, F., Lee, K. H., Scaglione, A and Sciuva, M Di, 1999, "Mesh design in finite element analysis of post-buckled delamination in composite laminates," Composite Structures, **47**, pp. 603-611.

[154] Buchholz, G., Rikards, R. and Wang, H., 1997, "Computational analysis of interlaminar fracture of laminated composites," International Journal of Fracture, **86**, pp. 37–57.

[155] Mukherjee, Y. X., Gulrajani, S. N., Mukherjee, S. and Netravali, A. N., 1994, "A numerical and experimental study of delaminated layered composites," Journal of Composite Materials, **28**, pp. 837-870.

[156] Whitcomb, J. D., 1992, "Analysis of a laminate with postbuckled delamination including contact effects," Journal of Composite Materials, **26**, pp. 1523-1325.

[157] Crocombe, A. D. and Adams, R. D., 1982, "An elasto-plastic investigation of the peel test," Journal of Adhesion, **13**, pp. 241-267.

[158] Tsai, M. Y., Oplinger, D. W. and Morton, J., 1998, "Improved theoretical solutions for adhesive lap joints," International Journal of Solids and Structures, **35**, pp. 1163-1185.

[159] Krüeger, R., 2004, "Virtual crack closure technique: history, approach and applications," ASME Transactions, Journal of Applied Mechanics Review, **57**, pp. 109-143.

[160] Delale, F., Erdogan, F. and Aydinogluy, M. N., 1982, "Stresses in adhesively bonded joints: A closed-form solution," Journal of Composite Materials, **15**, pp. 249-271.

[161] Wang, C. H. and Rose, L. R. F., 1997, "Determination of triaxial stresses in bonded joints," International Journal of Adhesion and Adhesives, **17** pp. 17-25.

[162] Raju, I. S., Sistla, R. and Krishnamurty, T. S., 1996, "Fracture mechanics analysis for skin-stiffener debonding," Engineering Fracture Mechanics, **54**, pp. 371-385.

[163] Pradhan, B. and Chakraborty, D., 1999, "Effect of ply thickness and fiber orientation on delamination initiation in broken ply composite laminates," Journal of Reinforced Plastics and Composites, **18**, pp. 735-757.

[164] Pradhan, B. and Panda, S. K., 2006, "The influence of ply sequence and thermoelastic stress field on asymmetric delamination crack growth behavior of embedded elliptical delaminations in laminated FRP composites," Composites Science and Technology, **36** pp. 417-426.

[165] Pradhan, B. and Panda, S. K., 2006, "Effect of material anisotropy and curing stresses on interface delamination propagation characteristics in multiply laminated FRP composites," ASME Transactions, Journal of Engineering Materials and Technology, **128**, pp. 383-392.

[166] Timoshenko, S. P. and Goodier, J. N., 1970, *Theory of Elasticity*, McGraw Hill Publication, Singapore.

[167] Tsai, M. Y. and Morton, J., 1994, "Three dimensional deformations in a single lap joint," Journal of Strain Analysis, **29**, pp. 137-145.

[168] Dattaguru, B., Jr R. A. Everett, Whitcomb, J. D. and Johnson, W. S., 1984, "Geometrically non linear analysis of adhesively bonded joints," ASME Transactions, Journal of Engineering Materials and Technology, **106**, pp. 59-65.

[169] Rybicki, E. F., Schmueser, D. W. and Fox, J., 1977, "An energy release rate approach for stable crack growth in free edge delamination problem," Journal of Composite Materials, **11**, pp. 470-487.

[170] Kelly, G., 2006, "Quasi-static strength and fatigue life of hybrid (bonded/bolted) composite single-lap joints," Composite Structures, **72**, pp. 119-129.

[171] Potter, K. D., Guild, F. J., Harvey, H. J., Wisnom, M. R. and Adams, R. D., 2001, "Understanding and control of adhesive crack propagation in bonded joints between carbon fiber composite adherends-I. Experimental," International Journal of Adhesion and Adhesives, **21**, pp. 435-443.

[172] Panigrahi, S. K. and Pradhan, B., 2007, "Three dimensional failure analysis and damage propagation behaviour of adhesively bonded single lap joints in laminated FRP composites," Journal of Reinforced Plastics and Composites, **26**, pp. 183-201.

[173] Delale, F., 1984, "Stress singularities in bonded anisotropic materials," International Journal of Solids and Structure, **20**, pp. 31-40.

[174] Groth, H. L., 1988, "Stress singularities and fracture at interface corners in bonded joints," International Journal of Adhesion and Adhesives, **8**, pp. 107-113.

[175] Quaresimin, M. and Ricotta, M., 2006, "Stress intensity factors and strain energy release rates in single lap bonded joints in composite materials," Composites Science and Technology, **66**, pp. 647-656.

[176] Wheeler, G. E., Madsen, B. S. and DeVries, K. L., 2005, "Fracture mechanics applied to adhesive joints," Journal of ASTM International, **2**, pp. 1-19.

[177] Krüeger, R., Paris, I. L., O'Brien, T. K. and Minguet, P. J., 2002, "Comparaison of 2D finite element modelling assumptions with results from 3D analysis for composite skin-stiffener debonding," Composite Structures, **57**, pp. 161-168.

[178] Chakraborty, D. and Pradhan, B., 2000, "Influence of interfacial resin layer on delamination initiation in broken ply composite laminates," Journal of Adhesion Science and Technology, **14**, pp. 1499-1513.

[179] Glaessgen, E. H., Riddell, W. T. and Raju, I. S., 1998, *Effect of shear deformation and continuity on delamination modeling with plate elements*, AIAA-98-2022.

[180] Panda, S. K. and Pradhan, B., 2005, "Analysis of thermoelastic interaction of manufacturing stresses along the interface on interlaminar delamination progression in multi-ply composite laminates," Journal of Adhesion Science and Technology, **19**, pp. 1305-1323.

[181] Wang, S. S., 1980, "An analysis of delamination in angle-ply fiber-reinforced composites," ASME Transactions, Journal of Applied Mechanics, **47**, pp. 64-70.

[182] Silva, L. F. M. da and Adams, R. D., 2007, "Techniques to reduce the peel stresses in adhesive joints with composites," International Journal of Adhesion and Adhesives, **27**, pp. 227-235.

[183] Jena, B., 1993, *Analysis of Adhesive Bonded Joints in FRP Composite Laminates and Tubes*, Ph.D Thesis, Department of Mechanical Engineering, IIT Kharagpur, India.

[184] Fernlund, G., 2007, "Stress analysis of bonded lap joints using fracture mechanics and energy balance," International Journal of Adhesion and Adhesives, **27**, pp. 584-592.

[185] Oplinger, D. W., 1994, "Effects of adherend deflections in single lap joints," International Journal of Solids and Structures, **31**, pp. 2565-2587.

[186] Wang, H. and Vu-Khanh, T., 1995, "Fracture mechanics and mechanisms of impact-induced delamination in laminated composites," Journal of Composite Materials, **29**, pp. 156-177.

[187] Finn, S. R. and Springer, G. S., 1993, "Delaminations in composite plates under transverse static or impact loads-A model," Composite Structures, **23**, pp. 177-190.

[188] Tay, T. E., 2003, "Characterization and analysis of delamination fracture in composites: An overview of developments from 1990 to 2001," ASME Transactions, Journal of Applied Mechanics Review, **56**, pp. 1-32.

[189] Rinderknecht, S. and Kröplin, B., 1995, "A finite element model for delamination in composite plates," Mechanics of Composite Materials and Structures, **2**, pp. 19-47.

[190] Penado, F. E., 2000, "Analysis of singular regions in bonded joints," International Journal of Fracture, **105**, pp. 1-25.

[191] Liljedahl, C. D., Crocombe, A. D., Wahab, M. A. and Ashcroft, I. A., 2006, "Damage modelling of adhesively bonded joints," International Journal of Fracture, **141**, pp. 147-161.

[192] Tong, L., 1998, "Strength of adhesively bonded single-lap and lap-shear joints," International Journal of Solids and Structures, **35**, pp. 2601-2616.

[193] Zou, G. P., Shahin, K. and Taheri, F., 2004, "An analytical solution for the analysis of symmetric composite adhesively bonded joints," Composite Structures, **65**, pp. 499-510.

[194] Pindera, J. T. and Wang, G., 1990, "Criticality of local three-dimensional stresses in a symmetric adhesively bonded joint," Theoretical Applied Fracture Mechanics, **13**, pp. 1-9.

[195] Anderson, G. P. and DeVries, K. L., 1989, "Predicting strength of adhesive joints from test results," International Journal of Fracture, **39**, pp. 191-200.

[196] Her, S. H., 1999, "Stress analysis of adhesively-bonded lap joints," Composite Structures, **47**, pp. 673-678.

[197] Tsai, S. W. and Wu, E. M., 1971, "A general theory of strength for anisotropic materials," Journal of Composite Materials, **5**, pp. 58-80.

[198] Tserpes, K. I., Labeas, G., Papanikos, P. and Kermanidis, Th., 2002, "Strength prediction of bolted joints in graphite/epoxy composite laminates," Composites-Part B: Engineering, **33**, pp. 521-529.

[199] Panda, S. K. and Pradhan, B., 2007, "Thermoelastic analysis of the asymmetries of interfacial embedded delamination characteristics in laminated FRP composites," Composites-Part A: Applied Science and Manufacturing, **38**, pp. 337-347.

[200] Raju, I. S., Shivakumar, K. N. and Crews, J. H., 1988, "Three dimensional elastic analysis of a double cantilever beam specimen," AIAA Journal, **26**, pp. 1493-1498.

[201] Rice, J. R., 1988, "Elastic fracture mechanics concepts for interfacial cracks," ASME Transactions, Journal of Applied Mechanics, **55**, pp. 98-103.

[202] Hashin, Z., 1980, "Failure criteria for unidirectional fiber composites," ASME Tranactions, Journal of Applied Mechanics, **47**, pp. 329-334.

[203] Crews, J. H. Jr, Shivakumar, K. N. and Raju, I. S., 1991, "Strain energy release rate distribution for double cantilever beam specimen," AIAA Journal, **29**, pp. 1686-1691.

PUBLICATIONS FROM THE THESIS

Referred Journals

[1] Panigrahi, S. K. and Pradhan, B., 2007, "Three-dimensional failure analysis and damage propagation behaviour of adhesively bonded single lap joints in laminated FRP composites," Journal of Reinforced Plastics and Composites, **26**, pp. 183-201.

[2] Panigrahi, S. K. and Pradhan, B., 2007, "Adhesion failure propagation in adhesively bonded single lap laminated FRP composite joints," Journal of Adhesion Science and Technology, **21**, pp. 379-398.

[3] Panigrahi, S. K. and Pradhan, B., "Delamination damage analyses of adhesively bonded lap shear joints in laminated FRP composites," International Journal of Fracture, (Under Review).

[4] Panigrahi, S. K. and Pradhan, B., "Through-the-width delamination damage propagation characteristics in single lap laminated FRP composite joints," International Journal of Adhesion and Adhesives, (Under Review).

[5] Panigrahi, S. K. and Pradhan, B., "Onset and growth of adhesion failure and delamination induced damages in double lap joint of laminated FRP composites," Composite Structures, (Under Review).

[6] Panigrahi, S. K. and Pradhan, B., "Development of load coupler profiles of spar wingskin joints with improved performance for integral structural construction of aircraft wings," Journal of Reinforced Plastics and Composites, (Under Review).

[7] Panigrahi, S. K. and Pradhan, B., "Delamination damage analyses of FRP composite spar wingskin joint with modified elliptical adhesive load coupler profiles," Composites-Part B: Engineering, (Communicated).

Proceedings (International Conferences)

[1] Panigrahi, S.K. and Pradhan, B., 2004, "A SERR approach for analysis of edge delamination propagation in adhesive bonded FRP composite laminates," 49th Congress of ISTAM, NIT Rourkela, December, 27-30, p. 49.

[2] Ramesh Babu, P., Panigrahi, S.K. and Pradhan, B., 2005, "Debond damage analyses of laminated FRP composites using SERR approach," 50th Congress of ISTAM, IIT Kharagpur, December 14-17, pp. 208-217.

[3] Panigrahi, S.K. and Pradhan, B., 2005, "MCCI based unified FE computation scheme of mode separation of SERR for delamination damage evolution studies

in adhesive bonded FRP composites, 50th Congress of ISTAM, IIT Kharagpur, December 14-17, pp. 87-88.

[4] Panigrahi, S.K. and Pradhan, B., 2006, "Damage mechanics of adhesive bonded single lap joints in laminated FRP composites with embedded adhesive failures", 21st Technical Conference of the American Society for Composites, University of Michigan, September 17-22.

[5] Panigrahi, S.K. and Pradhan, B., 2006, "Effect of through-the-width delamination on cohesive and adhesive failure initiation in laminated FRP composite single lap joint," 51st Congress of ISTAM, Andhra University, Visakhapatnam, December 18-21, pp. 257-265.

[6] Panigrahi, S.K. and Pradhan, B., 2006, "Effect of through-the-width delamination on cohesive and adhesive failure initiation in laminated FRP composite single lap joint," 51st Congress of ISTAM, Andhra University, Visakhapatnam, December 18-21, pp. 52-53.

[7] Panigrahi, S.K. and Pradhan, B., 2006, "3D layerwise stress analysis and damage prediction in adhesively bonded single lap joints of laminated FRP composites," 2nd ICCMS-16, IIT Guwahati, India, December 8-10, pp. 419-425.

[8] Panigrahi, S.K. and Pradhan, B., 2007, "Effect of through-the-width embedded delamination on damage prediction of Single lap FRP composite joints," 16th International Conference on Composite Materials, Kyoto, Japan, July 8-13, pp. 1222-1223.

[9] Panigrahi, S.K. and Pradhan, B., 2007, "Modelling and simulation of delamination damages in adhesively bonded single lap joints in FRP composites," International Conference on Computer Aided Engineering, IIT Madras, Chennai, India, December 13-15.

[10] Panigrahi, S.K. and Pradhan, B., 2007, "Effect of temperature on damage propagation in single lap joints of laminated FRP composites," 52nd Congress of ISTAM, BNMIT Bangalore, December 14-17.

Appendix I
Multi-Point Constraint elements (MPC184)

MPC184 comprises a general class of multipoint constraint elements that implement kinematic constraints. The elements are loosely classified here as "constraint elements" and "joint elements." These elements can be used in situations that require some type of kinematic constraint to be imposed. The constraint may be as simple as that of identical displacements at a joint. Constraints can also be more complicated, such as those involving modeling of rigid parts, or kinematic constraints that transmit motion between flexible bodies in a particular way. The type of constraint used depends on the desired application. For example, a structure may consist of some rigid parts and some moving parts connected together by some rotational or sliding connections. The rigid part of the structure may be modeled using the MPC184 Link/Beam elements, while the moving parts may be connected with the MPC184 slider, spherical, revolute, slot, or universal joint element.

Constraint Elements available in MPC184

- Link/beam
- Slider
- Spherical

Joint Elements available in MPC184

- Revolute joint
- Universal joint
- Slot joint

Method of using kinematic constraints

- Direct elimination method
- Lagrange multiplier method

The rigid beam/link MPC184 elements can use the direct elimination method or the Lagrange multiplier method. All other MPC184 element options use the Lagrange multiplier method.

Spherical joint element (used in this Thesis)

Figure A-I-1 shows "MPC184 Spherical Constraint Geometry" and node locations for this element. The two nodes (I and J) are expected to have identical spatial locations initially.

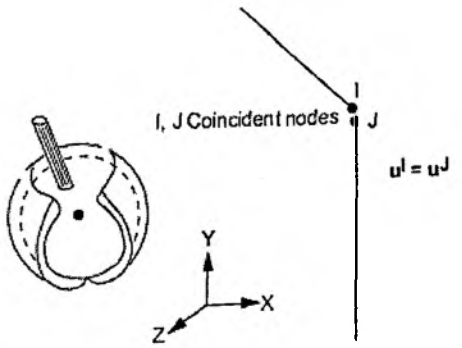

Figure A-I-1 MPC184 Spherical Constraint Geometry

The 3-D spherical element has three degrees of freedom (translations in x, y, and z directions) at each node. The spherical element imposes a kinematic constraint such that the displacements at the two nodes forming the element are identical. The rotational degrees of freedom, if any, are left unconstrained.

Appendix II
Contact or gap element (CONTA178)

Element Description

CONTA178 represents contact and sliding between any two nodes of any types of elements. The element has two nodes with three degrees of freedom at each node with translations in the X, Y, and Z directions. It can also be used in 2-D and axisymmetric models by constraining the UZ degree of freedom. The element is capable of supporting compression in the contact normal direction and Coulomb friction in the tangential direction. The element may be initially preloaded in the normal direction or it may be given a gap specification. A longitudinal damper option can also be included.

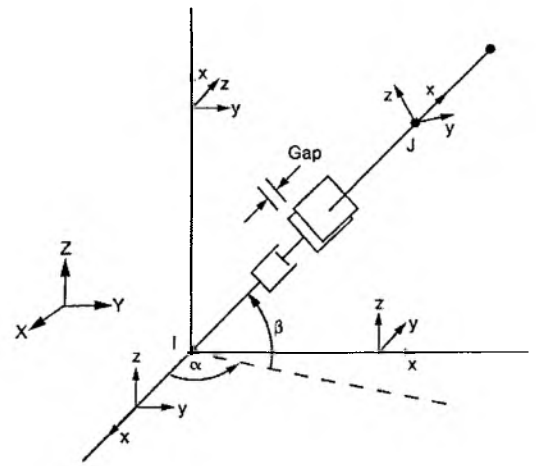

Figure A-II-1 CONTA178 Geometry

The geometry, node locations, and the coordinate system for this element are shown in the Fig. A-II-1. The element is defined by two nodes, an initial gap or interference (GAP), an initial element status (START), and damping coefficients CV1 and CV2. The orientation of the interface is defined by the node locations (I and J) or by a user specified contact normal direction. The interface is assumed to be perpendicular to the I-J line or to the specified gap direction. The element coordinate system has its origin at node I and the x-axis is directed toward node J or in the user specified gap direction. The interface is parallel to the element y-z plane.

Some of the salient features of CONTA 178 are as follows:

- The element operates bilinearly only in the static and the nonlinear transient dynamic analyses. If used in other analysis types, the element maintains its initial status throughout the analysis.
- The element is nonlinear and requires an iterative solution.
- Non-converged substeps are not in equilibrium.
- The element maintains its original orientation in either a small or a large deflection analysis unless the cylindrical gap option is used.

VITAE

Sashi Kanta Panigrahi, son of Late Sri Chakradhar Panigrahi and Smt. Ramamani Panigrahi was born on September 16, 1968 in Balasore district of Orissa State, India. He completed his 10th Class Board Examination from B. C. High School, Tentei, Balasore and 10+2 (Intermediate) CHSE Examination from U. N. College, Soro, Orissa, all in First Division. He received his Bachelor of Engineering in *Mechanical Engineering* in the year 1992 from University College of Engineering, Burla with First Division. He has been a recipient of many scholarships (Merit and National) and awards during his school and college days. From October 1992 to August 1994, he has joined the faculty of Mechanical Engineering Department of Orissa Engineering College, Bhubaneswar. He completed his Post-Graduate Degree with Specialization in *Machine Design and Analysis* securing highest marks from the Mechanical Engineering Department of National Institute of Technology, Rourkela (Formerly known as Regional Engineering College) in the month of January 1996. Since then till date, he is continuing as a faculty member in the Department of Mechanical Engineering of North Eastern Regional Institute Science and Technology (NERIST), Arunachal Pradesh (Deemed University), India. During the deputation period (2004-2007) to Indian Institute of Technology, Kharagpur under Quality Improvement Programme of Government of India, he has been engaged for the Ph.D. Dissertation work on "***Adhesion Failure and Delamination Damage Analyses of Bonded Joints in Laminated FRP Composites***". He has published some good quality research papers in International Journals of repute and presented several research papers in various International and National Conferences. He has been all along associated in Teaching and Research in the broad field of Solid Mechanics with special interest in the area of Damages in FRP Composite Materials, Finite Element Analysis and Computational Fracture Mechanics. His research interests also include damage analyses of bonded joints, especially for aircraft and automotive applications.